NASA Contractor Report 172507

Nonlinear Potential Analysis Techniques for Supersonic Aerodynamic Design

V. Shankar and K.Y. Szema

ROCKWELL INTERNATIONAL SCIENCE CENTER
Thousand Oaks, California 91360

CONTRACT NAS1-15820
1 MARCH 1985

National Aeronautics and Space Administration

Langley Research Center
Hampton, Virginia 23665

NASA Contractor Report 172507

NONLINEAR POTENTIAL ANALYSIS TECHNIQUES FOR SUPERSONIC AERODYNAMIC DESIGN

V. Shankar and K.Y. Szema

ROCKWELL INTERNATIONAL SCIENCE CENTER

Thousand Oaks, California 91360

CONTRACT NAS1-15820

March 1, 1985

FOREWORD

This final report was prepared by the Science Center of Rockwell International, Thousand Oaks, California, for the Langley Research Center, National Aeronautics and Space Administration, Hampton, Virginia. The work was performed under Contract No. NAS1–15820, "Development of Full Potential Analysis Aero Prediction Technology for Hypersonic Configuration Design." Mr. Noel Talcott and Mr. Kenneth Jones were the Project Monitors of this contract.

Mr. E. Bonner of the Los Angeles Division, Rockwell International, was the Program Manager; Drs. V. Shankar and K.Y. Szema of the Rockwell International Science Center were the Principal Investigators.

SUMMARY

A numerical method based on the conservation form of the full potential equation has been applied to the problem of three–dimensional supersonic flows with embedded subsonic regions. The governing equation is cast in a nonorthogonal coordinate system, and the theory of characteristics is used to accurately monitor the type–dependent flow field. A conservative switching scheme is employed to transition from the supersonic marching procedure to a subsonic relaxation algorithm and vice versa. The newly developed computer program can handle arbitrary geometries with fuselage, canard, wing, flow through nacelle, vertical tail and wake components at combined angles of attack and sideslip. Results are obtained for a variety of configurations that include a Langley advanced fighter concept with fuselage centerline nacelle, Rockwell's Advanced Tactical Fighter (ATF) with wing mounted nacelles, and the Shuttle Orbiter configuration.

CONTENTS

1. INTRODUCTION

An examination of the literature for supersonic/hypersonic aircraft provides an indication of the flexibility and generality required for a prediction technique. Typical configuration development variables include wing section, incidence, height, dihedral, planform, effectiveness of longitudinal control surfaces for trim, effectiveness of empennage for directional stability, and propulsion system–airframe interactions.

State–of–the–art response to these prediction requirements is provided by hypersonic impact methods as well as linearized analysis and design algorithms. These approaches can treat complex geometries with minimum response time and cost, with efficient predicted data coverage in terms of Mach number, angle of attack, trim deflection, yaw angle, etc. Shortcomings are present, however, in both the impact and linearized methods. For the former, interference between surface elements is totally ignored in implementations such as classical Newtonian, tangent wedge, and cone theories. Crossflow interactions and stagnation point singularities are also implicitly disregarded. In the latter, shocks, vorticity, and entropy wakes and layers are excluded. Furthermore, superposition of elementary solutions such as those for thickness and angle of attack freely used in linear models are, strictly speaking, invalid at hypersonic speeds.

A need exists for new aerodynamic prediction techniques to optimize vehicles designed to travel at supersonic/hypersonic speeds. One requirement of a new aerodynamic prediction technique is that it be more accurate than simple noninterfering panel methods. Another specification is that it be more computationally efficient than currently available explicit finite–difference methods so that it can be incorporated into a practical design

procedure. The new approach should include enough of the physics of the flow to allow realistic optimization and should permit consideration of appropriate interactions between components of promising arrangements, since this has been found to be the key to increasing aerodynamic efficiency using linear methodology. Nonlinear potential theoretical formulations hold the promise of meeting this objective and providing economic design codes which are responsive to conceptual vehicle definition efforts.

A nonlinear aerodynamic prediction technique based on the full potential equation in conservation form has been developed for the treatment of supersonic flows. References 1 and 2 contain the details of the theoretical development of the full potential analysis method. Detailed description of the method can be found in the publications in Appendix A. The second and third papers of the Appendix constitute a user's manual for the full potential analysis code. Contained therein is a brief description of the code organization, main program and subroutines, flow variables, input data format, and sample test cases.

The computer program entitled, "Nonlinear Supersonic Full Potential Analysis Program" can be obtained for a fee from:

Computer Software Management and Information Center (COSMIC)

112 Barrow Hall

University of Georgia

Athens, GA 30602

(404) 542–3265

Request the program package by the designation LAR–13413. The program is written in FORTRAN IV for use on the Control Data 6600 and the CYBER series of computers.

2. FULL POTENTIAL METHOD

The full potential equation in conservative or nonconservative form is frequently used for transonic flow analysis, where the local Mach number does not exceed approximately 1.4. If the assumptions of irrotationality and isentropicity are reasonably valid, then the full potential equation is expected to yield results comparable to Euler equations, even for supersonic/hypersonic flow fields. For conceptual design studies, where short response time is desired, the full potential methods can be an attractive substitute for expensive Euler methods and less accurate linear theory methods.

A nonlinear aerodynamic prediction technique based on the full potential equation in conservation form has been developed for the treatment of supersonic flows. A detailed description of the method has been presented in several published papers[1-6]. The most recent publications are enclosed in Appendix A for convenience. The first three papers[6-8] describe the method for the treatment of predominantly supersonic flows with regions of subsonic flow that usually occur at low supersonic Mach numberswith the 2nd and 3rd papers constituting a user's manual for the full potential analysis code. The final two papers[9,10] in the Appendix describe the method to treat the unsteady form of the full potential equation. Additional information on the unsteady treatment may be found in References 11 and 12. For blunt nosed configurations with a detached bow shock, the unsteady method is used to generate the starting solution for the marching code. Since the Appendix describes the full potential method, only the results not included in the published articles are presented here.

The following summarizes the salient features of the subject full potential code. Details can be found in the noted references.

- Equation in conservation form (see Refs. 1–6)
- Flux linearized upwind differencing in the marching direction (see Refs. 2–6)
- Conservative switch operators to treat embedded subsonic zones (see Refs. 2 and 3)
- Treatment of wakes (see Refs. 2–6)
- Yaw and angle of attack (see Refs. 2, 5, and 6)
- Complex geometry treatment (fuselage, canopy, wing, canard, nacelle, tail, multibody, etc.) (see Refs. 2, 5, and 6)
- Treatment of blunt nose using unsteady full potential methods (see Refs. 9–12)
- Numerical grid generation with constraints (see Refs. 2, 4, 5, and 6–8)
- Use of GEMPAK[13] or CDS[14] to generate geometry input files (fully automated) (see Refs. 2–8)

3. RESULTS

The full potential analysis code can handle complex aircraft geometries as well as multibody configurations. The following set of four different configuration studies clearly demonstrate the versatility and robustness of the code in handling a wide variety of non-linear flows.

The results to be presented here are

1) Langley's canard–wing fighter configuration, Figures 1 through 21.

Figures 1–2 indicate the complexity of the fighter geometry. Figure 3 schematically shows the variation of the cross plane geometry from the nose to the back end. Figures 4–11 show the cross–sectional geometry and the corresponding grid setup at various axial stations. Figure 12 shows the circumferential pressure distribution at an axial station where only the canard is present. Figure 13 shows the pressure contours, cross flow velocity vectors, and the cross flow streamlines at this axial station. The cross flow velocity vectors and cross flow streamlines are obtained by projecting the total velocity vector on a unit sphere whose center is at the nose of the geometry. Figures 14–19 show similar results at other axial stations. The formation of a shock around the inlet is clearly seen in Fig. 19. Figure 20 shows the computational geometry and the surface grid points for this Langley fighter. Figure 21 shows the pressure contours in the plane of symmetry.

2) Rockwell's Advanced Tactical Fighter with a flow through nacelle, Figures 22 through 24.

Figure 22 shows the geometry of an advanced tactical fighter with a nacelle mounted on the undersurface of the wing. The figure also shows the surface grid setup. Figure 23 shows the grid at an axial station where the nacelle is present. Figure 24 shows the pressure contours at this axial station and the corresponding crossflow velocity vectors.

3) Isolated Shuttle Orbiter flow, Figures 25 through 27,

Figure 25 shows the geometry of the Shuttle Orbiter. Figure 26 shows the upper surface chordwise pressure distribution at various span stations at $M_\infty = 1.4$ and $\alpha = -1.94°$. The agreement with experimental data is very good. Figure 27 shows the OMS pod shock formation and its impingement on the upper wing surface.

4) Shuttle Orbiter — External Tank mated configuration, Figures 28 through 31.

Figure 28 shows the multibody problem of the Shuttle mated configuration with the External Tank and the Solid Rocket Boosters present. Figure 29 shows a typical gridding for this multibody problem at an axial station where the OMS pod, External Tank/SRB, and the blockage are all present. Figure 29 shows the pressure contours at this axial station indicating the OMS pod shock and the detached shock in front of the blockage. Figure 30 shows the Orbiter lower surface chordwise pressure with and without the blockage effect. The comparison with experimental data is good when the blockage effect is accounted for. Figure 31 shows the computational geometry and surface gridding for the mated configuration. More results on this multibody problem can be found in Ref. 15.

The Shuttle Orbiter and the Orbiter/External Tank studies were performed as part of another contract from the Space Division of Rockwell International and funded by NASA–MSFC, Contract No. NAS9–14000. They are included in this contract report only for completeness in illustrating the overall capability of the full potential code.

4. CONCLUSIONS

The full potential analysis code has developed into a powerful nonlinear tool for the analysis of complex aerodynamic configurations: Modifications and enhancements allow analysis of complete configurations including fuselage, canard, wing, vertical and/or horizontal tail, nacelle (body or wing mounted), wake interference effects and multibody flows. Comparisons with available experimental data are in good agreement.

The code is operational on several computer systems, such as the CRAY–XMP, CYBER 203, CDC 7600, CYBER 176 and 175. A vectorized version of the code for the VPS–32 (modified CYBER 205) is currently in development. When fully developed and optimized, the vectorized code is expected to be able to analyze a complete fighter–like configuration in 20–30 seconds using the VPS–32 or CRAY–XMP class machine.

5. REFERENCES

1. Clever, W.C. and Shankar, V., "Nonlinear Potential Analysis Techniques for Supersonic/Hypersonic Configuration Design," NASA CR–166078, March 1983.

2. Shankar, V. and Clever, W.C., "Nonlinear Potential Analysis Techniques for Supersonic/Hypersonic Aerodynamic Design," NASA CR–172299, March 1984.

3. Shankar, V., Szema, K.Y., and Osher, S., "A Conservative Type–Dependent Full Potential Method for the Treatment of Supersonic Flows with Embedded Subsonic Regions," AIAA Paper No. 83–1887, July 1983.

4. Shankar, V., Rudy, S., and Szema, K.Y., "Application of a Two–Dimensional Grid Solver for Three–Dimensional Problems," ASME Paper Vol. No. G00222, June 1983.

5. Jones, K.M., Talcott, N.A., Jr., and Shankar, V., "Application of a Full Potential Method for Computation of Three–Dimensional Supersonic Flows," AIAA Paper No. 84–0139, January 1984.

6. Szema, K.Y. and Shankar, V., "Nonlinear Computation of Wing–Body–Vertical Tail–Wake Flows at Low Supersonic Speed," AIAA Paper No. 84–0427, January 1984.

7. Shankar, V. and Szema, K.Y., "Conservative Full Potential Implicit Marching Scheme for Supersonic Flows," Presented at the University of Tennessee Space Institute Work-

shop on Computational Fluid Dynamics, Article 6.1, UTSI Publication No. E01–4005–023–84, March 1984.

8. Bonner, E., "Supersonic Full Potential Analysis Program Operating Instructions," Rockwell International Report TFD 84–1654, July 1984.

9. Shankar, V., "Implicit Treatment of the Unsteady Full Potential Equation in Conservation Form," AIAA Paper No. 84–0262, January 1984.

10. Shankar, V., Ide, Hiroshi, and Gorski, Joseph, "Relaxation and Approximate Factorization Methods for the Unsteady Full Potential Equation," Presented at the 14th Congress of the International Council of the Aeronautical Sciences (ICAS), Toulouse, France, September 1984.

11. Shankar, V., Szema, K.Y., Gorski, J., and Ide, Hiroshi, "Nonlinear Steady and Unsteady Aerodynamic Prediction Methods Based on the Full Potential Equation," Presented at the Third International Conference on Boundary Interior Layers — Computational and Asymptotic Methods (BAIL III), Dublin, Ireland, June 1984.

12. Shankar, V., Szema, K.Y., Gorski, J., and Ide, Hiroshi, "Steady and Unsteady Nonlinear Flow Treatment Using the Full Potential Equation," Presented at the Ninth International Conference on Numerical Methods in Fluid Dynamics (IC9NMFD), Saclay, France, June 1984.

13. Stack, S.H., Edwards, C.L.W., and Small, W.J., "GEMPAK: An Arbitrary Aircraft Geometry Generator," NASA TP–1022, December 1977.

14. Raymer, D.P., "Configuration Development System," Rockwell International Report TFD–78–755–4, April 1983.

15. Szema, K.Y., Reba, W., Shankar, V., and Gorski, J., "Full Potential Treatment of Flows over Three–Dimensional Geometries Including Multibody Configurations," AIAA Paper No. 85–0272, 23rd Aerospace Sciences Meeting, Reno, Nevada, January 1985.

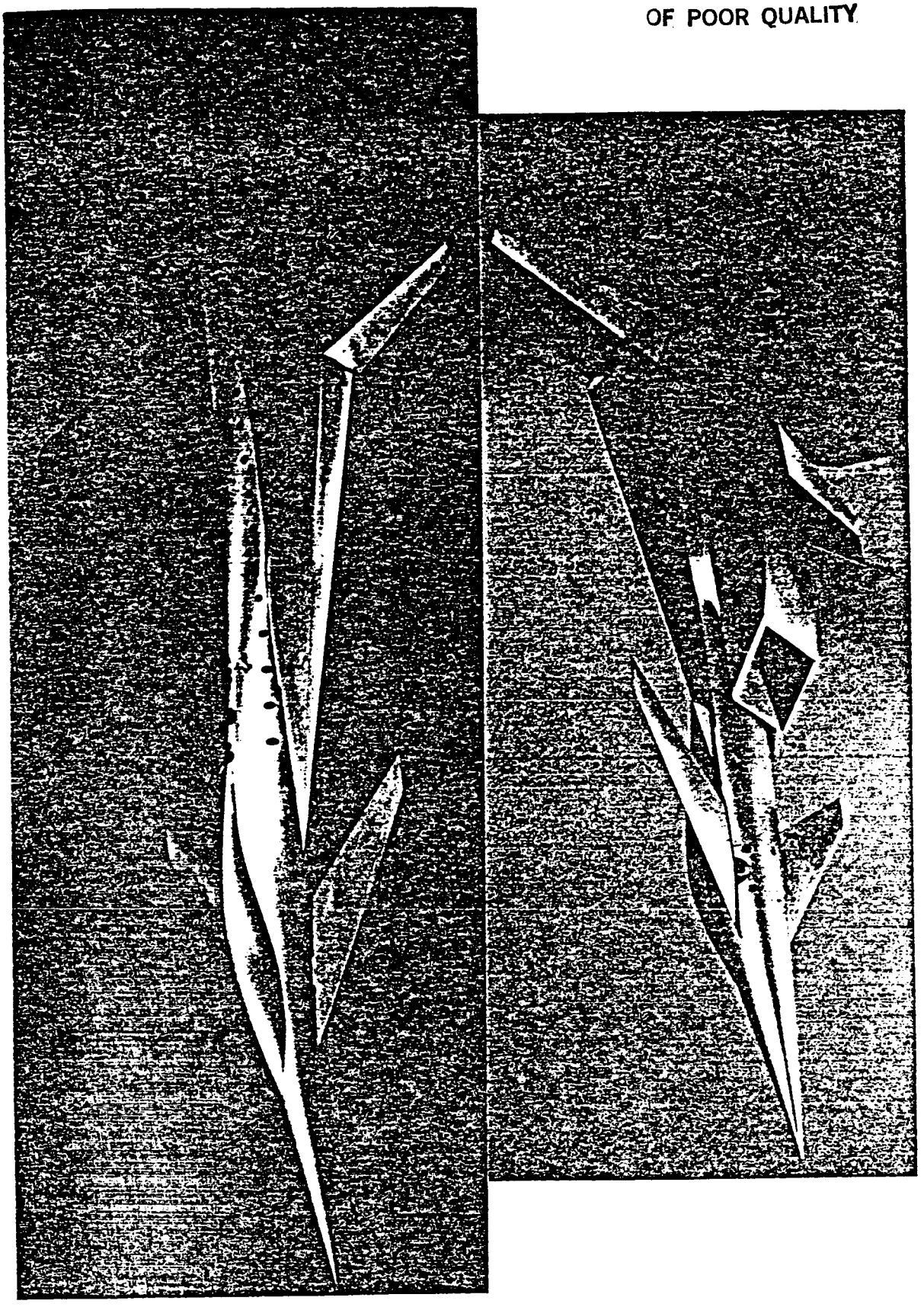

Fig. 1. Canard-wing fighter configuration.

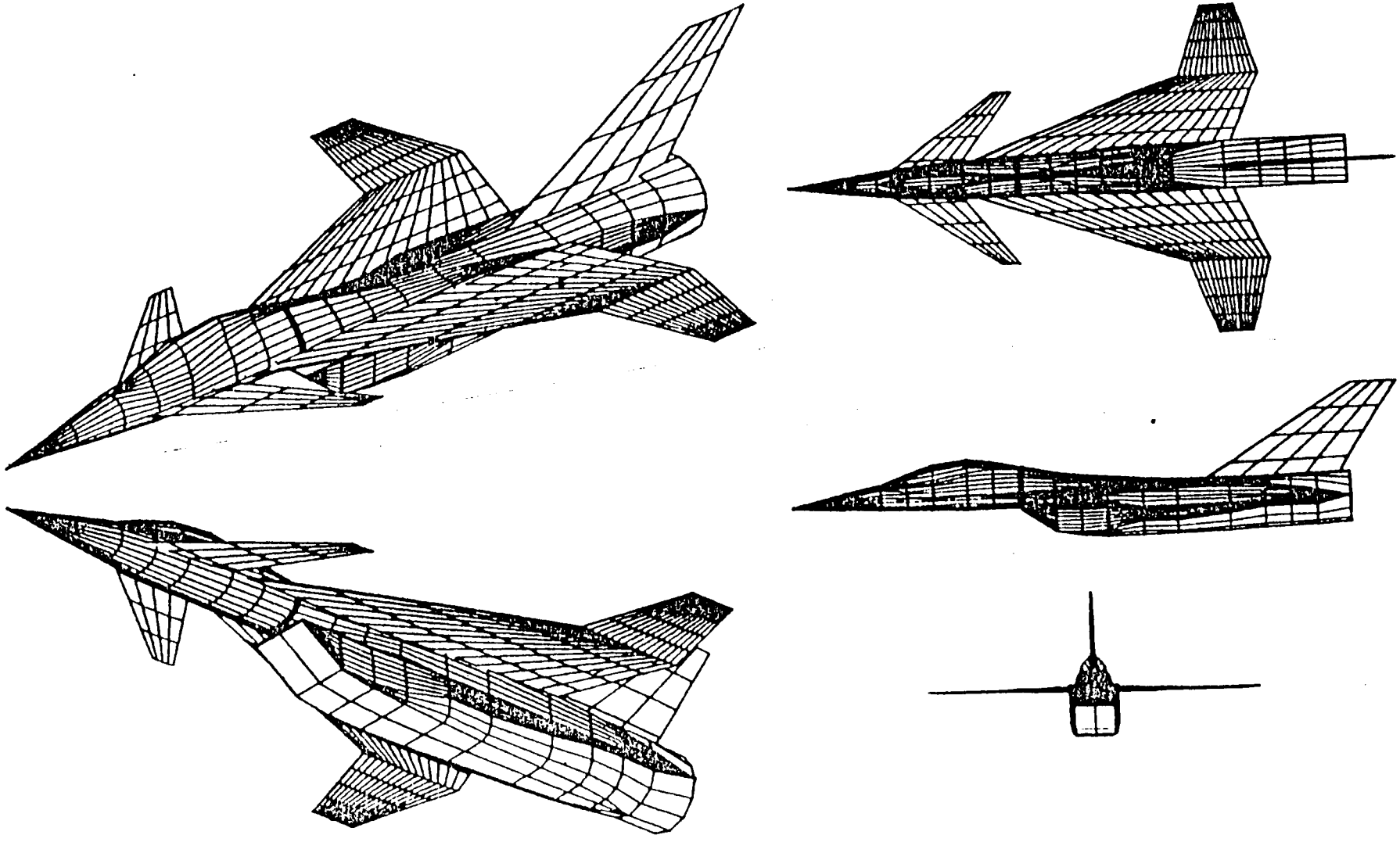

Fig. 2. Treatment of complex aerodynamic configurations.

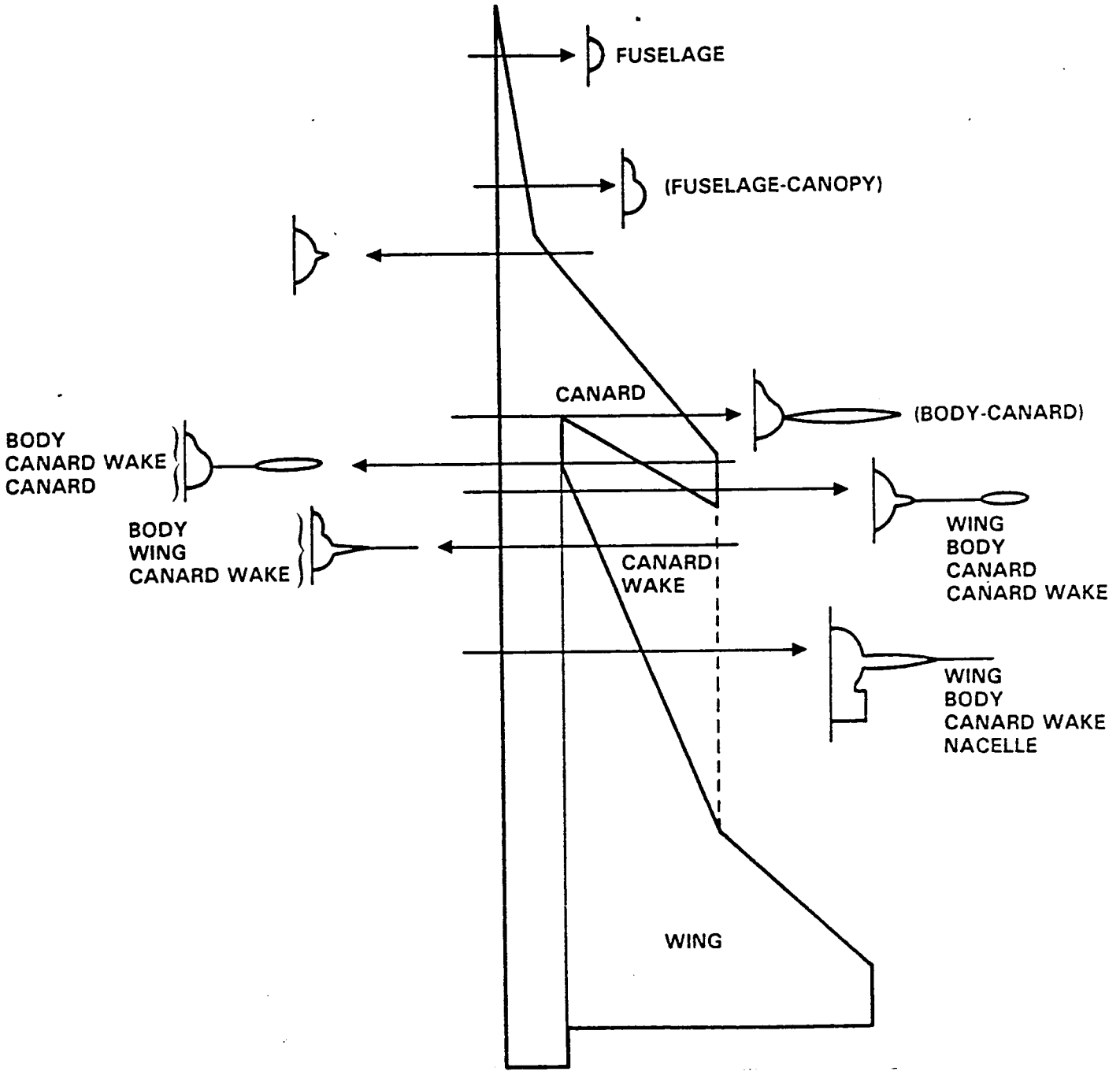

Fig. 3. Variation in cross–sectional shape.

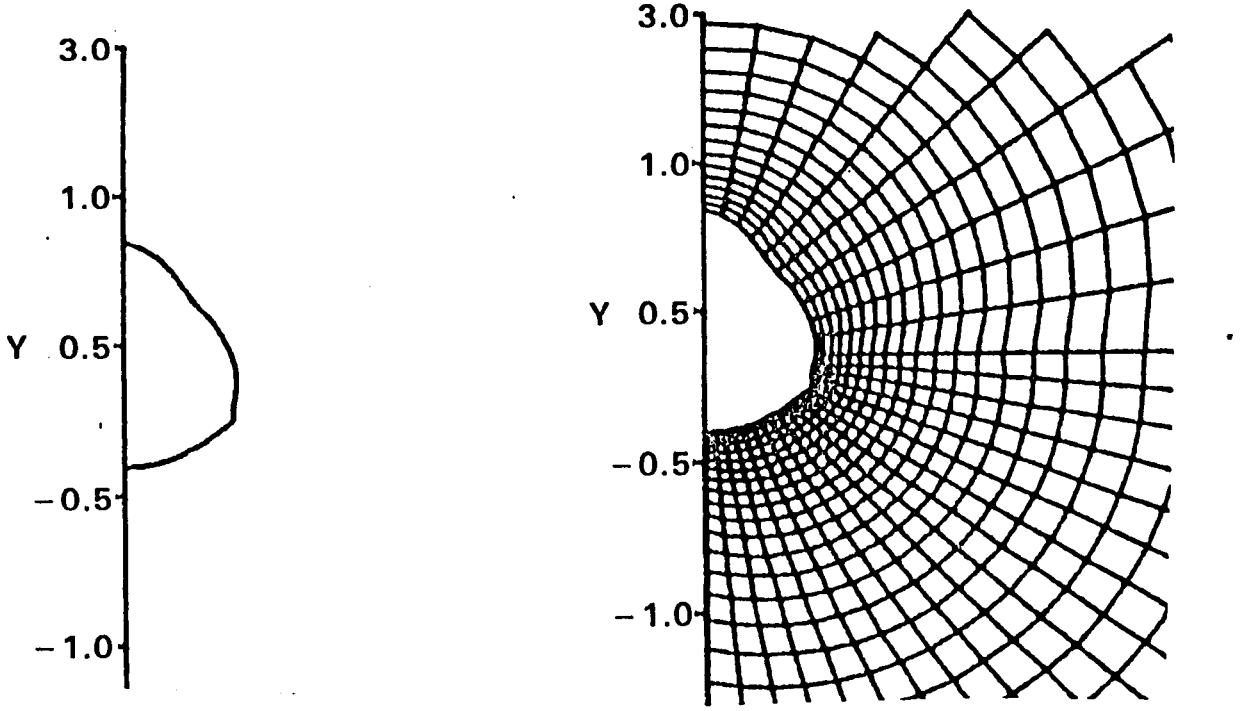

Fig. 4. Cross-section and grid at $x = 5$ (fuselage/canopy/beginning of canard).

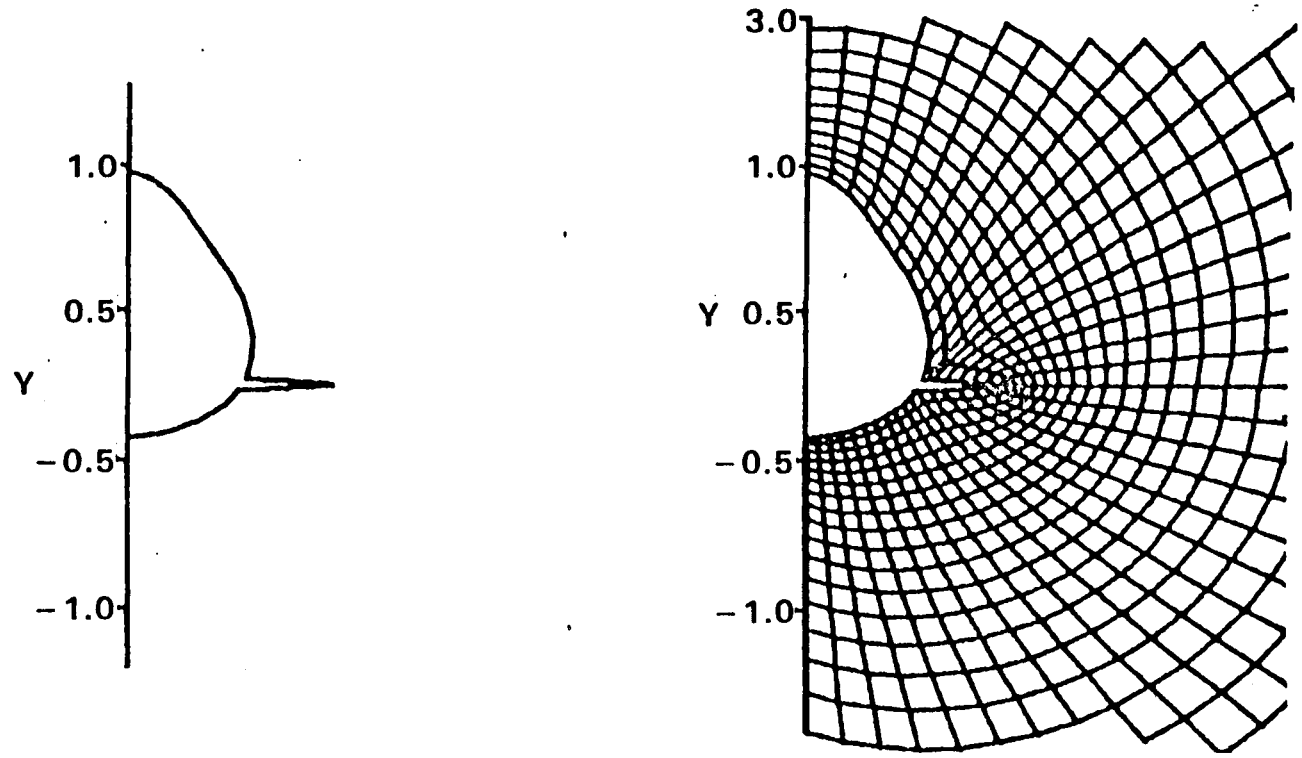

Fig. 5. Cross–section and grid at $x = 7$ (fuselage/canopy/canard).

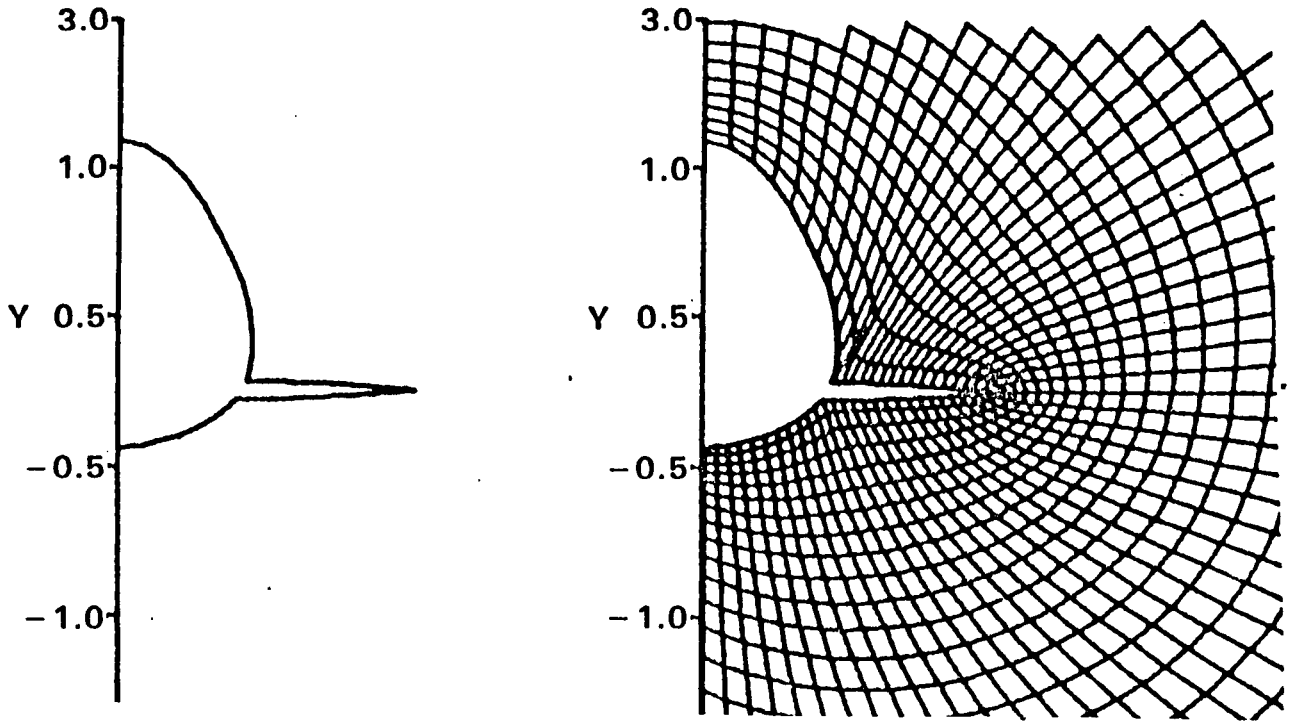

Fig. 6. Cross-section and grid at $x = 8$ (fuselage/canard).

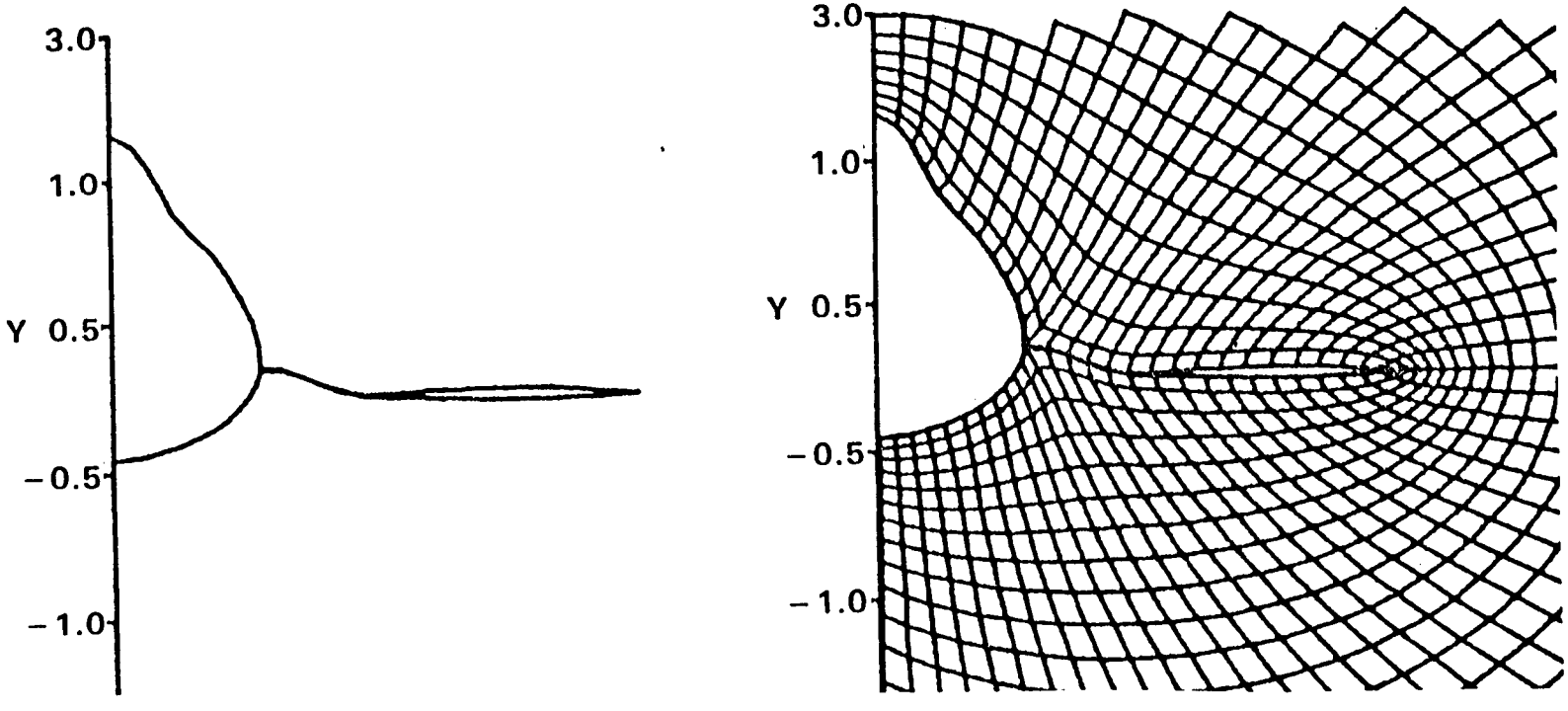

Fig. 7. Cross-section and grid at $x = 10.5$ (fuselage/canopy/canard/canard wake).

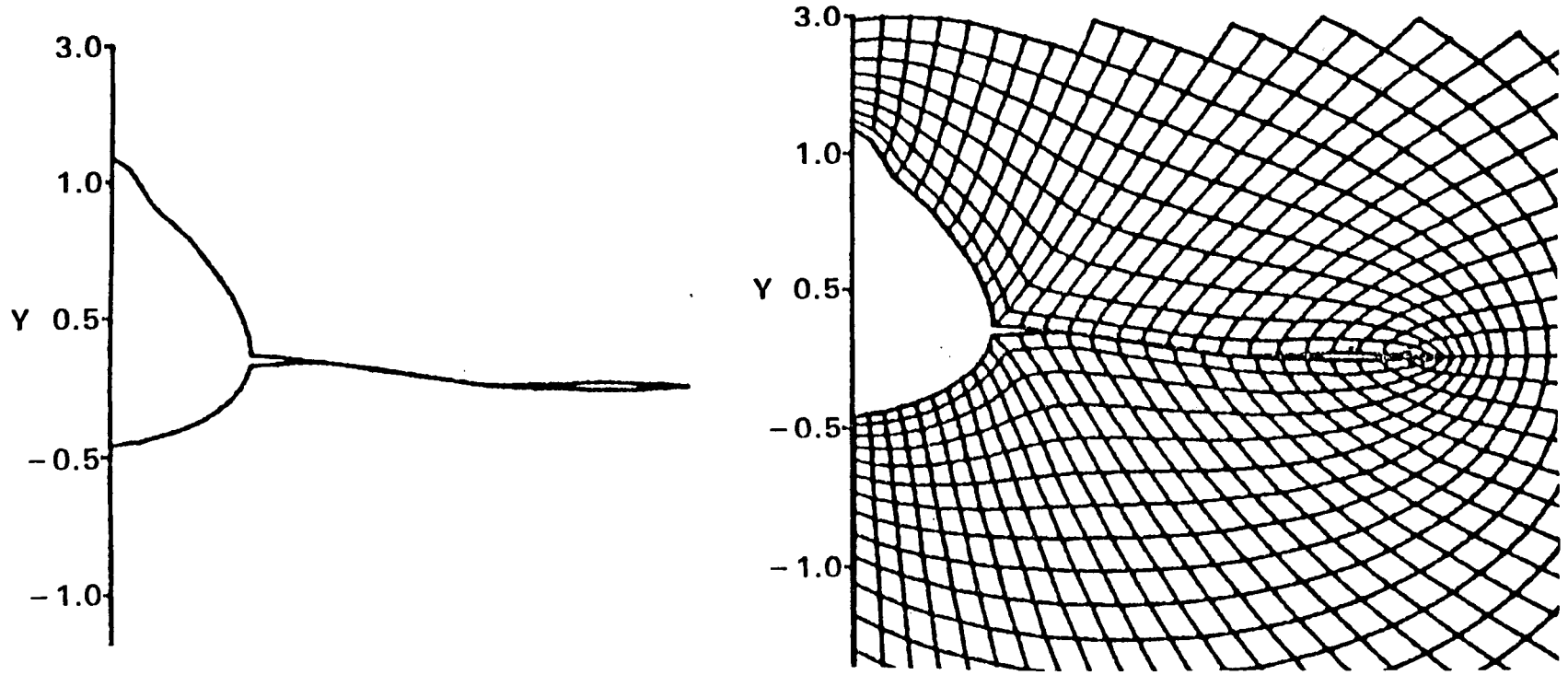

Fig. 8. Cross-section and grid at $x = 11.5$ (fuselage/canopy/wing/canard wake/canard).

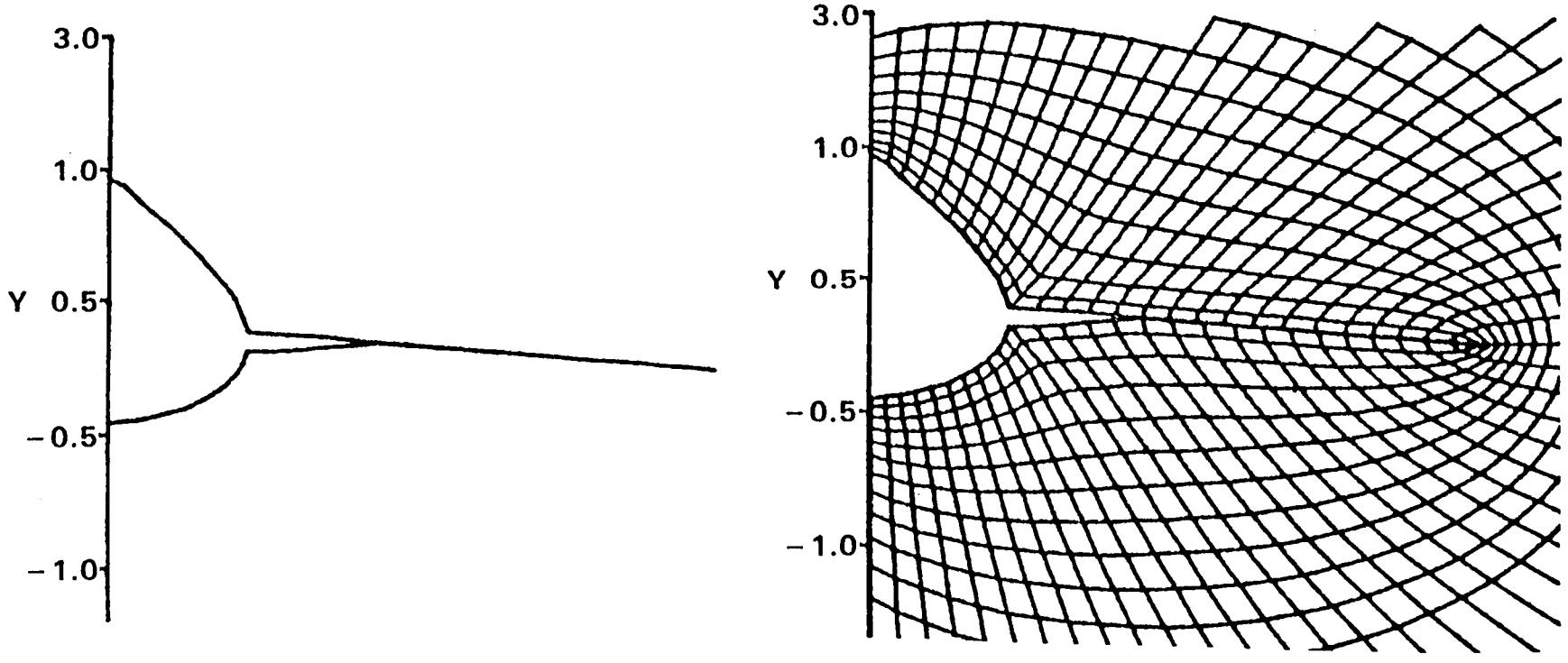

Fig. 9. Cross–section and grid at $x = 13.05$ (fuselage/wing/canard wake).

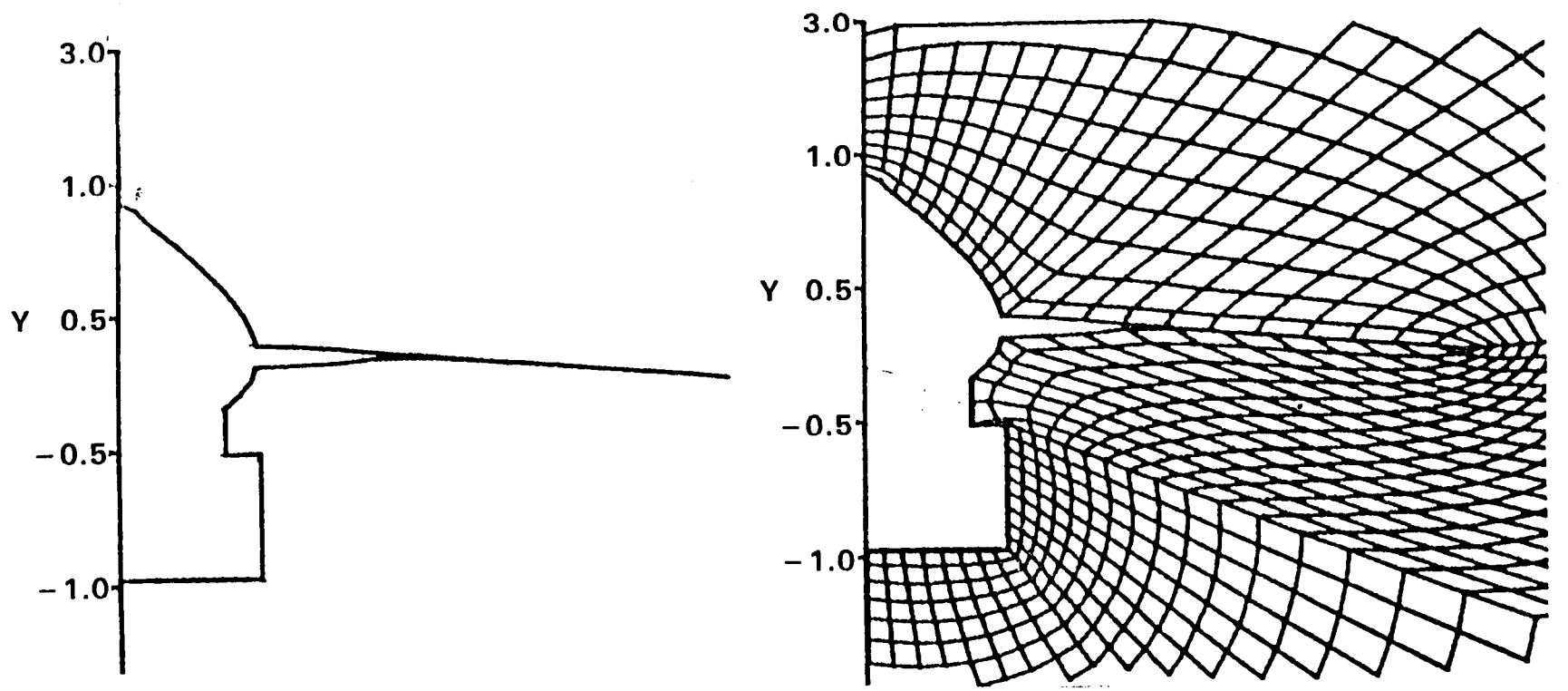

Fig. 10. Cross-section and grid at $x = 13.51$ (fuselage/wing/canard wake/nacelle).

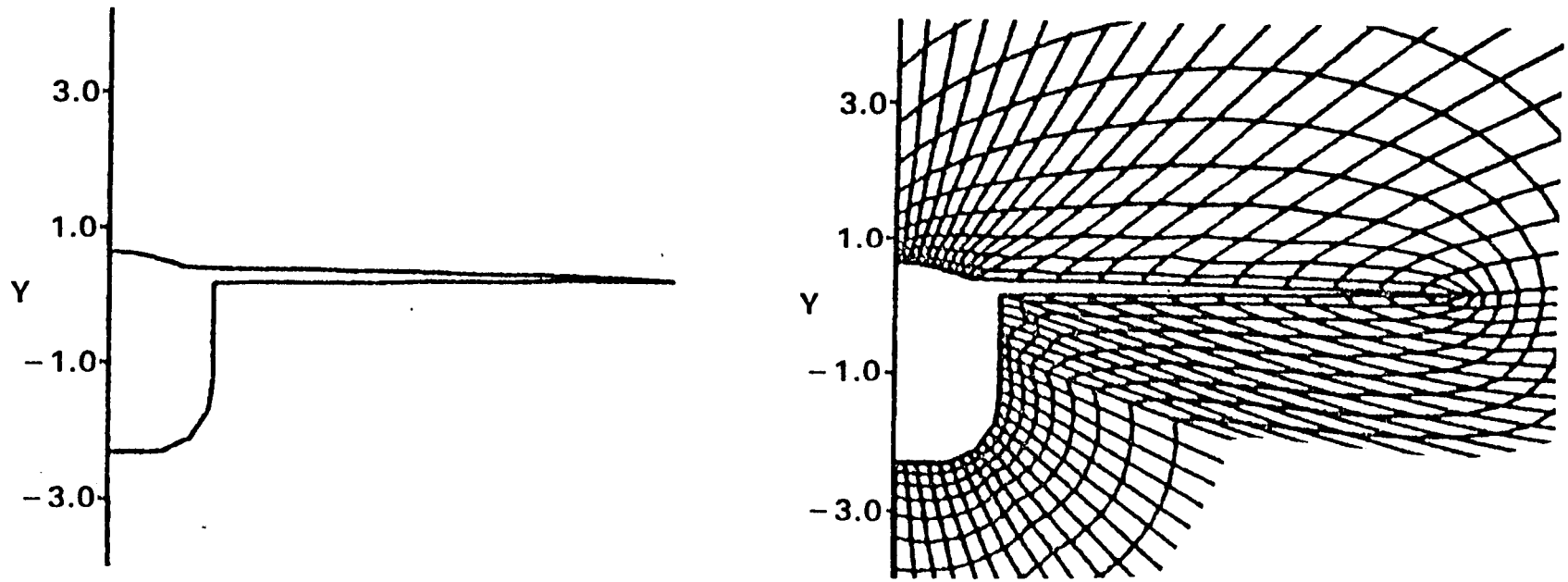

Fig. 11. Cross-section and grid at $x = 26$ (wing/nacelle).

$M_\infty = 2;\ \alpha = 4\,\text{deg};\ x/l = 0.22$

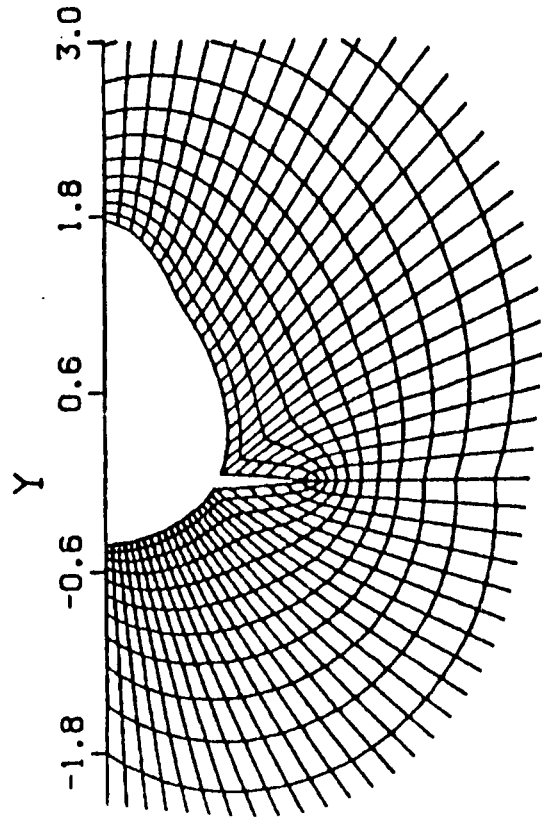

CROSS-SECTIONAL SHAPE

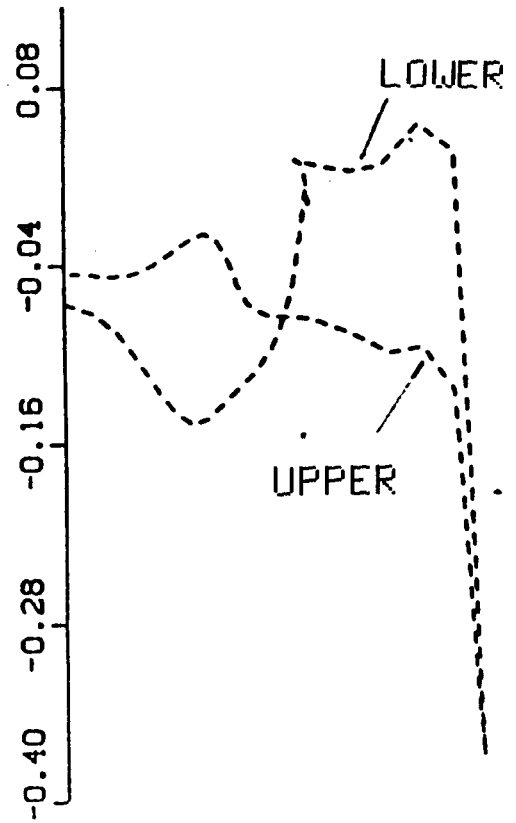

PRESSURE PROFILE

Fig. 12. Solution for Langley fighter configuration.

$M_\infty = 2;\ \alpha = 4\,\text{deg};\ x/l = 0.22$

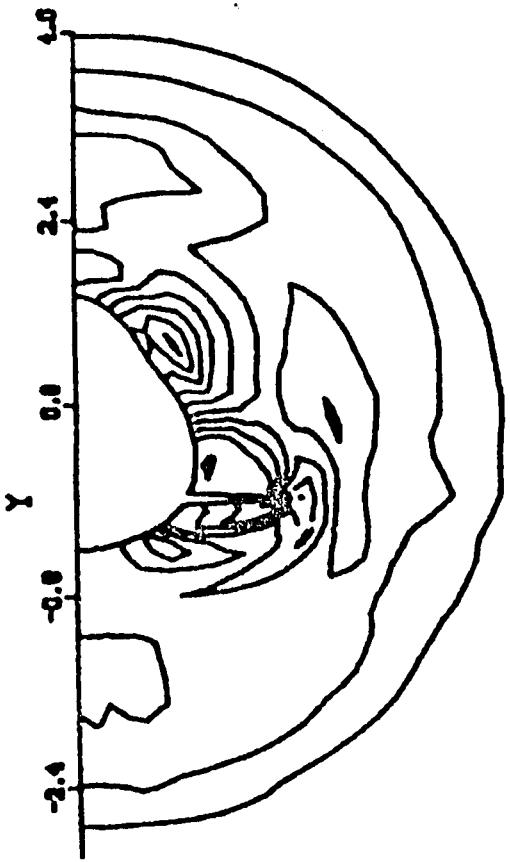

PRESSURE CONTOURS

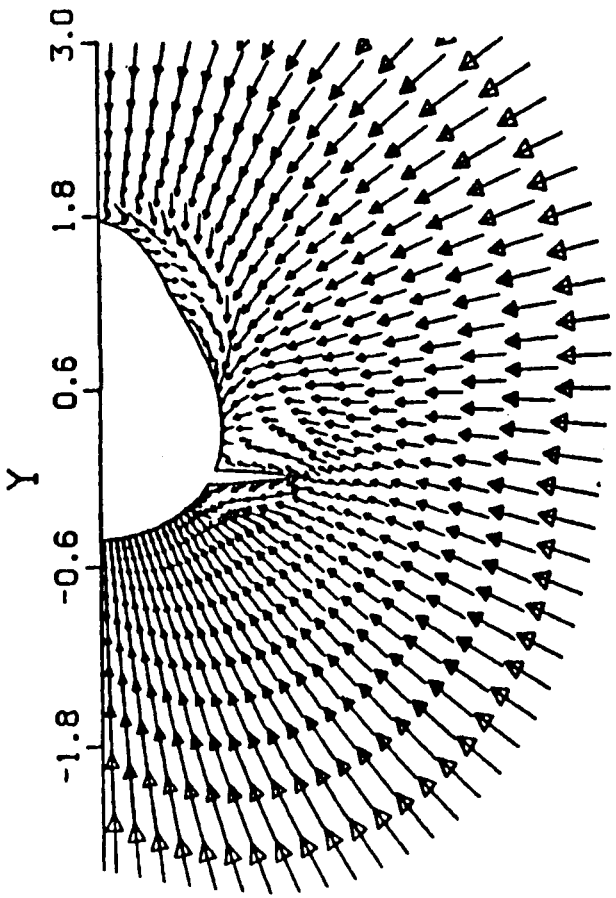

VELOCITY VECTORS

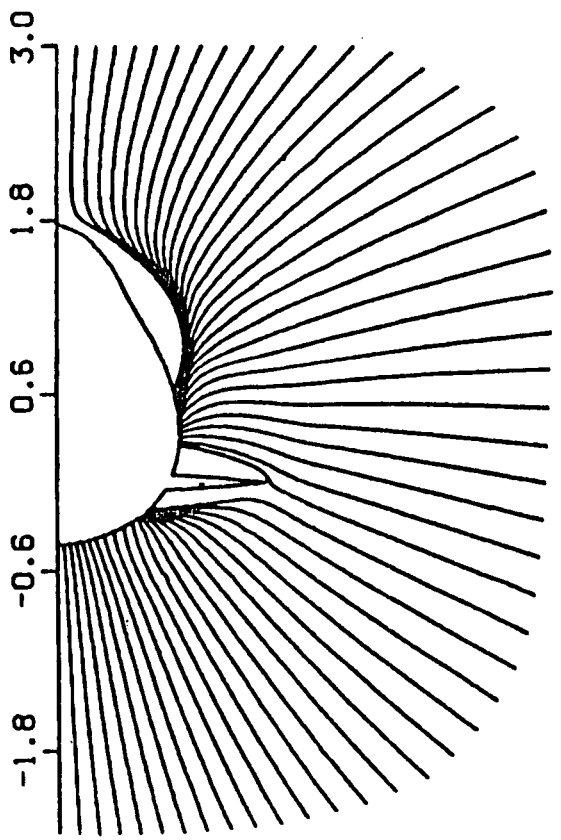

CROSSFLOW STREAMLINES

Fig. 13. Solution for Langley fighter configuration.

$M_\infty = 2;\ \alpha = 4\,\text{deg};\ x/l = 0.38$

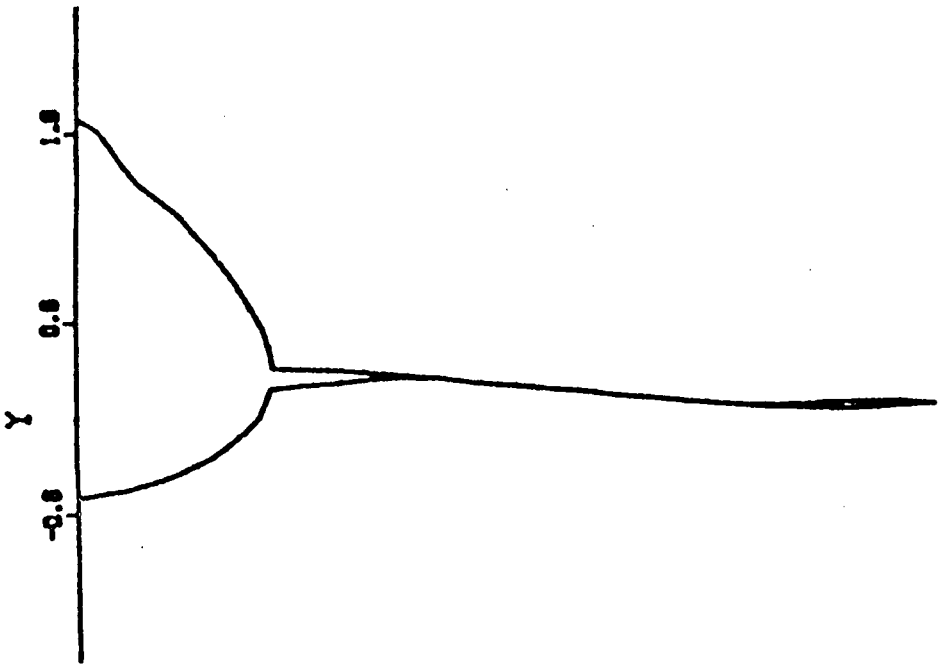

CROSS-SECTIONAL SHAPE

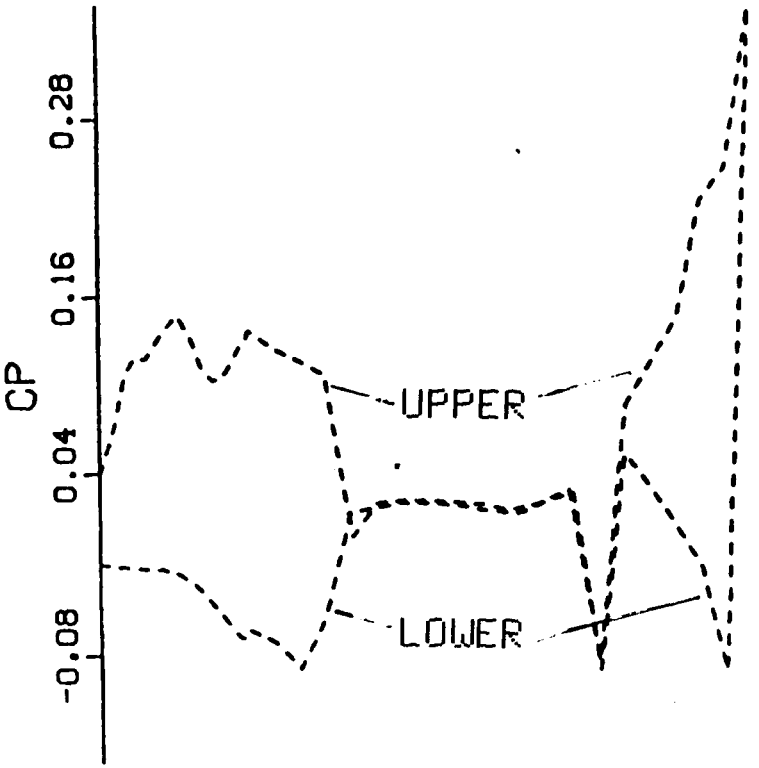

PRESSURE PROFILE

Fig. 14. Solution for Langley fighter configuration.

$M_\infty = 2;\ \alpha = 4\,\text{deg};\ x/l = 0.38$

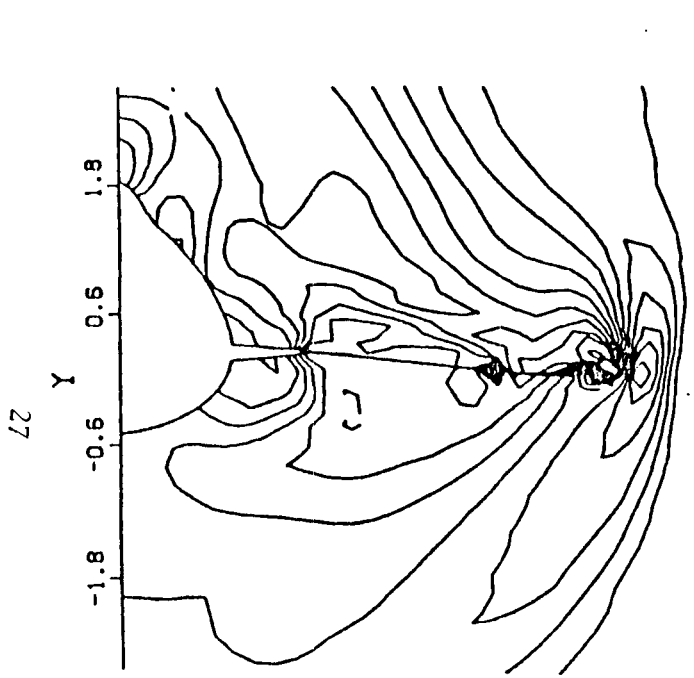

PRESSURE CONTOURS

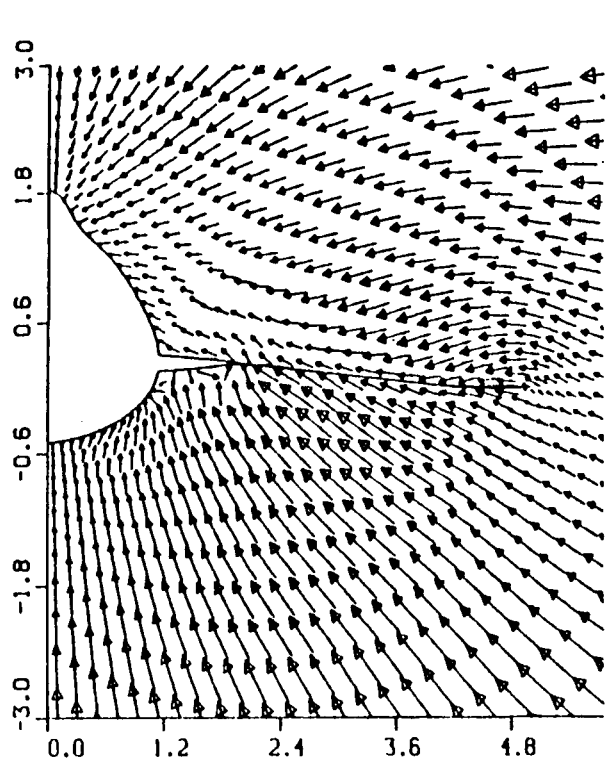

CROSSFLOW

VELOCITY VECTORS

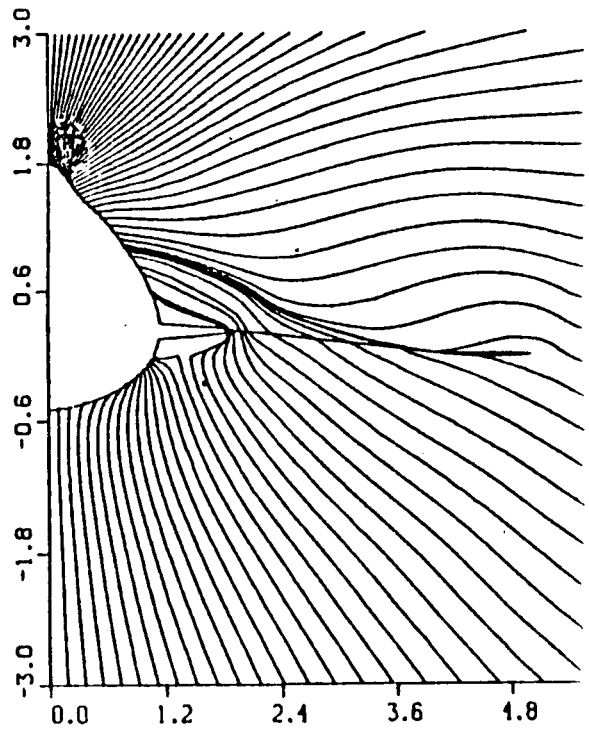

CROSSFLOW STREAMLINE

Fig. 15. Solution for Langley fighter configuration.

$M_\infty = 2$; $\alpha = 4$ deg; $x/l =$ 0.41

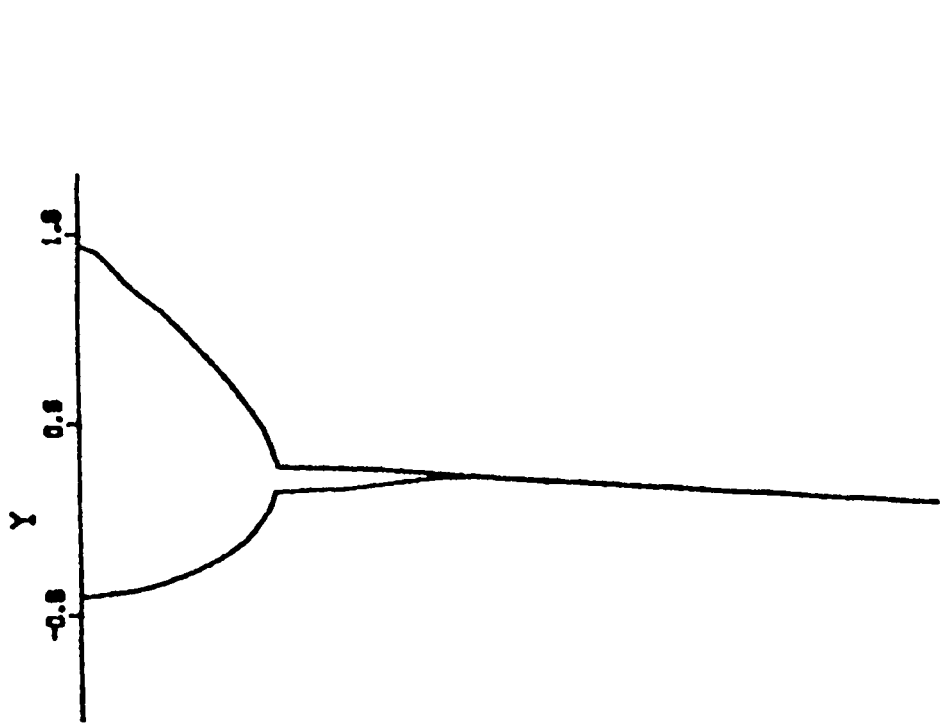

CROSS-SECTIONAL SHAPE

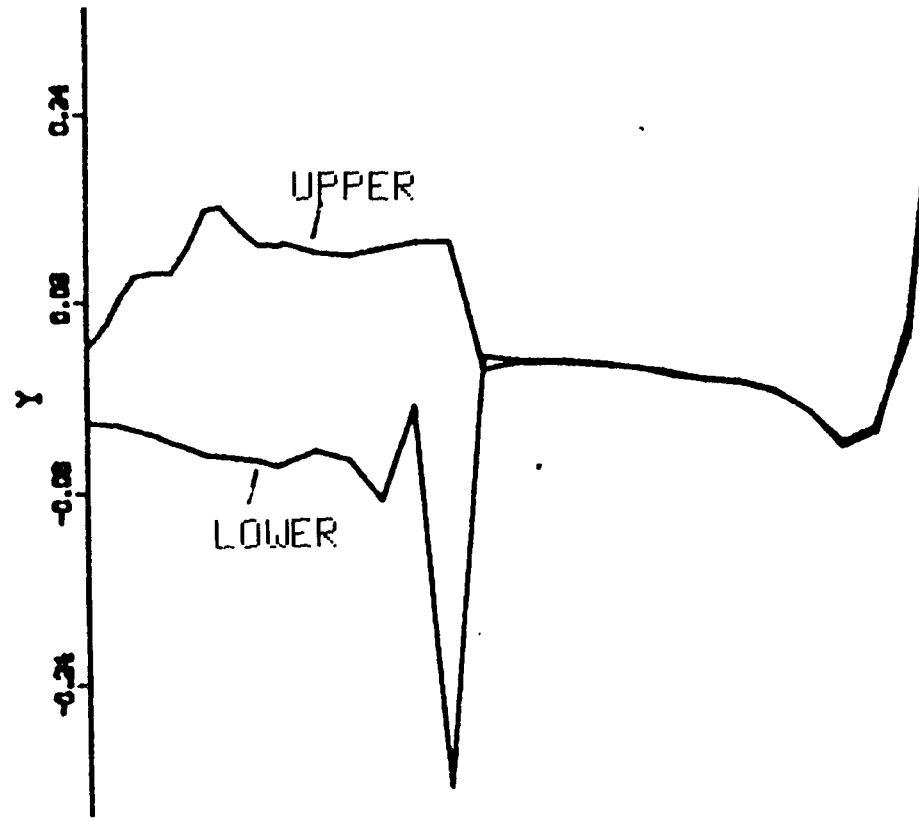

PRESSURE PROFILE

Fig. 16. Solution for Langley fighter configuration.

$M_\infty = 2;\ \alpha = 4\,\text{deg};\ x/l =$ 0.41

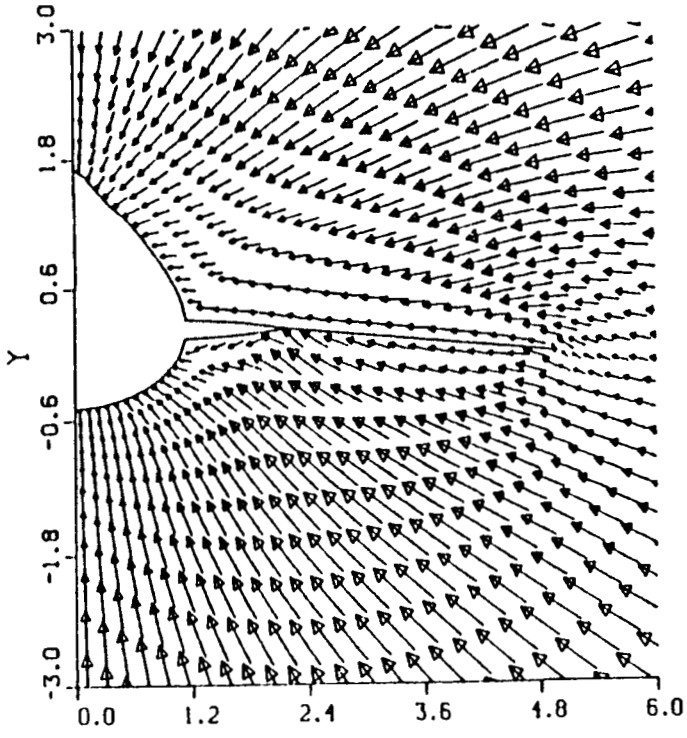

CROSSFLOW

VELOCITY VECTORS

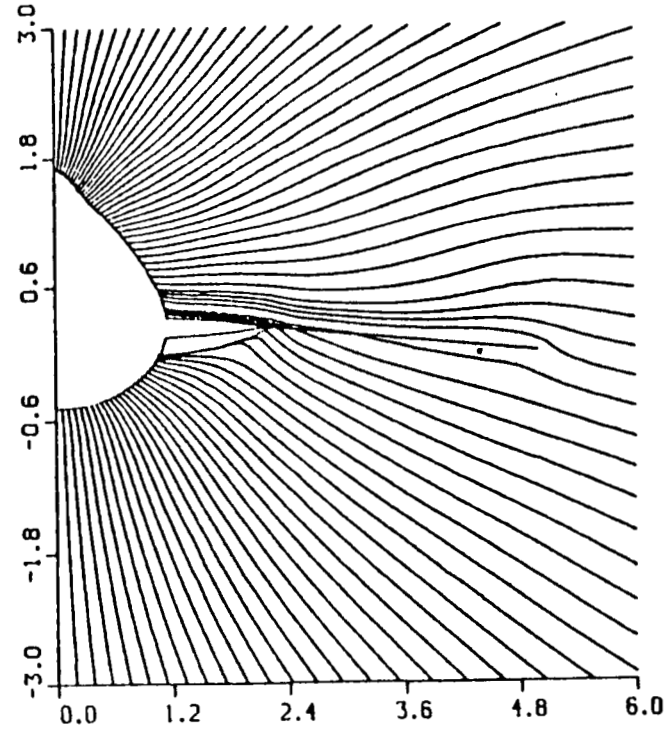

CROSSFLOW STREAMLINES

Fig. 17. Solution for Langley fighter configuration.

$M_\infty = 2;\ \alpha = 4\,\text{deg};\ x/l = 0.47$

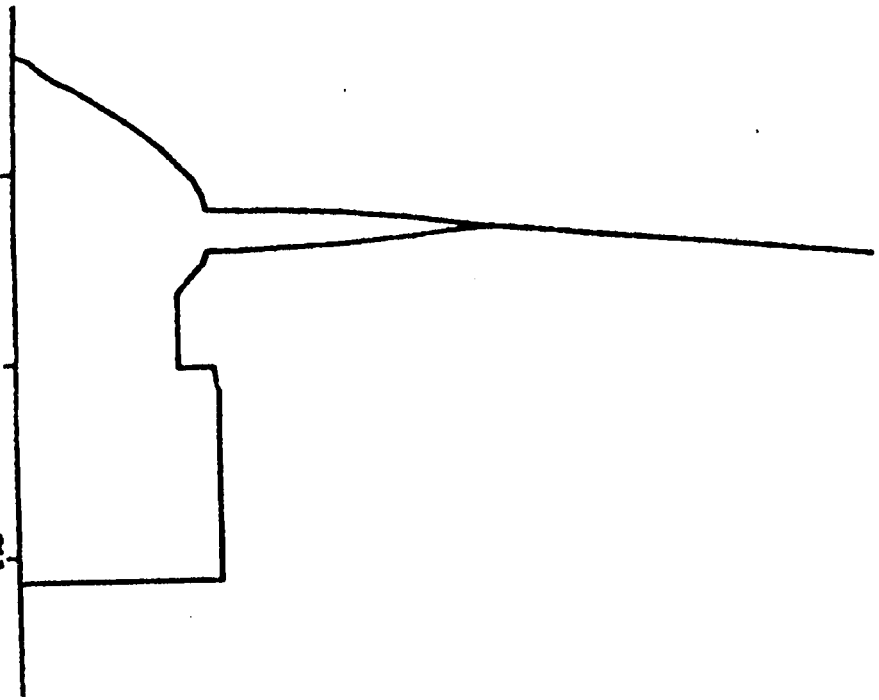

CROSS-SECTIONAL SHAPE

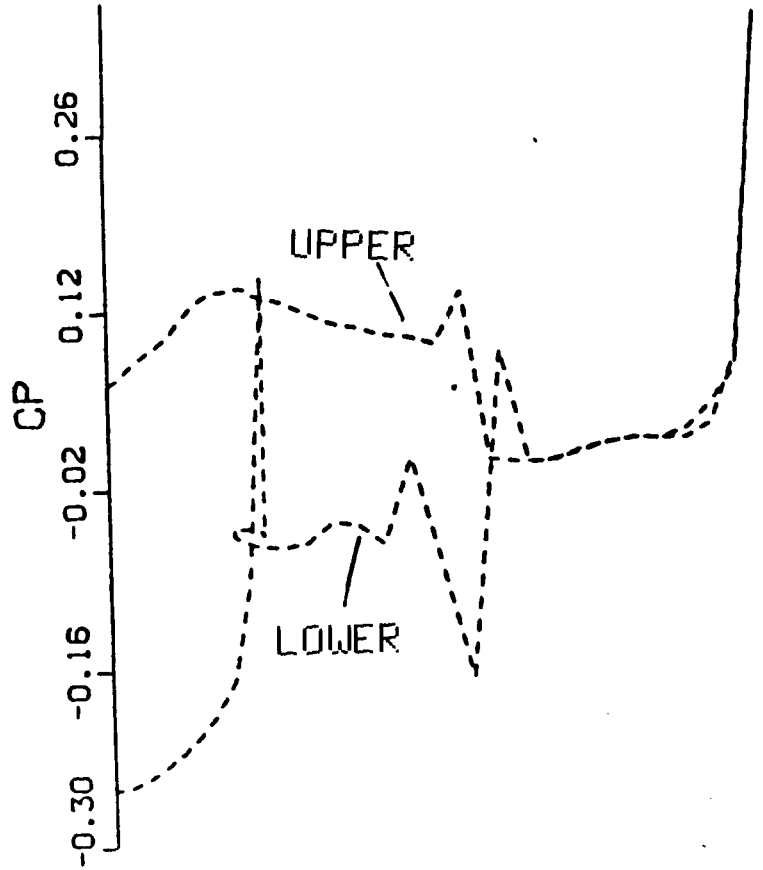

PRESSURE PROFILE

Fig. 18. Solution for Langley fighter configuration.

$M_\infty = 2;\ \alpha = 4\,\text{deg};\ x/l = 0.47$

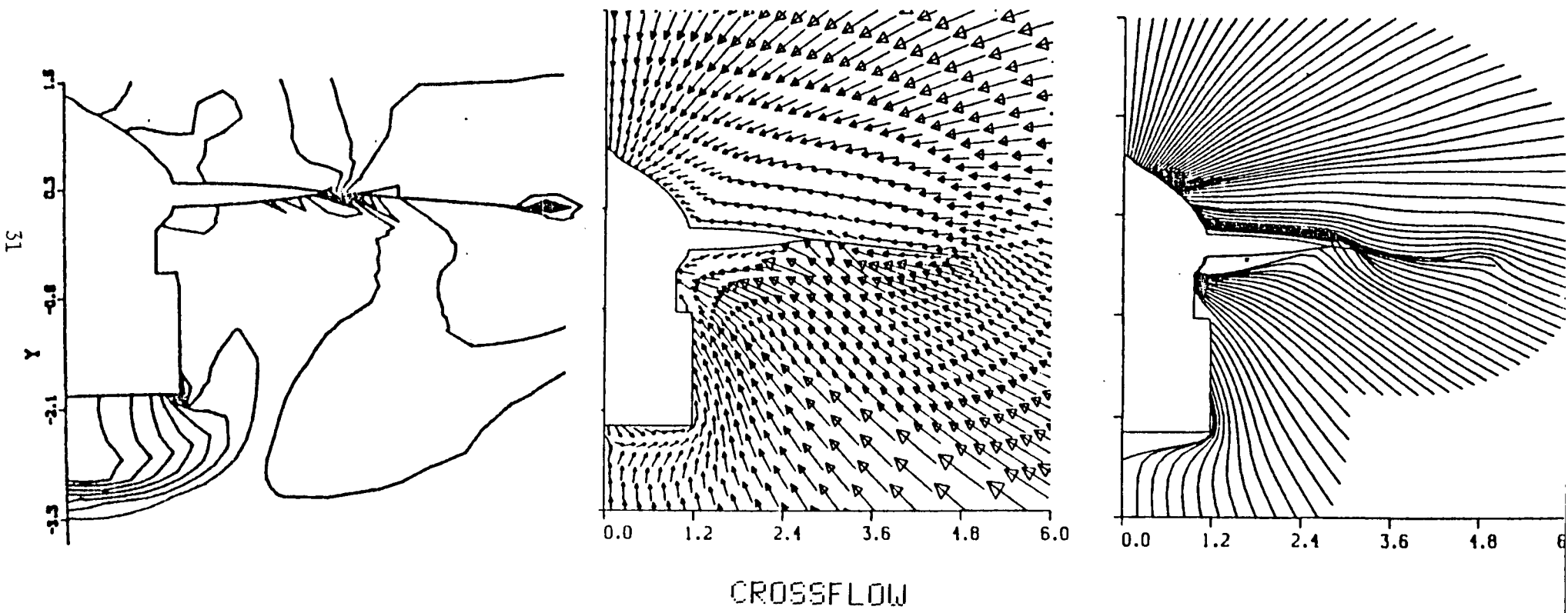

PRESSURE CONTOURS

VELOCITY VECTORS

CROSSFLOW STREAMLINES

Fig. 19. Solution for Langley fighter configuration.

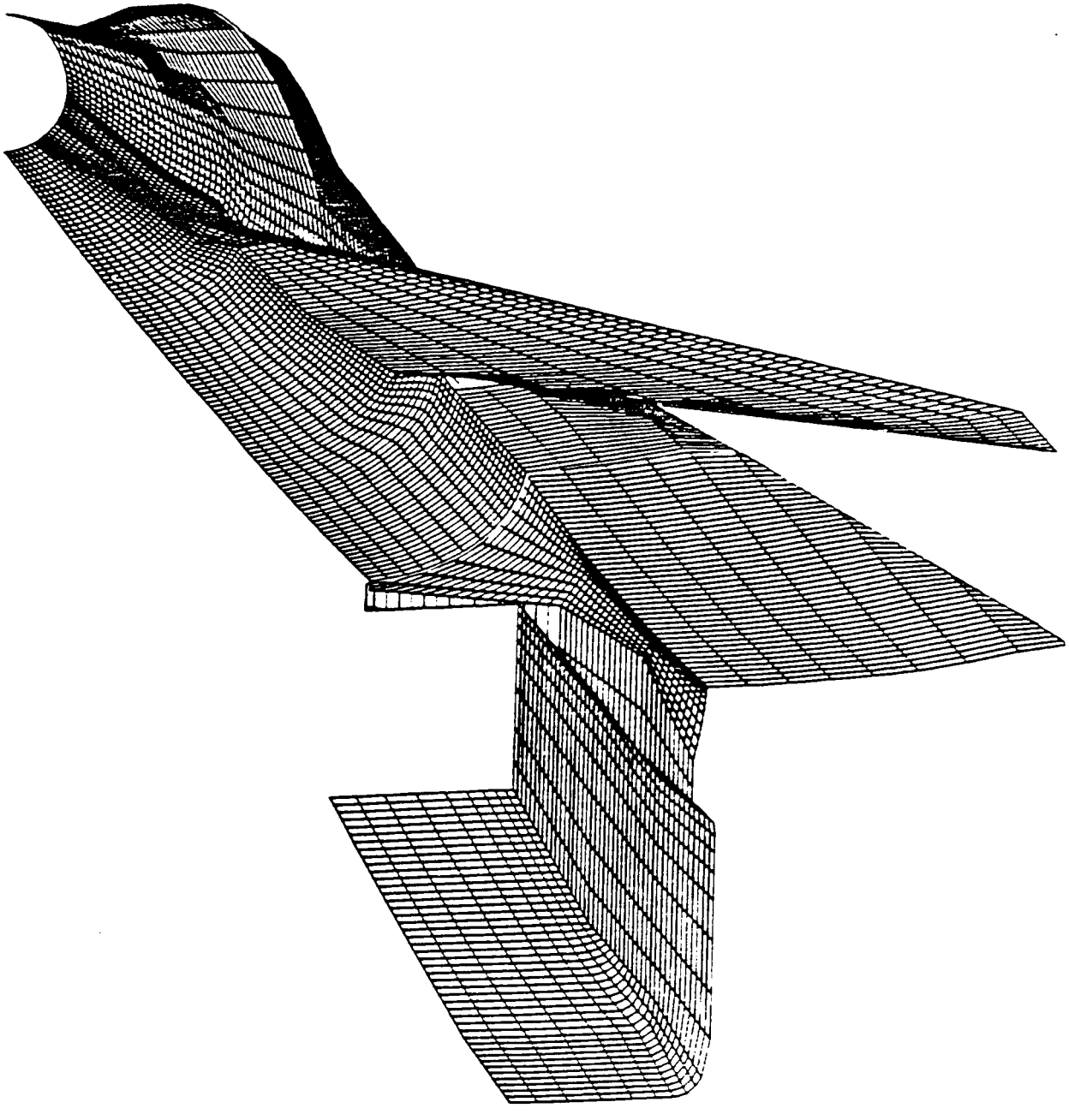

Fig. 20. Computational geometry and surface grid points.

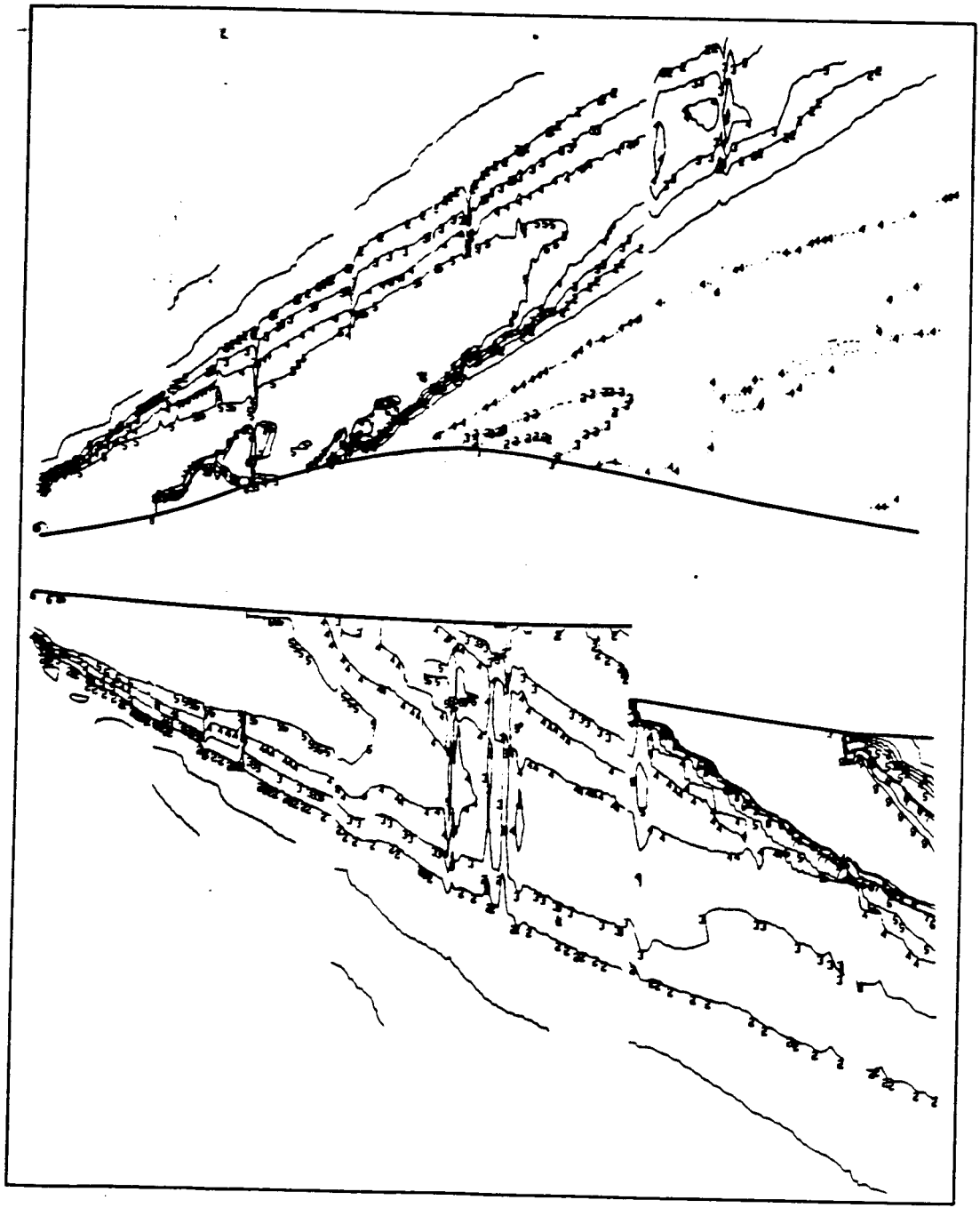

Fig. 21. Pressure contours in the plane of symmetry.

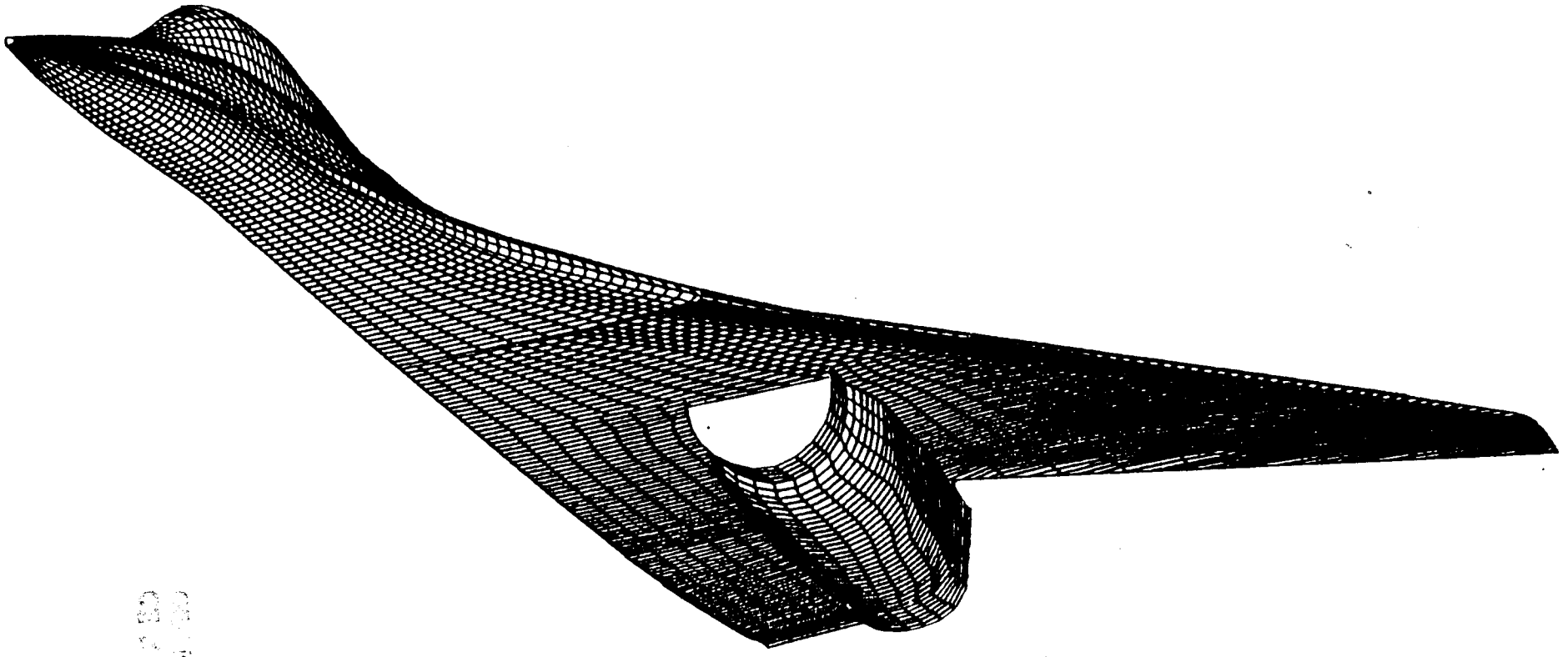

Fig. 22. Geometry of an advanced fighter with a nacelle.

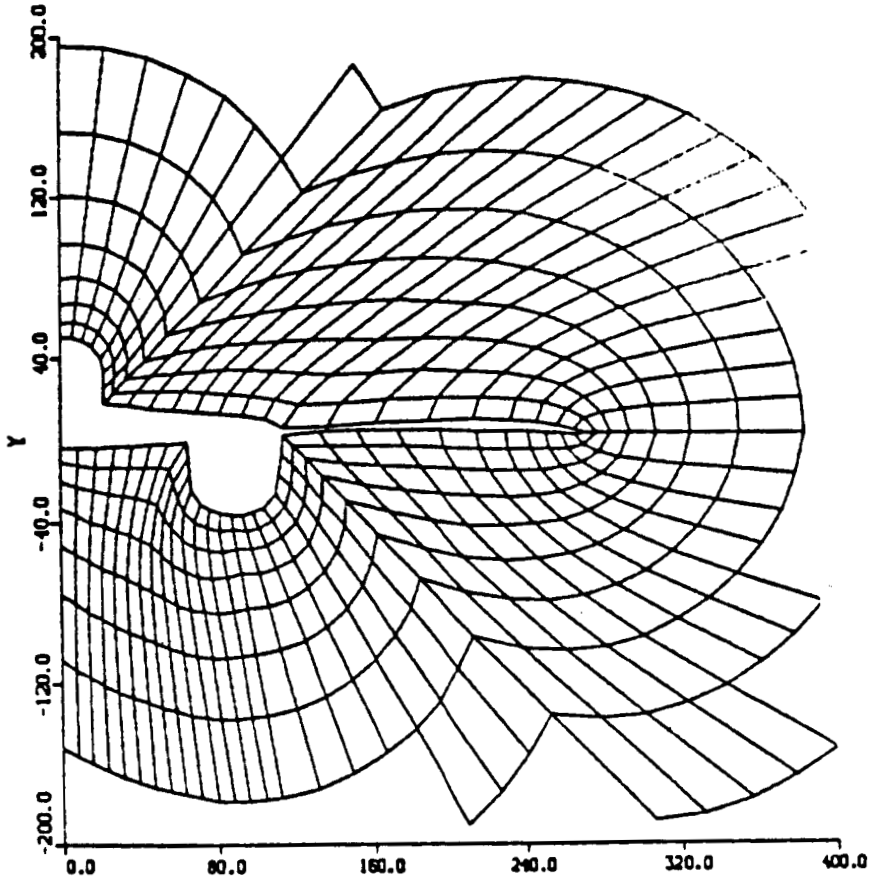

Fig. 23. Grid setup for a wing mounted nacelle.

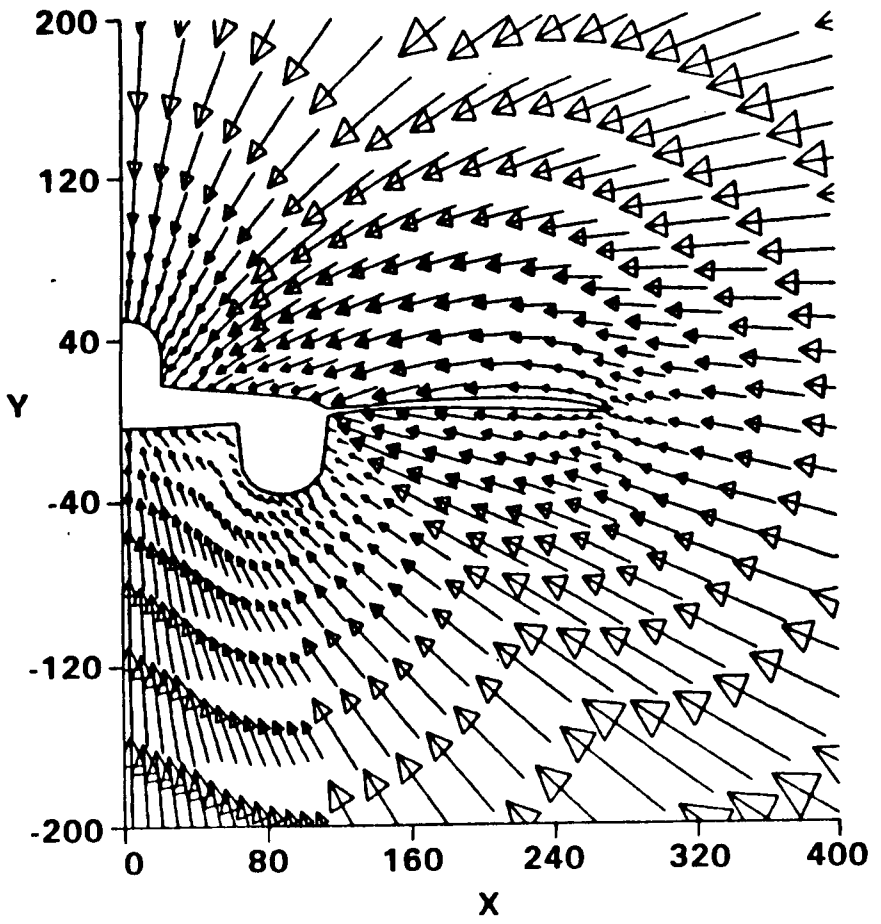

a) Cross flow velocity

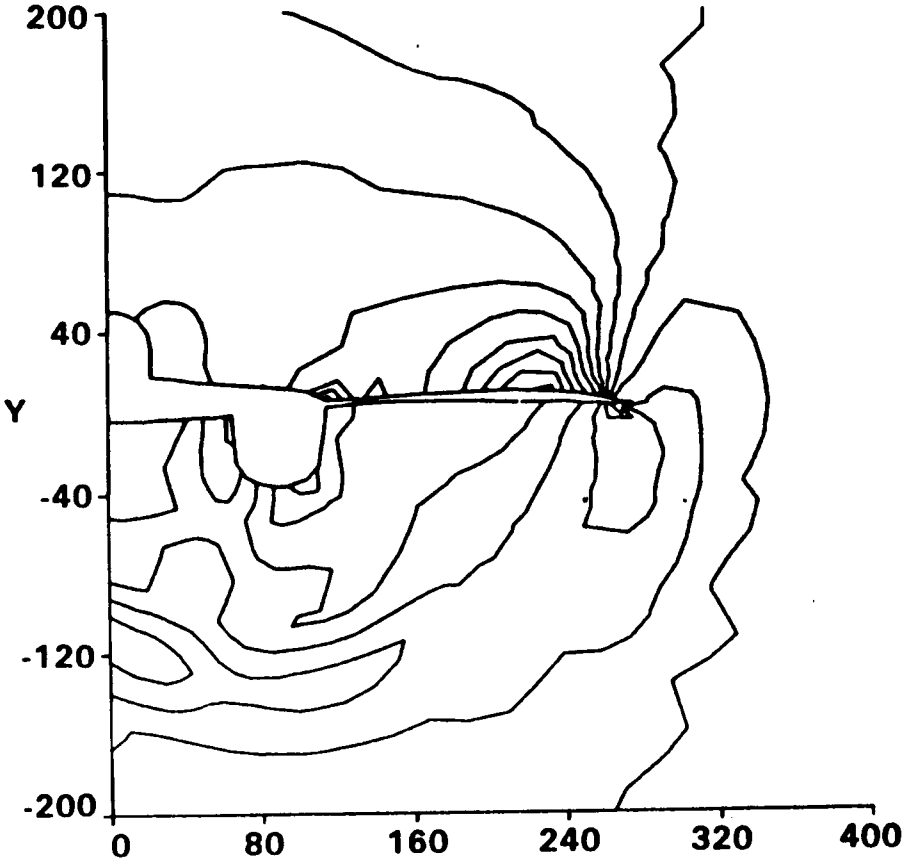

b) Pressure contours

Fig. 24. Tactical fighter results at $M_\infty = 1.6$, $\alpha = 5°$, $\frac{X}{L} = 0.65$

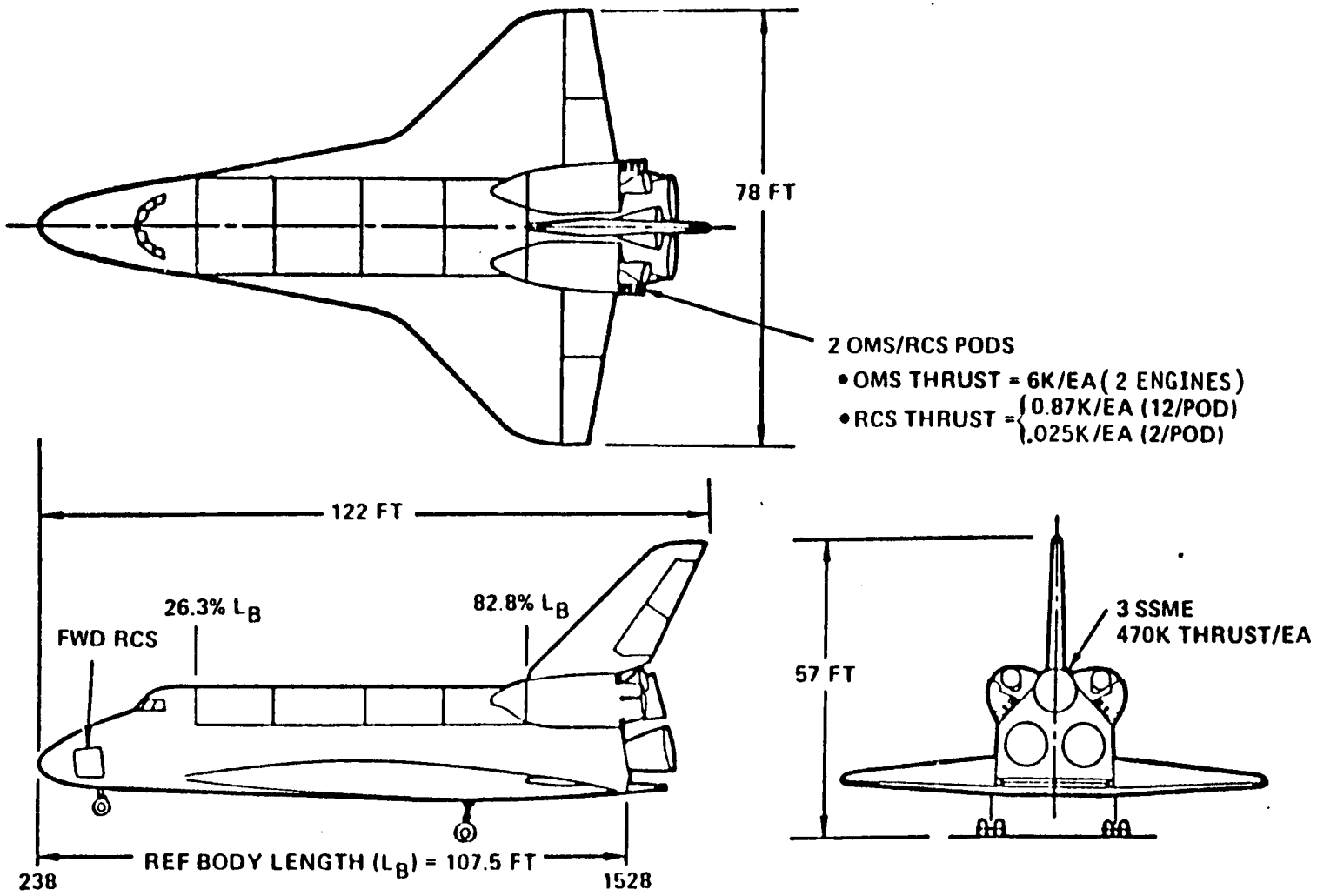

Fig. 25. Space Shuttle Orbiter.

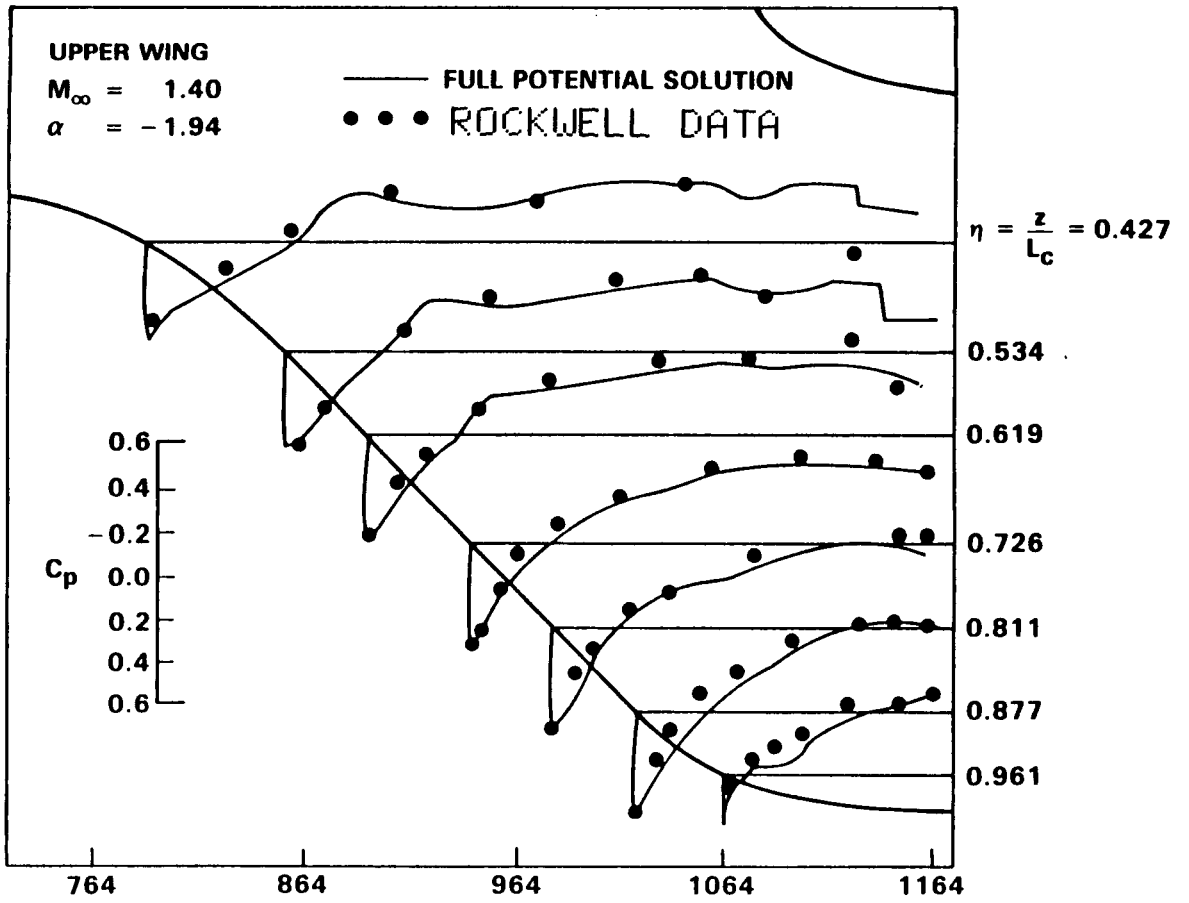

Fig. 26. Shuttle Orbiter upper surface pressure distribution; $M_\infty = 1.4$, $\alpha = 1.94$.

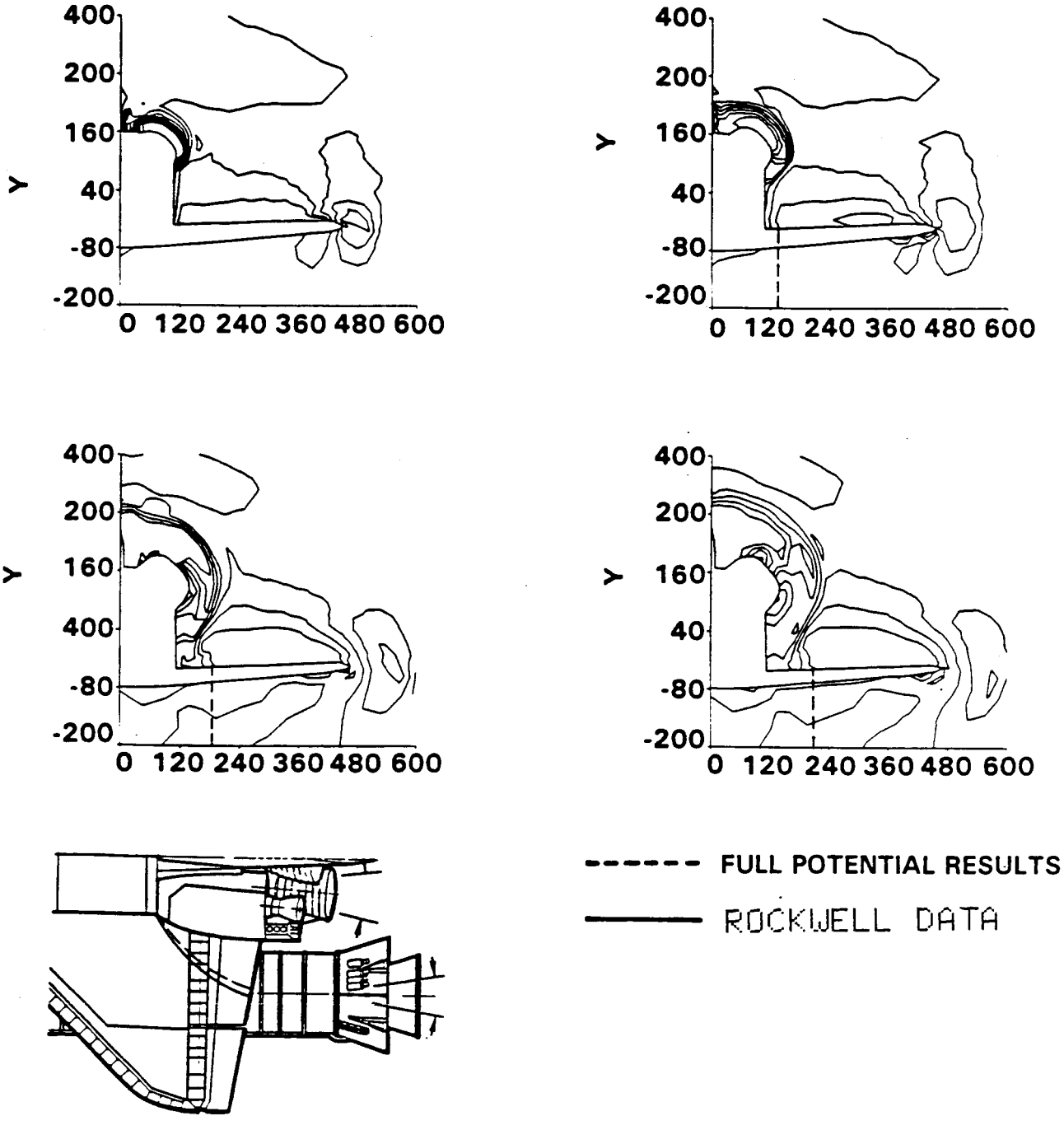

Fig. 27. The trace of OMS pod shock on the upper surface; $M_\infty = 1.4$, $\alpha = 1.94$.

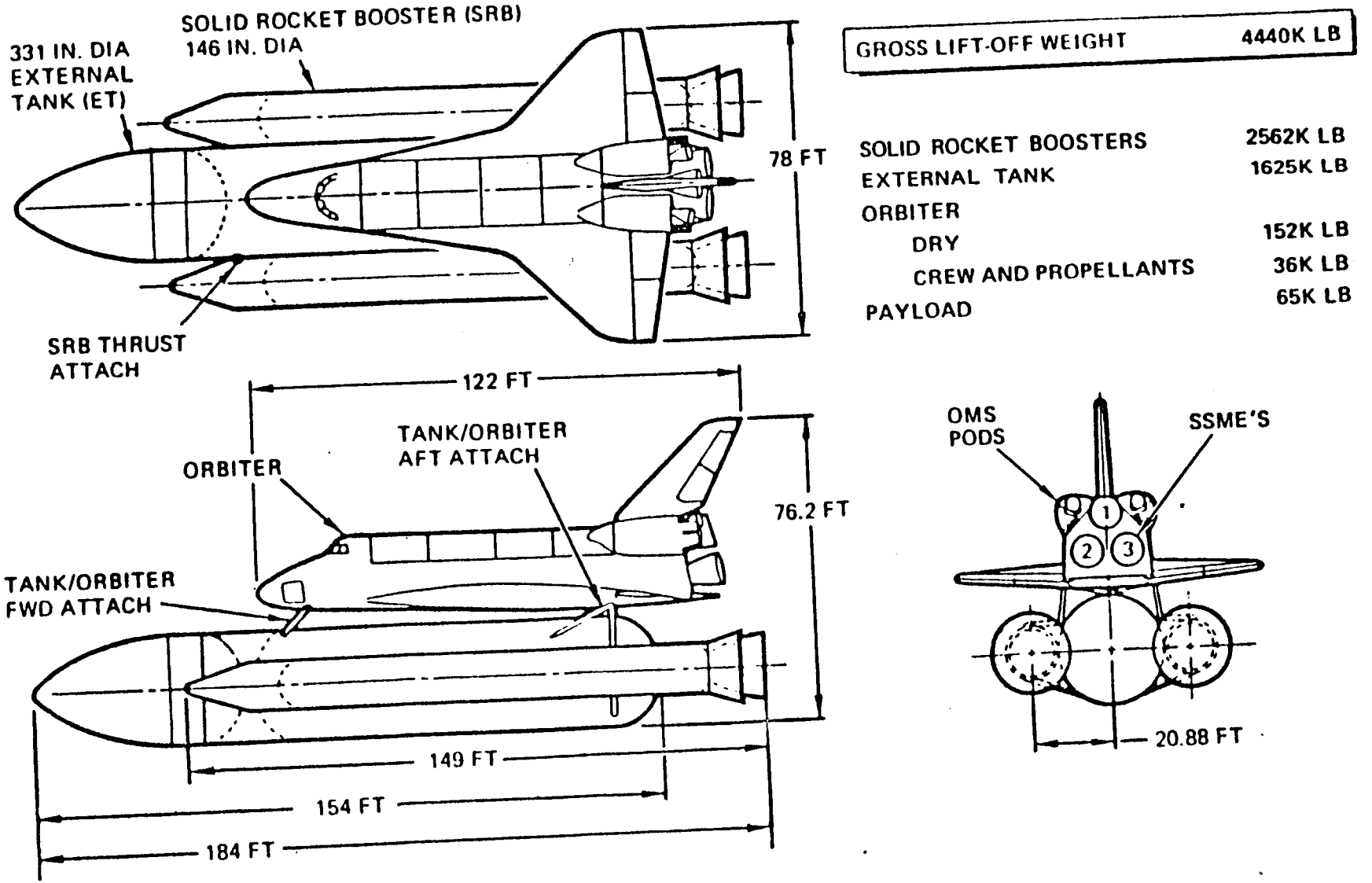

Fig. 28. Space Shuttle Vehicle — mated configuration.

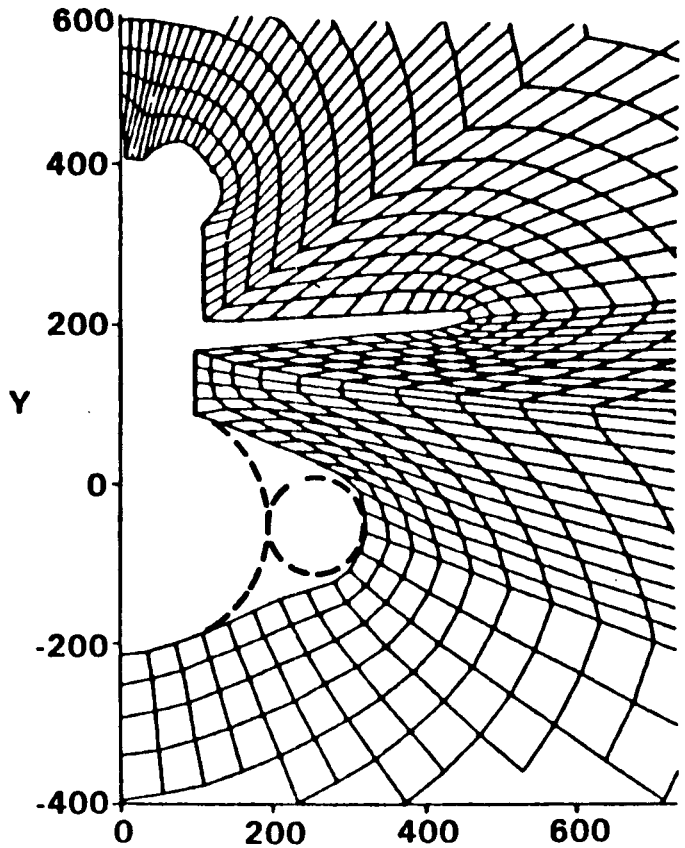

a) Computational grid

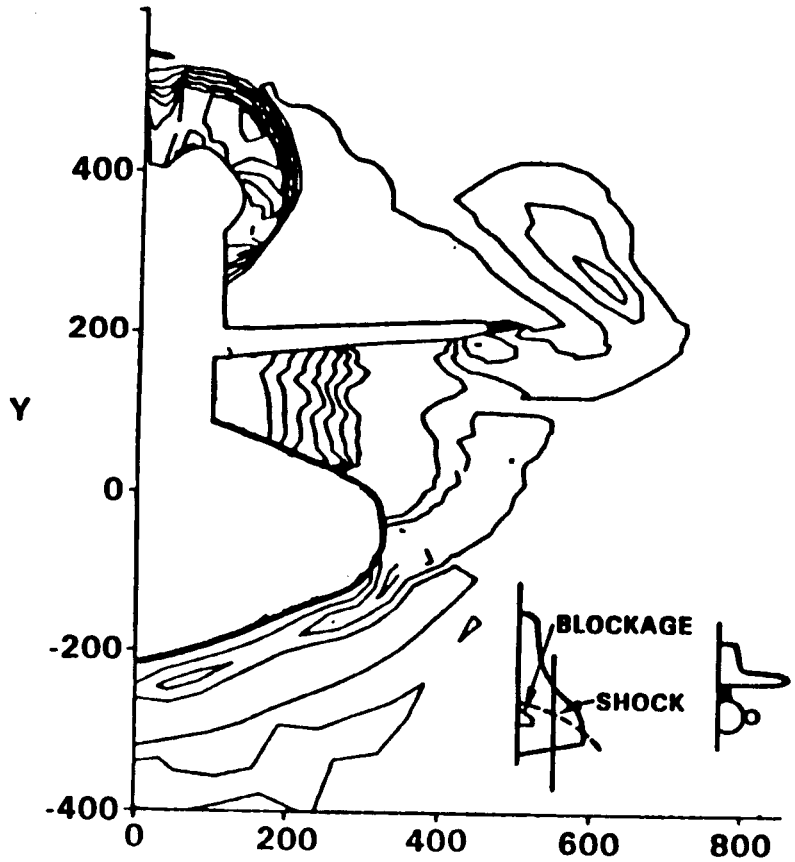

b) Pressure contours

Fig. 29. Multibody problem analysis at M = 1.6, α = -1.96°, $\frac{X}{L}$ = .65

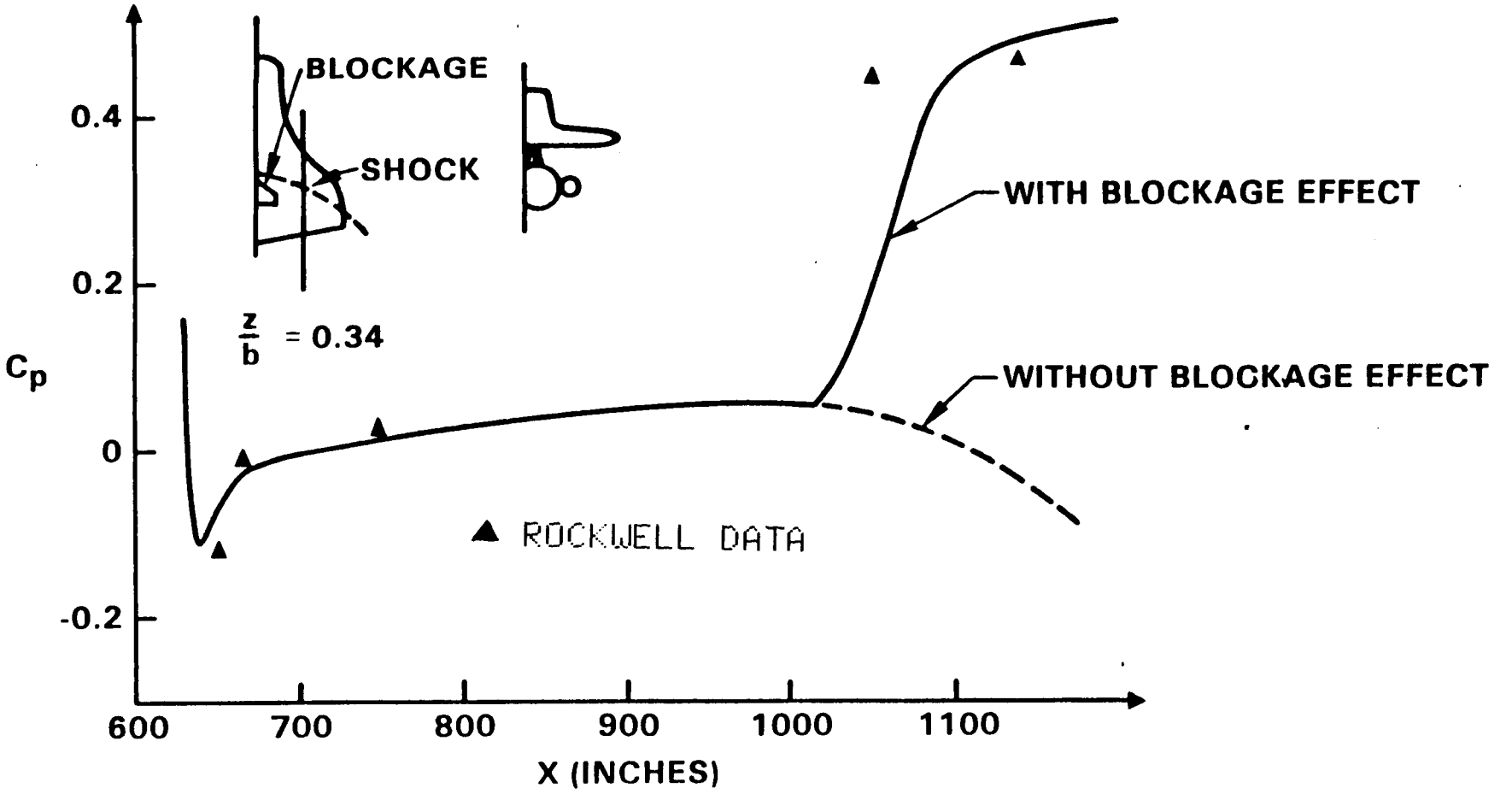

Fig. 30. Orbiter lower surface chordwise pressure distribution.

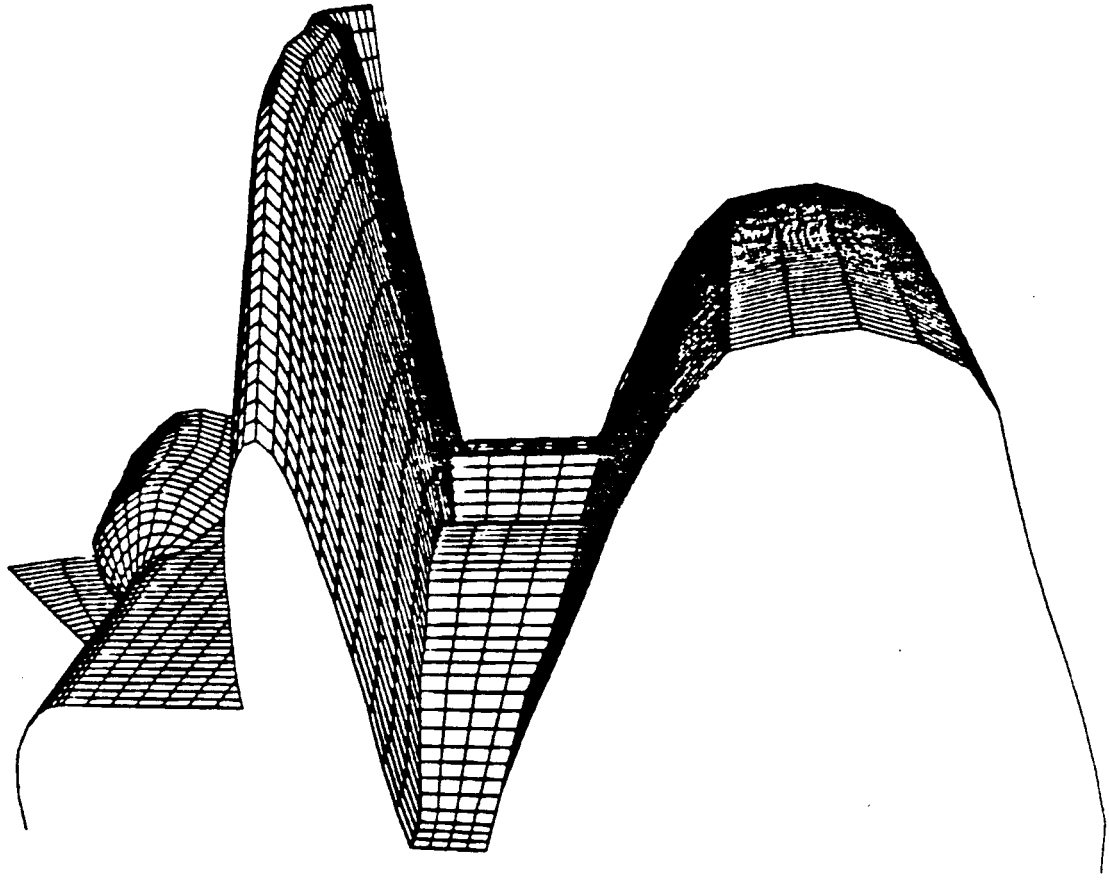

Fig. 31. Computational geometry and surface gridding for mated configuration.

APPENDIX A

CONTRACT PUBLICATIONS

1. AIAA Paper No. 84-0427.*

2. University of Tennessee Space Institute Workshop on Computational Fluid Dynamics — Article 6.1, UTSI Publication No. E02-4005-023-84.

3. Rockwell International Report, TFD 84-1654.

4. AIAA Paper No. 84-0262.*

5. ICAS-84-1.6.2, International Council of the Aeronautical Sciences Meeting, Toulouse, France, September 1984.*

*Permission to reprint these Papers was granted by AIAA, March 6, 1985

AIAA'84

AIAA-84-0427

Nonlinear Computation of Wing-Body-Vertical Tail-Wake Flows at Low Supersonic Speed

K.Y. Szema and V. Shankar, Rockwell International Science Center, Thousand Oaks, CA

AIAA 22nd Aerospace Sciences Meeting

January 9-12, 1984/Reno, Nevada

NONLINEAR COMPUTATION OF WING-BODY-VERTICAL TAIL-WAKE FLOWS AT LOW SUPERSONIC SPEEDS

Kuo-Yen Szema* and Vijaya Shankar**
Rockwell International Science Center
Thousand Oaks, California

Abstract

A numerical method based on the conservation form of the full potential equation has been applied to the problem of three-dimensional supersonic flows with embedded subsonic regions. The governing equation is cast in a nonorthogonal coordinate system, and the theory of characteristics is used to accurately monitor the type-dependent flow field. A conservative switching scheme is employed to transition from the supersonic marching procedure to a subsonic relaxation algorithm and vice versa. The newly developed computer program can handle arbitrary geometries with fuselage, wing, vertical tail and wake components at combined angle of attack and sideslip. Results are presented for a low supersonic mach numbers flow over the Shuttle orbiter (including the OMS pods and vertical tail), and for flows over a realistic fighter type configuration. Comparisons with experimental data are shown to be in good agreement for various cases.

I. Introduction

Currently available numerical algorithms to compute the low supersonic, inviscid flow about complex configurations are frequently either inadequate[1] or too costly to use for routine analysis.[2,3] For treatment of low supersonic flows, the full potential method[4] is an ideal substitute for the Euler methods to avoid the requirements of excessive computer time and memory.

Recently, Shakar et al[4] have developed a numerical method based on the characteristic theory to solve the problem of supersonic flow with embedded subsonic regions. Reference 4 describes the characteristic theory involved in determining the condition for a marching direction to exist. Once that condition is violated, the marching scheme is transitioned to a relaxation scheme through a conservative switching operator. For the marching condition violation, the total velocity q does not have to be subsonic. Even for a supersonic total velocity q, if the component in the marching direction is subsonic, a relaxation scheme is required. In order to properly produce the necessary artificial viscosity through density biasing, Reference 4 defines two situations: (1) the total velocity q is supersonic, but the marching direction component is subsonic (defined as Marching Subsonic Region (MSR)), and (2) the total velocity q is subsonic (termed as Total Subsonic Region (TSR)). The method of Reference 4 uses a numerical mapping technique to generate the body fitted, nonorthogonal curvilinear coordinates system. The key advantage is that it has no restrictions on its applicability to complex geometries and intricate shocked flow fields.

The main purpose of this study is to extend the methodology of Reference 4 to investigate supersonic flows with large embedded subsonic regions over complex configurations, and as well as extend the treatment to combined angle of attack and yaw cases. All the calculations reported in this paper were performed using the CDC CYBER 176 computer. A typical calculation over a complete configuration requires 15 minutes of CPU time on the CYBER system or 3 minutes on the CRAY 1.

II. Basic Formulation

The steady, conservative full potential equation cast in an arbitrary coordinate system defined by $\xi = \xi(x,y,z)$, $\eta = \eta(x,y,z)$ and $\zeta = \zeta(x,y,z)$ can be written as

$$\left(\rho \frac{U}{J}\right)_\xi + \left(\rho \frac{V}{J}\right)_\eta + \left(\rho \frac{W}{J}\right)_\zeta = 0 \qquad (1)$$

where the density ρ is given by

$$\rho = \left[1 - \left(\frac{\gamma-1}{2}\right) M_\infty^2 \left(U\phi_\xi + V\phi_\eta + W\phi_\zeta - 1\right)\right]^{1/(\gamma-1)} \qquad (2)$$

and M_∞ is the free stream mach number, a is the local speed of sound and U,V,W are the contravariant velocity components. Introducing the following notation for convenience.

$$\begin{array}{lll} U_1 = U & U_2 = V & U_3 = W \\ x = x_1 & y = x_2 & z = x_3 \\ \xi = X_1 & \eta = X_2 & \zeta = X_3 \end{array},$$

the contravariant velocity can be expressed as

$$U_i = \sum_{j=1}^{3} a_{ij}\phi_{X_j} \qquad i = 1,2,3$$

$$a_{ij} = \sum_{k=1}^{3} \frac{\partial X_i}{\partial x_k}\frac{\partial X_j}{\partial x_k} \qquad \begin{array}{l} i = 1,2,3 \\ j = 1,2,3 \end{array} \text{ (transformation metrics)} \qquad (3)$$

The Jacobian of the transformation J is represented by

$$J = \frac{\partial(\xi,\eta,\zeta)}{\partial(x,y,z)} = \begin{bmatrix} \xi_x & \xi_y & \xi_z \\ \eta_x & \eta_y & \eta_z \\ \zeta_z & \zeta_y & \zeta_z \end{bmatrix} \qquad (4)$$

*Member Technical Staff, Member AIAA
**Manager, CFD Group, Associate Fellow AIAA

The nature of Eq. (1) can be analyzed by studying the eigenvalue system of Eq. (1) combined with the irrotationality condition in the (ζ,η) and (ζ,ξ) planes. A detailed discussion on this can be found in Reference 4. Therefore, only the final results are presented here.

1. At a grid point, the marching direction ζ is <u>hyperbolic</u> and the total velocity q is supersonic, $\left(a_{11} - \frac{U^2}{a^2}\right) < 0$, $q > a$. This point will use the algorithm of Reference 5.

2. At a grid point, the marching direction ζ is <u>elliptic</u>, $\left(a_{11} - \frac{U^2}{a^2}\right) > 0$, but the total velocity q is supersonic, $q > a$. This point will be treated by a transonic operator with a built-in density biasing based on the magnitude of $\left(1 - \frac{a^2}{q^2}\right)$.

3. At a grid point, the direction ζ is <u>elliptic</u> and the total velocity q is <u>subsonic</u>, $q < a$. This point will be treated by a subsonic central differenced operator.

III. Method of Solution

Figure 1 shows the schematic of a fuselage-canopy forebody geometry with an embedded MSR and TSR present in a supersonic flow. To solve this problem, the marching scheme of Reference 5 is used when $\left(a_{11} - \frac{U^2}{a^2}\right)$ is negative, and a relaxation scheme is used when $\left(a_{11} - \frac{U^2}{a^2}\right)$ is positive. First, march from the nose up to the plane denoted by (A-B) in Fig. 1, using the method of Reference 5. Then, between (A-B) and (C-D), which embed the subsonic bubble (MSR and TSR), use a relaxation scheme and iterate until the subsonic bubble is fully captured. Then, resume the marching scheme from the plane (C-D), downstream of the body.

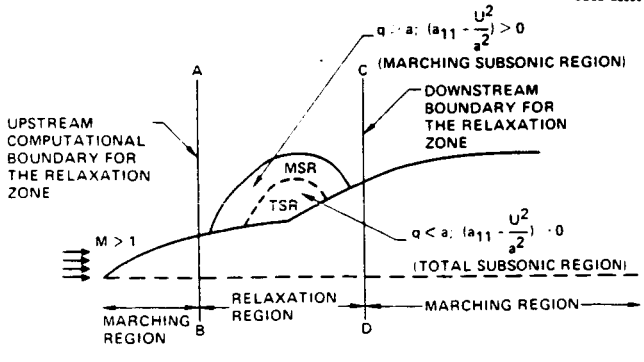

Fig. 1 Embedded subsonic bubble in a supersonic flow.

1. Treatment of $\partial/\partial\zeta\ (\rho\ U/J)$ Term

The finite-difference operator at point $(i+1, \xi, k)$ for the first term in Eq. (1) may be written as

$$\frac{\partial}{\partial\zeta}\left(\rho\,\frac{U}{J}\right) = \theta_i \underbrace{\frac{\overleftarrow{\delta}}{\partial\zeta}\left(\rho\,\frac{U}{J}\right)_{i+1}}_{\text{supersonic}} + (1 - \theta_{i+1}) \underbrace{\frac{\overrightarrow{\delta}}{\partial\zeta}\left(\tilde{\rho}\,\frac{U}{J}\right)_{i+1}}_{\text{marching subsonic}} \qquad (5)$$

where

$\overleftarrow{\delta}$ refers to backward differencing

$\overrightarrow{\delta}$ refers to forward differencing

$\theta_i = 1$ if $\left(a_{11} - \frac{U^2}{a^2}\right) < 0$

$= 0$ if $\left(a_{11} - \frac{U^2}{a^2}\right) > 0$.

The first term in Eq. (4) corresponds to the supersonic marching operator and the second term is the subsonic operator. By using a local linerization procedure, Eq. (5) can be expressed in term of ϕ only. Details of the procedure are given in Refs. 4 and 5.

2. Treatment of $\partial/\partial\eta\ (\rho\ V/J)$ Term

The finite difference operator for the second term in Eq. (1) is given as

$$\frac{\partial}{\partial\eta}\left(\rho\,\frac{V}{J}\right) = \theta_{i+1} \underbrace{\frac{\overleftarrow{\delta}}{\partial\eta}\left(\bar{\rho}\,\frac{V}{J}\right)_{j+1/2}}_{\text{supersonic}} + (1 - \theta_{i+1}) \underbrace{\frac{\overrightarrow{\delta}}{\partial\eta}\left(\tilde{\tilde{\rho}}\,\frac{V}{J}\right)_{j+1/2}}_{\text{marching subsonic}} \qquad (6)$$

where

$\theta_{i+1} = 1$ if $\left(a_{11} - \frac{U^2}{a^2}\right)_{i+1} < 0$ (supersonic point)

$\theta_{i+1} = 0$ if $\left(a_{11} - \frac{U^2}{a^2}\right)_{i+1} > 0$ (MSR) .

When $\theta_{i+1} = 1$, that is, the point is <u>supersonic</u> with respect to ζ, only the first term in Eq. (6) is used and the biased density ρ is defined by (for $V > 0$)

$$\bar{\rho}_{j+1/2} = (1 - \bar{\nu}_{j+1/2})\rho^*_{j+1/2} + \frac{1}{2}\,\bar{\nu}_{j+1/2}(\rho^*_j + \rho^*_{(j-1)}) \qquad (7)$$

where

$$\bar{\nu} = \max\left(0,\ 1 - a_{22}\,\frac{a^2}{V^2}\right) .$$

In Eq. (7), the evaluation of ρ^* depends on whether the flow is conical or nonconical. For conical flows, all ρ^* quantities are evaluated at the i^{th} plane. For nonconical flows, at each nonconical marching plane, initially ρ^* is seen to be the value at the i^{th} plane and then subsequently iterated to convergence by setting ρ^* to the

previous iterated value of ρ at the current i+1 plane.

When the point is elliptic, the density biasing is defined by

$$\tilde{\tilde{\rho}}^{n+1}_{j+1/2} = (1 - \tilde{\tilde{\nu}}_{J+1/2})\rho^{n}_{j+1/2} + \frac{1}{2}\tilde{\tilde{\nu}}_{j+1/2}\,(\rho^{n}_{j} + \rho^{n}_{j-1}) \tag{8}$$

where $\tilde{\tilde{\nu}} = \max\left(0,\ 1 - \frac{a^2}{q^2}\right)$. As before, the superscript n+1 denotes the current relaxation cycle for a subsonic bubble calculation. Note the difference in the definition of ν and $\tilde{\tilde{\nu}}$. The density biasing in the cross flow direction n is turned off when the total velocity q is less than the speed of sound a. The implicit treatment of V in the marching subsonic operator of Eq (6) is the same as that of the supersonic part, explained in Reference 5.

A similar procedure is implemented for $\left(\rho \frac{W}{J}\right)_{\zeta}$ term in Eq. (1).

3. Implicit Factorization Algorithm

Combining the various terms of Eq. (1) as represented by Eqs. (5)-(8) together with the terms arising from $\left(\rho \frac{W}{J}\right)_{\zeta}$ will result in a fully implicit model. This is solved using an approximate factorization implicit scheme. After some rearrangement of the terms, the factored implicit scheme becomes

$$\left[1 + \frac{A_3}{\beta\Delta\zeta}\frac{\partial}{\partial\zeta} + \frac{1}{\beta}\frac{\partial}{\partial\zeta}\left(\hat{\rho}\frac{a_{31}}{\Delta\zeta}\right) + \frac{1}{\beta}\frac{\partial}{\partial\zeta}\frac{\hat{\rho a}_{33}}{J}\frac{\partial}{\partial\zeta}\right] \times \left[1 + \frac{A_2}{\beta\Delta\zeta}\frac{\partial}{\partial\eta} + \frac{1}{\beta}\frac{\partial}{\partial\eta}\left(\frac{\hat{\rho a}_{21}}{J\Delta\zeta}\right) + \frac{1}{\beta}\frac{\partial}{\partial\eta}\frac{\hat{\rho a}_{22}}{J}\frac{\partial}{\partial\eta}\right]\Delta\phi = R \quad . \tag{9}$$

$$\begin{aligned} R = {} & \theta_i \left\{ \frac{1}{\Delta\zeta_1}\left[\frac{A_{1i}}{\Delta\zeta_2}\Delta\phi_i + A_{1i-1}\left(\frac{\Delta\phi_i}{\Delta\zeta_2} - \frac{\Delta\phi_{i-1}}{\Delta\zeta_3}\right) + A_{2i-1}\frac{\partial\Delta\phi}{\partial\eta} + A_{3i-1}\frac{\partial\Delta\phi_i}{\partial\zeta}\right] + \frac{\partial}{\partial\zeta}\left(\frac{\rho_i U_i}{J}\right)\right\} \\ & + (1 - \theta_{i+1})\left\{ \frac{1}{\beta\Delta\zeta_o}\left[\frac{\tilde{\tilde{\rho}}}{J}\left(a_{11}\frac{\Delta\phi}{\Delta\zeta_o} + a_{12}\phi_\eta + a_{13}\phi_\zeta\right)\right]_{i+2} \right. \\ & \left. + \frac{1}{\beta\Delta\zeta_o}\left[\left(\frac{\tilde{\tilde{\rho}}a_{12}}{J}\right)_{i+1}\frac{\partial\phi_i}{\partial\eta} + \left(\frac{\tilde{\tilde{\rho}}a_{13}}{J}\right)_{i+1}\frac{\partial\phi_i}{\partial\zeta}\right]\right\} \\ & - \frac{1}{\beta}\frac{\partial}{\partial\eta}\left[\left(\frac{\hat{\rho a}_{22}}{J}\frac{\partial\phi_i}{\partial\eta}\right) + \left(\frac{\hat{\rho a}_{23}}{J}\frac{\partial\phi_i}{\partial\zeta}\right)\right] \\ & - \frac{1}{\beta}\frac{\partial}{\partial\zeta}\left[\left(\frac{\hat{\rho a}_{32}}{J}\frac{\partial}{\partial\eta}\phi_i\right) + \frac{\hat{\rho a}_{33}}{J}\frac{\partial}{\partial\zeta}\phi_i\right] \\ & - \frac{1}{\beta}\frac{\partial}{\partial\eta}\left(\frac{\hat{\rho a}_{23}}{J}\frac{\partial}{\partial\zeta}\right)_{i+1}\Delta\phi_{i+1} - \frac{1}{\beta}\frac{\partial}{\partial\zeta}\left(\frac{\hat{\rho a}_{32}}{J}\frac{\partial}{\partial\eta}\right)_{i+1}\Delta\phi_{i+1} \end{aligned} \tag{10}$$

The density $\hat{\rho}$ appearing in Eq. (9) and Eq. (10) can be either ρ or $\tilde{\rho}$ depending on the sign of $\left(a_{11} - \frac{U^2}{a^2}\right)$ as illustrated in Eq. (6).

Equation (9) has the form $L_\zeta L_\eta(\Delta\phi) = R$ and it is implemented as follows:

$$L_\zeta(\Delta\phi)^* = R \quad L_\eta(\Delta\phi) = (\Delta\phi)^* \quad \phi_{i+1} = \phi_1 + \Delta\phi \quad .$$

The various quantities appearing in Eq. (9) are given by

$$B = \frac{1}{\Delta\zeta}\left[\theta_i A_1 - (1 - \theta_{i+1})\frac{\Delta\zeta}{\Delta\zeta_0}\left(\frac{\tilde{\rho}a_{11}}{J}\right)_{i+1}\right]$$

$$A_1 = \frac{\rho_i}{J_{i+1}}\left(a_{11} - \frac{U^2}{a^2}\right)$$

$$A_2 = \theta_i\left[\frac{\rho_i}{J_{i+1}}\left(a_{12} - \frac{UV}{a^2}\right)\right] - (1 - \theta_{i+1})\frac{\Delta\zeta}{\Delta\zeta_0}\left(\frac{\tilde{\rho}a_{12}}{J}\right)_{i+1}$$

$$A_3 = \theta_i\frac{\rho_i}{J_{i+1}}\left(a_{13} - \frac{UW}{a^2}\right) - (1 - \theta_{i+1})\frac{\Delta\zeta}{\Delta\zeta_0}\left(\frac{\tilde{\rho}a_{13}}{J}\right)_{i+1}$$

$$\Delta\zeta_0 = \zeta_{i+2} - \zeta_{i+1}$$

$$\Delta\zeta = \zeta_{i+1} - \zeta_i \tag{11}$$

If the flow field does not contain an embedded MSR or TSR, the implicit factored algorithm of Eq. (9) performs a pure marching procedure starting from an initial known data plane. In this situation, there is no need to go back to the upstream starting plane and iterate the solution. However, if a subsonic bubble is presnt (between planes AB and CD in Fig. 1, then the solution procedure of Eq. (9) performs a relaxation method, and iterates for the elliptic subsonic bubble to converge.

IV. Initial Conditions

For a pure supersonic flow, initial conditions are required at the starting plane. Usually, the starting plane is set close to the nose region of the configuration. For a sharp nosed configuration, conical solutions are prescribed, and for a blunt nose, the axisymmetric unsteady full potential solver of Reference 6 is used to obtain flow field in the transonic forbody region.

In the embedded subsonic region, when Eq. (5) is applied at an i+1 grid point, information on the Flux ρU at i+2 is required. For the first relaxation pass, sonic conditions are assumed at i+2.

$$\rho_{i+2} = \rho^* = \left(\frac{2}{\gamma+1} + \frac{\gamma-1}{\gamma+1} M_\infty^2\right)^{1/\gamma-1}$$

$$U_{i+2} = q^* \, (a_{11})^{1/2}_{i+2} \qquad (12)$$

where

$$q^* = [\rho^{*\gamma-1}/M_\infty^2]^{1/2}$$

The sonic values ρ^* and q^* are purely a function of the free-stream Mach number M_∞. For the second relaxation cycle and onwards, the conditions from the previous relaxation cycle is used.

V. Boundary Conditions

In order to solve the full potential equation, it is essential to specify appropriate boundary conditions of the body surface and outer boundary.

1. Body Surface

At a solid boundary, the contravariant velocity V is set to zero. Exact implementation of V = 0 in the implicit treatment of Eq. (9) is described in Reference 4.

2. Outer Boundary

The outer boundary is set away from the bow shock and the freestream velocity potential ϕ_∞ is imposed along that boundary. All discontinuities in the flow field are captured. The precise density biasing activator ν, based on the characteristic theory, allows for sharp capturing of shocks in the flow.

3. Symmetric Boundary Conditions

For yaw angle $\beta = 0$, only the half plane problem needs to be solved with the plane of symmetry boundary conditions imposed along K = 2 and (Kmax - 1), as shown in Fig. 2a. Imposing that the flow conditions along K = 1 are to be the same as the ones along K = 3, the L_F operator results in a tridiagonal system that can be easily solved.

SCB3-24987

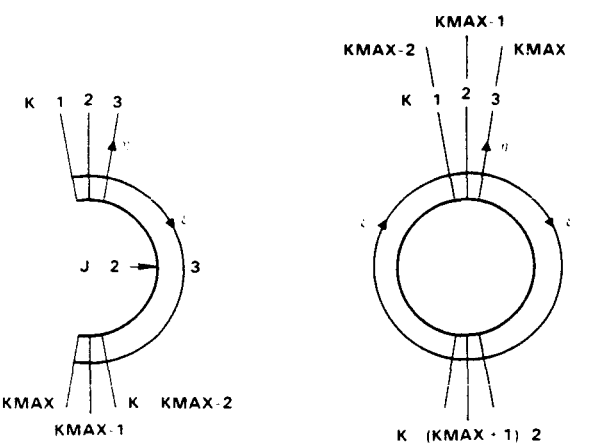

a) PLANE OF SYMMETRY (YAW ANGLE 0)

$\phi_{j,1} = \phi_{j,3}$

$\phi_{j,KMAX} = \phi_{j,KMAX-2}$

b) PERIODIC CONDITION FOR YAW TREATMENT

$\phi_{j,1} = \phi_{j,KMAX-2}$

$\phi_{j,KMAX} = \phi_{j,3}$

Fig. 2 Symmetry and periodic conditions.

4. Combined Yaw and Angle of Attack

Even for a symmetric configuration, when yaw angle is present the entire cross-flow plane needs to be solved as shown in Fig. 2b. In this case the flow conditons along K = 1 are set to be the same as the ones along K = (KMAX - 2). This destroys the tridiagonal nature of the L_F operator. A special routine has been developed to invert a matrix of the following type.

$$L_F = \begin{bmatrix} X & X & & & X & 0 \\ X & X & X & & 0 & 0 \\ & X & X & X & & 0 \\ & & & & & \\ & & & & & \\ 0 & 0 & & X & X & X \\ 0 & X & & & X & X \end{bmatrix} \qquad (13)$$

In the current formulation, positive angle of attack α represents a positive cartesian velocity v in the freestream and similarly positive yaw β produces a positive w in the free stream. When both angle of attack and yaw are present, first the freestream is turned by an angle β and then by α.

Let (x,y,z) be the inertial Cartesian system. After an initial yaw turn β let the wind axis system be (x',y',z'), and after a subsequent α turn let it become $(\tilde{x},\tilde{y},\tilde{z})$.

$$\begin{pmatrix} \tilde{x} \\ \tilde{y} \\ \tilde{z} \end{pmatrix} = \begin{bmatrix} \cos\alpha & \sin\alpha & 0 \\ -\sin\alpha & \cos\alpha & 0 \\ 0 & 0 & 1 \end{bmatrix} \begin{bmatrix} \cos\beta & 0 & \sin\beta \\ 0 & 1 & 0 \\ -\sin\beta & 0 & \cos\beta \end{bmatrix} \begin{pmatrix} x \\ y \\ z \end{pmatrix} \qquad (14)$$

$$= \begin{bmatrix} \cos\alpha\cos\beta & \sin\alpha & \cos\alpha\sin\beta \\ -\sin\alpha\cos\beta & \cos\alpha & 0 \\ -\sin\beta & 0 & \cos\beta \end{bmatrix} \begin{pmatrix} x \\ y \\ z \end{pmatrix}$$

The free stream is now along $\tilde{x}$. The normalized free stream velocity potential is given by

$$\phi_\infty = X\cos\alpha\cos\beta + y\sin\alpha + z\cos\alpha\sin\beta \qquad (15)$$

Using Eq. (14), the lift, drag and side forces are easily represented.

$$D = F_x\cos\alpha\cos\beta + F_y\sin\alpha + F_z\cos\alpha\sin\beta$$

$$L = -F_x\sin\alpha\cos\beta + F_y\cos\alpha \qquad (16)$$

5. Swept Trailing Edge Wake Treatment

Figure 3 shows a schematic of a swept trailing edge wake system. In order to treat the region behind the trailing edge, an artificial cut is created and the pressure jump [P] across this cut is imposed to be zero as a boundary condition. This is achieved by maintaining the jump in the velocity potential ϕ along a k = constant line (see Fig. 3) for j = 2 to be the same as the value $[\phi]$ at the trailing edge. The full potential equation is not solved at grid points on the wake cut. Instead, $\phi_{hh} = 0$ is solved to provide $[\phi_\eta] = 0$ across the wake cut. Maintaining $[\phi]$ constant along a k line provides $[\phi_\zeta] = 0$. The combination

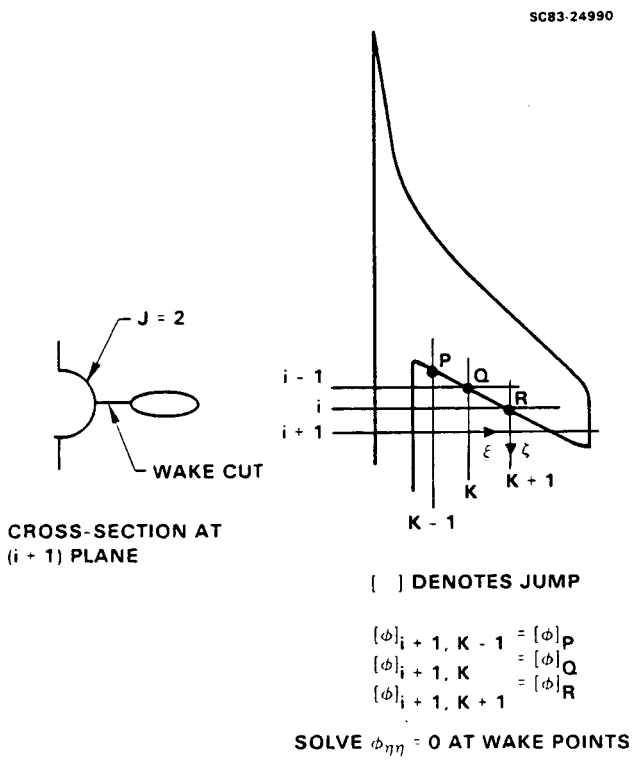

Fig. 3 Wake boundary condition.

of $[\phi_\xi] = 0$ and $[\phi_\eta] = 0$ across the cut satisfies $[P] = 0$ approximately.

6. Geometry and Grid System

The geometry of a configuration is prescribed at discrete points in a crossplane (usually x = constant plane) at various axial locations. These geometry input points are usually obtained from a geometry package such as GEMPACK or CDS. The input points are then divided into several patches, and at each patch a key-point system is established as shown in Fig. 4. The geometry at a marching plane is then obtained by joining the appropriate key-point for each patch. Using a cubic spline passing through the key points, a desired grid point distribution (clustering) is set up on the body surface. Then, using an appropriate outer boundary, the grid for the flowfield calculation is generated by using an elliptic grid generator.

VI. Results and Discussion

Four cases are presented to substantiate the recently developed code.

1. Flow over an arrow-wing body at M_∞ = 2.96, α = 10.01°.
2. Flow over a forebody configuration at M_∞ = 2.5, β = 5° and at M_∞ = 1.7, α = 10°, β = 5°.
3. Flow over the entire shuttle orbiter geometry at M_∞ = 1.4, α = 0°.
4. Flow over a realistic fighter configuration at different angles of attack and freestream mach numbers.

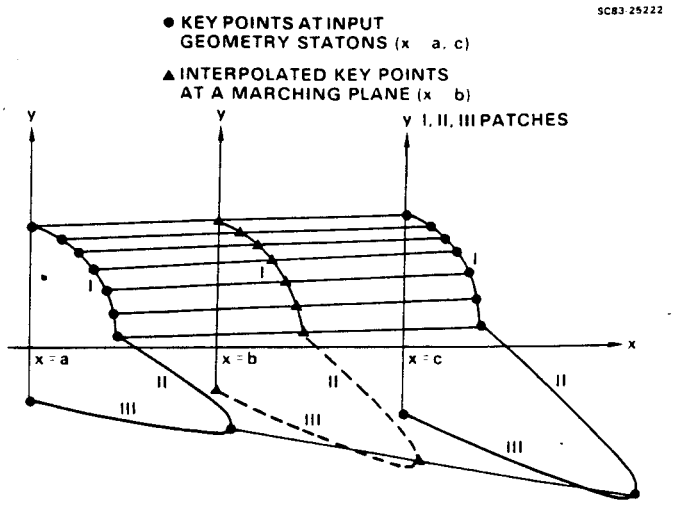

Fig. 4 Geometry setup.

Figure 5 shows the pressure distribution on the surface of an arrow-wing configuration at location $x/\ell = 0.8$ for $M_\infty = 2.9$, and $\alpha = 10°$. The improvement in the prediction capability achieved using the wake treatment is illustrated. The dashed line represents the result from "no wake" treatment (assumes a flat plate behind the trailing edge) and the solid line represents the modifications to the pressure distribution once a zero jump in pressure across the wake cut is imposed. The solid line pressures on the body agree very well with experiments. Without a proper wake cut treatment, the overall lift and drag forces and the pitching moment can be off by a considerable margin.

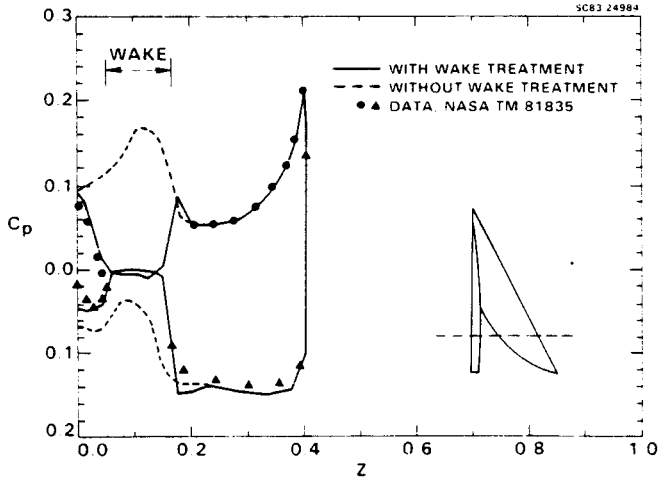

Fig. 5 Circumferential pressure distribution for the arrow-wing at $x/\ell = 0.81$, $M_\infty = 2.96$, $\alpha = 10°$.

Figure 6 presents the pressure distribution on a fully developed forebody[6] for $M_\infty = 2.5$ and yaw angle $\beta = 5°$. Figure 7 shows the circumferential pressure distribution for the same body at $x/\ell = 0.68$ for $M_\infty = 1.7$, $\alpha = 10°$ and $\beta = 5°$. The experimental data[7] are also given in these two figures. The results show that the present prediction is in excellent agreement with the experimental data.

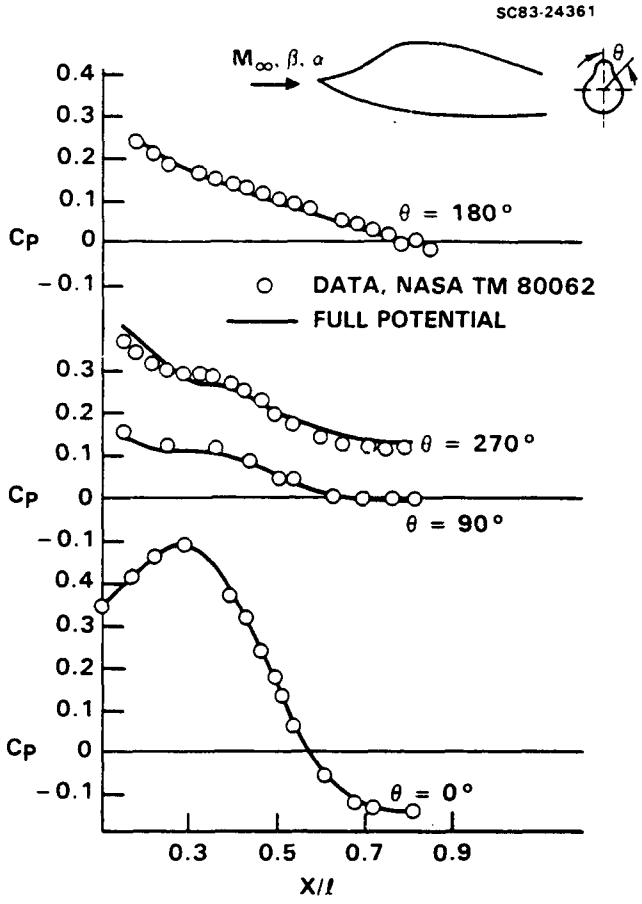

Fig. 6 Pressure distribution on a forebody in sideslip $M_\infty = 2.5$, $\beta = 5.02°$, $\alpha = 0°$.

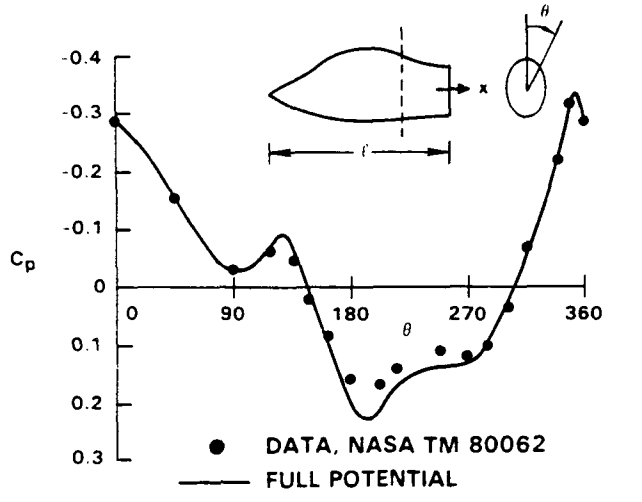

Fig. 7 Circumferential pressure distribution on a forebody at $x/\ell = 5.02°$, $\alpha = 0°$.

Figures 8 to 18 give the geometry and the corresponding flow field solutions for the shuttle orbiter. The side view, cross section and grid in the nose region are given in Fig. 8. The top views, cross-section, grid and chordwise cross-section are presented in Fig. 9. It should be mentioned here that for most of the previous space

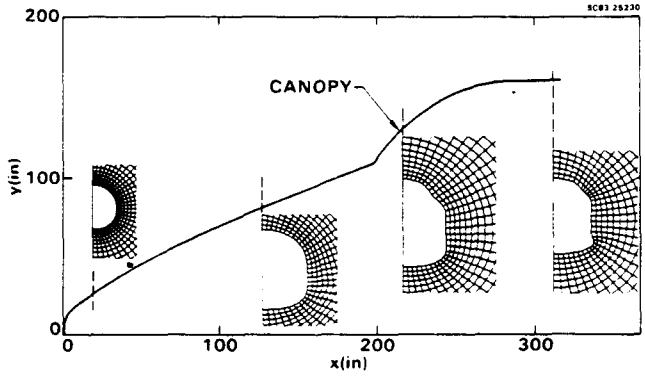

Fig. 8 Nose region geometry for Space Shuttle.

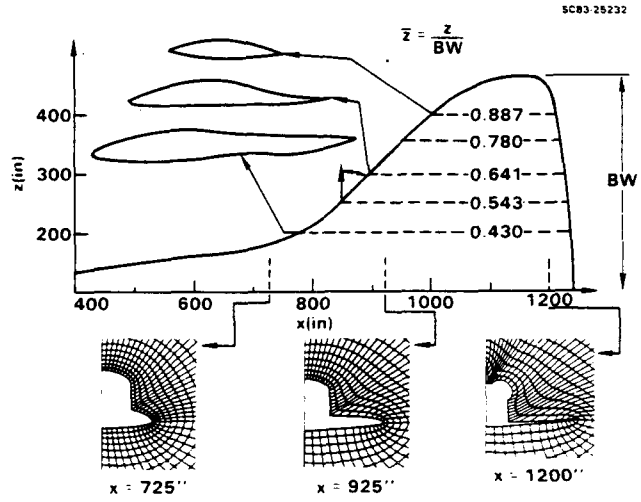

Fig. 9 Geometry and grid generation for Shuttle orbiter at axial cuts.

shuttle calculations[9,10] the geometry has been modified by smoothing out the canopy and increasing the wing sweep angle from 45 to 55 degrees in order to avoid the subsonic bubble. Since the present method is valid for supersonic flow with embedded subsonic region, the realistic shuttle orbiter geometry was used without any modification.

Figure 10 shows the surface pressure distribution along the leeward plane of symmetry. At x ≅ 170 in. which is the beginning of the canopy, the pressure increases rapidly from $C_p \cong 0.3$ to 1.0, approximately. In the canopy region an MSR/TSR is formed and required three relaxation cycles to develop the solution. The circumferential surface pressure distribution at x = 240 in. is shown in Fig. 11. The experimental data is also given in these figures and the agreement is very good. The surface pressure distribution along the wing leading edge is given in Fig. 12. It is seen that the present calculation agrees with the experiment data quite well along the entire wing leading edge except in the vicinity of the wing-fuselage junction, where a vortex flow may exist.

Figure 13 to Figure 17 present the orbiter chordwise pressure distribution on the upper and lower wing surface at $\bar{z} = z/bw = 0.471$, 0.530, 0.641, 0.780 and 0.887, respectively where bw is a semispan defined in Fig. 8. The results show that

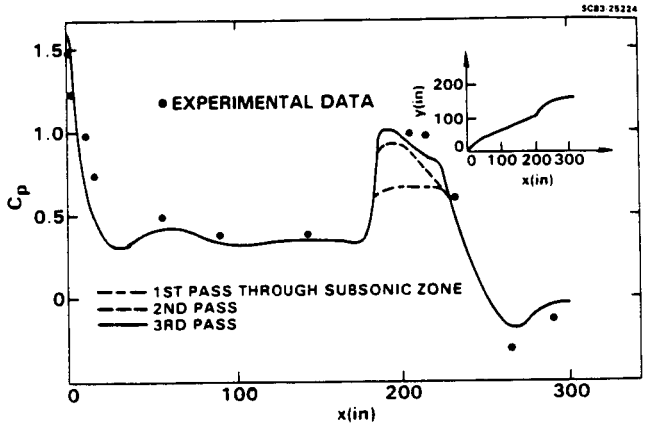

Fig. 10 Surface pressure distribution at leeward plane of symmetry.

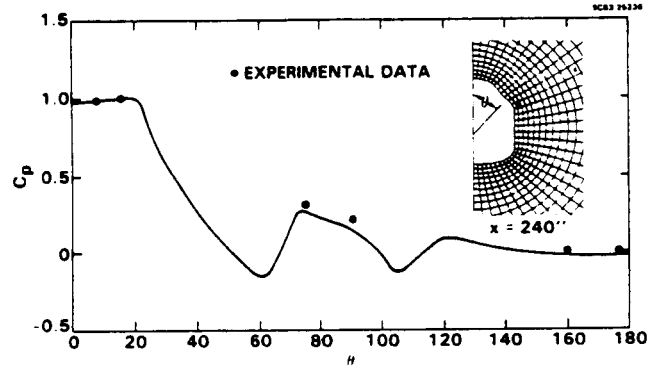

Fig. 11 Surface pressure distribution around the body.

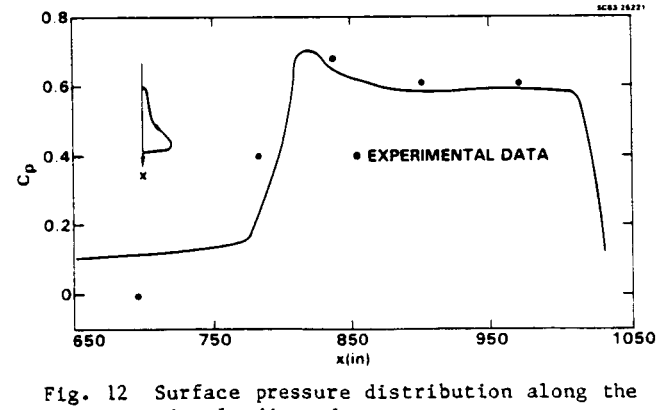

Fig. 12 Surface pressure distribution along the wing leading edge.

the present predictions are in very good agreement with the experimental data, except in the region near the trailing edge of the upper surface at $\bar{z}$ = 0.471 and 0.53 span stations. Here again, a vortex flow or separation may be causing the discrepancies. Figure 18 shows the circumferential pressure distribution for the orbiter at x = 1120 in. It is noted that the pressure at the vertical tail and OMS pods are well predicted.

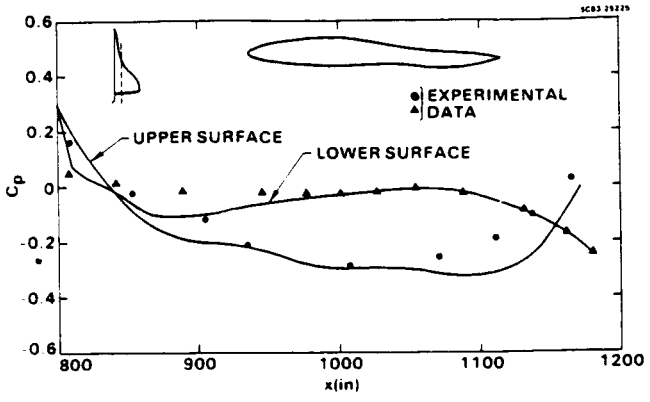

Fig. 13 Shuttle orbiter chordwise pressure distribution; M_∞ = 1.4, α = 0.0°, $\bar{z}$ = 0.471.

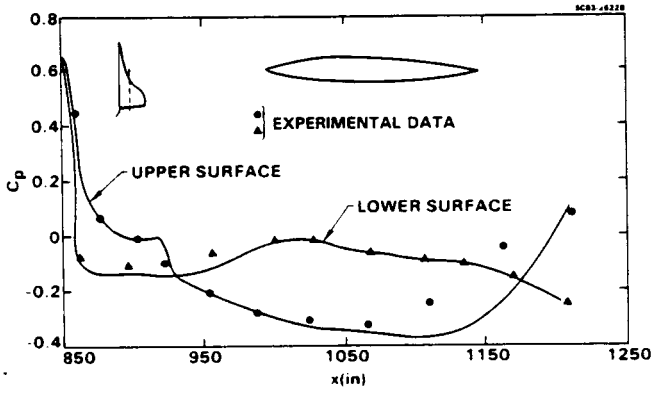

Fig. 14 Shuttle orbiter chordwise pressure distribution; M_∞ = 1.4, α = 0.0°, $\bar{z}$ = 0.53.

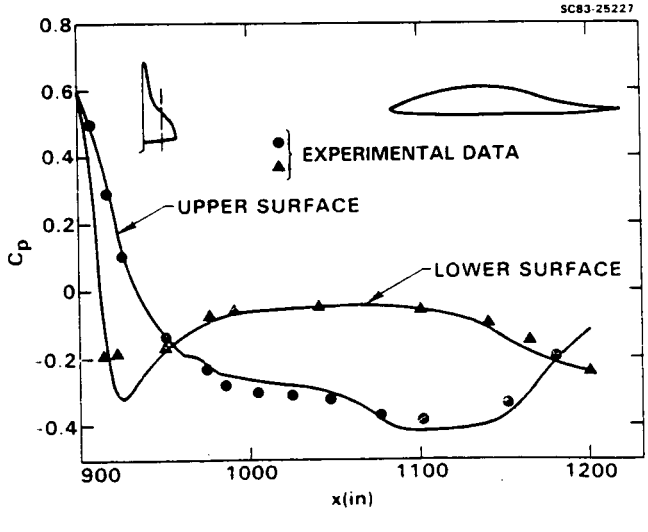

Fig. 15 Shuttle orbiter chordwise pressure distribution; M_∞ = 1.4, α = 0.0°, $\bar{z}$ = 0.641.

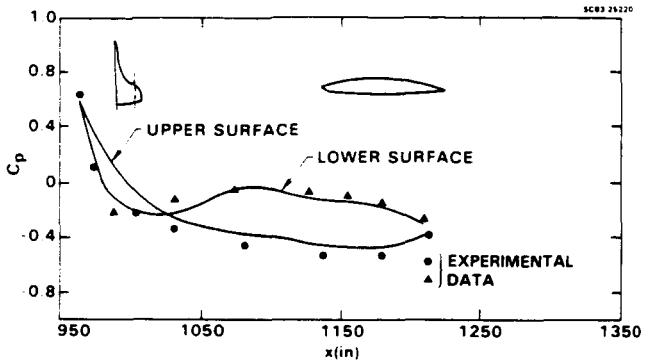

Fig. 16 Shuttle orbiter chordwise pressure distribution; $M_\infty = 1.4$, $\alpha = 0.0°$, $\bar{z} = 0.78$.

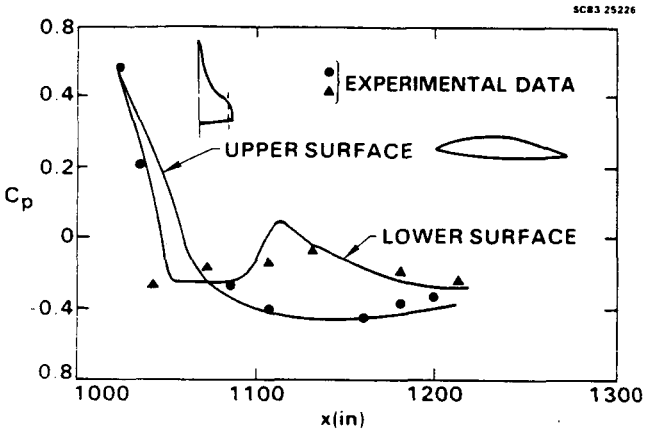

Fig. 17 Shuttle orbiter chordwise pressure distribution; $M_\infty = 1.4$, $\alpha = 0.0°$, $\bar{z} = 0.887$.

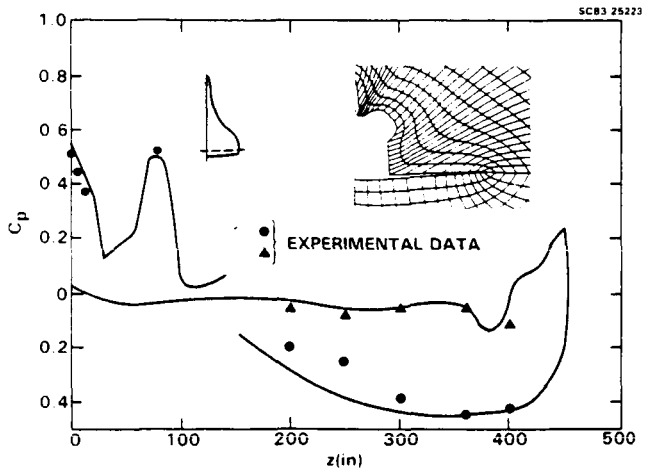

Fig. 18 Circumferential pressure distribution for the orbiter at x = 1120 in; $M_\infty = 1.4$, $\alpha = 0.0°$.

Figure 19 shows a supersonic fighter configuration with vertical tails. The free stream mach number, angle of attack and wing sweep angle for the calculation are summarized in Table 1.

Figure 20 presents the surface pressure at various axial stations and the corresponding grid distribution for the wing body geometry. For this case, the MSR/TSR starts around x = 0.4 at the leading edge, and remains subsonic all the way to the end of the wing. Figure 21 and 22 show the circumferential pressure distribution in the vertical tail and wake region of the fighter-like configuration. The pressure on the vertical tail surface is given separately along y-direction. The results clearly show that the present wake tretment provides the correct zero pressure jump condition across the wake. The chordwise pressure distributions from the center of the body to the top of the wing are given in Fig. 23. Figure 24 presents the pressure contour on the upper and lower surface of the fighter configuration.

The lift and drag coefficients from the present calculations for this fighter model are also given in Table 1. The comparison with experimental data show excellent agreement.

VII. Conclusions

A nonlinear full potential method has been applied to investigate the supersonic flows with embedded sobsonic regions over some very complex configurations. A conservative switching scheme is employed to transition from the supersonic marching algorithm to a subsonic relaxation procedure. The present predictions are in very good agreement with experiment data.

Work is now progressing to simulate the multibody interaction between the shuttle orbiter and the external tank. The present methodology will also be extended to treat all mach number flows (fully subsonic flow as well as subsonic flow with pockets of supersonic region (transonic case)).

Acknowledgment

This work was partially supported by NASA-Langley Research Center under Contract NAS1-15820.

References

1. Woodward, F.A., Tinoco, E.N., and Larsen, J.W., "Analysis and Design of Supersonic Wing-Body Combinations, Including Flow Properties in the Near Field. Part I - Theory and Application," NASA CR 73106, 1967.

2. Kutler, P., "Computation of Three-Dimensional Inviscid Supersonic Flows," in Lecture Notes in Physics 41, Springer-Verlag, New York, 1975.

3. Marconi, F., Salas, M., and Yeager, L., "Development of a Computer Code for Calculating the Steady Super/Hypersonic Inviscid Flow Around Real Configurations, Vol. I - Computational Techniques," NASA CR 2675, April 1976.

4. Shankar, V., Szema, K.Y., and Osher S., "A Conservative Type-Dependent Full Potential Method for the Treatment of Supersonic Flow with Imbedded Supersonic Region," AIAA Paper No. 83-1887, July 1983.

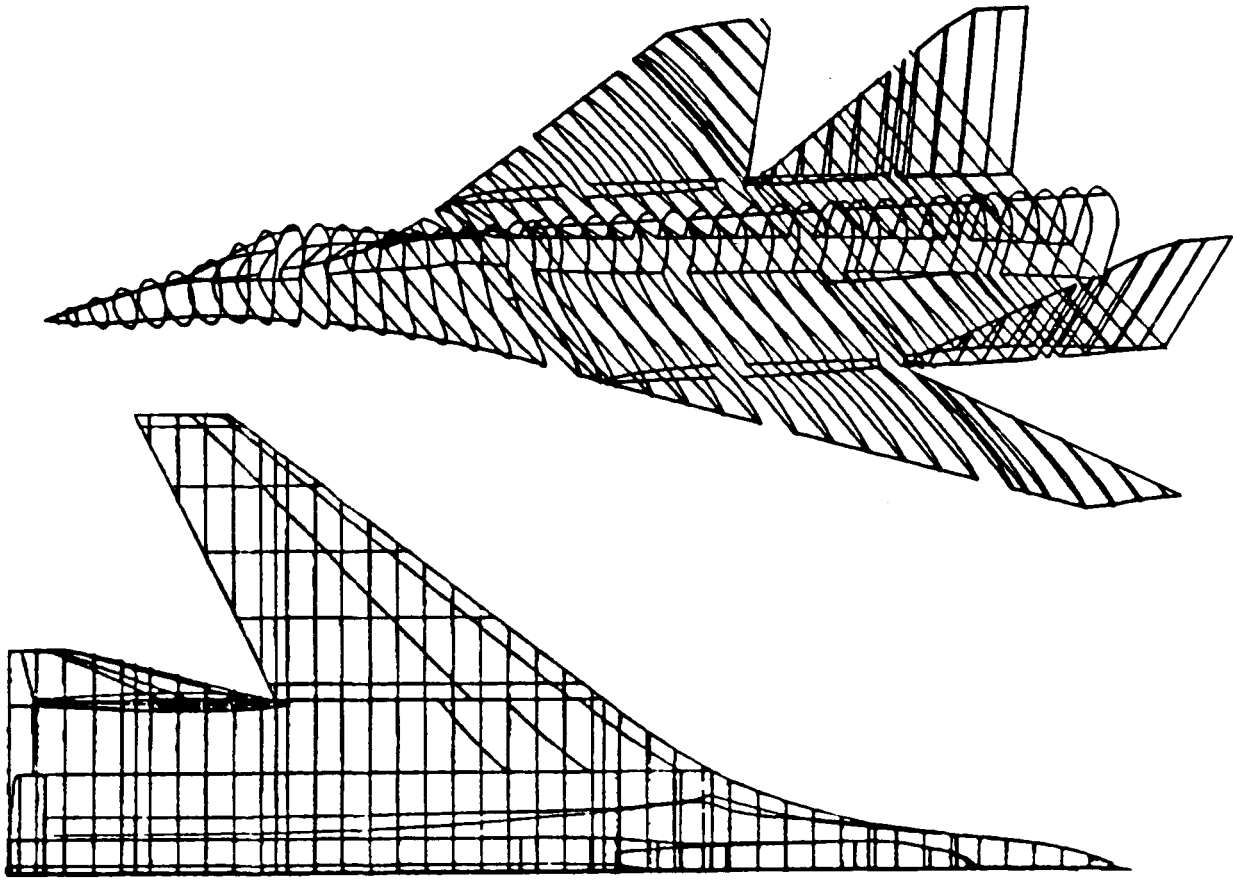

Fig. 19 Fighter-like configuration.

Table 1 Test cases for fighter-like configurations.

α		5°	5°	5°	5°
M_∞		1.6*	1.6†	1.4†	1.6†
Λ		48°	48°	48°	55°
C_L	CODE	0.298	0.3016	0.3561	0.29186
	DATA	0.277	0.295	0.342	0.3
C_D	CODE	0.0462	0.04916	0.04117	0.028129
	DATA	0.0457	0.0493	0.0425	0.0301

Λ = Wing sweep angle
*Without vertical tail
†With vertical tail

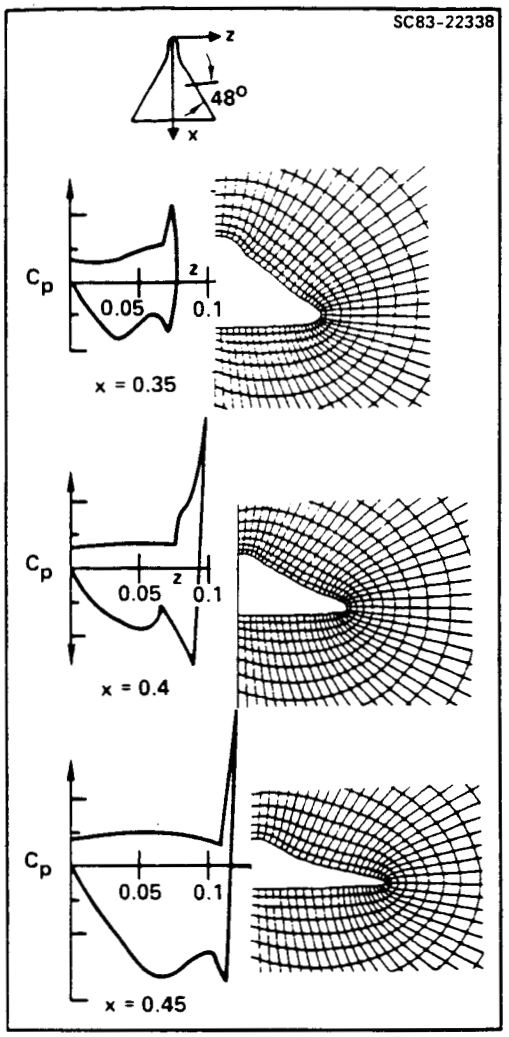

Fig. 20 Pressure distribution on a fighter-like configuration, M_∞ = 1.6, α = 5°.

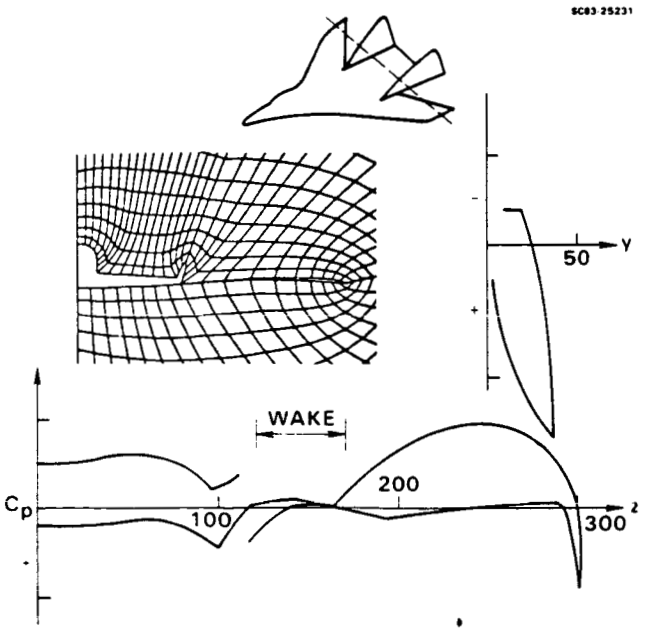

Fig. 21 Circumferential pressure distribution in the vertical tail and wing region of a fighter-like configuration, M_∞ 1.6, α = 4.46, x/ℓ = 0.82.

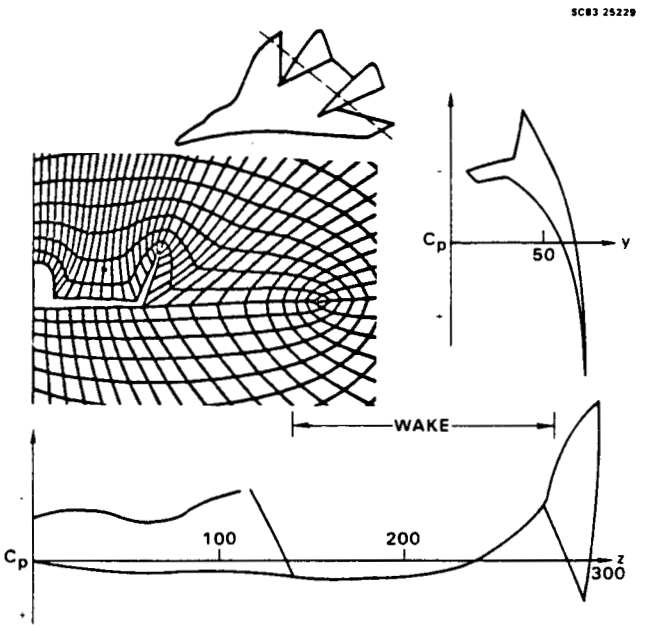

Fig. 22 Circumferential pressure distribution in the vertical tail and wing region of a fighter-like configuration, M_∞ 1.6, α = 4.46, x/ℓ = 0.90.

5. Shankar, V., and Osher, S., "An Efficient Full Potential Implicit Method Based on Characteristics for Analysis of Supersonic Flows," AIAA Paper No. 82-0974, June 1982.

6. Shankar, V., "Implicit Treatment of the Unsteady Full Potential Equation in Conservation Form," AIAA Paper No. 84-0262, January 1984.

7. Townsend, J.C., "Pressure Data for Four Analytically Defined Arrow Wings in Supersonic Flow," NASA TM 81835, September 1980.

8. Townsend, J.C., Howell, D.T., Collins, I.K., and Hayes, C., "Surface Pressure Data on a Series of Analytic Forebodies at Mach Numbers from 1.7 to 4.50 and Combined Angles of Attack and Sideslip," NASA TM 80062, June 1979.

9. Maus, J.R., Griffith, B.J., Szema, K.Y., and Best, J.T., "Hypersonic Mach Number and Real Gas Effects on Space Shuttle Orbiter Aerodynamics," AIAA Paper No. 83-0343, January 1983.

10. Venkatapathy, E., Rakich, J.V., and Tannehill, J.C., "Numerical Solution of Space Shuttle Orbiter Flow Field," AIAA Paper No. 82-0028, January 1982.

11. Rockwell International Space Division Data.

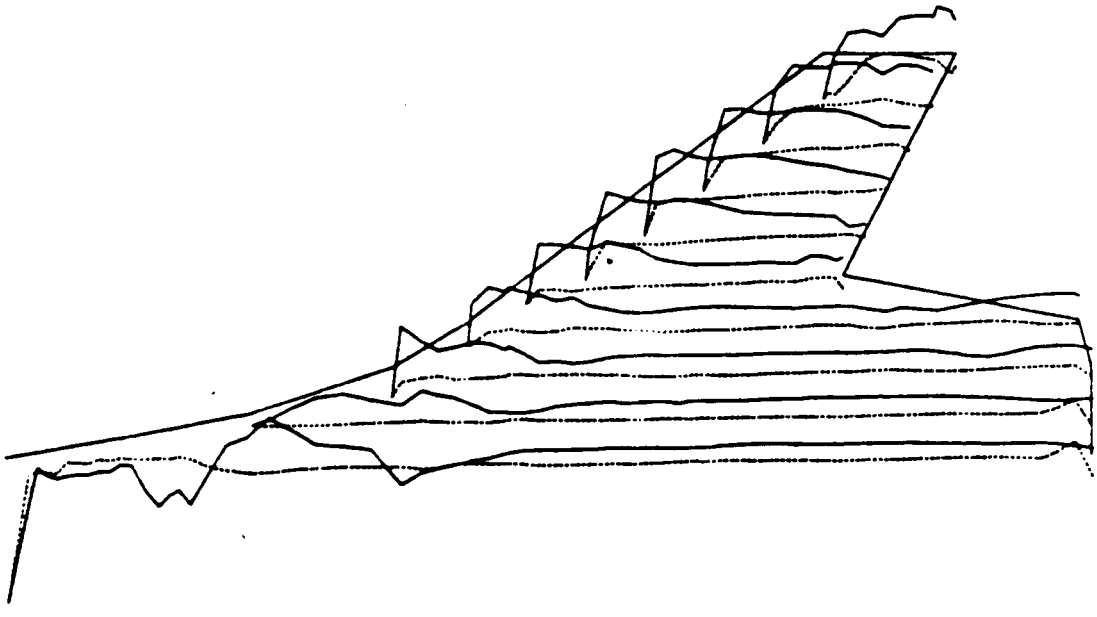

Fig. 23 Chordwise pressure distribution for a fighter-like configuration. M_∞ 1.6, α = 4.46.

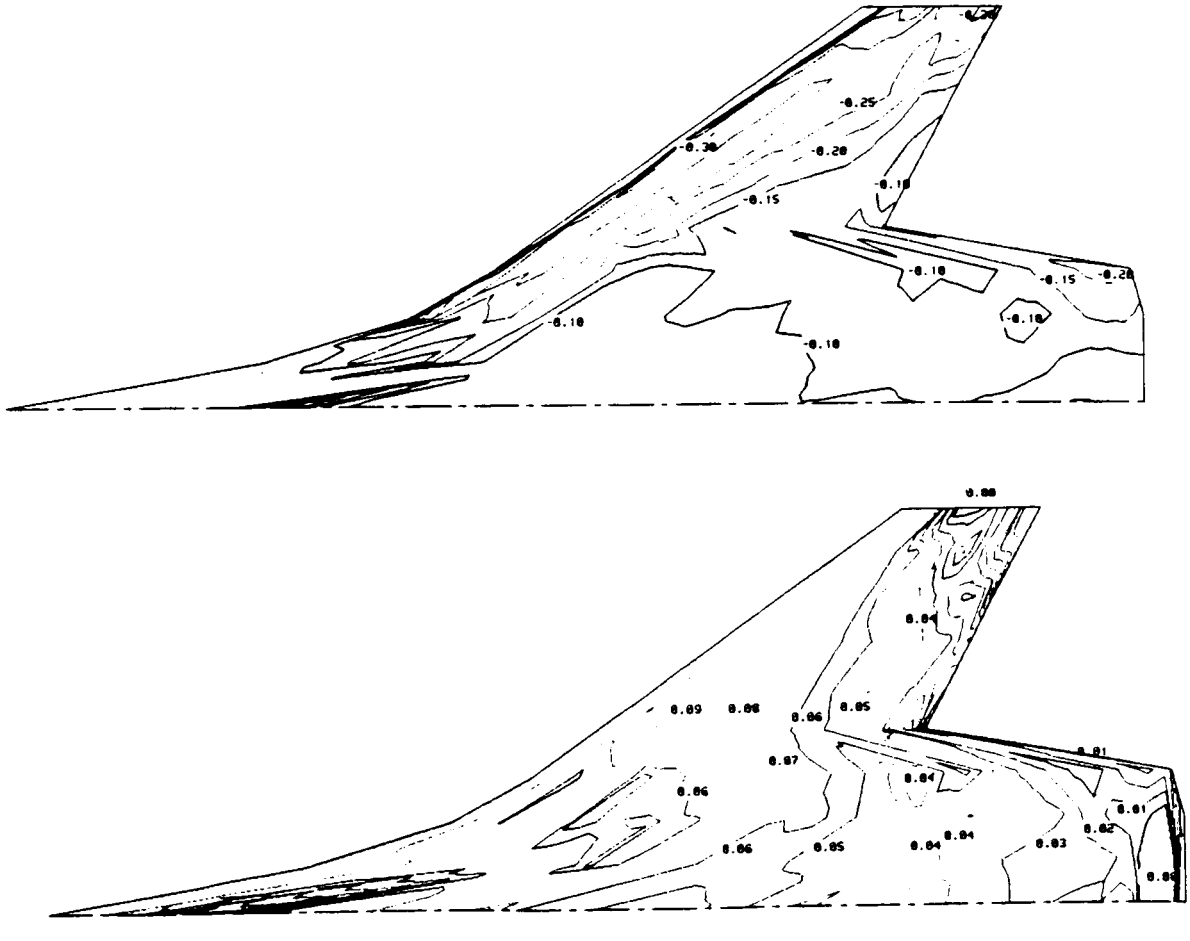

Fig. 24 Pressure contour on the upper and lower surface of the fighter-like configuration. M_∞ = 1.6, α = 4.46°.

CONSERVATIVE FULL POTENTIAL, IMPLICIT MARCHING SCHEME FOR SUPERSONIC FLOWS

VIJAYA SHANKAR and KUO-YEN SZEMA

Rockwell International Science Center
Thousand Oaks, California 91360

I. THEORY

ABSTRACT

A numerical method based on the conservation form of the full potential equation has been applied to three-dimensional supersonic flows with embedded subsonic regions. The governing equation is cast in a nonorthogonal coordinate system, and the theory of characteristics is used to accurately monitor the type-dependent flow field. A conservative switching scheme is employed to transition from the supersonic marching procedure to a subsonic relaxation algorithm and vice versa. The newly developed computer program can handle arbitrary geometries with fuselage, wing, vertical tail and wake components at combined angles of attack and sideslip. Example results in this report include the Shuttle Orbiter flow at a low supersonic Mach number, flow over a realistic fighter-type configuration, wake simulations for an arrow wing, and a forebody in sideslip. Comparisons with experimental data are shown to be in good agreement for various cases.

INTRODUCTION

Nonlinear aerodynamic prediction methods based on the full potential equation are used regularly for treating transonic[1,2] and supersonic[3-5] flows over realistic wing-body configurations. The transonic algorithms[1,2] are designed to treat predominantly subsonic flows with pockets of supersonic regions bounded by sonic lines and shocks. The supersonic methods[3-5] are based on a marching concept, and require the flow to remain supersonic in a given marching direction. Once the marching direction velocity becomes subsonic, the domain of dependence changes and a pure marching scheme[3-5] will violate the rules of characteristics signal propagation. The possibility of a marching velocity becoming subsonic in a supersonic flow is great, especially for low supersonic freestream Mach number flows (M_∞ = 1.3 ~ 1.7) over moderately swept fighter-like configurations (sweep angle Λ 45 ~ 50°) and over forebody shapes having a sizeable fuselage-canopy junction region. The methodology of

Refs. 6 and 7 is an extension to the marching scheme of Ref. 5 and is designed to treat embedded subsonic regions in a supersonic flow. In order to properly produce the necessary artificial viscosity through density biasing, Ref. 6 defines two situations: 1) the total velocity, q, is supersonic, but the marching direction component is subsonic (defined as Marching Subsonic Region (MRS)), and 2) the total velocity, q, is subaonic (termed as Total Subsonic Region (TSR).

The method of Refs. 4-7 is based on the characteristic theory of signal propagation and uses a generalized, nonorthogonal, curvilinear coordinate system. It has no restrictions (limitations of the full potential theory hold) on its applicability to complex geometries and intricate shocked flow fields. It is a conservative formulation and uses numerical mapping techniques to generate the body-fitted system.

This report presents a brief description of the overall methodology[4-7] along with some user information on code organization, input and output data, and sample results. A typical calculation over a complete configuration (wing-body-vertical tail-wake) requires fifteen minutes of CPU time on the Cyber 176 machine or three minutes on the Cray-1.

BASIC FORMULATION

The steady, conservative full potential equation cast in an arbitrary coordinate system defined by $\zeta = \zeta(x,y,z)$, $\eta = \eta(x,y,z)$ and $\Xi = \Xi(x,y,z)$ can be written as

$$\left(\rho \frac{U}{J}\right)_\zeta + \left(\rho \frac{V}{J}\right)_\eta + \left(\rho \frac{W}{J}\right)_\Xi = 0 \qquad (1)$$

where the density ρ is given by

$$\rho = \left[1 - \left(\frac{\gamma-1}{2}\right) M_\infty^2 \{U\phi_\zeta + V\phi_\eta + W\phi_\Xi - 1\}\right]^{1/(\gamma-1)} \qquad (2)$$

and M_∞ is the free stream Mach number, a is the local speed of sound and U,V,W are the contravariant velocity components. Introducing the following notation

for convenience

$$U_1 = U \quad U_2 = V \quad U_3 = W$$
$$x = x_1 \quad y = x_2 \quad z = x_3 \quad .$$
$$\zeta = X_1 \quad \eta = X_2 \quad \xi = X_3 \quad ,$$

the contravariant velocity can be expressed as

$$U_i = \sum_{j=1}^{3} a_{ij} \phi_{X_j} \qquad i = 1,2,3$$

$$a_{ij} = \sum_{k=1}^{3} \frac{\partial X_i}{\partial x_k} \frac{\partial X_j}{\partial x_k} \qquad \begin{matrix} i = 1,2,3 \text{ (transforma-} \\ j = 1,2,3 \text{ tion metrics)} \end{matrix} \tag{3}$$

The Jacobian of the transformation J is represented by

$$J = \frac{\partial(\zeta,\eta,\xi)}{\partial(x,y,z)} = \begin{vmatrix} \zeta_x & \zeta_y & \zeta_z \\ \eta_x & \eta_y & \eta_z \\ \xi_z & \xi_y & \xi_z \end{vmatrix} \tag{4}$$

The nature of Eq. (1) can be analyzed by studying the eigenvalue system of Eq. (1) combined with the irrotationality condition in the (ζ,η) and (ζ,ξ) planes. A detailed discussion on this can be found in Reference 6. Therefore, only the final results are presented here.

1. At a grid point, the marching direction ζ is <u>hyperbolic</u> and the total velocity q is supersonic, $\left(a_{11} - \frac{U^2}{a^2}\right) < 0$, $q > a$. This point will use the algorithm of Reference 5.

2. At a grid point, the marching direction ζ is <u>elliptic</u>, $\left(a_{11} - \frac{U^2}{a^2}\right) > 0$, but the total velocity q is supersonic, $q > a$. This point will be treated by a transonic operator with a built-in density biasing based on the magnitude of $\left(1 - \frac{a^2}{q^2}\right)$.

3. At a grid point, the direction ζ is <u>elliptic</u> and the total velocity q is <u>subsonic</u>, $q < a$. This point will be treated by a subsonic central differenced operator.

METHOD OF SOLUTION

Figure 1 shows the schematic of a fuselage-canopy forebody geometry with an embedded MSR and TSR present in a supersonic flow. To solve this problem, the marching scheme of Reference 5 is used when $\left(a_{11} - \frac{U^2}{a^2}\right)$ is negative, and a relaxation scheme is used when $\left(a_{11} - \frac{U^2}{a^2}\right)$ is positive. First, march from the nose up to the plane denoted by (A-B) in Fig. 1, using the method of Reference 5. Then, between (A-B) and (C-D), which embed the subsonic bubble (MSR and TSR), use a relaxation scheme and iterate until the subsonic bubble is fully captured. Then, resume the marching scheme from the plane (C-D), downstream of the body.

<u>Treatment of $\partial/\partial\zeta\ (\rho\ U/J)$ Term</u>

At a grid point $(i + 1, j, k)$, the derivative in the marching direction ζ is given by

$$\frac{\partial}{\partial\zeta}\left(\rho\,\frac{U}{J}\right) = \theta_i \underbrace{\frac{\overleftarrow{\delta}}{\partial\zeta}\left(\rho\,\frac{U}{J}\right)_{i+1}}_{\text{supersonic}} + (1 - \theta_{i+1}) \underbrace{\frac{\overrightarrow{\delta}}{\partial\zeta}\left(\tilde{\rho}\,\frac{U}{J}\right)_{i+1}}_{\substack{\text{marching} \\ \text{subsonic}}} \tag{5}$$

where

$\overleftarrow{\delta}$ refers to backward differencing

$\vec{\delta}$ refers to forward differencing

$$\theta_i = 1 \text{ if } \left(a_{11} - \frac{U^2}{a^2}\right) < 0$$

$$= 0 \text{ if } \left(a_{11} - \frac{U^2}{a^2}\right) > 0 \quad .$$

The first term in Eq. (5) corresponds to the supersonic marching operator and the second term is the subsonic operator. By using a local linearization procedure, Eq. (5) can be expressed in terms of ϕ only. Details of the procedure are given in Refs. 4 and 5.

Treatment of $\partial/\partial\eta\ (\rho\ V/J)$ Term

$$\frac{\partial}{\partial\eta}\left(\rho\,\frac{V}{J}\right) = \theta_{i+1}\,\frac{\vec{\delta}}{\partial\eta}\left(\bar{\rho}\,\frac{V}{J}\right)_{j+1/2}$$

supersonic

$$+ (1 - \theta_{i+1})\,\frac{\overleftarrow{\delta}}{\partial\eta}\left(\bar{\rho}\,\frac{V}{J}\right)_{j+1/2} \qquad (6)$$

marching subsonic

When $\theta_{i+1} = 1$, that is, the point is supersonic with respect to ξ, only the first term in Eq. (6) is used and the biased density $\bar{\rho}$ is defined by (for $V > 0$)

$$\bar{\rho}_{j+1/2} = (1 - \bar{\nu}_{j+1/2})\rho^*_{j+1/2} + \frac{1}{2}\,\bar{\nu}_{j+1/2}(\rho^*_j + \rho^*_{j-1}) \qquad (7)$$

where $\bar{\nu} = \max\left(0,\ 1 - a_{22}\,\frac{a^2}{V^2}\right)$.

In Eq. (7), the evaluation of ρ^* depends on whether the flow is conical or nonconical. For conical flows, all ρ^* quantities are evaluated at the i^{th} plane. For nonconical flows, at each nonconical marching plane, initially ρ^* is set to be the value at the i^{th} plane and then subsequently iterated to convergence by setting ρ^* to the previous iterated value of ρ at the current $i+1$ plane.

When the point is elliptic in the marching direction, the density biasing is defined by

$$\overset{=}{\rho}^{n+1}_{j+1/2} = (1 - \overset{=}{\nu}_{J+1/2})\rho^{n}_{j+1/2} + \frac{1}{2}\overset{=}{\nu}_{j+1/2}\,(\rho^{n}_{j} + \rho^{n}_{j-1}) \tag{8}$$

where $\overset{=}{\nu} = \max(0,\ 1 - \frac{a^2}{q^2})$. As before, the superscript n+1 denotes the current relaxation cycle for subsonic bubble calculation. Note the difference in the definition of $\bar{\nu}$ and $\overset{=}{\nu}$. The density biasing in the cross-flow direction η is turned off when the total velocity, q, is less than the speed of sound a. The implicit treatment of V in the marching subsonic operator of Eq. (6) is the same as that of the supersonic part, explained in Reference 5.

A similar procedure is implemented for $(\rho \frac{W}{J})_{\xi}$ term in Eq. (1).

Implicit Factorization Algorithm

Combining the various terms of Eq. (1) as represented by Eqs. (5)-(8) together with the terms arising from $(\rho \frac{W}{J})_{\xi}$ will result in a fully implicit model. This is solved using an approximate factorization implicit scheme. After some rearrangement of the terms, the factored implicit scheme becomes

$$\left[1 + \frac{A_3}{B\Delta\zeta}\frac{\partial}{\partial\xi} + \frac{1}{\beta}\frac{\partial}{\partial\xi}\left(\frac{\hat{\rho}}{J}\frac{a_{31}}{\Delta\zeta}\right) + \frac{1}{\beta}\frac{\partial}{\partial\xi}\frac{\hat{\rho a}_{33}}{J}\frac{\partial}{\partial\xi}\right]$$

$$\times \left[1 + \frac{A_2}{B\Delta\zeta}\frac{\partial}{\partial\eta} + \frac{1}{\beta}\frac{\partial}{\partial\eta}\left(\frac{\hat{\rho a}_{21}}{J\Delta\zeta}\right)\right.$$

$$\left. + \frac{1}{\beta}\frac{\partial}{\partial\eta}\frac{\hat{\rho a}_{22}}{J}\frac{\partial}{\partial\eta}\right]\Delta\phi = R \quad . \tag{9}$$

The density $\hat{\rho}$ appearing in Eq. (9) can be either $\bar{\rho}$ or $\overset{=}{\rho}$ depending on the sign of $(a_{11} - \frac{U^2}{a^2})$ as illustrated in Eq. (6).

Equation (9) has the form $L_{\xi}L_{\eta}(\Delta\phi) = R$ and it is implemented as follows:

$$L_\xi(\Delta\phi)^* = R,\ L_\eta(\Delta\phi) = (\Delta\phi)^*,\ \phi_{i+1} = \phi_i + \Delta\phi \quad .$$

INITIAL CONDITIONS

For a pure supersonic flow, initial conditions are required at the starting plane. Usually, the starting plane is set close to the nose region of the configuration. For a sharp nosed configuration, conical solutions are prescribed, and for a blunt nose, the axisymmetric unsteady full potential solver of Reference 8 is used to obtain flow field in the transonic forebody region.

In the embedded subsonic region, when Eq. (5) is applied at an i+1 grid point, information on the flux ρU at i+2 is required. For the first relaxation pass, sonic conditions are assumed at i+2.

$$\rho_{i+2} = \rho^* = \left(\frac{2}{\gamma+1} + \frac{\gamma-1}{\gamma+1} M_\infty^2\right)^{1/\gamma-1}$$

$$U_{i+2} = q^* \, (a_{11})_{i+2}^{1/2} \tag{10}$$

where

$$q^* = [\rho^{*\gamma-1}/M_\infty^2]^{1/2}$$

The sonic values ρ^* and q^* are purely a function of the free-stream Mach number M_∞. For the second relaxation cycle and onwards, the conditions from the previous relaxation cycle is used.

BOUNDARY CONDITIONS

In order to solve the full potential equation, it is essential to specify appropriate boundary conditions on the body surface and at the outer boundary.

1. Body Surface

At a solid boundary, the contravariant velocity V is set to zero. Exact implementation of V = 0 in the implicit treatment of Eq. (9) is described in Reference 4.

2. Outer Boundary

The outer boundary is set away from the bow shock and the free-stream velocity potential ϕ_∞ is imposed along that boundary. All discontinuities in the flow field are captured. The precise density biasing activator, ν, based on the characteristic theory, allows for sharp capturing of shocks in the flow.

3. Symmetric Boundary Conditions

For yaw angle $\beta = 0$, only the half plane problem needs to be solved with the plane of symmetry boundary conditions imposed along K = 2 and (KMAX - 1), as shown in Fig. 2a. Imposing that the flow conditions along K = 1 are to be the same as the ones along K = 3, the L_ξ operator results in a tridiagonal system that can be easily solved.

4. Combined Yaw and Angle of Attack

Even for a symmetric configuration, when yaw angle is present the entire cross-flow plane needs to be solved as shown in Fig. 2b. In this case the flow conditions along K = 1 are set to be the same as the ones along K = (KMAX - 2). This destroys the tridiagonal nature of the L_ξ operator. A special routine has been developed to invert a matrix of the following type.

$$L_\xi = \begin{vmatrix} X & X & & & X & 0 \\ X & X & X & & 0 & 0 \\ & X & X & X & & 0 \\ & & & & & \\ 0 & 0 & & X & X & X \\ 0 & X & & & X & X \end{vmatrix} \qquad (11)$$

In the current formulation, positive angle of attack α represents a positive Cartesian velocity v in the free-stream and similarly positive yaw β produces a positive w in the free-stream. When both angle of attack and yaw are present, first the free-stream is turned by an angle β and then by α.

The normalized free stream velocity potential is given by

$$\phi_\infty = x \cos\alpha \cos\beta + y \sin\alpha + z \cos\alpha \sin\beta \tag{12}$$

The lift and drag forces are represented by

$$D = F_x \cos\alpha \cos\beta + F_y \sin\alpha + F_z \cos\alpha \sin\beta$$

$$L = -F_x \sin\alpha \cos\beta + F_y \cos\alpha \tag{13}$$

5. Swept Trailing Edge Wake Treatment

Figure 3 shows a schematic of a swept trailing edge wake system. In order to treat the region behind the trailing edge, an artificial cut is created and the pressure jump [p] across this cut is imposed to be zero as a boundary condition. This is achieved by maintaining the jump in the velocity potential ϕ along a k = constant line (see Fig. 3) for j = 2 to be the same as the value $[\phi]$ at the trailing edge. The full potential equation is not solved at grid points on the wake cut. Instead, $\phi_{\eta\eta} = 0$ is solved to provide $[\phi_\eta] = 0$ across the wake cut. Maintaining $[\phi]$ constant along a k line provides $[\phi_\zeta] = 0$. The combination of $[\phi_\zeta] = 0$ and $[\phi_\eta] = 0$ across the cut satisfies $[p] = 0$ approximately.

6. Geometry and Grid System

The geometry of a configuration is prescribed at discrete points in a crossplane (usually x = constant plane) at various axial locations. These geometry input points are usually obtained from a geometry package such as the GEMPACK or CDS. The input points are then divided into several patches, and at each patch a key-point system is established as shown in Fig. 4. The geom-

etry at a marching plane is then obtained by joining the appropriate key-point for each patch, as shown in Fig. 5. Using a cubic spline passing through the key points, a desired grid point distribution (clustering) is set up on the body surface. Then, using an appropriate outer boundary, the grid for the flow-field calculation is generated by using an elliptic grid generator.[9]

II. CODE ORGANIZATION

The program is written in FORTRAN language. It can be executed on any CDC machine (Cyber 176, CDC 7600), as well as on the Cray 1. At present, the code is not optimized for a vector machine like the Cray or Cyber 205. for a cross-plane (η,ξ) grid of 30 x 60, the program requires a storage of 230,000 words octal. The program consists of a main routine and several subroutines. A brief description of the main program and other pertinent subroutines are given in this section.

Program Main

Program Main coordinates the entire operation. A flowchart describing the various operations performed by the Main program is given in Fig. 6. The Main program sets up the initial (known) data plane and the body-fitted grid system, and performs the L_ξ and L_η operators to advance the solution. The marching step size $\Delta\zeta$ can either be prescribed or computed at each marching plane from a given Courant number and the maximum eigenvalue. The various read and write tapes used in the calculation are listed below.

Program Main (Tape 1, Tape 2, Tape 3, Tape 4, Tape 5, Tape 7, Tape 8, Output, Tape 6 = Output)

Tape 1: Output solutions for plot.
Tape 2: Output solutions for restart.
Tape 4: Output solutions for restart.
Tape 3: Read in starting solutions.
Tape 5: Input data.

Tape 6: Solution output.

Tape 7: Read tape containing solutions for subsonic region.

Tape 8: Write tape for subsonic bubble calculation.

Subroutine EIGEN (EIGENY, EIGENZ)

This subroutine computes the maximum eigenvalue EIEGNY in the (ζ,η) plane and the maximum eigen value EIGENZ in the (ζ,ξ) plane. The expression used for calculating the eigenvalue is given in Ref. 5. The maximum eigenvalue information is then used to compute a marching step-size $\Delta\zeta$ for a specified Courant number.

Subroutine NFORCE (PX, PY, PM, AREA, KG)

At the end of each marching plane calculation, this subroutine computes the axial force, PX, vertical force, PY, and the side force, PM, by integrating the pressure force acting on an elemental area, dA. The elemental area, dA, is computed from the transformation matrice using the formula (at a body point j = 2)

$$dA = \{[y_\zeta z_\xi - z_\zeta y_\xi]^2 + [x_\xi z_\zeta - x_\zeta z_\xi]^2 + [y_\xi x_\zeta - y_\zeta x_\xi]^2\}^{1/2} \, d\zeta d\xi \, .$$

KG = 0, conical or blunt body nose force calculation

= 1, rest of the body force calculation.

The program also prints the C_L and C_D information based on a prescribed reference area, and C_M about a given reference point (X_0, Y_0).

Subroutine GEOM (N9, NRP)

N9 = 0, geometry data at X_1 are read in

= 1, geometry data at X_1 are updated

NRP = 0, X-plane geometry calculation

= 1, spherical plane geometry calculation.

Subroutine GEOM sets up the body grid points from a prescribed geometry shape. As illustrated in Fig. 4, the geometry is input in different patches (the number of patches to be used is left to the discretion of the user). From the input geometry points, a key point system is established using cubic splines. These key points are then joined from one prescribed geometry station to the other to provide the geometry at any intermediate marching plane. A flowchart describing GEOM is given in Fig. 7.

Subroutine Grid

Once the body points are obtained at a marching plane from GEOM, subroutine GRID sets up the entire crossflow plane grid using an elliptic grid solver that satisfies certain grid constraints. Figure 8 gives the flowchart for GRID.

Subroutine Metric

This subroutine computes all the necessary transformation metrics and Jacobians at various node and half node locations as required by the solution algorithm (L_ξ and L_η operators).

Subroutine UVW

This subroutine computes all the contravariant velocities U, V and W, and the density ρ.

Subroutine RHOBIAS

This subroutine performs the density biasing in the (η,ξ) plane based on a characteristic theory. This operation is essential to treat crossflow supersonic regions and to capture shock waves.

III. INPUT DATA

Input data includes specifications of flow parameters, grid parameters, read and write tape parameters, and geometry data in patches at various

axial stations. A sample inut is presented here.

Input cards 1 through 45 are self-explained. The rest of the input cards are explained below.

	Format	Symbol	Description
Card 46			
Col. 1-80	10F8.4	ZTAPT(10)	Location of detail flow field printout
Card 47			
Col. 1-5	I5	ISC	Number of patch (geometry)
Card 48			
Col. 1-50	10I5	NPT (10)	Number of output points in each patch
Card 49			
Col. 1-15	F15.6	X1	x location at which the geometry cross-section is given.
Col. 16-20	I5	ISC1	Number of input patch at this location
Card 50			
Col. 1-5	I5	ITH	Patch number
Col. 6-10	I5	IPT	Number of input points
Col. 11-15	I5	ND	Clustering control parameter 0: equal space 1: clustering at the beginning of the patch 2: clustering at the end of patch
Card 51			
Col. 1-15	F15.6	y	y-value
Col. 16-30	F15.6	z	z-value

SAMPLE INPUT

```
100-   120        NMAX    I5      NO. OF STREAMWISE STEP.
110-    20        JMAX            NO. OF POINT IN NORMAL DIR.
120-    26        KMAX            NO. OF POINT IN CIRCUM. DIR.
130-    20        JMAXO           OLD JMAX FOR RESTARTING.
140-    26        KMAXO           OLD KMAX FOR RESTARTING.
150-    17        KTEMP           K AT MAX Z
160-     2        NRM             NO.DOFEGRIDNSECTION.
170-    10        NU0             K FOR FIRST SECTION GRID IF NRM>2
180-    05        NP              OUTPUT FOR EVERY NP STEPS.
190-     1        KWKCTR          1:WAKE IS CONTROL BY K; 2:BY Z
200-    18        KWKST           WAKE START PT.
210-    36        KWKED           WAKE END PT.
220-    30        NCON            INITIAL CONICAL DATA ITERATIONS,
230-    30        NITER           NO. OF ITERATION FOR GRID.
240-     2        NSPTI           NO. OF PTS FOR ENTIRE FLOW FIELD OUTPUT.
250-     2        ITERGN          NEW THT USED AFTER NO. OF GLOB ITERATION.
260-     1        ITERGE          NO. OF GLOB ITERATION.
270-   999        KLE             NOT USED
280-   1.4        FSM    F10.5    FREE STREAM MACH NO.
290-  -1.94       ALFA            ANGLE OF ATTACK.
300-    70.       THTO            OUTER BOUNDARY. (DEGREE)
310-   0.1        DETA            STEP SIZE IN ETA DIR.
320-   0.1        DXI             STEP SIZE IN XI DIR.
330-   3.00       DZTA            STEP SIZE IN ZTA DIR. (STREAM)
340-   400.000    ZTA1            STARTING X LOCATION.
350-  1200.0      XEND            LAST X LOCATION.
360-    1.75       SWEEP           NOT USED.
370-    1.         AMU1            1:1ST ORDER,2:2ND ORDER ACCURATE.
380-    0.         AMU2            0:1ST ORDER,1:2ND ORDER ACCURATAXE.
390-   1500.0      XWAKE           WAKE START LOCATION.(X)
400-    0.188      ZWAKE           WAKE START LOCATION.(Z)
410-    001.       CHL             CHARACTERISTIC LENGTH
420-    -26.8      PTNOSE          NOSE LOCATION.(X)
430-    0.627      XM0             REF. X POINT FOR PITCH MOMENT.
440-    0.0        YM0             .....Y .....  ..............
450-    0.186      AAA             REF. AREA.
```

```
460-    0.291    ALL              REF. LENGTH FOR PITCH MOMENT.
470-    1.75     OMEGA            RELAXIATION FACTOR.
480-     T       PLANEOS          NOT USED.
490-     T       NUGRID    L3     NUMERICAL GRID GENERATION?
500-     T       IREAD            T:INPUT BODY GEOM;F:ANALYTIC GEOM.
510-     F       RPLANE           R-MARCHING
520-     T       TAPER            RESTART DATA FROM TAPE?
530-     T       TAPEW            WRITE RESTART DATA ON UNIT 2 & 4
540-     T       FORCE            DO FORCE CALCULATION
550-100.     200.0    300.0    400.0    500.0    600.0
560-     5       ISC              NO. OF PATCH. (GEOMETRY)
570-    04   05   05   06   08
580- 338.81                5
590-     1    4    0
600-   100.34                    0.00
610-    95.99                   30.83
620-    87.52                   58.14
630-    74.35                   74.08
640-     2    5    0
650-    74.35                   74.08
660-    63.18                   84.63
670-    52.29                   95.44
680-    44.26                  101.59
690-    36.22                  105.18
700-     3    5    0
710-    36.22                  105.18
720-    11.73                  105.62
730-    -9.88                  105.62
740-   -35.18                  105.62
750-   -65.87                  103.07
760-     4    3    2
770-   -65.87                  103.07
780-   -78.54                  109.55
790-   -90.72                  112.20
800-     5    7    1
810-   -90.72                  112.20
820-   -99.15                  110.39
```

PATCH I

PATCH II

PATCH III

PATCH IV

PATCH V

INPUT CROSS-SECTION AT X=388.81

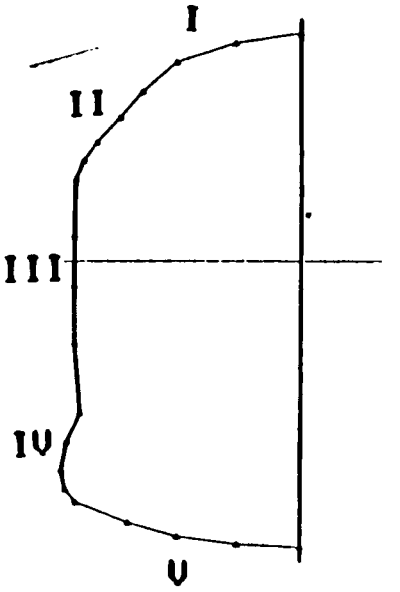

```
830-  -104.90                105.46
840-  -113.79                 80.81
850-  -119.75                 57.81
860-  -123.31                 30.04
870-  -124.64                  0.00
880-  387.41                5
890-     1     3     0
900-    99.47                  0.00
910-    95.81                 29.21
920-    89.47                 53.41
930-     2     5     0
940-    89.47                 53.41
950-    79.11                 75.76
960-    61.71                 98.21
970-    52.94                103.83
980-    44.11                105.70
990-     3     4     0
1000-    44.11               105.70
1010-    -8.94               106.05
1020-   -36.99               106.40
1030-   -63.82               108.84
1040-    4     5     2
1050-   -63.82               108.84
1060-   -76.69               116.04
1070-   -87.81               119.41
1080-   -96.76               119.20
1090-  -106.24               112.73
1100-    5     6     1
1110-  -106.24               112.73
1120-  -109.89               105.76
1130-  -112.21                92.84
1140-  -121.50                63.21
1150-  -125.54                30.98
1160-  -126.72                 0.00
1170-  454.23                5
1180-    1     3     0
1190-   99.47                  0.00
```

OUTPUT CROSS-SECTION AND GRID AT X=400

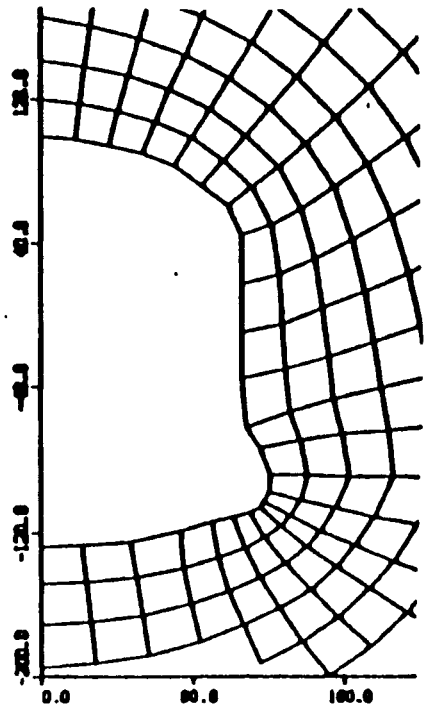

SAMPLE OUTPUT

ITER= 1 DZTA= 3.00000 ZTA1= 410.41814

J	K	RHO	CP	PHI	U	V	W	X	Y	Z
2	1	1.082483	.085533	368.148453	0.000000	0.000000	0.000000	410.418140	157.540064	-11.436041
2	2	1.091121	.094845	368.052851	.953648	0.000000	0.000000	410.418140	168.981000	0.000000
2	3	1.082483	.085533	368.148463	.957929	0.000000	.000123	410.418140	157.540064	11.436041
2	4	1.065946	.068168	368.308630	.966106	0.000000	.000219	410.418140	156.111638	22.871964
2	5	1.044297	.045508	368.727952	.976818	0.000000	.000303	410.418140	154.017090	34.187025
2	6	1.023306	.023802	369.182420	.986914	0.000000	.000424	410.418140	151.097415	45.337222
2	7	1.008144	.008147	369.852573	.997365	0.000000	.000621	410.418140	147.823567	56.373895
2	8	.955528	-.044971	370.828713	1.010527	0.000000	.000939	410.418140	143.631000	67.110000
2	9	.915739	-.084567	371.684815	1.037524	0.000000	.001311	410.418140	139.491203	74.289388
2	10	.883163	-.116377	372.629158	1.053169	0.000000	.001455	410.418140	135.167265	81.359857
2	11	.861988	-.136827	373.881636	1.062300	0.000000	.001651	410.418140	130.466393	88.182320
2	12	.847083	-.150250	374.888474	1.066703	0.000000	.001906	410.418140	125.122754	94.507390
2	13	.845543	-.152680	376.282041	1.065180	0.000000	.002147	410.418140	118.962725	100.037776
2	14	.850190	-.148133	377.772114	1.061968	0.000000	.002207	410.418140	111.716041	103.934170
2	15	.860942	-.129165	379.232969	1.058410	0.000000	.001888	410.418140	103.621000	105.700000
2	16	.874617	-.124649	381.091440	1.058399	0.000000	.000731	410.418140	87.084271	105.847319
2	17	.900271	-.099692	382.989192	1.045774	0.000000	.000732	410.418140	70.547191	105.994642
2	18	.923198	-.077147	384.613520	1.036304	0.000000	.000612	410.418140	54.010120	106.141958
2	19	.950344	-.050161	385.620213	1.024012	0.000000	.000496	410.418140	37.473086	106.289545
2	20	.946284	-.054207	386.377658	1.026787	0.000000	.000444	410.418140	20.935999	106.425505
2	21	.941654	-.058833	386.866847	1.029816	0.000000	.000319	410.418140	4.399613	106.230860
2	22	.946894	-.054487	386.694503	1.027286	0.000000	.000349	410.418140	-12.136424	106.000000
2	23	.959595	-.040894	386.974480	1.017431	0.000000	.000124	410.418140	-18.592232	119.448326
2	24	.978304	-.021031	388.196697	.991048	0.000000	.000089	410.418140	-30.633516	129.977876
2	25	.985104	-.015155	389.715170	.996016	0.000000	.001287	410.418140	-43.400110	122.912745
2	26	.995427	-.005060	390.759384	.998154	0.000000	.000837	410.418140	-50.448659	109.238657
2	27	.987780	-.012439	391.425802	1.003557	0.000000	.000403	410.418140	-55.358001	94.662599
2	28	.998556	-.001473	391.899897	.999084	0.000000	.000337	410.418140	-58.924438	81.403841
2	29	1.024813	.025444	392.221493	.986532	0.000000	.000230	410.418140	-62.490417	68.204936
2	30	1.026163	.026836	392.339406	.986365	0.000000	.000130	410.418140	-64.291899	54.632023
2	31	1.014509	.014848	392.328706	.992385	0.000000	.000078	410.418140	-65.838708	41.018623
2	32	1.019308	.019778	392.350656	.990419	0.000000	.000065	410.418140	-66.985000	27.373132
2	33	1.024350	.024977	392.386412	.987488	0.000000	.000039	410.418140	-67.619499	13.686654
2	34	1.028849	.029604	392.413489	.985085	0.000000	0.000000	410.418140	-68.247628	0.000000
2	35	1.024359	.024977	392.386412	0.000000	0.000000	0.000000	410.418140	-67.619499	-13.686654

J	K	RHO	CP	PHI	U	V	W	X	Y	Z
1	2	1.100731	.104817	367.909457	0.000000	0.000000	0.000000	410.418140	147.455536	0.000000
2	2	1.091121	.094845	368.052851	.953648	0.000000	0.000000	410.418140	168.981000	0.000000
3	2	1.100731	.104817	367.909457	.948370	-.000226	0.000000	410.418140	170.506465	0.000000
4	2	1.090524	.103638	367.383143	.948279	-.000355	0.000000	410.418140	183.330164	0.000000
5	2	1.077825	.090631	366.670066	.969093	-.000384	0.000000	410.418140	197.598332	0.000000
6	2	1.026877	.026541	365.873568	.985685	-.000384	0.000000	410.418140	213.473674	0.000000
7	2	.996633	-.003434	365.088734	1.001008	-.000371	0.000000	410.418140	231.137222	0.000000
8	2	.987749	-.012471	364.466279	1.006007	-.000354	0.000000	410.418140	250.796482	0.000000
9	2	.977198	-.023161	364.162812	1.011639	-.000353	0.000000	410.418140	272.657327	0.000000
10	2	.967420	-.033027	364.285392	1.016640	-.000420	0.000000	410.418140	296.987354	0.000000
11	2	1.014720	.015064	364.379894	.992492	-.000523	0.000000	410.418140	324.057927	0.000000
12	2	1.057717	.059567	364.410100	.970455	-.000573	0.000000	410.418140	354.177745	0.000000
13	2	1.083725	.086841	365.505553	.956238	-.000602	0.000000	410.418140	387.690275	0.000000
14	2	1.104822	.109159	367.752940	.944226	-.000672	0.000000	410.418140	424.977674	0.000000
15	2	1.107506	.112010	370.884531	.941858	-.000784	0.000000	410.418140	466.465145	0.000000
16	2	1.078436	.079171	374.847869	.958455	-.000971	0.000000	410.418140	512.625787	0.000000

IV. OUTPUT DATA

The program provides an output of the flowfield after every NP marching steps (NP is user specified). A small portion of the output is presented here. It provides the flow variable information (density, C_p, ϕ, contravariant velocities, U, V and W, and the grid point location x, y and z) along the body surface (J = 2) and along the planes of symmetry (K = 2 and KMAX-1). Besides this printout for every NP marching steps, the code also prints the Courant number and maximum eigenvalues in the η and ξ crossflow directions, and the rms change in density. A detailed output of the entire flowfield in the crossplane (η,ξ) for all J and K can also be obtained at selected marching plane locations prescribed by the user in the input at card number 46 (see Section III).

The code also stores the results for plotting purposes in Tape 1, and a separate plotting package is used to plot contours and other forms of visual output.

V. RESULTS

Four cases are presented to illustrate the capability of the code.

1. Flow over an arrow-wing body at M_∞ = 2.96. α = 10.01°.
2. Flow over a forebody configuration at M_∞ = 2.5, β = 5° and at M_∞ = 1.7, α = 10°, β = 5°.
3. Flow over the entire Shuttle Orbiter geometry at M_∞ = 1.4, α = 0°.
4. Flow over a realistic fighter configuration at different angles of attack and free-stream Mach numbers.

For an attached shock at the nose (pointed nose configurations), a conical solution is generatd and used as an initial data plane for the nonconical marching calculation. If the nose is blunt and has a detached shock, then an unsteady full potential code[8] is used to generate the initial blunt

body solution (free-stream Mach number less than 1.5 is recommended). This initial flow calculation usually takes 40 to 60 iterations. At the beginning of each marching plane calculation, the grid is generated using an elliptic grid solver. Usually, the grid solver requires 30 relaxation cycles to provide an acceptable grid distribution.

Figure 9 shows the pressure distribution on the surface of an arrow-wing configuration at location $x/\ell = 0.8$ for $M_\infty = 2.9$, and $\alpha = 10°$. The improvement in the prediction capability achieved using the wake treatment is illustrated. The dashed line represents the result from "no wake" treatment (assumes a flat plate behind the trailing edge) and the solid line represents the modifications to the pressure distribution once a zero jump in pressure across the wake cut is imposed. The solid line pressures on the body agree very well with experiments.[10] Without a proper wake cut treatment, the overall lift and drag forces and the pitching moment can be off by a considerable margin.

Figure 10 presents the pressure distribution on a fully developed forebody[11] for $M_\infty = 2.5$ and yaw angle $\beta = 5°$. Figure 11 shows the circumferential pressure distribution for the same body at $x/\ell = 0.68$ for $M_\infty = 1.7$, $\alpha = 10°$ and $\beta = 5°$. The experimental data[11] are also given in these two figures. The results show that the present prediction is in excellent agreement with the experimental data.

Figures 12 to 22 give the geometry and the corresponding flow field solutions for the Shuttle Orbiter. The side view, cross-section and grid in the nose region are given in Fig. 12. The top view, cross-section, grid and chordwise cross-sections are presented in Fig. 13. It should be mentioned here that for most of the previous Space Shuttle calculations[12,13] the geometry has been modified by smoothing out the canopy and increasing the wing sweep angle from 45 to 55 degrees in order to avoid the subsonic bubble. Since the present method is valid for supersonic flow with embedded subsonic region, the realistic Shuttle Orbiter geometry was used without any modification.

Figure 14 shows the surface pressure distribution along the leeward

plane of symmetry. At x ≅ 170 in. which is the beginning of the canopy, the pressure increases rapidly from $C_p \cong 0.3$ to 1.0, approximately. In the canopy region an MSR/TSR is formed and required three relaxation cycles to develop the solution. The circumferential surface pressure distribution at x = 240 in. is shown in Fig. 15. The experimental data is also given in these figures and the agreement is very good. The surface pressure distribution along the wing leading edge is given in Fig. 16. It is seen that the present calculation agrees with the experimental data quite well along the entire wing leading edge except in the vicinity of the wing-fuselage junction, where a vortex flow may exist.

Figure 17 to Figure 21 present the Orbiter chordwise pressure distribution on the upper and lower wing surface at $\bar{z} = z/bw = 0.471$, 0.530, 0.641, 0.780 and 0.887, respectively where bw is a semispan defined in Fig. 12. The results show that the present predictions are in very good agreement with the experimental data, except in the region near the trailing edge of the upper surface at $\bar{z} = 0.471$ and 0.53 span stations. Here again, a vortex flow or separation may be causing the discrepancies. Figure 22 shows the circumferential pressure distribution for the Orbiter at x = 1120 in. It is noted that the pressure at the vertical tail and OMS pods are well predicted.

Figure 23 shows a supersonic fighter configuration with vertical tails. The free-stream Mach number, angle of attack and wing sweep angle for the calculation are summarized in Table 1.

Figure 24 presents the surface pressure at various axial stations and the corresponding grid distribution for the wing body geometry. For this case, the MSR/TSR starts around x = 0.4 at the leading edge, and remains subsonic all the way to the end of the wing. Figure 25 and 26 show the circumferential pressure distribution in the vertical tail and wake region of the fighter-like configuration. The pressure on the vertical tail surface is given separately along the y-direction. The results clearly show that the present wake tretment provides the correct zero pressure jump condition across the wake. The chordwise pressure distributions from the center of the body to the tip of the wing are given in Fig. 27. Figure 28 presents the pressure contour on the upper and lower surface of the fighter configuration.

The lift and drag coefficients from the present calculations for this fighter model are also given in Table 1. The comparison with experimental data show excellent agreement.

VI. CONCLUSIONS

A nonlinear full potential method has been developed to analyze supersonic flows with embedded subsonic regions over some very complex configurations. A conservative switching scheme is employed to transition from the supersonic marching algorithm to a subsonic relaxation procedure. The predictions are in very good agreement with experiment data.

Work is now progressing to simulate the multibody interaction between the Shuttle Orbiter and the external tank, and canard-wing fighter geometries. The present methodology will also be extended to treat all Mach number flows (fully subsonic flow, as well as subsonic flow with pockets of supersonic region (transonic case)).

ACKNOWLEDGMENT

This work was partially supported by NASA-Langley Research Center under Contract NAS1-15820. The authors express their appreciation to Prof. Stanley Osher of UCLA for many valuable discussions.

REFERENCES

1. Jameson, A., "Transonic Potential Flow Calculations using Conservation Form," AIAA 2nd Computational Fluid Dynamics Conf. Proc., 1975, pp. 148-155.

2. Holst, T.L., "Fast, Conservative Algorithm for Solving the Transonic Full Potential Equation," AIAA Journal, Vol. 18, No. 12, December, 1980, pp. 1431-1439.

3. Siclari, M.J., "Computation of Nonlinear Supersonic Potential Flow over Three-Dimensional Surfaces," AIAA Paper No. 82-0167, presented at the AIAA 20th Aerospace Sciences Mtg., Orlando, Florida, January 1982.

4. Shankar, V., "A Conservative Full Potential, Implicit Marching Scheme for Supersonic Flows," AIAA Journal, Vol. 20, No. 11, November, 1982, pp. 1508-1514.

5. Shankar, V. and Osher, S., "An Efficient Full Potential Implicit Method Based on Characteristics for Analysis of Supersonic Flows," AIAA Journal, Vol. 21, No. 9, p. 1262, September, 1983.

6. Shankar, V., Szema, K.Y. and Osher S., "A Conservative Type-Dependent Full Potential Method for the Treatment of Supersonic Flow with Embedded Subsonic Regions," AIAA Paper No. 83-1887, July 1983.

7. Szema, K.Y. and Shankar, V., "Nonlinear Computation of Wing-Body-Vertical Tail-Wake Flows at Low Supersonic Speeds," AIAA Paper No. 84-0427, January, 1984.

8. Shankar, V., "Implicit Treatment of the Unsteady Full Potential Equation in Conservation Form," AIAA Paper No. 84-0262, January 1984.

9. Shankar, V., Rudy, S., and Szema, K.-Y., "Application of a Two-Dimensional Grid Solver for Three-Dimensional Problems," ASME Applied Mechanics, Bioengineering and Fluids Eng. Conf., Vol. No. G00222, June 20-22, 1983.

10. Townsend, J.C., "Pressure Data for Four Analytically Defined Arrow Wings in Supersonic Flow," NASA TM 81835, September 1980.

11. Townsend, J.C., Howell, D.T., Collins, I.K., and Hayes, C., "Surface Pressure Data on a Series of Analytic Forebodies at Mach Numbers from 1.7 to 4.50 and Combined Angles of Attack and Sideslip," NASA TM 80062, June 1979.

12. Maus, J.R., Griffith, B.J., Szema, K.Y., and Best, J.T., "Hypersonic Mach Number and Real Gas Effects on Space Shuttle Orbiter Aerodynamics," AIAA Paper No. 83-0343, January 1983.

13. Venkatapathy, E., Rakich, J.V., and Tannehill, J.C., "Numerical Solution of Space Shuttle Orbiter Flow Field," AIAA Paper No. 82-0028, January 1982.

14. Rockwell International Space Division Data.

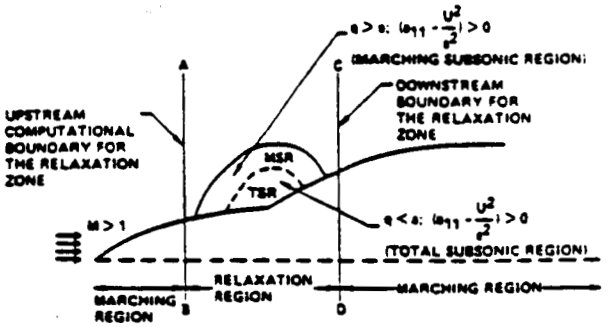

Fig. 1 Embedded subsonic bubble in a supersonic flow.

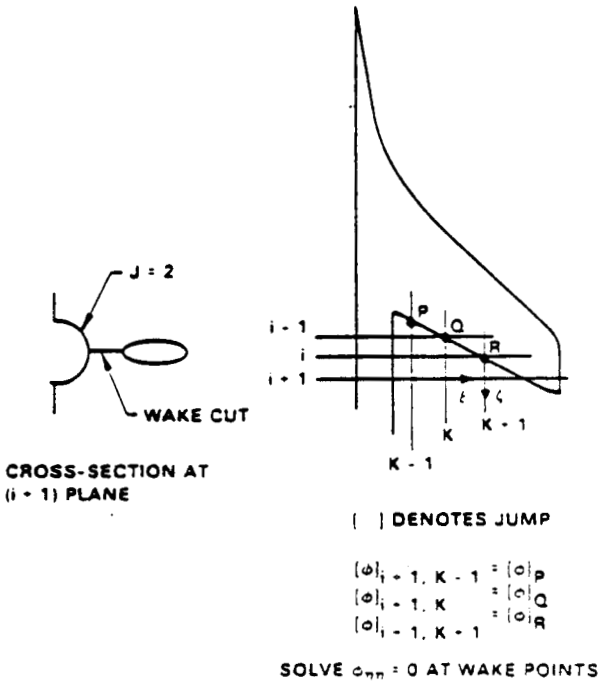

Fig. 3 Wake boundary condition.

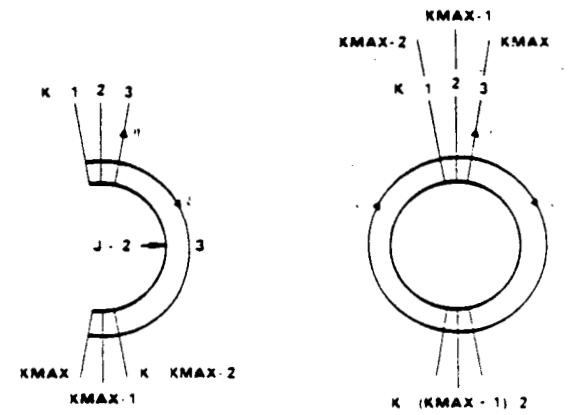

Fig. 2 Symmetry and periodic conditions.

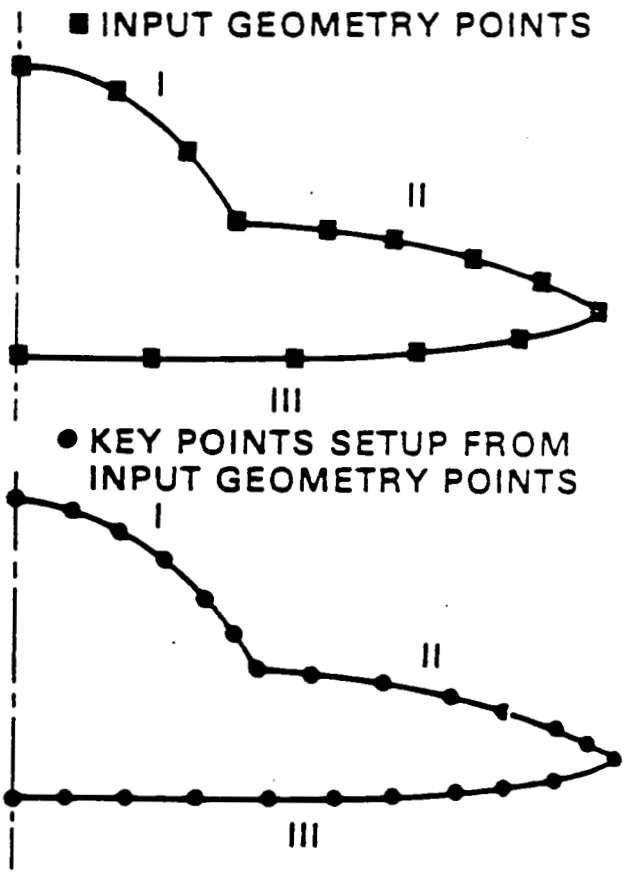

Fig. 4 Input geometry points and setup of key points.

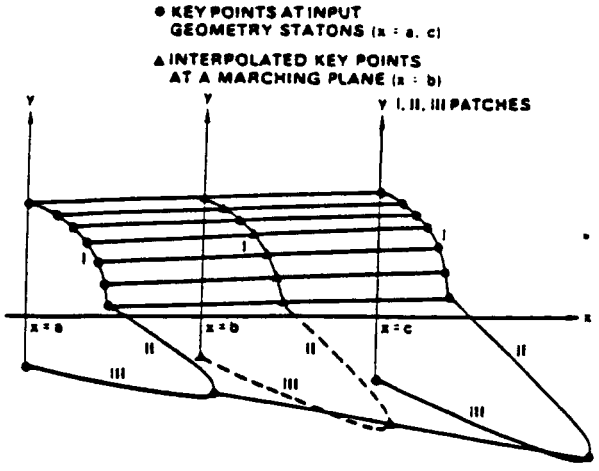

Fig. 5 Geometry setup.

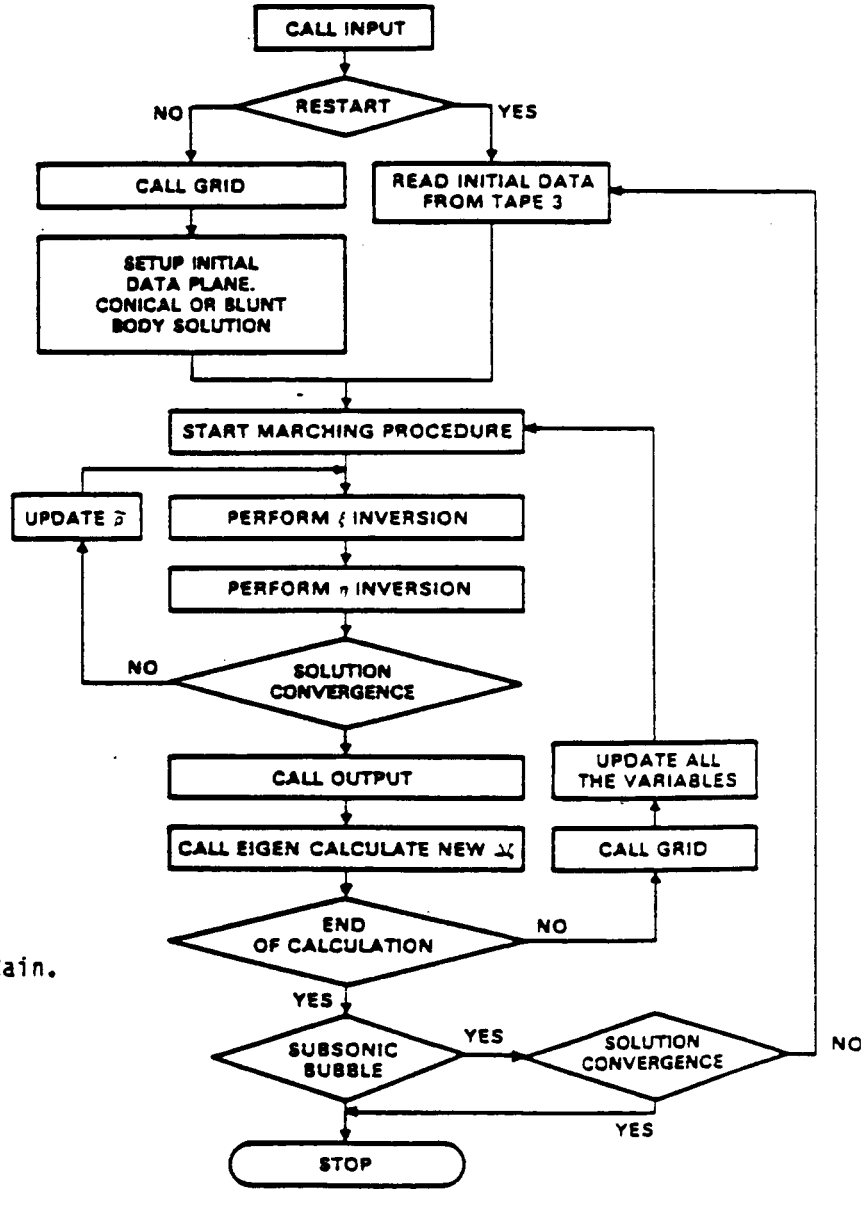

Fig. 6 Flowchart of program Main.

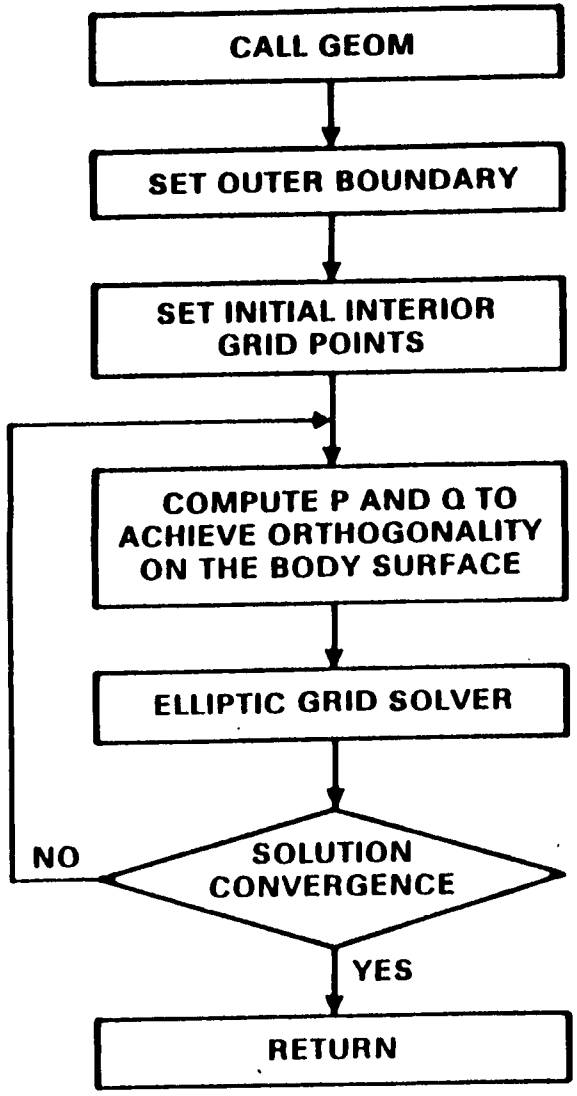

Fig. 7 Flowchart of subroutine GEOM.

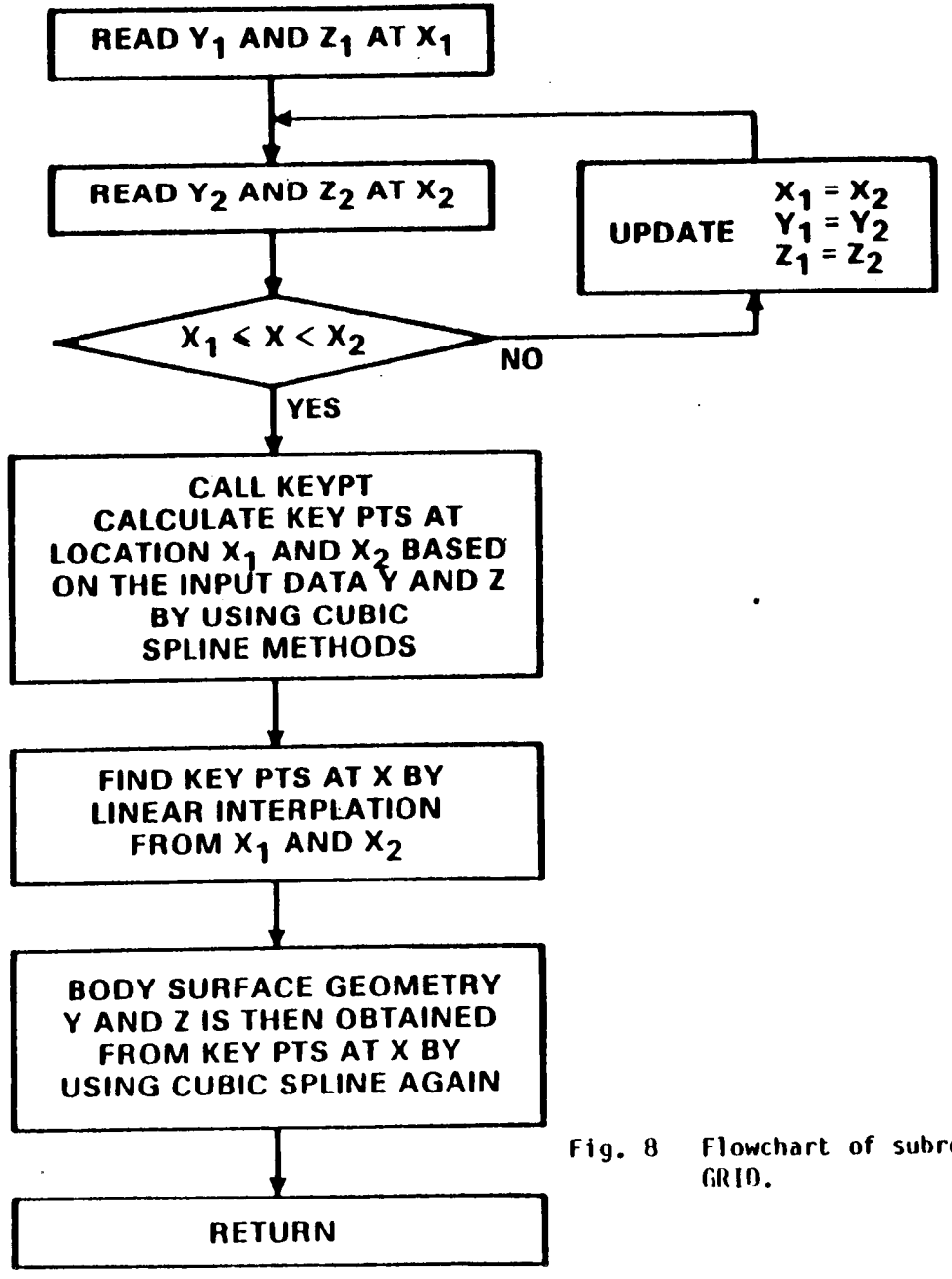

Fig. 8 Flowchart of subroutine GRID.

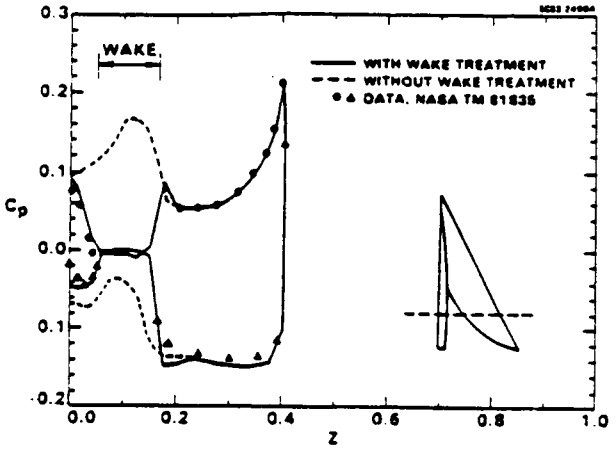

Fig. 9 Circumferential pressure distribution for the arrow-wing at $x/\ell = 0.81$, $M_\infty = 2.96$, $\alpha = 10°$.

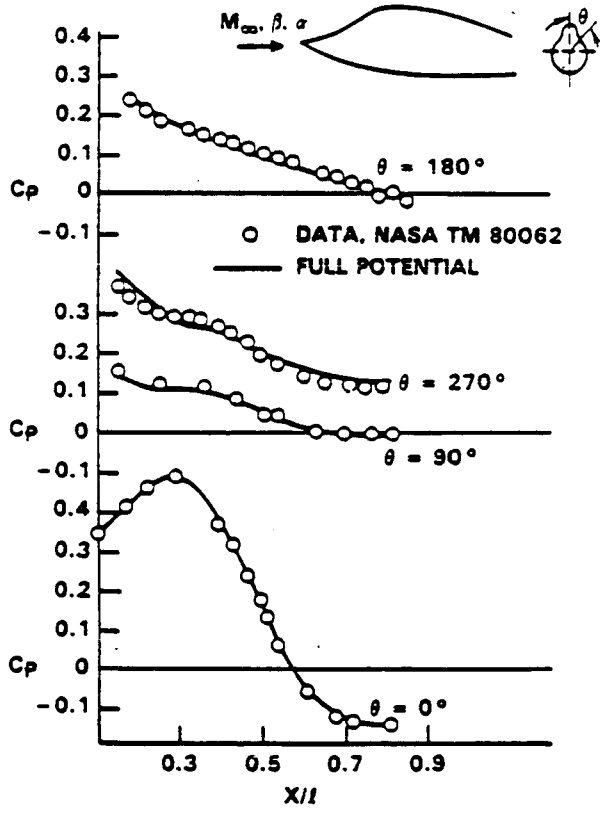

Fig. 10 Pressure distribution on a forebody in slideslip $M_\infty = 2.5$, $\beta = 5.02°$, $\alpha = 0°$.

ORIGINAL PAGE IS
OF POOR QUALITY

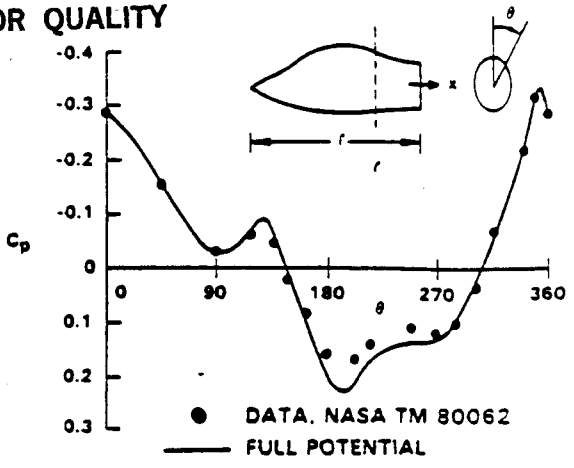

Fig. 11 Circumferential pressure distribution on a forebody at $x/\ell = 5.02°$, $\alpha = 0°$.

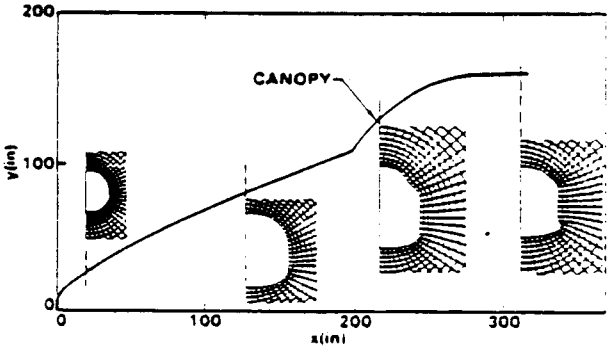

Fig. 12 Nose region geometry for Space Shuttle.

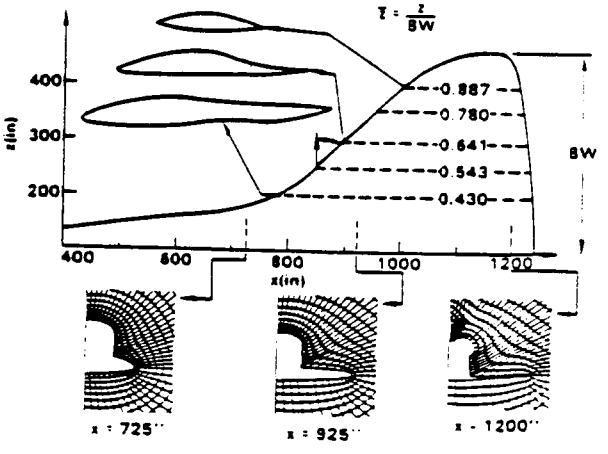

Fig. 13 Geometry and grid generation for Shuttle Orbiter at axial cuts.

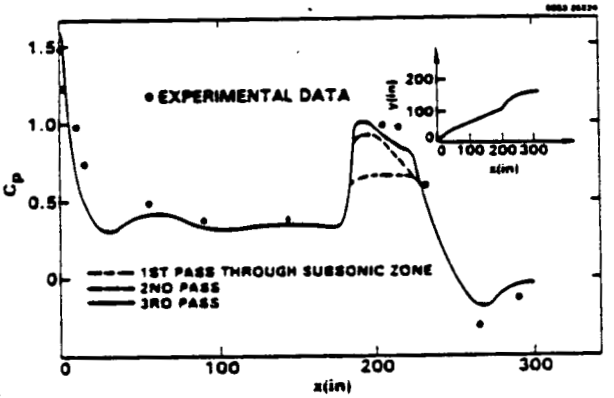

Fig. 14 Surface pressure distribution at leeward plane of symmetry.

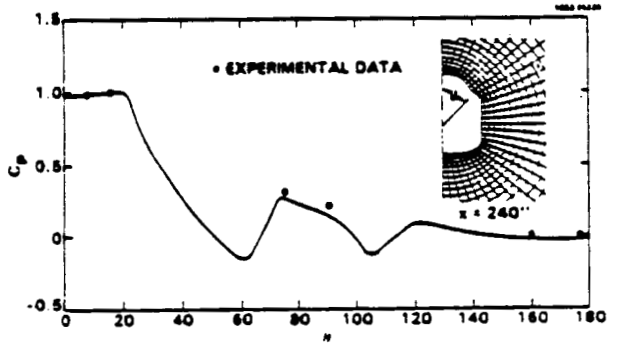

Fig. 15 Surface pressure distribution around the body.

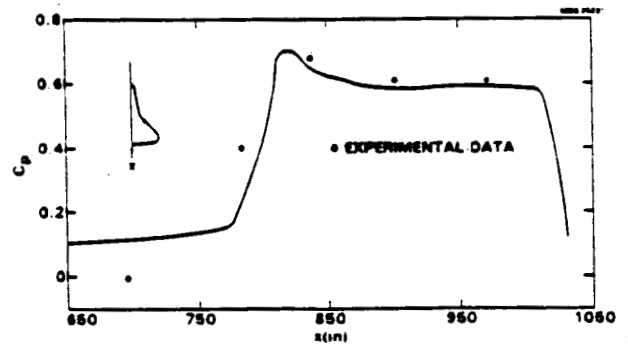

Fig. 16 Surface pressure distribution along the wing leading edge.

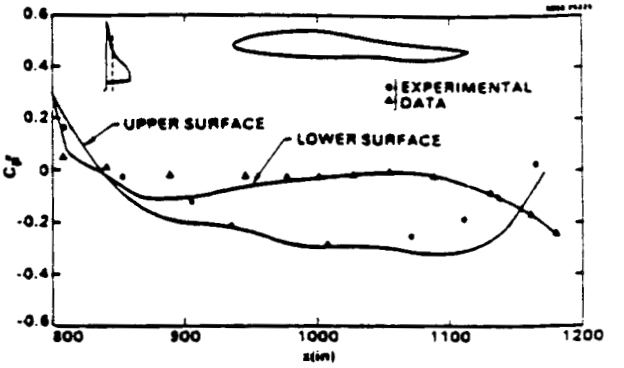

Fig. 17 Shuttle Orbiter chordwise pressure distribution; M_∞ = 1.4, α = 0.0°, $\bar{z}$ = 0.471.

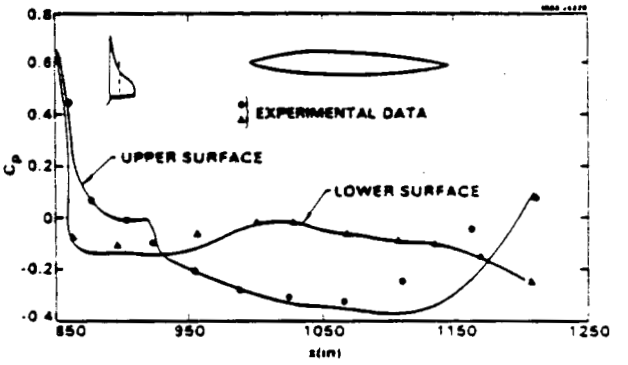

Fig. 18 Shuttle Orbiter chordwise pressure distribution; M_∞ = 1.4, α = 0.0°, $\bar{z}$ = 0.53.

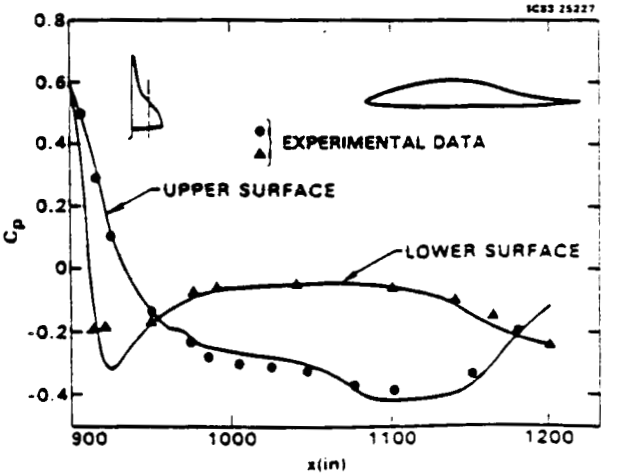

Fig. 19 Shuttle Orbiter chordwise pressure distribution; M_∞ = 1.4, α = 0.0°, $\bar{z}$ = 0.641.

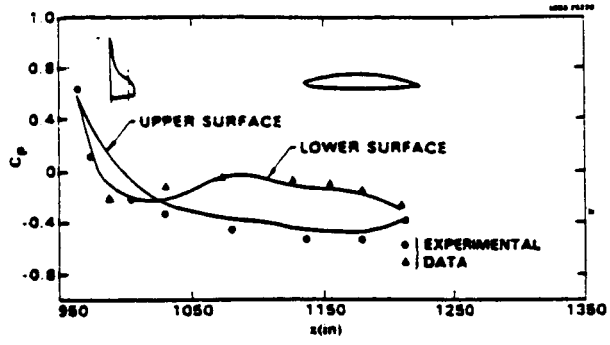

Fig. 20 Shuttle Orbiter chordwise pressure distribution; M_∞ = 1.4, α = 0.0°, $\bar{z}$ = 0.78.

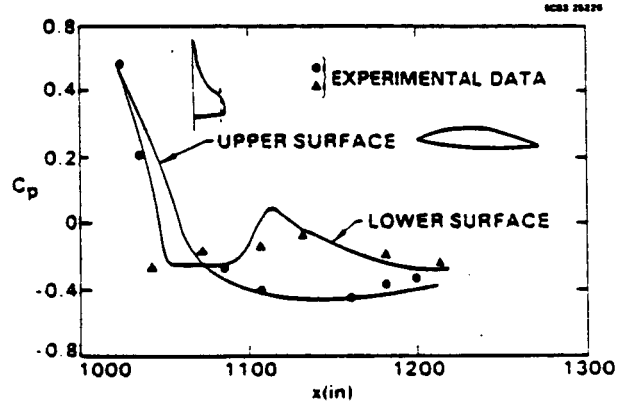

Fig. 21 Shuttle Orbiter chordwise pressure distribution; M_∞ = 1.4, α = 0.0°, $\bar{z}$ = 0.887.

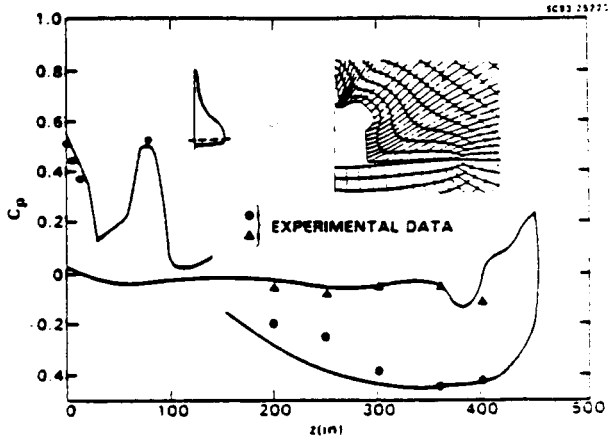

Fig. 22 Circumferential pressure distribution for the Orbiter at x = 1120 in; M_∞ = 1.4, α = 0.0°.

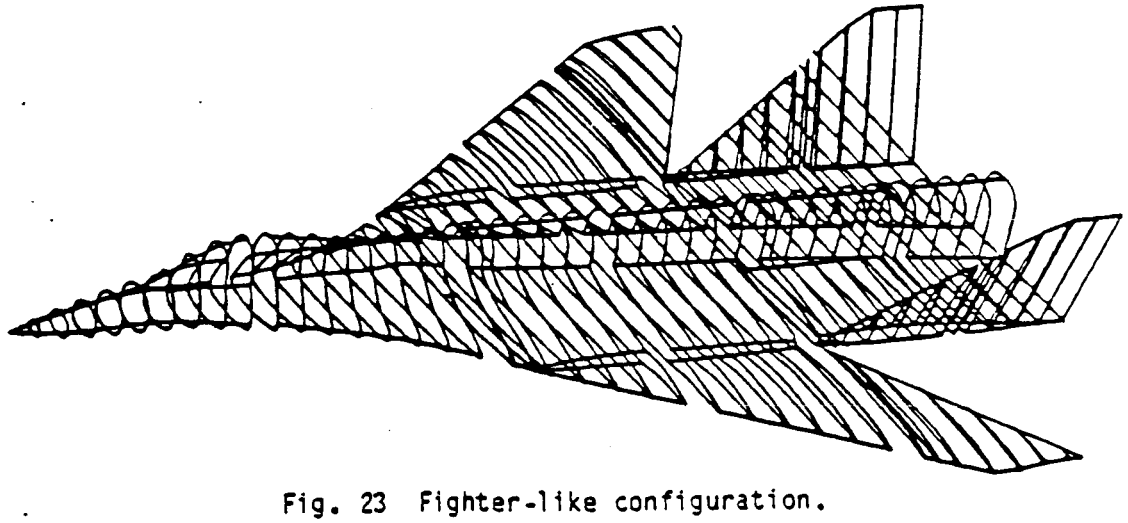

Fig. 23 Fighter-like configuration.

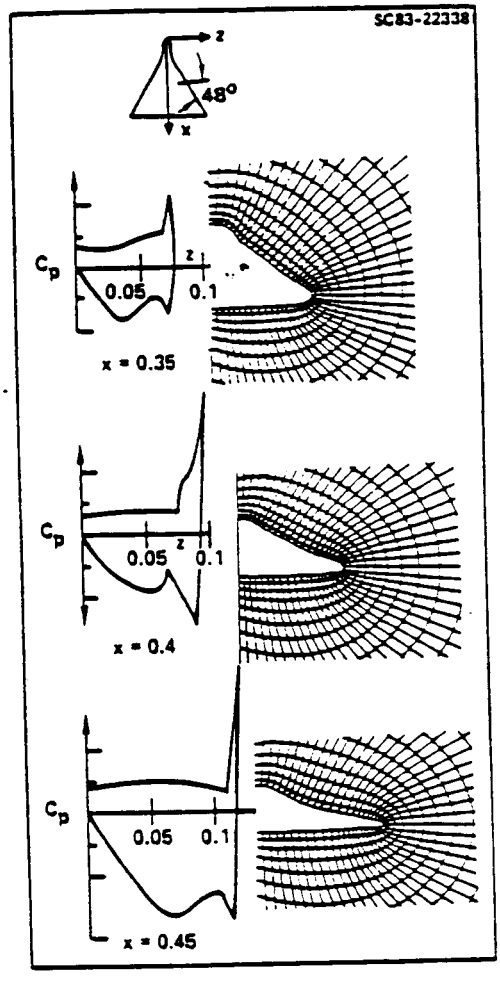

Fig. 24 Pressure distribution on a fighter-like configuration, $M_\infty = 1.6$, $\alpha = 5°$.

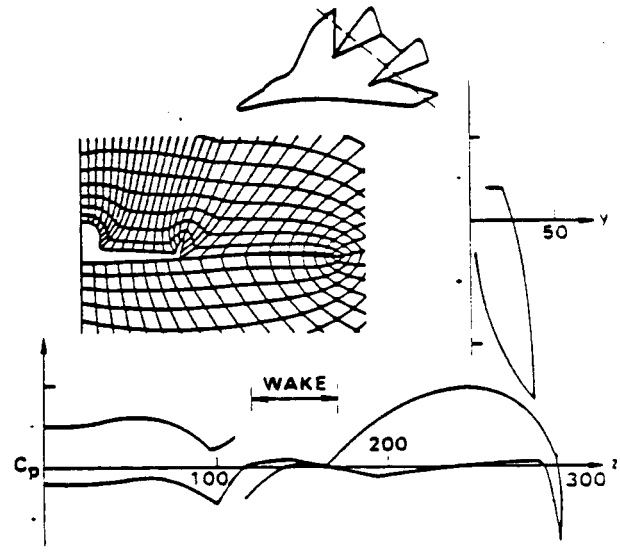

Fig. 25 Circumferential pressure distribution in the vertical tail and wing region of a fighter-like configuration, M_∞ 1.6, $\alpha = 4.46$, $x/\ell = 0.82$.

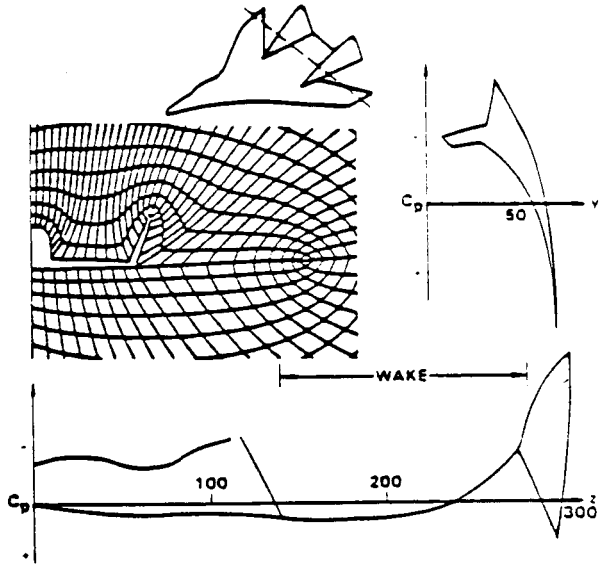

Fig. 26 Circumferential pressure distribution in the vertical tail and wing region of a fighter-like configuration, M_∞ 1.6, $\alpha = 4.46$, $x/\ell = 0.90$.

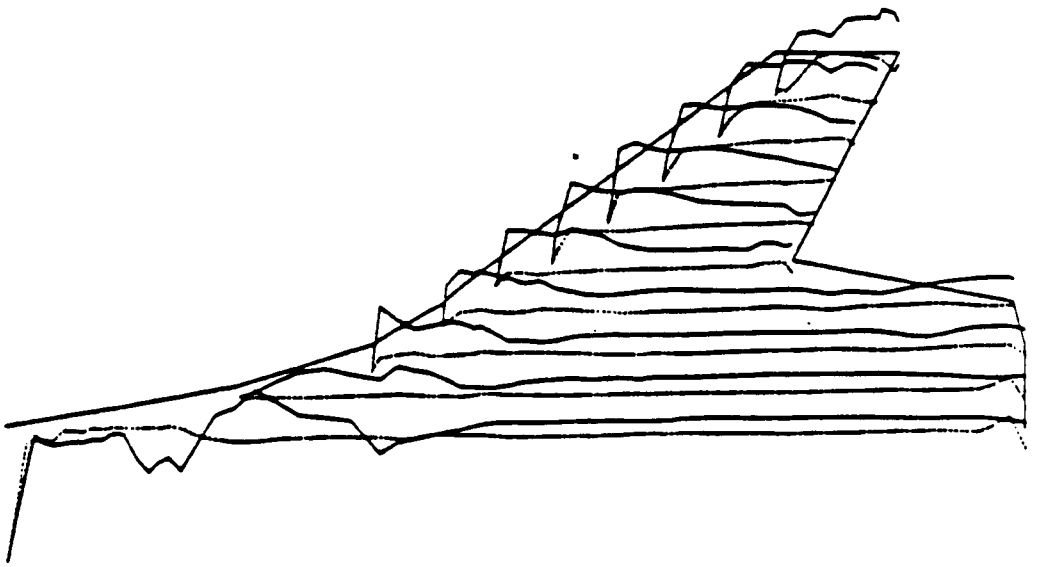

Fig. 27 Chordwise pressure distribution for a fighter-like configuration. M_∞ 1.6, α = 4.46.

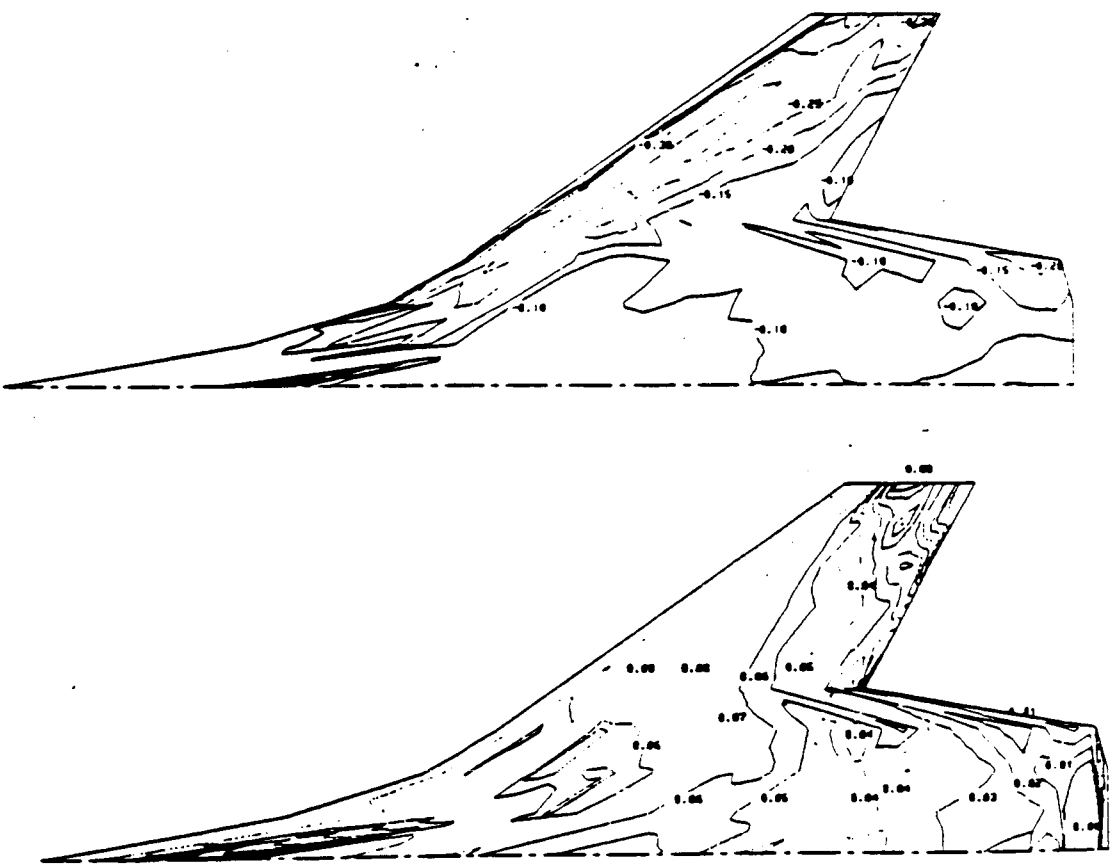

Fig. 28 Pressure contour on the upper and lower surface of the fighter-like configuration. M_∞ = 1.6, α = 4.46°.

α		5°	5°	5°	5°
M_∞		1.6*	1.6†	1.4†	1.6†
Λ		48°	48°	48°	55°
C_L	CODE	0.298	0.3016	0.3561	0.29186
	DATA	0.277	0.295	0.342	0.3
C_D	CODE	0.0462	0.04916	0.04117	0.028129
	DATA	0.0457	0.0493	0.0425	0.0301

Λ = Wing sweep angle
*Without vertical tail
†With vertical tail

Table 1 Test cases for fighter-like configurations.

SUPERSONIC FULL POTENTIAL ANALYSIS PROGRAM OPERATING INSTRUCTIONS

E. BONNER

Rockwell International Corporation
North American Aircraft Operations
Los Angeles, California 90009

ABSTRACT

Description of input/output data and operating instructions are presented for a recently developed supersonic full potential analysis program. Solution pre and post processors are also discussed for completeness. The latter includes a three dimensional finite difference boundary layer program interface

TABLE OF CONTENTS

INTRODUCTION

The supersonic full potential analysis method,[1-3] in conjuction with three dimensional boundary layer analysis[4] is currently being used to derive nonlinear supersonic cruise and maneuver designs to support aerodynamic advance configuration studies. The fundamental advance of full potential methodology relative to linear solutions is the ability to shock capture. The analysis consequently provides the means to achieve necessary conditions of shock weakening and separation elimination /management through appropriate redesign. In this regard, it provides a capability similar to relaxation solvers that are routinely used to develop efficient transonic flows.

Supersonic full potential analysis also provides the ability to accurately assess the impact of sweep, thickness, and lift for a range of design space for which linear theory is unsatisfactory.

DISCUSSION

The supersonic full potential (SFP) analysis code of Shankar[1-3] is applicable to arbitrary wing-body-nacelle-tail arrangements from moderate supersonic Mach number to values of the hypersonic similarity parameter $M\delta \sim O(1)$. The lower code limit is governed by the extent of embedded subsonic flow while the upper limit results from a breakdown in the isentropic assumption for strong shock waves. Also, since potential theory is irrotional, the modeling of vortices is not treated.

The current version of the pilot code is operational on the CDC 875 and is stored as program library FPF7PL.

CASE DESCRIPTION

Four types of data are required to define a problem: a) header data describing mesh information, Mach number, angle of attack, aerodynamic coefficient reference quanities, center of gravity location, etc.; b) detailed geometric coordinates defining configuration cross plane contours; c) program update file directives defining code modifications, wake data, etc.; and d) job control directives defining program and input/output file allocations.

GEOMETRY DATA

A configuration is defined by several regions* of crossplane sections as indicated in figure 1. The number of patches (segments) defining a section is constant for a given region and typically increases from one region to the next.

For the wing-body-vertical case under discussion, a three (3) patch initial region, a six (6) patch center region, and and eight (8) patch final region as indicated on figure 2. Zero length patches are not permissable. Since the analysis is marching in nature, a complete geometry data set is not required to begin and partially process a problem. Appropriate use of restart solutions allows continuation of the analysis as new or modified geometry becomes available.

*The overlap must be sufficient to encompass at least the final three (3) marching data planes of the prior region.

C-2

The format for a typical station is shown below. The group of cards is repeated for each station of a region. The last point of each patch (except for the last patch of a station) should have the same coordinates as the first point of the next patch.

Card#	Format	Field	Name	Description
A1	F15.6,I5	1	X1	The x value (longitudinal) of this station.
		2	ISC1	The number of patches for this section. $1 \leq$ ISC1 ≤ 15

The group of cards A2 thru A3 are repeated ISC1 times.

A2	3I5	1	ITH	Patch number ≤ 15
		2	IPT1	Number of points in this patch. $2 \leq$ IPT1 ≤ 30
		3	ND	Mesh spacing parameter*. Typically the same for all stations of a region

The A3 card is repeated IPT1 times.

A3	2F15.6	1	Y1	Vertical location of point (positive upwards). Points start at top centerline.
		2	Z1	Spanwise location of point.

Cubic spline interpolation is performed on input patch data to derive the boundary at the mesh points. Linear interpolation is performed to define the boundary at a marching plane between input stations.

Sample geometry data for the problem of figure 1 is presented on Table I and was developed using CDS[5].

---

*FOR SEGMENT $\overline{AB}$

0 Equal space
1 Bunch near A
2 Bunch near B

TABLE I GEOMETRY DATA

ORIGINAL PAGE IS
OF POOR QUALITY

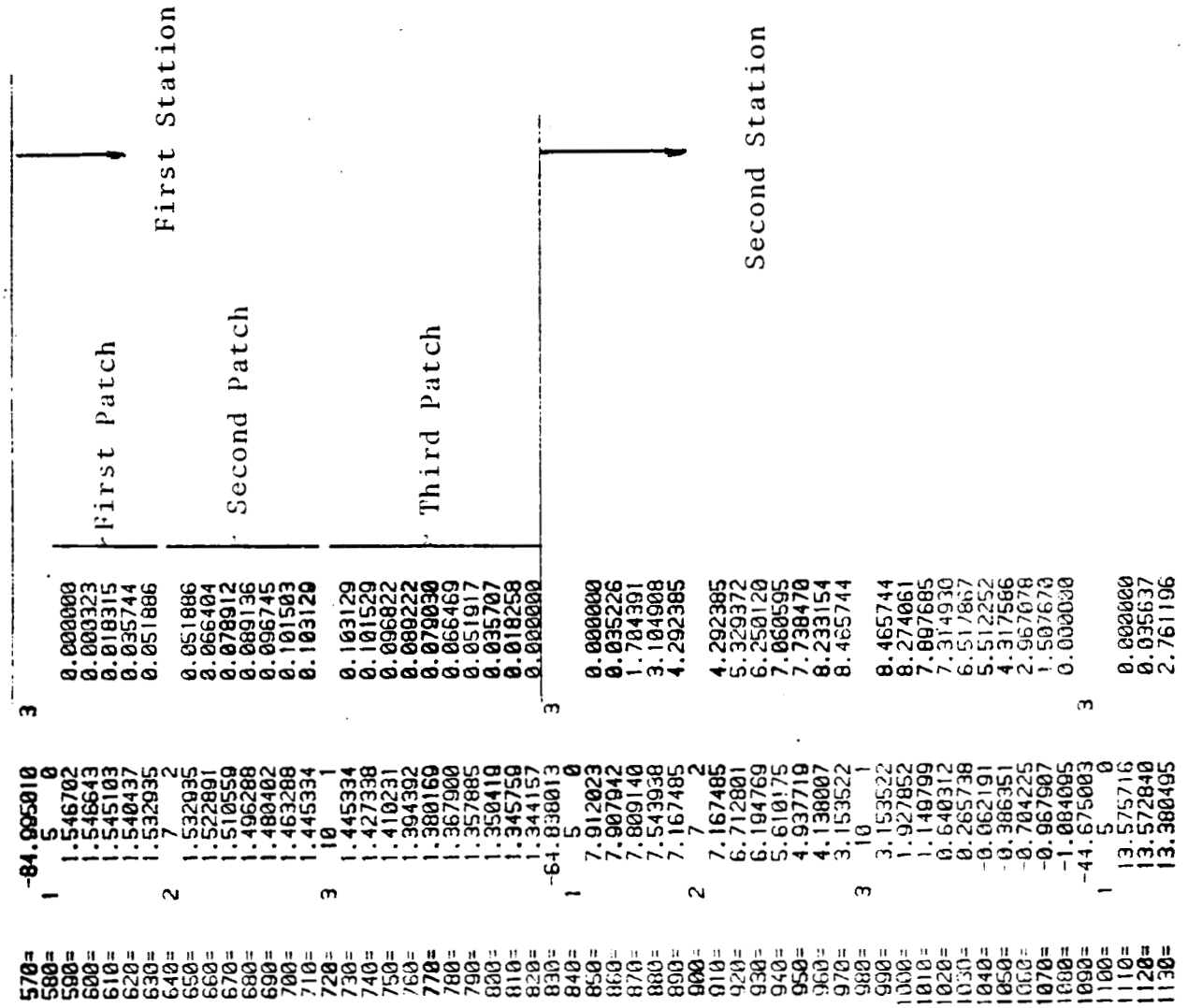

```
8380=     289.670959     3                    <-- End of Region 1
8390=  1   13    0
8400=      49.958420       0.000000
8410=      49.958382       1.937543
8420=      49.958420       4.388307
8430=      49.680511       7.428109
8440=      48.879784      10.266657
8450=      47.604164      12.876740
8460=      45.899948      15.224077
8470=      43.811752      17.267170
8480=      41.382515      18.957480
8490=      38.653473      20.239323
8500=      35.664185      21.049873
8510=      32.452553      21.319206
8520=      30.713291      21.295483
8530=  2   30    2
8540=      30.713291      21.295483
8550=      29.147690      23.898067
8560=      26.650154      28.498608
8570=      24.242348      33.629456
8580=      22.121189      38.922287
8590=      20.874866      42.500359
8600=      19.281048      47.515938
8610=      17.635311      53.495407
8620=      16.076260      61.088318
8630=      15.763639      65.987915
8640=      15.355867      68.569077
8650=      14.472219      73.730820
8660=      13.490191      78.891434
8670=      12.402630      84.404892
8680=      11.482655      88.847702
8690=      10.837719      91.780429
8700=      10.246025      94.368530
8710=       9.555044      97.232849
8720=       8.931576      99.526596
8730=       8.207584     102.105409
8740=       7.425758     104.684341
8750=       6.573520     107.263199
8760=       5.626501     109.842041
8770=       4.722771     112.048233
8780=       4.134672     113.304123
8790=       3.615775     114.227844
8800=       3.348063     114.597412
8810=       3.147207     114.708508
8820=       2.919736     114.946838
8830=       2.698931     114.993576
8840=  3   29    1
8850=       2.698931     114.993756
8860=       2.579846     114.980423
8870=       2.459620     114.933670
8880=       2.363239     114.838547
8890=       2.245280     114.634491
8900=       2.062772     113.952515
8910=       1.905408     112.792099
8920=       1.762813     111.139282
8930=       1.631411     109.008453
8940=       1.515947     106.502197
8950=       1.424684     103.794922
8960=       1.356829     101.145477
8970=       1.204087      96.947678
8980=       1.005896      94.368591
8990=       0.917631      90.622635
9000=       0.640761      86.630768
9010=       0.257428      81.430713
9020=      -0.130081      76.311234
9030=      -0.450283      71.150040
9040=      -0.645550      65.987915
9050=      -0.994209      61.978348
9060=      -1.161518      57.469460
9070=      -1.294488      52.036896
9080=      -1.417318      45.268186
9090=      -1.456881      36.659615
9100=      -1.600638      27.491192
9110=      -1.781296      18.323032
9120=      -1.914585       9.163094
9130=      -1.960516       0.000000
9140=     257.762939     6                    <-- Beginning of Region 2
9150=  1   6    0
9160=      50.010979       0.000000
9170=      50.010979       0.611856
9180=      49.824493       3.408121
9190=      49.187645       6.642947
9200=      48.033119       9.893850
9210=      46.359802      12.845306
9220=  2   6    0
9230=      46.359802      12.845306
9240=      44.232117      15.282759
9250=      41.780586      17.095585
9260=      39.201439      18.276600
9270=      36.756943      18.921902
9280=      34.538315      19.328766
9290=  3   10   0
9300=      34.538315      19.328766
9310=      32.809967      21.765694
9320=      29.693047      26.516281
9330=      26.462524      31.830555
9340=      23.469040      37.253181
9350=      21.147877      42.008942
9360=      20.279148      43.921326
9370=      19.470787      46.044807
9380=      18.717278      48.341698
9390=      17.326115      53.398514
9400=  4   18   2
9410=      17.326115      53.398514
9420=      15.954689      59.162178
9430=      14.366322      65.999817
9440=      13.750040      68.714981
9450=      13.192150      71.150070
9460=      12.580235      73.730789
9470=      11.938618      76.311203
9480=      11.212303      78.891495
9490=      10.451161      81.471466
```

TABLE I Continued


```
24360=     528.031982    6                    <-- End of Region 2
24370=  1    7    0
24380=      50.007111          0.000000
24390=      50.007019          2.742154
24400=      50.005111          4.956256
24410=      49.731850          7.991484
24420=      48.936188         10.803526
24430=      47.665405         13.500030
24440=      45.965707         16.014454
24450=  2    8    0
24460=      45.965707         16.014454
24470=      43.864506         18.106064
24480=      41.460543         19.809887
24490=      38.769760         21.076782
24500=      35.834053         21.863373
24510=      32.715767         22.132114
24520=      25.660957         22.127000
24530=      16.874676         22.126163
24540=  3   17    0
24550=      16.874676         22.126163
24560=      16.113289         30.029079
24570=      15.296806         39.139084
24580=      14.629675         48.051239
24590=      14.137501         56.337900
24600=      13.470024         65.099817
24610=      13.089699         71.150040
24620=      12.432905         78.801418
24630=      11.775507         86.630768
24640=      11.325478         91.789383
24650=      10.802713         96.947571
24660=      10.042408        104.684296
24670=       9.567081        109.842010
24680=       9.088606        113.689621
24690=       8.620909        114.515457
24700=       7.802448        114.869385
24710=       4.650239        114.999863
24720=  4   29    2
24730=       4.650239        114.999863
24740=       5.103719        123.433228
24750=       5.596378        130.728241
24760=       6.415631        141.596466
24770=       7.474397        155.155457
24780=       8.102022        164.025568
24790=       8.563284        174.694519
24800=       8.874420        184.462860
24810=       9.115057        194.230164
24820=       9.400442        208.878906
24830=       9.506882        223.523987
24840=       9.463659        233.285553
24850=       9.169333        243.043579
24860=       8.811359        248.582214
24870=       8.448650        262.708920
24880=       7.926655        257.676614
24890=       7.303553        262.513306
24900=       6.501266        267.634949
24910=       5.575104        272.557800
24920=       4.080721        275.272766
24930=       4.621628        276.748108
24940=       4.288194        278.013977
24950=       3.983303        279.084778
24960=       3.708123        279.972534
24970=       3.461858        280.685852
24980=       3.242233        281.231323
24990=       3.045500        281.613525
25000=       2.866371        281.836182
25010=       2.697999        281.901428
25020=  5   30    1
25030=       2.697999        281.901428
25040=       2.555275        281.812378
25050=       2.455352        281.571533
25060=       2.390040        281.174377
25070=       2.356306        280.615479
25080=       2.347210        279.888855
25090=       2.360858        278.988037
25100=       2.395871        277.904968
25110=       2.451631        276.630676
25120=       2.360858        278.988037
25130=       2.451631        276.630676
25140=       2.687582        272.557922
25150=       2.998391        267.635010
25160=       3.381361        262.630127
25170=       3.833046        256.580478
25180=       4.020399        248.358643
25190=       4.345508        240.274780
25200=       4.592886        232.240451
25210=       4.820795        223.524078
25220=       5.055776        213.761658
25230=       5.270200        201.888916
25240=       5.500740        189.346741
25250=       5.704358        179.578674
25260=       5.881357        169.810730
25270=       5.711005        160.040466
25280=       5.460247        150.270203
25290=       5.115679        140.499298
25300=       4.824990        130.728210
25310=       4.676602        123.433243
25320=       2.500000        115.000000
25330=  6   16    0
25340=       2.500000        115.000000
25350=       0.234524        112.990997
25360=       0.205185        109.842010
25370=       0.049130        104.684326
25380=      -0.214951         96.947586
25390=      -0.615489         86.630768
25400=      -0.909250         78.891403
25410=      -1.228700         71.160055
25420=      -1.472983         65.987900
25430=      -1.646140         59.730128
25440=      -1.985137         50.456306
25450=      -2.540106         40.541016
25460=      -3.078060         28.682934
25470=      -3.383003         16.579712
25480=      -3.529747          8.129135
25490=      -3.599054          0.000000
25500=     499.712952    8                    <-- Beginning of Region 3
```

TABLE I Continued

```
25510=    1    7    0
25520=      50.007126        0.000000
25530=      50.007095        2.742039
25540=      50.005126        4.956260
25550=      49.737724        7.991527
25560=      48.950752       10.893637
25570=      47.682236       13.590189
25580=      45.974167       16.014576
25590=    2    8    0
25600=      45.974167       16.014576
25610=      43.874220       18.105961
25620=      41.436035       19.809288
25630=      38.718979       21.075272
25640=      35.788315       21.860439
25650=      32.715111       22.127048
25660=      26.359161       22.127010
25670=      18.414383       22.127018
25680=    3   10    0
25690=      18.414383       22.127018
25700=      17.814026       26.774406
25710=      16.923122       34.597984
25720=      16.013092       43.651665
25730=      15.325804       52.031616
25740=      14.666439       60.607819
25750=      13.918823       68.569077
25760=      13.272402       76.311203
25770=      12.510948       84.051117
25780=      11.722996       91.789398
25790=    4    4    2
25800=      11.722996       91.789398
25810=      10.950851       99.526520
25820=      10.160648      107.263123
25830=       9.658892      112.420868
25840=    5    3    1
25850=       9.658892      112.420868
25860=       7.128384      115.000000
25870=       5.126293      117.956802
25880=    6   29    2
25890=       5.126293      117.956802
25900=       5.853478      125.842819
25910=       6.825004      133.837067
25920=       8.132015      145.828949
25930=       8.799452      153.823059
25940=       9.262857      161.816805
25950=       9.645087      173.806427
25960=       9.769035      181.708798
25970=       9.833309      193.786194
25980=       9.785547      201.776581
25990=       9.639191      209.766571
26000=       9.360663      217.755157
26010=       8.956194      226.046539
26020=       8.400652      233.096222
26030=       7.648726      239.993317
26040=       6.849148      245.704193
26050=       5.749837      251.973328
26060=       5.238540      254.410126
26070=       4.662115      256.886719
26080=       4.369453      258.021057
26090=       4.097445      259.004211
26100=       3.846460      259.842285
26110=       3.616040      260.540894
26120=       3.404875      261.104858
26130=       3.210836      261.537364
26140=       3.102296      261.720947
26150=       3.030086      261.841614
26160=       2.861572      262.018860
26170=       2.697999      262.070618
26180=    7   30    1
26190=       2.697999      262.070618
26200=       2.627872      262.051697
26210=       2.569114      262.012207
26220=       2.513620      261.944702
26230=       2.458793      261.845003
26240=       2.418955      261.742126
26250=       2.378328      261.578125
26260=       2.319113      261.204773
26270=       2.278214      260.722534
26280=       2.259218      260.128967
26290=       2.242231      259.419250
26300=       2.243885      258.591797
26310=       2.257326      257.642151
26320=       2.282346      256.567322
26330=       2.368329      254.016083
26340=       2.521813      250.454346
26350=       2.709336      246.293915
26360=       3.116043      235.725586
26370=       3.460886      221.033502
26380=       3.839483      206.437592
26390=       4.086307      195.451019
26400=       4.351102      184.462891
26410=       4.600918      173.473694
26420=       4.703060      166.146942
26430=       4.687814      158.819366
26440=       4.501820      151.102020
26450=       3.955967      140.499268
26460=       3.023705      127.743134
26470=       2.482436      116.711746
26480=       1.313319      114.999817
26490=    8   13    0
26500=       1.313319      114.999817
26510=       0.154916      112.420914
26520=       0.021698      107.263168
26530=      -0.209001       99.526550
26540=      -0.567024       89.210129
26550=      -0.849183       81.471390
26560=      -1.263398       71.150055
26570=      -1.696522       59.699020
26580=      -2.194694       50.229889
26590=      -2.726831       40.469147
26600=      -3.224504       28.843315
26610=      -3.657449       16.538712
26620=      -3.791033        0.000000
26630=     519.784912    8
26640=    1    7    0
26650=      50.007103        0.000000
```

```
41690=     721.499878    8
41700=   1    7    0
41710=      50.007126       0.000000
41720=      50.007111       2.190936
41730=      50.007126       4.956260
41740=      49.737625       7.991241
41750=      48.950493      10.892822
41760=      47.681923      13.589085
41770=      45.974007      16.013924
41780=   2   15    0
41790=      45.974007      16.013924
41800=      43.874474      18.106983
41810=      41.436966      19.813690
41820=      38.720818      21.085270
41830=      35.791206      21.878693
41840=      32.719025      22.156746
41850=      29.372906      22.153980
41860=      26.042725      22.151500
41870=      22.696865      22.149929
41880=      19.303780      22.149937
41890=      15.831873      22.152149
41900=      12.249571      22.157227
41910=       8.525335      22.165813
41920=       4.627600      22.178566
41930=       0.524876      22.196121
41940=   3    2    0
41950=       0.524876      22.196121
41960=       1.755000     112.214996
41970=   4    2    2
41980=       1.755000     112.214996
41990=     103.760986     148.779999
42000=   5    2    1
42010=     103.760986     148.779999
42020=       1.755000     112.214996
42030=   6    2    2
42040=       1.755000     112.214996
42050=       5.874999     306.528992
42060=   7    2    1
42070=       5.874999     306.528992
42080=       1.755000     112.214996
42090=   8    3    0
42100=       1.755000     112.214996
42110=       0.524876      22.196121
42120=       0.525000       0.000000
42130=*EOF
```

End of Region 3

TABLE I Concluded

HEADER DATA

The present problem requires a minimum of four (4) marching solutions to complete the analysis of the three region sample geometry of figure 1 - one each for region one and two and two solutions for region three. The latter is a consequence of increasing the number of mesh points on the vertical tail as its local span increased with marching distance. It also illustrates the wake restart procedure.

Each solution has a different set of header instructions for describing grid parameters, wake information if pertinent, restart directions, and number of mesh points for each patch of the region. This information precedes the geometric data discussed in the previous section. The header data used for the sample problem and a description of the various parameters is presented on Table II.

The last header data set is coordinated with the wake update file described in the next section. The pertinent nomenclature is depicted below.

KWAK**	RESTART
1	Standard (geometry)
2	Wake

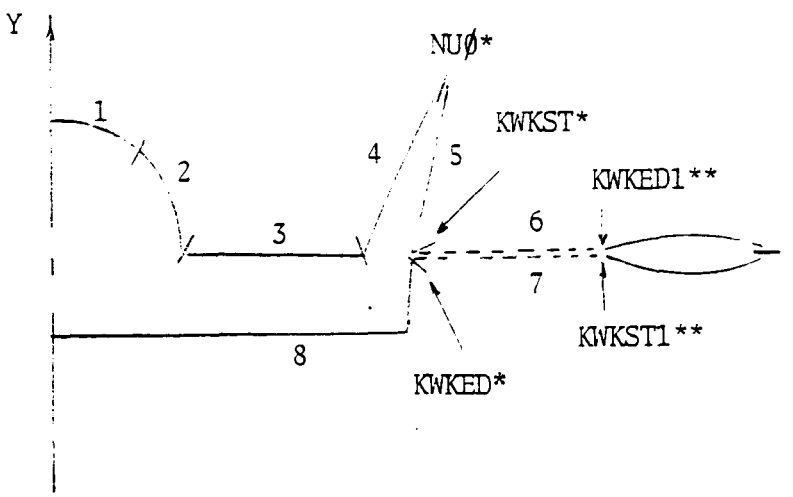

NOTE: Reindex K of VORT (K) to allow for increase of points for patches 4 and 5

---

* TAPE 5
** Update file

TABLE II HEADER DATA


```
100=  175      NMAX   I5      NO. OF AXIAL STEP
110=   15      JMAX           NO. OF PTS IN NORMAL DIR.<26
120=   33      KMAX           NO. OF PTS IN CIRCUM DIR;ISC1+ISC2-1+ISC3+1<81
130=    2      NRM            NO. GRID REGIONS<7;B&WB-2,WBV-3,WBNV-5
140=   13      NU0            SECOND SHARP EDGE K.
150=    2      NP             OUTPUT FOR EVERY NP STEPS
160=   18      KWKST          WAKE START K.
170=   36      KWKED          WAKE END K.
180=   30      NCON           NO. CONE STARTING SOL. STEPS.
190=   30      NITER          NO. OF GRID ITERATIONS.
200=    6      NSPTI          NO. OF ZTA FOR FLOW FIELD OUTPUT.
210=    1      ITERGE         NO. OF GLOB ITERATION.
220=  5.0      CFLIN F10.5    CFL NUMBER
230=  2.5      DZTAIN         IF>0 FIXED STEP SIZE.IF<0 CFL NO.
240=  3.0      DZMAX          MAX. AXIAL STEP SIZE
250=  1.0      DZMIN          MIN. AXIAL STEP SIZE
260=  1.6      FSM            FREE STREAM MACH NO.
270=  4.46     ALFA           ANGLE OF ATTACX-DEG.
280=   60.     THTO           OUTER BOUNDARY-DEG.
290=  0.1      DETA           STEP SIZE IN ETA DIR.
300=  0.1      DXI            STEP SIZE IN XI DIR.
310=   1.5     DZTA           FIRST STEP AFTER CONE START, SOL.
320=  15.00    ZTAI           STARTING ZTA >3*DZTAIN.
330= 371.0     XEND           END ZTA<MAX INPUT ZTA-DZTAIN.
340=   1.      AMU1           1:FIRST ORDER,2:2ND ORDER.
350=   0.      AMU2           0:FIRST ORDER,1:2ND ORDER.
360=  614.     XWAKE          WAKE MINIMUM ZTA.
370=  117.     ZWAKE          WAKE MINIMUM .
380=   1.0     CHL            GEOMETRY SCALE FACTOR
390=   85.0    PTNOSE         AXIAL GEOMETRY SHIFT FOR ZTA>0.
400=   0.      YSHIFT         VERTICAL GEOMETRY SHIFT
410=  500.     XO             AXIAL C.G. ZTA.
420=   0.      YO             VERTICAL C.G.
430=125280.    AAA            REFERENCE AREA.
440=234.627    ALL            REFERENCE LENGTH.
450=   1.75    OMEGA          RELAXATION FACTOR.
460=    T      PLANEOS        PLANE OF SYM.?
470=    T      NUGRID         GENERATE GRID?
480=    T      IREAD          INPUT GEOMETRY?
490=    F      RPLANE         R-MARCHING?
500=    F      TAPER          RESTART DATA FROM TAPE?
510=    T      TAPEW          WRITE RESTART DATA ON UNIT 2 & 4?
520=    F      TAPEBW         WRITE SUBSONIC RESTART DATA ON UNIT 8?
530=    T      FORCE          CALCULATE FORCES?
540=   18                     GRID REGION TERMINAL K,5I5;ISC1+ISC2-1+..+ISCN
550=   0.       00.0        00.0     00.0          POLAR ANGLE-DEG;5F10.4
560=100.    150.    200.    250.    300.    350.   FLOW FIELD OUTPUT ZTA
570=    3      ISC                                 NO. GEOM. SEGMENTS
580=    8   18   15                               NO. MESH PTS/SEGMENT
590=    0                    NAUS
```

a) Region 1

TABLE II CONTINUED

```
100=   125        NMAX    I5      NO. OF AXIAL STEPS
110=    15        JMAX            MESH PTS IN NORMAL DIR.<26
120=    57        KMAX            MESH PTS IN CIRCUM DIR;ISC1+ISC2-1+..+ISC6+1<81
130=     2        NRM             NO. GRID REGIONS<7;B&WB-2,WBV-3,WBNV-5
140=    13        NU0             SECOND SHARP EDGE K.
150=     2        NP              OUTPUT FOR EVERY NP STEPS.
160=    28        KWKST           WAKE START K;ISC1+ISC2-1...+ISC5
170=    47        KWKED           WAKE END K;ISC1+ISC2-1+...+ISC7
180=    30        NCON            NO CONE STARTING SOL. STEPS.
190=    30        NITER           NO. OF GRID ITERATIONS.
200=     6        NSPTI           NO. OF ZTA FOR FLOW FIELD OUTPUT.
210=     1        ITERGE          NO. OF GLOB ITERATION.
220=   5.0        CFLIN  F10.5    CFL NUMBER.
230=   2.5        DZTAIN          IF>0 FIXED STEP SIZE.IF<0 CFL NO.
240=   3.0        DZMAX           MAX. AXIAL STEP SIZE
250=   1.0        DZMIN           MIN. AXIAL STEP SIZE
260=   1.6        FSM             FREE STREAM MACH NO.
270=  4.46        ALFA            ANGLE OF ATTACK-DEG.
280=   60.        THTO            OUTER BOUNDARY-DEG.
290=   0.1        DETA            STEP SIZE IN ETA DIR.
300=   0.1        DXI             STEP SIZE IN XI DIR.
310=   1.5        DZTA            FIRST STEP AFTER CONE START. SOL.
320= 371.0        ZTA1            STARTING ZTA.
330= 611.0        XEND            END ZTA<MAX INPUT ZTA-DZTAIN.
340=    1.        AMU1            1:FIRST ORDER,2:2ND ORDER.
350=    0.        AMU2            0:FIRST ORDER,1:2ND ORDER.
360=   614.       XWAKE           WAKE MINIMUM ZTA.
370=   117.       ZWAKE           WAKE MINIMUM Z.
380=     1.0      CHL             GEOMETRY SCALE FACTOR
390=    85.0      PTNOSE          AXIAL GEOMETRY SHIFT FOR ZTA>0.
400=    0.0       YSHIFT          VERTICAL GEOMETRY SHIFT
410=   500.       XO              AXIAL C.G. ZTA.
420=     0.       YO              VERTICAL C.G.
430=125280.       AAA             REFERENCE AREA.
440=234.627       ALL             REFERENCE LENGTH.
450=    1.75      OMEGA           RELAXIATION FACTOR.
460=     T        PLANEOS         PLANE OF SYM.?
470=     T        NUGRID          GENERATE GRID?
480=     T        IREAD           INPUT GEOMETRY?
490=     F        RPLANE          R-MARCHING?
500=     T        TAPER           RESTART DATA FROM TAPE?
510=     T        TAPEW           WRITE RESTART DATA ON UNIT 2 & 4?
520=     F        TAPEBW          WRITE SUBSONIC RESTART DATA ON UNIT 8?
530=     T        FORCE           CALCULATE FORCES?
540=    32   00   00   00         GRID REGION TERMINAL K,5I5;ISC1+ISC2-1+..+ISCN
550=   0.0       0.00       00.0      00.0  "          POLAR ANGLE;5F10.4
560=400.     450.     500.     550.     575.     600.  FLOW FIELD OUTPUT ZTA
570=     6        ISC                                  NO. GEOM. SEGMENTS
580=    04   05   10   15   15   11                    NO. MESH PTS/SEGMENT
590=     0                   NAJS
```

b) Region 2

ORIGINAL PAGE IS
OF POOR QUALITY

TABLE II CONTINUED

ORIGINAL PAGE IS
OF POOR QUALITY

```
100=    50        NMAX    I5      NO. OF AXIAL STEPS
110=    15        JMAX            MESH PTS IN NORMAL DIR.<26
120=    63        KMAX            MESH PTS IN CIRCUM DIR;ISC1+ISC2-1+..+ISC8+1<81
130=     3        NRM             NO. GRID REGIONS<7;8&WB-2,WBV-3,WBNV-5
140=    21        NUB             TAIL EDGE K;ISC1+ISC2-1+...+ISC4
150=     2        NP              OUTPUT FOR EVERY NP STEPS
160=    24        KWKST           WAKE START K;ISC1+ISC2-1+...+ISC5
170=    52        KWKED           WAKE END K;ISC1+ISC2-1+...+ISC7
180=    30        NCON            NO. CONE STARTING SOL. STEPS.
190=    30        NITER           NO. OF GRID ITERATIONS.
200=     3        NSPTI           NO. OF ZTA FOR FLOW FIELD OUTPUT.
210=     1        ITERGE          NO. OF GLOB ITERATION.
220=   5.0        CFLIN  F10.5    CFL NUMBER.
230=   2.5        DZTAIN          IF>0 FIXED STEP SIZE.IF<0 CFL NO.
240=   3.0        DZMAX           MAX. AXIAL STEP SIZE
250=   1.0        DZMIN           MIN. AXIAL STEP SIZE
260=   1.6        FSM             FREE STREAM MACH NO.
270=  4.46        ALFA            ANGLE OF ATTACK-DEG.
280=   60.        THTO            OUTER BOUNDARY-DEG.
290=   0.1        DETA            STEP SIZE IN ETA DIR.
300=   0.1        DXI             STEP SIZE IN XI DIR.
310=   1.5        DZTA            FIRST STEP AFTER CONE START. SOL.
320= 611.0        ZTA1            STARTING ZTA.
330= 685.0        XEND            END ZTA<MAX INPUT ZTA-DZTAIN.
340=    1.        AMU1            1:FIRST ORDER,2:2ND ORDER.
350=    0.        AMU2            0:FIRST ORDER,1:2ND ORDER.
360=   614.       XWAKE           WAKE MINIMUM ZTA.
370=   117.       ZWAKE           WAKE MINIMUM Z.
380=     1.0      CHL             GEOMETRY SCALE FACTOR
390=    85.0      PTNOSE          AXIAL GEOMRTRY SHIFT FOR ZTA>0.
400=    0.0       YSHIFT          VERTICAL GEOMETRY SHIFT.
410=   500.       XO              AXIAL C.G. ZTA.
420=     0.       YO              VERTICAL C.G.
430=125280.       AAA             REFERENCE AREA
440=234.627       ALL             REFERENCE LENGTH.
450=   1.75       OMEGA           RELAXATION FACTOR.
460=      T       PLANEOS         PLANE OF SYM.?
470=      T       NUGRID          GENERATE GRID?
480=      T       IREAD           INPUT GEOMETRY?
490=      F       RPLANE          R-MARCHING?
500=      T       TAPER           RESTART DATA FROM TAPE?
510=      T       TAPEW           WRITE RESTART DATA ON UNIT 2 & 4?
520=      F       TAPEBW          WRITE SUBSONIC RESTART DATA ON UNIT 8?
530=      T       FORCE           CALCULATE FORCES?
540=     21    38    00    00     GRID REGION TERMINAL K,5I5;ISC1+ISC2-1+..+ISCN
550=   70.0        0.00          00.0      00.0   "        POLAR ANGLE;5F10.4
560=625.      650.      675.                               FLOW FIELD OUTPUT ZTA
570=      8       ISC                                      NO. GEOM. SEGMENTS
580=     04    05    10    04     04    15    15    11     NO. MESH PTS/SEGMENT
590=      0                      NAJS
```

c) Region 3, Solution 1

TABLE II COMPLETED

ORIGINAL PAGE IS
OF POOR QUALITY

```
100=    75        NMAX    I5      NO. OF STEP
110=    15        JMAX            MESH PTS IN.NORMAL DIR.<26
120=    68        KMAX            MESH PTS IN CIRCUM DIR;ISC1+ISC2-1+..+ISC8+1<81
130=     3        NRM             NO. GRID REGIONS<7;B&WB-2,WBV-3,WBNV-5
140=    24        NU0             TAIL EDGE K;ISC1+ISC2-1+...+ISC4
150=     2        NP              OUTPUT FOR EVERY NP STEPS
160=    30        KWKST           WAKE START K;ISC1+ISC2-1+...+ISC5
170=    58        KWKED           WAKE END K;ISC1+ISC2-1+...+ISC7
180=    30        NCON            NO. CONE STARTING SOL. STEPS.
190=    30        NITER           NO. GRID OF ITERATIONS.
200=     5        NSPTI           NO. OF ZTA FOR FLOW FIELD OUTPUT.
210=     1        ITERGE          NO. OF GLOB ITERATION.
220=   5.0        CFLIN   F10.5   CFL NUMBER.
230=   2.5        DZTAIN          IF>0 FIXED STEP SIZE.IF<0 CFL NO.
240=   3.0        DZMAX           MAX. AXIAL STEP SIZE
250=   1.0        DZMIN           MIN. AXIAL STEP SIZE
260=   1.6        FSM             FREE STREAM MACH NO.
270=  4.46        ALFA            ANGLE OF ATTACK-DEG.
280=    60.       THTO            OUTER BOUNDARY-DEG.
290=   0.1        DETA            STEP SIZE IN ETA DIR.
300=   0.1        DXI             STEP SIZE IN XI DIR.
310=    1.5       DZTA            FIRST STEP AFTER CONE START. SOL.
320=  685.0       ZTAI            STARTING ZTA.
330=  804.0       XEND            END ZTA<MAX INPUT ZTA-DZTAIN.
340=    1.        AMU1            1:FIRST ORDER,2:2ND ORDER.
350=    0.        AMU2            0:FIRST ORDER,1:2ND ORDER.
360=   614.       XWAKE           WAKE MINIMUM ZTA.
370=   117.       ZWAKE           WAKE MINIMUM Z.
380=     1.0      CHL             GEOMETRY SCALE FACTOR
390=    85.0      PTNOSE          AXIAL GEOMETRY SHIFT FOR ZTA>0.
400=    0.0       YSHIFT          VERTICAL GEOMETRY SHIFT.
410=   500.       XO              AXIAL C.G. ZTA.
420=     0.       YO              VERTICAL C.G.
430=125280.       AAA             REFERENCE AREA
440=234.627       ALL             REFERENCE LENGTH.
450=    1.75      OMEGA           RELAXATION FACTOR.
460=     T        PLANEOS         PLANE OF SYM.?
470=     T        NUGRID          GENERATE GRID?
480=     T        IREAD           INPUT GEOMETRY?
490=     F        RPLANE          R-MARCHING?
500=     T        TAPER           RESTART DATA FROM TAPE?
510=     T        TAPEW           WRITE RESTART DATA ON UNIT 2 & 4?
520=     F        TAPE8W          WRITE SUBSONIC RESTART DATA ON UNIT 8?
530=     T        FORCE           CALCULATE FORCES?
540=    24   44   00   00        GRID REGION TERMINAL K,515:ISC1+ISC2-1+..+ISCN
550=    70.0      0.00          00.0      00.0                POLAR ANGLE;SF10.4
560=700.      725.      750.     775.      800.                FLOW FIELD OUTPUT ZTA
570=     8        ISC                                         NO. GEOM. SEGMENTS
580=    04   05   10    7    7   15   15   11                NO. MESH PTS/SEGMENT
590=     1   04   04   05   04NAJS,NPTCHA,NODPTA,NPTCHB,NODPTB
```

d) Region 3, Solution 2

UPDATE FILE DATA

The purpose of this data is to define specialized information logic which has not been incorporated into the pilot code. It is anticipated that this type of input will be progressively eliminated as a production status evolves.

Two basic update files (see table III) are typically used. One for a standard (i.e. geometry) restart and a second for a wake restart. The former defines certain potential averaging, leading edge mesh, nacelle directives, etc. In addition, the wake restart file describes the vorticity distribution which is output by the prior (for the present case the third) solution.

The update files also contain modifications to the pilot code which have not been incorporated permanently. These directives do not need to be changed (but must be included) for a new problem.

TABLE III UPDATE FILE DIRECTIVES

```
100=*IDENT HRDWIRE
110=*I MAIN.14
120=C       TAPE9: OUTPUT PRESSURE DISTRIBUTIONS AT SPECIFIED Z
130=*D MAIN.55,MAIN.72
140=C
150=C    RESTART DIRECTIVE;KWAK=1-SOLID BOUNDARY,=2-WAKE
160=C
170=      KWAK=1
180=*D INVSETA.175,INVSETA.176
190=C    AVERAGE PHI AT MAX Z
200=      IF(ZTAI .LT. 371.0 ) PHI(1,2,KTEMP)=
210=     *(PHI(1,2,KTEMP+1)+PHI(1,2,KTEMP-1))/2.0
220=*D NFORCE.151
230=    18 FORMAT (2X,'PITCH MOMENT=',E12.4,3X,'CM=',E12.4,
240=*D INPUT.27
250=      DO 10 NAA=1,50
260=*D METRIC.51,METRIC.52
270=C    CONST.FOR ZTAI SHOULD BE CHANGE AT VERY THIN,SHARP
280=C    LEADING EDGE USING METRIC 56-79
290=*EOF
```

a) Region 1

```
100=*IDENT HRDWIRE
110=*I MAIN.14
120=C       TAPE9: OUTPUT PRESSURE DISTRIBUTIONS AT SPECIFIED Z
130=*D MAIN.55,MAIN.72
140=C
150=C    RESTART DIRECTIVE;KWAK=1-SOLID BOUNDARY,=2-WAKE
160=C
170=      KWAK=1
180=*D NFORCE.151
190=    18 FORMAT (2X,'PITCH MOMENT=',E12.4,3X,'CM=',E12.4,
200=*D GEOM.175
210=C    INCREASE NO. OF MESH POINTS IN WING L.E. REGION
220=      DS=SSS/(NPT(IS)*3.5)
230=*D GEOM.186
240=C    INCREASE NO. OF MESH POINTS IN WING L.E. REGION
250=      DS=SSS/(AD*3.5)
260=*D INPUT.27
270=      DO 10 NAA=1,50
280=*D METRIC.51,METRIC.52
290=C    CONST.FOR ZTAI SHOULD BE CHANGE AT VERY THIN,SHARP
300=C    LEADING EDGE USING METRIC 56-79
310=*EOF
```

b) Region 2

```
100=*IDENT HRDWIRE
110=*I MAIN.14
120=C       TAPE9: OUTPUT PRESSURE DISTRIBUTIONS AT SPECIFIED Z
130=*D MAIN.55,MAIN.72
140=C**
150=C**  RESTART DIRECTIVE;KWAK=1-SOLID BOUNDARY,=2-WAKE
160=C**
170=      KWAK=1
180=*D MAIN.308
190=C    DEFINE WING T.E. EQUATION
200=      ZWAKE1=1.8622*ZTAI-1026.53
210=*D MAIN.315,MAIN.316
220=C    SPECIFY MAXIMUM WAKE Z(I.E. WING HALF SPAN)
230=      IF (ZWAKE1 .GT. 306.53) KWKST1=KTEMP
240=      IF (ZWAKE1 .GT. 306.53) GO TO 54
250=*D MAIN.360,MAIN.361
260=C    OUTPUT VORTICITY FOR WAKE RESTART
270=      IF (NI .NE. 29) GO TO 138
280=*D INVSETA.175,INVSETA.176
290=C    AVERAGE PHI AT OR NEAR WING TIP
300=      IF(ZTAI .GT. 645.0 .AND. ZTAI .LT. 717.0) PHI(1,2,KTEMP)=
310=     *(PHI(1,2,KTEMP+1)+PHI(1,2,KTEMP-1))/2.0
320=      IF(ZTAI .GT. 645.0 .AND. ZTAI .LT. 717.0) PHI(1,2,KTEMP+1)=
330=     *(PHI(1,2,KTEMP)+PHI(1,2,KTEMP+2))/2.0
340=*D NFORCE.151
350=    18 FORMAT (2X,'PITCH MOMENT=',E12.4,3X,'CM=',E12.4,
360=*D GEOM.175
370=C    INCREASE NO. OF MESH POINTS IN WING L.E. REGION
380=      DS=SSS/(NPT(IS)*3.5)
390=*D GEOM.186
400=C    INCREASE NO. OF MESH POINTS IN WING L.E. REGION
410=      DS=SSS/(AD*3.5)
420=*D INPUT.27
430=      DO 10 NAA=1,50
440=*D METRIC.51,METRIC.52
450=C    CONST.FOR ZTAI SHOULD BE CHANGE AT VERY THIN,SHARP
460=C    LEADING EDGE USING METRIC 56-79
470=*EOF
```

c) Region 3, Solution 1

TABLE III COMPLETED

```
100=*IDENT HROWIRE
110=*I MAIN.14
120=C       TAPE9: OUTPUT PRESSURE DISTRIBUTIONS AT SPECIFIED Z
130=*D MAIN.55,MAIN.72
140=C
150=C    RESTART DIRECTIVE;KWAK=1-SOLID BOUNDARY,=2-WAKE
160=C    KWED1-MAX U.S. WAKE K; KWKST1-MIN L.S. WAKE K
170=C    D703-15A 55 DEG W.T. MODEL DESIGN;M=1.6,ALPHA=4.46
180=C    USE NACELLE OFF FILE 055C,ITER=29 WITH REINDEXED K
190=C
200=       KWAK=2
210=       KWED1=36
220=       KWKST1=52
230=       VORT(30)=28.51
240=       VORT(31)=28.27
250=       VORT(32)=27.52
260=       VORT(33)=27.49
270=       VORT(34)=26.03
280=       VORT(35)=23.31
290=       VORT(36)=19.83
300=       VORT(52)=-19.84
310=       VORT(53)=-23.31
320=       VORT(54)=-26.04
330=       VORT(55)=-27.49
340=       VORT(56)=-27.52
350=       VORT(57)=-28.57
360=       VORT(58)=-28.82
370=*D MAIN.308
380=C    DEFINE WING T.E. EQUATION
390=       ZWAKE1=1.8622*ZTA1-1026.53
400=*D MAIN.315,MAIN.316
410=C    SPECIFY MAXIMUM WAKE Z(I.E. WING HALF SPAN)
420=       IF (ZWAKE1 .GT. 306.53) KWKST1=KTEMP
430=       IF (ZWAKE1 .GT. 306.53) GO TO 54
440=*D MAIN.360,MAIN.361
450=C    OUTPUT VORTICITY FOR WAKE RESTART
460=       IF (NI .NE. 48) GO TO 138
470=*D INVSETA.175,INVSETA.176
480=C    AVERAGE PHI AT OR NEAR WING TIP
490=       IF(ZTA1 .GT. 648.0 .AND. ZTA1 .LT. 717.0) PHI(1,2,KTEMP)=
500=      *(PHI(1,2,KTEMP+1)+PHI(1,2,KTEMP-1))/2.0
510=       IF(ZTA1 .GT. 648.0 .AND. ZTA1 .LT. 717.0) PHI(1,2,KTEMP+1)=
520=      *(PHI(1,2,KTEMP)+PHI(1,2,KTEMP+2))/2.0
530=C    AVERAGE PHI AT OR NEAR VERTICAL TIP
540=       IF(ZTA1 .GT. 760.) PHI(1,2,24)=(PHI(1,2,23)+PHI(1,2,25))/2.
550=       IF(ZTA1 .GT. 760.) PHI(1,2,25)=PHI(1,2,24)
560=*D NFORCE.151
570=    18 FORMAT (2X,'PITCH MOMENT=',E12.4,3X,'CM=',E12.4,
580=*D GRID.133
590=C    INCREASE GRID CELL AREA IN VERTICAL/WAKE CORNER
600=       FAC1=.75
610=*I GRID.162
620=C    CONVERGE MORE SLOWLY TO AVOID GRID DIVERGANCE
630=       IF(NN .EQ. 1) OP=.005
640=       IF(NN .GE. 2) OP=.01
650=*D INPUT.27
660=       DO 18 NAA=1,50
670=*D METRIC.51,METRIC.52
680=C    CONST.FOR ZTA1 SHOULD BE CHANGE AT VERY THIN,SHARP
690=C    LEADING EDGE USING METRIC 56-78
700=*EOF
```

d) Region 3, Solution 2

JOB CONTROL

The final type of information required to process a problem is program/update and input/output file declarations. These directives change from solution to solution in order to properly process and save data.

The pertinent submit files for the CDC 875 under NOS Operating System 2.1 are presented on table IV for the sample problem. The file functions are:

TAPE 1: Last X Plot Data
TAPE 2: Output Marching Plane Restart Data
TAPE 3: Input Marching Plane Restart Data
TAPE 4: Output Marching Plane Restart Data Backup
TAPE 5: Input Data
TAPE 7: Input Subsonic Region Data: 30 Step Limit
TAPE 8: Output Subsonic Region Data: 30 Step Limit
TAPE 9: Output Pressure Distribution at Specified Z for Post Processor

TABLE IV SAMPLE JOB CONTROL DIRECTIVES

```
100=S55A,EC700,T300,P3.
110=USER,D0236,XXXXXX.
120=CHARGE,*011,XXXX.
130=ACCT(BONNER     ST18422401*011XXXX)
140=RFL,EC=700.
150=ATTACH,OLDPL=SFP7PL/UN=D0835.
160=GET,INP=U55A.
170=UPDATE,I=INP.
180=FTN5,I,OPT=2,LCM=I,L=0,PL=20000.
190=ATTACH,TAPE5=AT55A.
200=PURGE,PL55A/NA.
210=DEFINE,TAPE1=PL55A.
220=PURGE,R55A1/NA.
230=DEFINE,TAPE2=R55A1.
240=PURGE,R55A2/NA.
250=DEFINE,TAPE4=R55A2.
260=PURGE,P55/NA.
270=DEFINE,TAPE9=P55.
280=ATTACH,LIB1=SFP7LGO/UN=D0835.
290=COPYL,LIB1,LGO,LGO1.
300=LGO1.
310=*EOF
```

a) Region 1

```
100=S55B,EC700,T500,P3.
110=USER,D0236,XXXXXX.
120=CHARGE,*011,XXXX.
130=ACCT(BONNER     ST18422401*011XXXX)
140=RFL,EC=700.
150=ATTACH,OLDPL=SFP7PL/UN=D0835.
160=GET,INP=U55B.
170=UPDATE,I=INP.
180=FTN5,I,OPT=2,LCM=I,L=0,PL=20000.
190=ATTACH,TAPE5=AT55B.
200=ATTACH,TAPE3=R55A1.
210=PURGE,PL55B/NA.
220=DEFINE,TAPE1=PL55B.
230=PURGE,R55B1/NA.
240=DEFINE,TAPE2=R55B1.
250=PURGE,R55B2/NA.
260=DEFINE,TAPE4=R55B2.
270=ATTACH,TAPE9=P55/M=A.
280=SKIPEI,TAPE9.
290=ATTACH,LIB1=SFP7LGO/UN=D0835.
300=COPYL,LIB1,LGO,LGO1.
310=LGO1.
320=*EOF
```

b) Region 2

```
100=S55C,EC700,T200,P3.
110=USER,D0236,XXXXXX.
120=CHARGE,*011,XXXX.
130=ACCT(BONNER     ST18422401*011XXXX)
140=RFL,EC=700.
150=ATTACH,OLDPL=SFP7PL/UN=D0835.
160=GET,INP=U55C.
170=UPDATE,I=INP.
180=FTN5,I,OPT=2,LCM=I,L=0,PL=20000.
190=ATTACH,TAPE5=AT55C.
200=ATTACH,TAPE3=R55B1.
210=PURGE,PL55C/NA.
220=DEFINE,TAPE1=PL55C.
230=PURGE,R55C1/NA.
240=DEFINE,TAPE2=R55C1.
250=PURGE,R55C2/NA.
260=DEFINE,TAPE4=R55C2.
270=ATTACH,TAPE9=P55/M=A.
280=SKIPEI,TAPE9.
290=ATTACH,LIB1=SFP7LGO/UN=D0835.
300=COPYL,LIB1,LGO,LGO1.
310=LGO1.
320=*EOF
```

c) Region 3, Solution 1

```
100=S55D,EC700,T300,P3.
110=USER,D0236,XXXXXX.
120=CHARGE,*011,XXXX.
130=ACCT(BONNER     ST18422401*011XXXX)
140=RFL,EC=700.
150=ATTACH,OLDPL=SFP7PL/UN=D0835.
160=GET,INP=U55D.
170=UPDATE,I=INP.
180=FTN5,I,OPT=2,LCM=I,L=0,PL=20000.
190=ATTACH,TAPE5=AT55D.
200=ATTACH,TAPE3=R55C1.
210=PURGE,PL55D/NA.
220=DEFINE,TAPE1=PL55D.
230=PURGE,R55D1/NA.
240=DEFINE,TAPE2=R55D1.
250=PURGE,R55D2/NA.
260=DEFINE,TAPE4=R55D2.
270=ATTACH,TAPE9=P55/M=A.
280=SKIPEI,TAPE9.
290=ATTACH,LIB1=SFP7LGO/UN=D0835.
300=COPYL,LIB1,LGO,LGO1.
310=LGO1.
320=*EOF
```

d) Region 3, Solution 2

ANALYSIS

It is recommended that a general file nomenclature be developed prior to the analysis in order to achieve a consistent function/code/problem seven character descriptor. The following is provided as an example.

FUNCTION	FILE
Submit	SXYYYY A, B, C, D (X: Function; YYYY: Code; A, B, C, D: Solutions; YYYY: Case)
Input	I
Sectional Plot	X
Restart	R
Printed Output	O
Pressure Plot	P

A review of the submit, header input, and update files should be completed before processing each solution. A check list which has been found to be useful in this regard is

SOLUTION	TAPE 5	UPDATES
Region 1	Taper=F NAJS=0	Modify as appropriate
Region 2	Taper=T	———
Region 3 Solution 1	NRM=3, NUØ KWST,KWKED, XWAKE	Main. 360, VORT (k) Output
Region 3 Solution 2	NAJS=1, etc	KWAK= 2, Reindex KWKED1,KWKST1, and VORT (k)

Typical problem (one Mach number and angle of attack) run time on the CDC 875 under OPT = 2 compilation is

SOLUTION	ZTA1	J	K	ITER	CPU-SEC	SEC/STEP
Region 1	0-370	15	33	172	121	.7
Region 2	370-455	15	57	34	60	1.76
Region 3	455-610	15	68	62	111	1.78
Region 4 Solution 1	610-685	15	74	30	79	2.65
Region 4 Solution 2	685-802.5	15	80	47	133	2.82
					504	

PRE-PROCESSOR

A pre-processor is available for evaluating input geometry and grid quality. It may be accessed and executed using

```
GET,SFPPLTX/UN=D0235

SFPPLTX,XPFN,DOXXX
```

The file XPFN is generated for ZTA1 by the supersonic full potential analysis as tape 1 when NMAX=0, TAPER=F.

Typical grid program prompt response is

```
get,sfppltx
/sfppltx,p48j5c,d0096
      .1600E-01   .1590E-01   .6085E+03   20   51
IPLOT...IS
        =   2 FOR MACH NO. CONTOURS
        =   3 FOR PRESSURE CONTOURS
        =  10 FOR COMPUTATIONAL      GRID
        =  12 FOR MACH NO. PROFILES
        =  13 FOR PRESSURE PROFILES
---------0---------0---------0---------0
? 10
XMIN=  0.                XMAX=   .9409186SE+03
YMIN=  -.90619733E+03YMAX=   .88599023E+03
XMIN,XMAX,YMIN,YMAX...4F10.4
X  IS THE PLOTIS X COORDINATE
Y  IS THE PLOTIS Y COORDINATE
Y  IS THUS  MACH NO. FOR IPLOT=12
Y  IS THUS  PRESSURE FOR IPLOT=13
Y  IS OTHERWISE THE PHYSICAL Y COORDINATE
X IS ALWAYS THE PHYSICAL X COORDINATE
XMIN=  0.                XMAX=   .9409186SE+03
YMIN=  -.90619733E+03YMAX=   .88599023E+03
---------0---------0---------0---------0
XMIN=  0.                XMAX=   .9409186SE+03
YMIN=  -.90619733E+03YMAX=   .88599023E+03
? 0.        400.       -200.        200.
```

ORIGINAL PAGE IS OF POOR QUALITY

Typical output is shown below. The grid is truncated at Z=400 and Y=±200 as specified in the input above

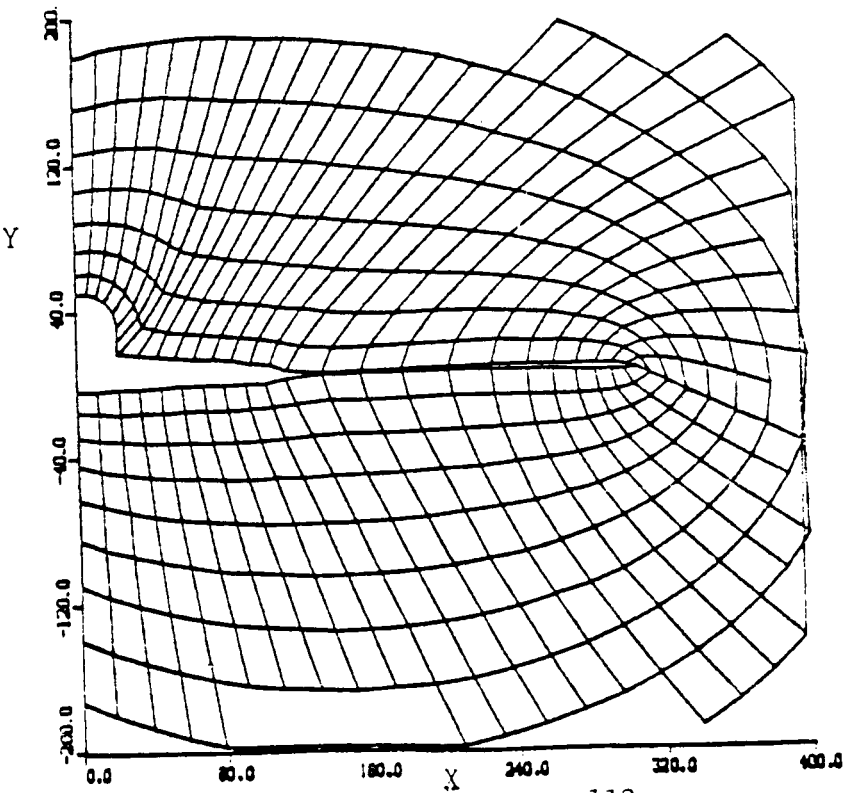

OUTPUT DATA

Sample printed output data is presented on table V for region 3, solution 2. Standard tabulated data is produced every NP marching steps as defined in the header data. More detailed physical plane data can be output at specified stations using the parameter NSPTI and the tabulated stations following the true/false header data input. Cartesion coordinates, velocities, and mesh indices are indicated in the following sketch. The axial velocity component, U, is positive out of the plane of the paper.

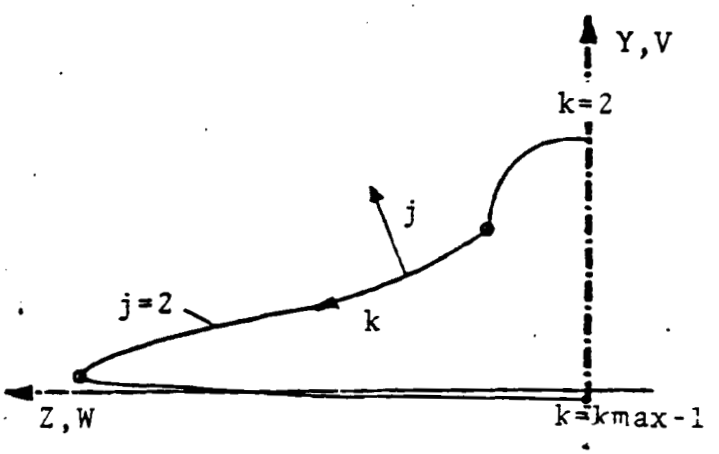

Crossplane data and tabulated surface pressure coefficient data at constant span stations (i.e. z) are output via tapes 1 and 9 respectively. These files are displayed using the pre and post processors described in this document.

ITER= 5 (STEP) DZTA= 2.50000 ZTA1= 696.58838

TABLE V SAMPLE OUTPUT DATA

J	K	RHO	ρ/ρ_∞	C_p CP	PHI	Contravariant Velocities U	V	W	X	Y	Z
2	1	.872616		-.096915	714.215315	I	I	I	696.588384	49.946005	-5.649278
2	2	.872623		-.096910	714.204622	1.050623	0.000000	0.000000	696.588384	50.007111	0.000000
2	3	.872618		-.096915	714.218316	1.050518	0.000000	.000071	696.588384	49.946006	5.649278
2	4	.873174		-.096503	714.248745	1.050269	0.000000	.000147	696.588384	48.830548	11.157859
2	5	.874366		-.095620	714.305288	1.049668	0.000000	.000251	696.588384	45.976709	16.013771
2	6	.872136		-.097271	714.504990	1.050287	0.000000	.000103	696.588384	38.523018	21.151141
2	7	.862499		-.104383	714.836467	1.053838	0.000000	-.000019	696.588384	29.496730	22.217937
2	8	.850378		-.113283	715.239224	1.058207	0.000000	-.000116	696.588384	20.360161	22.099892
2	9	.841292		-.119921	715.803286	1.060812	0.000000	-.000339	696.588384	11.222849	22.130118
2	10	.848717		-.114499	715.640282	1.057427	0.000000	-.000116	696.588384	10.635839	34.678301
2	11	.856343		-.108909	715.548134	1.054818	0.000000	-.000163	696.588384	10.167200	47.231016
2	12	.862010		-.104742	715.215639	1.051803	0.000000	-.000364	696.588384	9.980513	59.791822
2	13	.896769		-.078948	714.493998	1.036773	0.000000	-.000598	696.588384	9.546090	72.346230
2	14	.878214		-.092769	713.454512	1.044120	0.000000	-.000634	696.588384	9.033332	84.897888
2	15	.855106		-.109817	712.639572	1.055693	0.000000	-.000403	696.588384	8.453547	97.446525
2	16	.796150		-.152476	712.355240	1.079943	0.000000	-.000323	696.588384	7.656034	109.983178
2	17	.750268		-.184816	711.603647	1.098479	0.000000	-.001455	696.588384	19.543347	114.612843
2	18	.571523		-.303054	710.240655	1.178196	0.000000	-.002982	696.588384	34.426618	120.638436
2	19	.988565		-.024403	709.952537	1.011578	0.000000	-.004748	696.588384	46.562350	125.885400
2	20	1.384285		.321751	710.068089	.851226	0.000000	-.008015	696.588384	53.717897	129.180570
2	21	1.687214		.602611	709.537858	.731483	0.000000	-.009591	696.588384	58.456765	131.626700
2	22	1.203788		.165454	710.328615	.688019	0.000000	-.023466	696.588384	61.448687	133.958279
2	23	1.187687		.151942	708.419447	.856460	0.000000	.004271	696.588384	57.404383	133.773184
2	24	1.211263		.171750	707.036204	.905288	0.000000	.005404	696.588384	51.839495	132.488912
2	25	.938402		-.047523	706.321779	1.021979	0.000000	.003958	696.588384	43.679468	130.254218
2	26	.814356		-.139434	705.713319	1.074143	0.000000	.002269	696.588384	30.141000	126.154023
2	27	.747032		-.187067	706.033838	1.102131	0.000000	.001185	696.588384	13.799620	120.801278
2	28	.778193		-.165224	706.225323	1.088395	0.000000	.000573	696.588384	.867854	116.363281
2	29	1.040903		.032214	707.005377	.983751	.000066	.000109	696.588384	2.142344	140.624250
2	30	1.047007		.037067	707.509698	.981139	.000330	-.000188	696.588384	3.497559	166.660347
2	31	1.020956		.016441	706.811346	.989676	.000578	-.000335	696.588384	4.974130	195.631517
2	32	.997484		-.001964	705.783749	.998770	.000690	-.000321	696.588384	6.431195	224.529098
2	33	.905790		-.072188	705.017271	1.033382	.000656	-.000571	696.588384	7.684317	247.718921
2	34	.851733		-.112290	702.271378	1.052011	.000490	-.000891	696.588384	8.262393	264.931600
2	35	.358600		-.425012	701.901114	1.275561	0.000000	-.001226	696.588384	8.611518	278.402489
2	36	.387657		-.409959	698.181106	1.230990	0.000000	-.002962	696.588384	8.829093	289.487817
2	37	.549374		-.316780	694.830364	1.097884	0.000000	-.005217	696.588384	8.753903	298.793426
2	38	.457297		-.371424	690.329619	1.008294	0.000000	-.014518	696.588334	7.796446	306.528992
2	39	1.008353		.006537	688.484540	.978897	0.000000	-.002028	696.588304	7.459420	298.747500
2	40	1.072089		.057120	687.482653	.962986	0.000000	-.001175	696.588384	7.958001	289.456406
2	41	1.272637		.224039	686.206321	.885956	0.000000	-.001111	696.588384	8.007882	278.373004
2	42	.864753		-.102722	684.305635	1.051430	.000004	-.000468	696.588384	7.946608	264.900973
2	43	.908679		-.070017	684.290840	1.035219	-.000708	-.000280	696.588384	7.716527	247.684785
2	44	.998102		-.001482	683.209029	.998665	-.000577	-.000280	696.588384	6.419963	224.503204
2	45	1.020192		.015038	681.803950	.990154	-.000501	-.000267	696.588384	5.010471	195.610113
2	46	1.042044		.033121	680.575873	.982155	-.000397	-.000253	696.588384	3.548817	166.645427
2	47	1.031691		.024915	679.795940	.984745	-.000376	-.000346	696.588384	2.174109	140.616372
2	48	1.032494		.025550	677.918751	.985072	0.000000	-.000445	696.588384	.867854	116.363281
2	49	1.029608		.023267	677.213594	.987619	0.000000	-.000394	696.588384	.522167	101.820516
2	50	1.028351		.022274	676.758143	.988580	0.000000	-.000264	696.588384	.069392	87.274129
2	51	1.044217		.034847	676.523870	.982598	0.000000	-.000167	696.588384	-.411646	72.728832
2	52	1.047296		.037297	676.410182	.981438	0.000000	-.000118	696.588384	-.962648	58.179577
2	53	1.038723		.030485	676.318889	.984731	0.000000	-.000096	696.588384	-1.203779	43.640848
2	54	1.029345		.023060	676.204160	.988351	0.000000	-.000077	696.588384	-1.889275	29.101001
2	55	1.026936		.021157	676.126533	.989269	0.000000	-.000042	696.588384	-2.116542	14.552648
2	56	1.027394		.021518	676.096079	.989098	0.000000	0.000000	696.588384	-2.257743	0.000000
2	57	1.026936		.021157	676.126533	I	I	I	696.588384	-2.116542	-14.552648

15 56	1.006286	.004917	652.950876	.994820	-.000576	0.000000	696.588384	-530.992758	0.000000
16 56	1.000046	.000036	645.388007	.996996	-.000649	0.000000	696.588384	-629.183474	0.000000
17 56	1.001168	.000913	636.587362	.996560	-.000719	0.000000	696.588384	-742.906384	0.000000
18 56	1.000015	.000011	626.447526	.997006	-.000793	0.000000	696.588384	-874.618431	0.000000
19 56	.998826	-.001073	614.629798	.997515	-.000871	0.000000	696.588384	-1027.165207	0.000000
20 56	1.000000	0.000000	600.864805	1	-.000963	1	696.588384	-1203.842432	0.000000

RMS DENSITY= .08857158

+++UPER SURFACE+++ C_p P/P_∞

X= .69659E+03	Z= 0.	CP= -.969106-01	RHO= .87262E+00	IU= 1	
X= .69689E+03	Z= .30600E+02	CP= -.11826E+00	RHO= .84830E+00	IU= 2	
X= .69659E+03	Z= .61200E+02	CP= -.10188E+00	RHO= .86991E+00	IU= 3	
X= .69659E+03	Z= .91800E+02	CP= -.10215E+00	RHO= .86550E+00	IU= 4	
X= .69659E+03	Z= .12240E+03	CP= -.20914E+00	RHO= .70533E+00	IU= 5	
X= .69659E+03	Z= .15300E+03	CP= .34521E-01	RHO= .10438E+01	IU= 6	
X= .69659E+03	Z= .18360E+03	CP= .25006E-01	RHO= .10318E+01	IU= 7	
X= .69659E+03	Z= .21420E+03	CP= .46142E-02	RHO= .10059E+01	IU= 8	
X= .69659E+03	Z= .24480E+03	CP= -.63349E-01	RHO= .91733E+00	IU= 9	
X= .69689E+03	Z= .27540E+03	CP= -.36854E+00	RHO= .46844E+00	IU= 10	
X= .69659E+03	Z= .30653E+03	CP= -.37142E+00	RHO= .90433E+00	IU=	

LEADING EDGE

+++LOWER SURFACE+++

SPECIFIED Z SURFACE PRESSURE COEFFICIENT

X= .69659E+03	Z= 0.	CP= .21518E-01	RHO= .10274E+01	IU= 1	
X= .69659E+03	Z= .30600E+02	CP= .23824E-01	RHO= .10303E+01	IU= 2	
X= .69689E+03	Z= .61200E+02	CP= .36788E-01	RHO= .10467E+01	IU= 3	
X= .69659E+03	Z= .91800E+02	CP= .22583E-01	RHO= .10287E+01	IU= 4	
X= .69659E+03	Z= .12240E+03	CP= .25391E-01	RHO= .10323E+01	IU= 5	
X= .69659E+03	Z= .15300E+03	CP= .28819E-01	RHO= .10366E+01	IU= 6	
X= .69659E+03	Z= .18360E+03	CP= .23005E-01	RHO= .10293E+01	IU= 7	
X= .69659E+03	Z= .21420E+03	CP= .46942E-02	RHO= .10060E+01	IU= 8	
X= .69659E+03	Z= .24480E+03	CP= -.61488E-01	RHO= .91981E+00	IU= 9	
X= .69659E+03	Z= .27540E+03	CP= .15193E+00	RHO= .11826E+01	IU= 10	

RMSR3= .17218125E-01 NN= 312 NR3ITER= 2
RMSR3= .16891918E-01 NN= 312 NR3ITER= 3
RMSR3= .11200030E-04 NN= 312 NR3ITER= 4

EIGENY= .92064673E-01 CFLE= .23016168E+01 EIGENZ= .78797052E-01 CFLX= .1970E+01 DZTA= .2500E+01
KST,KED1,KST1,KED,KS,KE,KIA,KAWK 28 35 41 48 35 35 1 2
VORT,PHM,K .16133E+02 .68830E+03 35
KST,KED1,KST1,KED,KS,KE,KIA,KAWK 28 35 41 48 41 41 2 2
VORT,PHM,K -.16135E+02 .70444E+03 41
L= .31948E+05 D= .28019E+04 CL= .25501E+00 CD= .22365E-01 SURFACE A= .36979E+06 REF. A= .12828E+06
PITCH MOMENT= -.4698E+06 CP= -.1598E-01 XO= .5000E+03 YO= 0. .1545E+03 .1603E+05 .2346E+03

FLOW FIELD AT ZTA= 699.0884

J	K	RHO ρ/ρ_∞	P P/P_∞	U-VEL u/V_∞	V-VEL v/V_∞	W-VEL w/V_∞	A $T_{t\infty}/T_t$	M	X	Y	Z
2	2	.8731E+00	.8270E+00	.1050E+01	.7814E-06	0.	.6083E+00	.1727E+01	.6991E+03	.5001E+02	0.
3	2	.8758E+00	.8306E+00	.1049E+01	-.1508E-01	0.	.6086E+00	.1724E+01	.6991E+03	.6383E+02	0.
4	2	.8764E+00	.8314E+00	.1049E+01	-.1420E-01	0.	.6087E+00	.1723E+01	.6991E+03	.7985E+02	0.
5	2	.8801E+00	.8362E+00	.1047E+01	-.9394E-02	0.	.6092E+00	.1719E+01	.6991E+03	.9845E+02	0.
6	2	.8890E+00	.8481E+00	.1044E+01	-.7727E-03	0.	.6108E+00	.1710E+01	.6991E+03	.1200E+03	0.
7	2	.8963E+00	.8579E+00	.1041E+01	.9083E-02	0.	.6115E+00	.1702E+01	.6991E+03	.1450E+03	0.
8	2	.9038E+00	.8679E+00	.1038E+01	.1903E-01	0.	.6125E+00	.1695E+01	.6991E+03	.1740E+03	0.
9	2	.9099E+00	.8762E+00	.1035E+01	.2816E-01	0.	.6133E+00	.1688E+01	.6991E+03	.2077E+03	0.
10	2	.9238E+00	.8950E+00	.1029E+01	.3802E-01	0.	.6152E+00	.1674E+01	.6991E+03	.2467E+03	0.
11	2	.9404E+00	.9175E+00	.1022E+01	.4930E-01	0.	.6174E+00	.1658E+01	.6991E+03	.2919E+03	0.
12	2	.9633E+00	.9490E+00	.1012E+01	.6413E-01	0.	.6203E+00	.1635E+01	.6991E+03	.3444E+03	0.

TABLE V CONTINUED

```
  7 56   .1065E+01   .1092E+01   .9745E+00   .2535E-01  0.          .6329E+00   .1540E+01   .6991E+03  -.1020E+03  0.
  8 56   .1071E+01   .1101E+01   .9721E+00   .2646E-01  0.          .6336E+00   .1535E+01   .6991E+03  -.1323E+03  0.
  9 56   .1071E+01   .1101E+01   .9718E+00   .3007E-01  0.          .6337E+00   .1534E+01   .6991E+03  -.1675E+03  0.
 10 56   .1061E+01   .1086E+01   .9756E+00   .3697E-01  0.          .6324E+00   .1544E+01   .6991E+03  -.2083E+03  0.
 11 56   .1052E+01   .1074E+01   .9787E+00   .4351E-01  0.          .6314E+00   .1551E+01   .6991E+03  -.2555E+03  0.
 12 56   .1051E+01   .1072E+01   .9790E+00   .4806E-01  0.          .6312E+00   .1553E+01   .6991E+03  -.3102E+03  0.
 13 56   .1046E+01   .1065E+01   .9806E+00   .5437E-01  0.          .6307E+00   .1557E+01   .6991E+03  -.3736E+03  0.
 14 56   .1028E+01   .1039E+01   .9872E+00   .5436E-01  0.          .6284E+00   .1574E+01   .6991E+03  -.4470E+03  0.
 15 56   .1006E+01   .1009E+01   .9948E+00   .7363E-01  0.          .6258E+00   .1594E+01   .6991E+03  -.5321E+03  0.
 16 56   .1000E+01   .1000E+01   .9970E+00   .7722E-01  0.          .6250E+00   .1600E+01   .6991E+03  -.6307E+03  0.
 17 56   .1001E+01   .1002E+01   .9966E+00   .7717E-01  0.          .6251E+00   .1599E+01   .6991E+03  -.7449E+03  0.
 18 56   .1000E+01   .1000E+01   .9970E+00   .7724E-01  0.          .6250E+00   .1600E+01   .6991E+03  -.8773E+03  0.
 19 56   .9986E+00   .9980E+00   .9975E+00   .7771E-01  0.          .6248E+00   .1601E+01   .6991E+03  -.1031E+04  0.

     ITER=    6 ZTA1= 699.08838 DZTA1=   2.50000
RMSR3=    .23415121E-01      NN=  313      NR3ITER=    2
RMSR3=    .16881968E-01      NN=  313      NR3ITER=    3
RMSR3=    .92558456E-05      NN=  313      NR3ITER=    4
  EIGENY=    .21338727E+00  CFLE= .53346819E+01  EIGENZ=    .63246441E-01  CFLX=       .1581E+01  DZTA=       .2500E+01
 L= .32070E+05   D= .28180E+04   CL= .25599E+00   CD= .22494E-01   SURFACE A= .37196E+06   REF. A= .12528E+06
 PITCH MOMENT=  -.4946E+06   CP=  -.1883E-01   XO=  .5000E+03   YO=  0.          .1578E+03   .1610E+05   .2346E+03

     ITER=    7 ZTA1= 701.58838 DZTA1=   2.50000
RMSR3=    .16894983E-01      NN=  314      NR3ITER=    2
RMSR3=    .19344000E-01      NN=  314      NR3ITER=    3
RMSR3=    .17461672E-04      NN=  314      NR3ITER=    4
     COMPLEX EIGEN VALUE  J=    2  K=   22  NN=  314  Q2ETA=    .20812154E-04  Q2XI=   -.32109857E-04
  EIGENY=    .24856313E-01  CFLE=    .62140783E+00  EIGENZ=    .42286298E-01  CFLX=       .1057E+01  DZTA=       .2500E+01
 L= .32201E+05   D= .28350E+04   CL= .25703E+00   CD= .22629E-01   SURFACE A= .37414E+06   REF. A= .12528E+06
 PITCH MOMENT=  -.5214E+06   CP=  -.1774E-01   XO=   .5000E+03   YO=  0.          .1612E+03   .1618E+05   .2346E+03

     ITER=    8 ZTA1= 704.08838 DZTA1=   2.50000
RMSR3=    .19873105E-01      NN=  315      NR3ITER=    2
RMSR3=    .19259946E-01      NN=  315      NR3ITER=    3
RMSR3=    .16920610E-04      NN=  315      NR3ITER=    4
     COMPLEX EIGEN VALUE  J=    2  K=   22  NN=  315  Q2ETA=    .10370612E-04  Q2XI=   -.74477587E-03
  EIGENY=    .18347013E-01  CFLE=    .45867532E+00  EIGENZ=    .29677634E-01  CFLX=       .7419E+00  DZTA=       .2500E+01
 KST,KED1,KST1,KED,KS,KE,KIA,KAWK   28   36   40   48   36   36    1    2
 VORT,PHM,K     .14187E+02     .69610E+03    36
 KST,KED1,KST1,KED,KS,KE,KIA,KAWK   28   36   40   48   40   40    2    2
 VORT,PHM,K    -.14187E+02     .71029E+03    40
 L= .32302E+05   D= .28506E+04   CL= .25784E+00   CD= .22754E-01   SURFACE A= .37624E+06   REF. A= .12528E+06
 PITCH MOMENT=  -.5426E+06   CP=  -.1846E-01   XO=   .5000E+03   YO=  0.          .1650E+03   .1621E+05   .2346E+03

     ITER=    9 ZTA1= 706.58838 DZTA1=   2.50000
RMSR3=    .24927062E-01      NN=  316      NR3ITER=    2
RMSR3=    .19872039E-01      NN=  316      NR3ITER=    3
RMSR3=    .20722912E-04      NN=  316      NR3ITER=    4
     COMPLEX EIGEN VALUE  J=    2  K=   22  NN=  316  Q2ETA=    .10124578E-04  Q2XI=   -.78430692E-03
  EIGENY=    .15843887E-01  CFLE=    .39609718E+00  EIGENZ=    .23966680E-01  CFLX=       .5992E+00  DZTA=       .2500E+01
 L= .32412E+05   D= .28674E+04   CL= .25872E+00   CD= .22888E-01   SURFACE A= .37835E+06   REF. A= .12528E+06
 PITCH MOMENT=  -.5658E+06   CP=  -.1925E-01   XO=   .5000E+03   YO=  0.          .1691E+03   .1627E+05   .2346E+03
        +++++RESTART DATA WRITE ON UNIT  4+++++
```

TABLE V CONCLUDED

POST PROCESSOR

A graphics geometry and surface pressure coefficient output processor for the Techtronix 4114 has been recently developed to support advance design effort using the supersonic full potential analysis. It may accessed and executed using

```
GET,SFPPLT/UN=D0235
SFPPLT,FPIN,FPOUT,DOXXX
```

The pertinent files are

NAME	TYPE	DESCRIPTION
SFPPLT	ID	Proc for Post Processor
FPIN	DA	SFP Output Data Set ≤ 5 Characters. UN=DOXXX
FPOUT	DA	Created to Store Post Processor Output for Debug if necessary.

The input file FPIN is generated by supersonic full potential analysis as tape 9 output. This file must be edited as follows:

1. Delete *EOR's and repetitious results.
2. Delete cone starting solution off front end.
3. Add the following data at the beginning.

   (a) Title Card
   (b) Mach Number and Angle of Attack. One card, format 2E12.5.
   (c) Number of trailing edge points. One card, format I3.
   (d) Planform trailing edge data. Input trailing edge X from root to tip, for each section stored in FPIN. Format 5E12.5

4. Check end of data set to make sure the last x-station is fully represented. If it is not, (examine previous x-station to see a fully represented example) delete these incomplete data.

5. If you do not want a particular z-value (3rd column) to be included in the data you will process, delete any reference to such data out of the 3rd column at the very end of the data set.

Sample graphics post processor input data is presented on Table VI.

The following nine post processor options are available to the analyst.

```
0  TO END
1  TO DISPLAY PLANFORM
2  TO DISPLAY 3-D VIEW OF WING Z/C
3  TO DISPLAY 3-D VIEW OF WING CP S
4  TO DISPLAY SECTION     CP S
5  TO DISPLAY SECTION     Z/C
6  TO DISPLAY SPANWISE    CL,CD,XCP
7  TO DISPLAY PLANFORM    ISOBARS
8  TO CREATE  BOUNDARY LAYER DATA FILE
```

The last creates a boundary layer analysis[4] input file FPINBL for the upper and lower surface. This data must be edited to remove the first STOP card, update case identification, static pressure and temperature, and specified transition point location.

TABLE VI POST PROCESSOR INPUT FILE STRUCTURE


```
100= D703-15A 55 DEG SWEEP MAN. POINT DESIGN DERIVATIVE
110=   .1600E+01   .4462E-01
120= 21
130=   .8000E+03   .8000E+03   .8000E+03   .8000E+03   .8000E+03
140=   .8000E+03   .8000E+03   .8000E+03   .6171E+03   .6253E+03
150=   .6336E+03   .6418E+03   .8500E+03   .6582E+03   .6665E+03
160=   .6747E+03   .6829E+03   .6912E+03   .6994E+03   .7076E+03
170=   .7159E+03
180=   .1500E+02   .6292E+01   .0000E+00   .3742E+00
190=   .1502E+02   .2716E+01   .6324E+01   .3653E+00
200=   .1500E+02  -.4622E+00   .0000E+00   .1749E+00
210=   .2000E+02   .7861E+01   .0000E+00   .1507E+00
220=   .2000E+02   .3140E+01   .8300E+01   .1317E+00
230=   .2000E+02  -.1865E+01   .0000E+00   .2620E+00
240=   .2500E+02   .9271E+01   .0000E+00  -.1004E+00
250=   .2500E+02   .3631E+01   .9502E+01  -.5543E-01
260=   .2500E+02  -.1340E+01   .0000E+00   .7038E-01
270=   .3000E+02   .1868E+02   .0000E+00   .4053E-01
280=   .3000E+02   .4124E+01   .1076E+02   .6944E-02
290=   .3000E+02  -.1624E+01   .0000E+00   .7075E-01
300=   .3500E+02   .1200E+02   .0000E+00   .8464E-01
310=   .3500E+02   .4618E+01   .1192E+02   .1335E+00
320=   .3500E+02  -.1898E+01   .0000E+00   .8600E-01
330=   .4000E+02   .1348E+02   .0000E+00   .1205E+00
340=   .4000E+02   .5111E+01   .1300E+02   .2134E+00
350=   .4000E+02  -.2172E+01   .0000E+00   .8487E-01
360=   .4500E+02   .1487E+02   .0000E+00   .1579E+00
370=   .4500E+02   .5694E+01   .1380E+02   .7023E-01
380=   .4500E+02  -.2246E+01   .0000E+00   .6772E-02
390=   .5000E+02   .1625E+02   .0000E+00   .1763E+00
400=   .5000E+02   .6283E+01   .1467E+02   .7084E-01
410=   .5000E+02  -.2306E+01   .0000E+00   .1026E-01
420=   .5500E+02   .1763E+02   .0000E+00   .1664E+00
430=   .5500E+02   .8039E+01   .1533E+02   .8658E-01
440=   .5500E+02   .6872E+01   .1545E+02   .8729E-01
450=   .5500E+02  -.2367E+01   .0000E+00   .1621E-01
460=   .5500E+02   .5844E+01   .1533E+02   .8118E-01
470=   .6000E+02   .1900E+02   .0000E+00   .1563E+00
480=   .6000E+02   .1176E+02   .1533E+02   .1106E+00
490=   .6000E+02   .7462E+01   .1622E+02   .9605E-01
500=   .6000E+02  -.2427E+01   .0000E+00   .2754E-01
510=   .6000E+02   .3186E+01   .1533E+02   .7508E-01
520=   .6500E+02   .2032E+02   .0000E+00   .1271E+00
530=   .6500E+02   .1366E+02   .1533E+02   .7140E-01
540=   .6500E+02   .8044E+01   .1682E+02   .3206E-01
550=   .6500E+02  -.2363E+01   .0000E+00  -.4588E-02
560=   .6500E+02   .2674E+01   .1533E+02   .1547E-01
570=   .7000E+02   .2164E+02   .0000E+00   .1267E+00
580=   .7000E+02   .1548E+02   .1533E+02   .8662E-01
590=   .7000E+02   .8625E+01   .1730E+02   .4700E-01
600=   .7000E+02  -.2285E+01   .0000E+00   .1194E-01
```

ADDED HEADER DATA

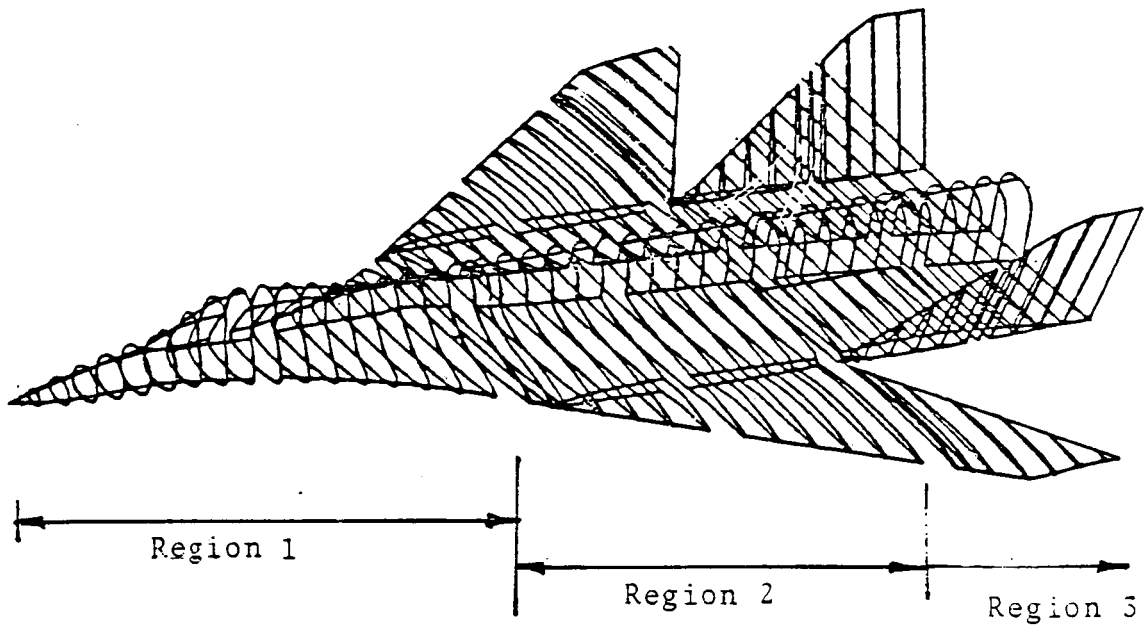

Figure 1. Sample Problem

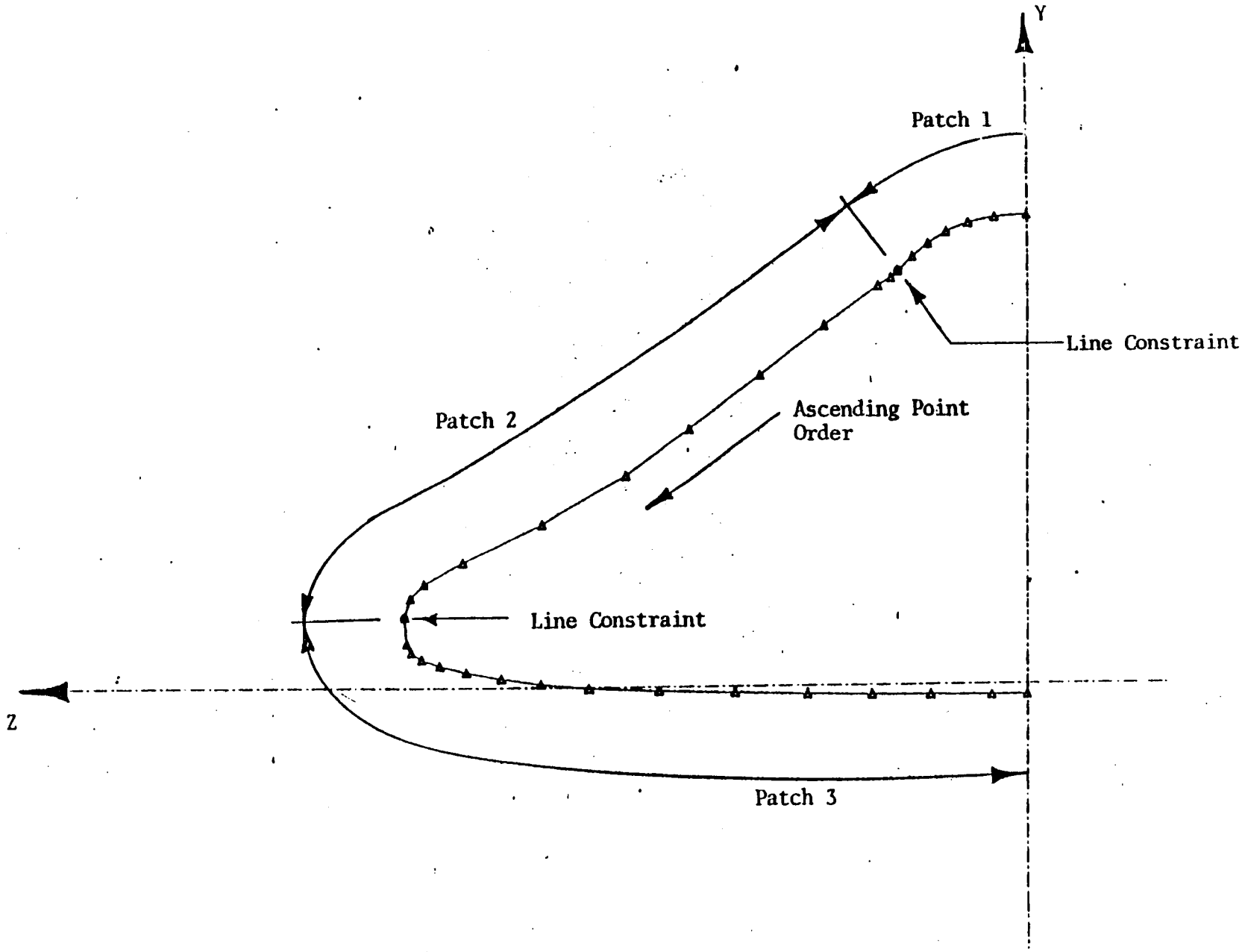

Figure 2. Region 1 Patching

REFERENCES

1. Shankar, V., "A Conservative Full Potential, Implicit, Marching Scheme for Supersonic Flows," AIAA Journal, Vol. 20, No. 11, November, 1982, pp. 1508-1514.

2. Shankar, v. and Osher, S., "An Efficient Full Potential Implicit Method Based on Charateristics for Analysis of Supersonic Flows," AIAA Paper No. 82-0974, June, 1982; also to appear in AIAA Journal, August, 1983.

3. Shankar, V., Szema, K.Y. and Osher, S., "A Conservative Type-Dependent Full Potential Method for the Treatment of Supersonic Flows with Embedded Subsonic Regions," AIAA Paper No. 83-1887. July 1983.

4. Nash, J. and Scrugs, R. "An Implicit Method for Calculation of Three Dimension Boundary Layers on Finite Thick Wings, "AFFDl TR-77-122 February, 1977.

5. Crehan, M, "Supersonic Full Potential Analysis Modeling Using CDS," to be published.

AIAA'84

AIAA-84-0262

Implicit Treatment of the Unsteady Full Potential Equation in Conservation Form

V. Shankar, Rockwell International Science Center, Thousand Oaks, CA

AIAA 22nd Aerospace Sciences Meeting

January 9-12, 1984/Reno, Nevada

IMPLICIT TREATMENT OF THE UNSTEADY FULL POTENTIAL EQUATION IN CONSERVATION FORM

Vijaya Shankar*

Rockwell International Science Center
Thousand Oaks, California 91360

Abstract

An implicit, conservative treatment for the unsteady full potential equation in two-dimensions is presented. The method employs a local time linearization for density, and introduces flux biasing concepts based on sonic conditions for the generation of artificial viscosity to capture shocks without any overshoots. The boundary condition is treated implicitely using a splitting procedure consistent with the approximate factorization scheme. This allows for extremely large Courant numbers, even for nonorthogonal grid at the body. The method has application not only to unsteady problems, but also to generate the starting blunt body solution for a supersonic full potential marching code. Results are presented for flows over cylinders, spheres and airfoils. Comparisons are made with available Euler and full potential results, and are in excellent agreement.

I. Introduction

Nonlinear aerodynamic prediction methods based on the steady form of the full potential equation are used ragularly for treating transonic[1,2] and supersonic[3-6] flows over realistic wing-body configurations. Numerical algorithms to compute the unsteady form of the full potential equation is still in a developmental stage, and several researchers[7-11] have recently made significant progress in this area. There are several issues involved in the construction of a robust and efficient numerical algorithm for the unsteady full potential equation. They are: 1) proper treatment of boundary conditions in a nonorthogonal grid system, 2) correct formulation for the production of artificial viscosity to capture sharp shocks, and 3) proper time linearization concepts.

The objective of the present paper is to present a numerical treatment of the unsteady full potential equation that properly takes into account the importance of the above three listed items. The paper discusses a local time linearization procedure for treating the time derivative term, a flux biasing concept based on sonic conditions (instead of the usual density biasing procedures) for the treatment of spatial derivative terms, and a split boundary condition procedure for incorporation into an approximately factored implicit algorithm. The resulting unsteady method has application not only to unsteady problems in transonics, but also to generate the starting blunt body solution for a full potential supersonic marching code.[6] The unsteady method of this paper, when combined with the steady methods of Refs. 4-6, provides a complete treatment of the full potential equations.

Results are presented for flows over cylinders, spheres and airfoils at various Mach numbers, and some comparisons are made with Euler solutions. Use of the split boundary condition technique, combined with the flux biasing concepts,[12,13] has produced a very robust method which, even for a difficult case with a fish-tail shock at the trailing edge of an airfoil, did not require any user specified "constants", such as the ones discussed in Ref. 2.

The paper also presents the results from a "hybrid" calculation, wherein the spherical blunt body solution from the unsteady code has been effectively used to provide the initial data plane for a supersonic marching calculating performed over the Shuttle Orbiter geometry.

II. Formulation

The two-dimensional/axisymmetric unsteady full potential equation written in a body-fitted coordinate system represented by $\tau = t$, $\zeta = \zeta(x,y,t)$ and $\eta = \eta(x,y,t)$ takes the form

$$\left(\frac{\rho}{J}\right)_\tau + \left(\rho\,\frac{U}{J}\right)_\zeta + \left(\rho\,\frac{V}{J}\right)_\eta + S\rho\,\frac{v}{yJ} = 0 \qquad (1)$$

where,

$S = 0$ for two dimensions, $= 1$ for axisymmetric

$$\rho = \text{density} = \left[1 - \frac{\gamma-1}{2} M_\infty^2 (2\phi_\tau + \bar{U}\phi_\zeta + \bar{V}\phi_\eta - 1)\right]^{1/(\gamma-1)}$$

$$U = \zeta_t + a_{11}\phi_\zeta + a_{12}\phi_\eta;\quad \bar{U} = U + \zeta_t$$

$$V = \eta_t + a_{12}\phi_\zeta + a_{22}\phi_\eta;\quad \bar{V} = V + \eta_t$$

$$a_{11} = \zeta_x^2 + \zeta_y^2;\quad a_{12} = \zeta_x\eta_x + \zeta_y\eta_y;$$

$$a_{22} = \eta_x^2 + \eta_y^2$$

$$J = \text{Jacobian} = \zeta_x\eta_y - \zeta_y\eta_y$$

The density ρ and the fluxes ρU and ρV are complicated nonlinear functions of ϕ, the velocity potential. Hence, to solve for ϕ from Eq. (1) will require a local linearization.

Let 'n' be the running index in the time direction, 'k' in the ζ direction and 'j' in the η direction leading out of the surface. The objective is to solve Eq. (1) for $\phi_{j,k}^{n+1}$ at the current time plane, knowing the information at n, n-1, n-2,... planes.

---

* Manager, Computational Fluid Dynamics Group, Associate Fellow AIAA.

A. Treatment of $\frac{\partial}{\partial\tau}(\frac{\rho}{J})$ in Eq. (1)

$$\frac{\partial}{\partial\tau}(\frac{\rho}{J})^{n+1} =$$

$$\frac{(a_1-\theta b_1)\{(\frac{\rho}{J})^{n+1} - (\frac{\rho}{J})^{n}\} - \theta b_1\{(\frac{\rho}{J})^{n}-(\frac{\rho}{J})^{n-1}\}}{a_1\Delta\tau_1-\theta b_1(\Delta\tau_1 + \Delta\tau_2)}$$

where

$a_1 = (\Delta\tau_1 + \Delta\tau_2)^2$
$b_1 = \Delta\tau_1^2$
$\theta = 0$ for first order time accuracy
$\theta = 1$ for second order accuracy
$\Delta\tau_1 = \tau^{n+1} - \tau^{n}$
$\Delta\tau_2 = \tau^{n} - \tau^{n-1}$

In order to write Eq. (2) in terms of ϕ^{n+1}, a local time linearization procedure is introduced.

$$\rho^{n+1} \doteq \rho^{n} + (\frac{\partial\rho}{\partial\phi})^{n}\Delta\phi + \ldots \qquad (3)$$

where $\Delta\phi = (\phi^{n+1} - \phi^{n})$. The term $(\frac{\partial\rho}{\partial\phi})$ is a differential operator given by

$$(\frac{\partial\rho}{\partial\phi})^{n} = -\frac{\rho^{n}}{a^2}(\frac{\partial}{\partial\tau} + U^{n}\frac{\partial}{\partial\zeta} + V^{n}\frac{\partial}{\partial\eta}) \qquad (4)$$

where 'a' is the local speed of sound.

Combining Eqs. (3) and (4), the nonlinear density function in terms of ϕ has been linearized, and the coefficients multiplying $\Delta\phi$ are evaluated at the known previous time level. To maintain conservation form, both ρ^{n+1} and ρ^{n} appearing in the first term of Eq. (2) are linearized according to Eq. (3).

B. Treatment of $\frac{\partial}{\partial\zeta}(\rho\frac{U}{J})$ in Eq. (1)

$$(\rho\frac{U}{J})_{\zeta}^{n+1} = \overleftarrow{\delta}_{\zeta}(\frac{\tilde{\rho}^{*}_{j,k+1/2}\,U^{n+1}_{j,k+1/2}}{J_{j,k+1/2}})$$

$$= \overleftarrow{\delta}_{\zeta}\{\frac{\tilde{\rho}^{*}}{J}(a_{11}\{\Delta\phi + \phi^{n}\}_{\zeta} \qquad (5)$$

$$+ a_{12}\{\Delta\phi + \phi^{n}\}_{\eta})\}_{j,k+1/2}$$

where $\rho^{n+1}_{j,k+1/2}$ appearing in the spatial derivative term has been linearized to $\tilde{\rho}^{*}_{j,k+1/2}$. The symbol $\sim$ appearing over ρ denotes that the density has been modified to produce the necessary artificial viscosity. The modified density is obtained from a flux biasing concept to be described later in this paper. For a genuine unsteady problem (where a time asymptotic steady state does not exist), initially, $\tilde{\rho}^{*}$ is set to $\tilde{\rho}^{n}$ and then subsequently iterated to convergence by setting $\tilde{\rho}^{*}$ to the previously iterated value of ρ at the current n+1 time plane. For problems where the steady state exists and is of interest (steady transonic flow over airfoils or blunt objects), $\tilde{\rho}^{*}$ is always set to $\tilde{\rho}^{n}$ and requires no internal iterations at n+1 plane.

The only unknown in Eq. (5) is $\Delta\phi$.

C. Treatment of $\frac{\partial}{\partial\eta}(\rho\frac{V}{J})$ in Eq. (1)

$$(\rho\frac{V}{J})_{\eta}^{n+1} \doteq \overleftarrow{\delta}_{\eta}(\tilde{\rho}^{*}\frac{V^{n+1}}{J^{n+1}})_{j+1/2,k}$$

$$= \overleftarrow{\delta}_{\eta}\{\frac{\tilde{\rho}^{*}}{J^{n+1}}(a_{12}\{\Delta\phi + \phi^{n}\}_{\zeta} \qquad (6)$$

$$+ a_{22}\{\Delta\phi + \phi^{n}\}_{\eta})\}_{j+1/2,k}$$

Similarly, $\tilde{\rho}^{*}_{j+1/2,k}$ is a modified density based on flux biasing.

D. Flux Biasing Procedure

The density $\tilde{\rho}$ appearing in Eqs. (5) and (6) is modified according to a flux biasing formula given by

$$\left.\begin{array}{l}
\text{for } U > 0 \\
\tilde{\rho}_{j,k+1/2} = \frac{1}{q_{j,k+1/2}}\{\rho q - \Delta\zeta\overleftarrow{\delta}_{\zeta}(\rho q)^{-}\}_{j,k+1/2} \\
\text{for } U < 0 \\
\quad = \frac{1}{q_{j,k+1/2}}\{\rho q + \Delta\zeta\overrightarrow{\delta}_{\zeta}(\rho q)^{-}\}_{j,k+1/2} \\
\text{for } V > 0 \\
\tilde{\rho}_{j+1/2,k} = \frac{1}{q_{j+1/2,k}}\{\rho q - \Delta\eta\overleftarrow{\delta}_{\eta}(\rho q)^{-}\}_{j+1/2,k} \\
\text{for } V < 0 \\
\quad = \frac{1}{q_{j+1/2,k}}\{\rho q + \Delta\eta\overrightarrow{\delta}_{\eta}(\rho q)^{-}\}_{j+1/2,k}
\end{array}\right\} \qquad (7)$$

where

$(\rho q)^{-} = (\rho q - \rho^{*}q^{*})$ if $q > q^{*}$
$\quad = 0$ if $q < q^{*}$

$\overleftarrow{\delta}$ = backward difference operator

$\overrightarrow{\delta}$ = forward difference opertor.

The quantities $\rho^{*}q^{*}$, ρ^{*} and q^{*} represent sonic values of the flux, density and total velocity, respectively. These sonic conditions are given by (using the density and speed of sound relationships)

$$(q^{*})^2 = \frac{1 + \frac{(\gamma-1)}{2}M_{\infty}^2(1-2\phi_{\tau})}{\frac{\gamma+1}{2}M_{\infty}^2} \qquad (8)$$

$$\rho^{*} = (q^{*}M_{\infty})^{2/(\gamma-1)} .$$

Note that for steady flows, the sonic conditions ρ^* and q^* are only a function of the free-stream Mach number, and for a given flow they are constants. For unsteady flows, ρ^* and q^* need to be computed everywhere due to the presence of ϕ_τ in Eq. (8).

Now, the following four cases can be defined.

a) Subsonic Flow ($q < q^*$ at $(j,k+1/2)$ and $(j,k-1/2)$) for $U > 0$, the modified density in Eq. (7) becomes

$$\tilde{\rho}_{j,k+1/2} = \frac{1}{q_{j,k+1/2}} \{(\rho q)_{j,k+1/2} - [(\rho q)^-_{j,k+1/2} - (\rho q)^-_{j,k-1/2}]\} \tag{9}$$

$$= \rho_{j,k+1/2}$$ (since $(\rho q)^-$ at $(j,k+1/2)$ and $(j,k-1/2)$ is zero, according to Eq. (8).

b) Supersonic Flow ($q > q^*$ at $(j,k+1/2)$ and $(j,k-1/2)$ for $U > 0$,

$$\tilde{\rho}_{j,k+1/2} = \frac{1}{q_{j,k+1/2}} \{(\rho q)_{j,k+1/2} - [(\rho q - \rho^* q^*)_{j,k+1/2} - (\rho q - \rho^* q^*)_{j,k-1/2}]\}$$

$$= \frac{(\rho q)_{j,k-1/2}}{q_{j,k+1/2}} + \frac{1}{q_{j,k+1/2}} [\{(\rho^* q^*)_{j,k+1/2} - (\rho^* q^*)_{j,k-1/2}\}] \tag{10}$$

For steady supersonic flows where $(\rho^* q^*)$ is a constant everywhere, Eq. (10) reduces to

$$\tilde{\rho}_{j,k+1/2} = \rho_{j,k-1/2} \left\{\frac{q_{j,k-1/2}}{q_{j,k+1/2}}\right\} \tag{11}$$

c) Transition Through Sonic Line ($q > q^*$ at $k+1/2$ and $q < q^*$ at $k-1/2$. Refer to Fig. 1a). For $U > 0$,

$$\tilde{\rho}_{j,k+1/2} = \frac{1}{q_{j,k+1/2}} \{(\rho q)_{j,k+1/2} - [(\rho q - \rho^* q^*)_{j,k+1/2} - \cancel{(\rho q)^-_{j,k-1/2}}^{\,0}]\} \tag{12}$$

$$= \frac{\rho^* q^*}{q_{j,k+1/2}}$$

d) Transition Through Shock ($q > q^*$ at $k-1/2$ and $q < q^*$ at $k+1/2$. Refer to Fig. 1b). For $U > 0$,

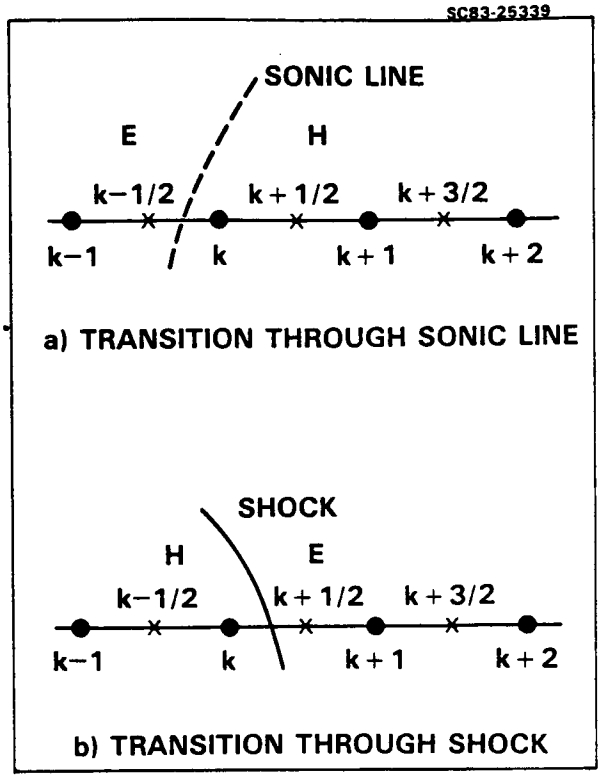

Fig. 1 Notation for flux biasing.

$$\tilde{\rho}_{j,k+1/2} = \frac{1}{q_{j,k+1/2}} \{(\rho q)_{j,k+1/2} - \cancel{(\rho q)^-_{j,k+1/2}}^{\,0} - (\rho q - \rho^* q^*)_{j,k-1/2}\} \tag{13}$$

$$= \rho_{j,k+1/2} + \frac{1}{q_{j,k+1/2}} \{\rho q - \rho^* q^*\}_{j,k-1/2}$$

For steady flows where $\rho^* q^*$ is a constant, it can be shown that at a pure supersonic point (case b above), the flux biasing procedure and the usual density biasing technique of Ref. 2 are identical. Using the following relationships:

$$\frac{\partial \rho}{\partial q} = -\frac{\rho}{a^2} q \tag{14}$$

$$\frac{\partial \rho}{\partial \zeta} = \frac{\partial \rho}{\partial q}\frac{\partial q}{\partial \zeta} = -\frac{\rho}{a^2} q\, q_\zeta \tag{15}$$

$$\frac{\partial}{\partial \zeta}(\rho q)^- = \frac{\partial}{\partial \zeta}(\rho q - \rho^* q^*)$$

$$= \frac{\partial}{\partial \zeta}(\rho q)$$ (for steady flows only)

$$= \rho_\zeta q + \rho q_\zeta \tag{16}$$

Using Eq. (15)

$$\frac{\partial}{\partial \zeta}(\rho q)^- = \rho_\zeta q \left\{1 - \frac{a^2}{q^2}\right\} = \rho_\zeta q \left\{1 - \frac{1}{M^2}\right\} \tag{17}$$

Using Eq. (17), thus, for a pure supersonic point, Eq. (7) becomes, for U > 0

$$\tilde{\rho}_{j,k+1/2} = \frac{1}{q_{j,k+1/2}} \left\{\rho q - \Delta\zeta \overset{+}{\rho}_{\zeta} q \left(1 - \frac{1}{M^2}\right)\right\}_{j,k+1/2} \tag{18}$$

Using $\nu = \left(1 - \frac{1}{M^2}\right)$, Eq. (18) can be written as

$$\tilde{\rho}_{j,k+1/2} = \rho_{j,k+1/2} - \nu(\rho_{j,k+1/2} - \rho_{j,k-1/2}) \tag{19}$$

$$= (1-\nu)\,\rho_{j,k+1/2} + \nu\rho_{j,k-1/2} \quad .$$

Equation (19) is the usual density biasing technique of Holst.[2] However, while transitioning through a sonic line (case c) or through a shock (case d), the flux biasing procedure of Eq. (7) accurately monitors the sonic conditions ρ^* and q^*, as given by Eqs. (12) and (13).

The advantages of flux biasing over the density biasing[2] scheme are:

1. Does not require any user specified constants (the parameter 'c' in Ref. 2) that depend on the severity of the flow.
2. Provides a monotone profile through the shock wave (for details, see Refs. 12 and 13).
3. Allows for larger Courant numbers to be taken during the calculation (by not producing undesired pressure overshoots at shocks, which could cause instability during transient calculations).
4. Provides a two point transition through a shock wave.

A detailed mathematical description of the flux biasing procedure can be found in the works of Osher[12] and Hafez.[13]

E. Implicit Approximate Factorization

Combining the various terms of Eq. (1) given by Eqs. (2-6) will result in a fully implicit model. This is solved using an approximate factorization implicit algorithm. After some rearrangement of the terms, the factored implicit scheme becomes

$$L_{\zeta} L_{\eta} \Delta\phi = R \tag{20}$$

where

$$L_{\zeta} = \left[1 + \Delta\tau_1 U \frac{\partial}{\partial\zeta} + \frac{\alpha}{\beta}\frac{\partial}{\partial\zeta}\frac{\tilde{\rho}^*}{J} a_{11}\frac{\partial}{\partial\zeta}\right]$$

$$L_{\eta} = \left[1 + \Delta\tau_1 V \frac{\partial}{\partial\eta} + \frac{\alpha}{\beta}\frac{\partial}{\partial\eta}\frac{\tilde{\rho}^*}{J} a_{22}\frac{\partial}{\partial\eta}\right]$$

$$\beta = -\left(\frac{\rho^n}{J^{n+1}(a^n\Delta\tau_1)^2}\right)_{j,k}$$

$$\alpha = (1-\theta) + \theta\left[\{a_1 - b_1(\Delta\tau_1 + \Delta\tau_2)/\Delta\tau_1\}/\{a_1 - b_1\}\right]$$

and R consists of various known terms at n, n-1 and n-2 levels.

Equation (20) is solved at the (n+1) plane in two steps.

$$L_{\zeta}\,\overline{\Delta\phi} = R, \quad \text{Step 1}$$

$$L_{\eta}\,\Delta\phi = \overline{\Delta\phi}, \quad \text{Step 2}$$

$$\phi^{n+1}_{j,k} = \phi^{n}_{j,k} + \Delta\phi_{j,k}$$

Both L_{ζ} and L_{η} result in tridiagonal matrices.

F. Boundary Condition

The direction ζ is along the body surface and η leads out of the surface. The boundary condition for the L_{ζ} operator usually depends on the problem. It can be a plane of symmetry condition, a periodic condition or a jump in ϕ condition that goes with a lifting airfoil. All these conditions are easily implemented in the L_{ζ} operator. Special attention needs to be given for the boundary condition that is required in the L_{η} operator. For inviscid flows, the surface flow tangency condition dictates that the contravariant velocity, V, be zero at the body. Implementation of the condition, V = 0, in the L_{η} operator is a crucial step in achieving a true implicit scheme. Usually, the boundary condition V = 0 is set only in the right hand side term R of Eq. (2), and a careless or no boundary condition treatment is imposed in the left hand side L_{η} operator.[2] In the present method, the condition V = 0 is imposed on both sides of the Eq. (20). Let j = J denote the body point. Then,

$$V = (a_{12}\phi_{\zeta} + a_{22}\phi_{\eta})_{J,k} = 0 \tag{21}$$

or

$$(\phi_{\eta})_{J,k} = -\left(\frac{a_{12}}{a_{22}}\phi_{\zeta}\right)_{J,k} \quad . \tag{22}$$

Now, the following adjustments are made for body points (using Eqs. (21) and (22)):

1. Set V = 0 in Eq. (4).
2. Replace $a_{12}(\Delta\phi + \phi^n)_{\eta}$ by $-\frac{a_{12}^2}{a_{22}}(\Delta\phi + \phi^n)_{\zeta}$ in Eq. (5).
3. Replace $\frac{\partial}{\partial\eta}\left(\rho\frac{V}{J}\right)$ by $\frac{2}{\Delta\eta}\left[\frac{\tilde{\rho}^*}{J}\{a_{12}(\Delta\phi + \phi)_{\zeta} + a_{22}(\Delta\phi + \phi)_{\eta}\}\right]_{J+1/2}$ in Eq. (6). This assumes $\left(\rho\frac{V}{J}\right)_{J-1/2} = -\left(\rho\frac{V}{J}\right)_{J+1/2}$.

The approximate factorization at a body point, J, is done after the above three boundary condition steps are implemented. This leads to the following approximate factored scheme for a body point, J.

$$\bar{L}_{\zeta}\bar{L}_{\eta}\,\Delta\phi = R \tag{23}$$

where

$$\bar{L}_\zeta = [1 + \Delta\tau_1 (U - V \overset{0}{\cancel{a_{12}/a_{22}}}) \frac{\partial}{\partial\zeta}$$

$$+ \frac{\alpha}{\beta} \frac{\partial}{\partial\zeta} \frac{\tilde{\rho}^*}{J} (a_{11} - \frac{a_{12}^2}{a_{22}}) \frac{\partial}{\partial\zeta}]$$

$$\bar{L}_\eta = [1 + \frac{2}{\Delta\eta} \frac{\alpha}{\beta} (\frac{\tilde{\rho}^*}{J} a_{22} \frac{\partial}{\partial\zeta})_{J+1/2}]$$

$\bar{R}$ = modified form of R in Eq. (20) after imposing $V^n = 0$.

In Eq. (23), the boundary condition is split between the two operators, L_ζ and L_η. Even for nonorthogonal mesh at the body ($a_{12}{}^\eta \neq 0$), the boundary condition is set implicitly. This allows for large time steps, or Courant numbers, to be taken during the calculation. Imposing Eq. (21) directly into the L_η operator in the approximate factorization of Eq. (20) would lead to an explicit treatment for the part $a_{12}\phi_\zeta$ in Eq. (21).

For all calculations to be reported in this paper, the above split boundary condition approach has proved to be an efficient and robust method, even for highly nonorthogonal grid at the body.

III. Results

Results are presented for various steady flows computed using the unsteady code for time-asymptotic steady state solution. The time-step $\Delta\tau_1$ appearing in Eq. (2) is computed from a prescribed Courant number. When impulsively starting the calculation from free-stream, the Courant number is usually set at 30 ~ 50, and as the iteration proceeds, the Courant number is rapidly increased to very large values such as 500 ~ 2000.

Figures 2 and 3 show the results of a flow over a cylinder at $M_\infty = 0.4$ and 0.45. At $M_\infty = 0.4$, the flow is barely critical, and a comparison with an efficient Euler code[14] is excellent. At $M_\infty = 0.45$, a shock is formed on the cylinder surface. The flux biasing procedure of Eq. (7) produces a shock with no overshoots and requires no user specified 'constants'[2] to stabilize the calculation. Calculations of Figs. 2 and 3 required 40 time-step iterations.

Figures 4 to 6 show results for supersonic flows over a sphere at different low Mach numbers 1.08, 1.2 and 1.4. The density distribution for all these cases are compared with a bench mark type Euler calculation.[15] The present full potential calculation required 80 time-steps to converge for all these cases. It is worth noting at this point that the Euler calculations of Ref. 15 for Mach number 1.08 required in excess of 20,000 interations.

Figure 7 shows the flow over NACA 0012 airfoil at Mach 0.75 and $\alpha = 2°$. The pressure distribution compares well with other full potential methods.[2] Since there are no user specified parameters in the dissipation part of the calculation (flux biasing), there is only one flow solution for the shock in the present method, and it has no overshoots. This calculation required 200 iterations to converge (residual 10^{-5}).

Figures 8 and 9 show the flow over NACA 0012 airfoil at $M_\infty = 0.98$ and $\alpha = 0°$ and 2°, respectively. The fish-tail shock pattern reported in Ref. 2 is nicely reproduced for the zero degree case with 250 time-step iterations. At 4° angle of attack, the trailing edge shock pattern is changed, as seen in Fig. 9. The trailing edge shock on the lower surface is weakened, while the one on the upper surface grew in strength compared to $\alpha = 0°$ case. Even these severe flow cases with complex shock shapes required only minimal time-step iterations and produced no unnecessary 'wiggles' near shocks.

Figure 10 shows the schematic of a hybrid calculation where the unsteady code is used to generate the blunt body solution for setting up the initial data plane for the full potential marching code.[16] A hybrid calculation was performed for the flow over the Shuttle Orbiter at $M_\infty = 1.4$, $\alpha = 0°$. The results of Fig. 6 were used as a starting solution for the marching calculation. The nose region geometry and the pressure distribution along the leeside symmetry of the Orbiter are shown in Figs. 11 and 12.

IV. Conclusions

An implicit method for the unsteady full potential equation is presented. The method employs a local time linearization process, a flux biasing technique for generation of artificial viscosity, and a split boundary condition scheme consistent with the approximate factorization algorithm. Results for flows over airfoils, cylinders and spheres are presented, along with a 'hybrid' calculation performed for the Shuttle Orbiter, using the unsteady and steady codes. Extensions of this work into three dimensions is currently in progress. Appropriate relaxaton schemes[14] will replace the approximate factorization procedure in three dimensions.

Acknowledgement

The author expresses his thanks to Prof. Osher of UCLA, and Drs. Chakravarthy and Szema of Rockwell for many valuable discussions. This work was partially funded by NASA Langley Research Center under Contract NAS1-15820.

References

1. Jameson, A., "Transonic Potential Flow Calculations Using conservation Form," AIAA 2nd Computational Fluid Dynamic Conference Proceedings, 1975, pp. 148-155.

2. Holst, T.L., "Fast, Conservative Algorithm for Solving the Transonic Full Potential Equation," AIAA Journal, Vol. 18, No. 12, December, 1980, pp. 1431-1439.

3. Siclari, M.J., "Computation of Nonlinear Supersonic Potential Flow Over Three-Dimensional Surfaces," AIAA Paper No. 82-0167, presented at the AIAA 20th Aerospace Sciences Meeting, Orlando, Florida, January, 1982.

4. Shankar, V., "A Conservative Full Potential, Implicit, Marching Scheme for Supersonic Flows," AIAA Journal, Vol. 20, No. 11, November, 1982, pp. 1508-1514.

5. Shankar, V. and Osher, S., "An Efficient Full Potential Implicit Method Based on Characteristics for Analysis of Supersonic Flows," AIAA Paper No. 82-0974, June, 1982; also to appear in AIAA Journal, August, 1983.

6. Shankar, V., Szema, K.Y. and Osher, S., "A Conservative Type-Dependent Full Potential Method for the Treatment of Supersonic Flows with Embedded Subsonic Regions," AIAA Paper No. 83-1887

7. Chipman, R. and Jameson, A., "An Alternating Direction Implicit Algorithm for Unsteady Potential Flow," Presented at AIAA 19th Aerospace Sciences Meeting, January, 1981.

8. Goorjian, P.M., "Compuations of Unsteady Transonic Flow Governed by the conservative Full Potential Equation Using an Alternating Direction Implicit Algorithm," NASA CR-152274, June, 1979.

9. Sankar, N.L. and Tassa, Y., "An Algorithm for Unsteady Transonic Potential Flow Past Airfoils," paper presented at 7th International Conference on Numerical Methods in Fluid Dynamics, June, 1980.

10. Steger, J. and Caradonna, F., "A Conservative Implicit Finite Difference Algorithm for the Unsteady Transonic Full Potential Equation," AIAA paper No. 80-1368, presented at the 13th Fluid and Plasma Dynamics Conference, July, 1980.

11. Malone, J.B. and Sankar, N.L., "Numerical Simulation of 2-D Unsteady Transonic Flows Using the Full Potential Equation," AIAA Paper No. 83-0233.

12. Osher, S., "Scheme Design for Transonic Unsteady Aerodynamics Based on Riemann Solvers and the Entropy Condition," Transonic Unsteady Aerodynamics and Aeroelasticity Workshop, NASA Langley Research Center, June 22-23, 1983.

13. Hafez, M., "Entropy Inequality for Transonic Flows," Transonic Unsteady Aerodynamics and Aeroelasticity Workshop, NASA Langley Research Center, June 22-23, 1983.

14. Sukamar, C.R., "Implicit Upwind Schemes Without Approximate Factorization," AIAA Paper No. 84-0165.

15. Salas, M.D., "Flow Properties for a Spherical Body at Low Supersonic Speeds," Symposium on Computers in Aerodynamics, 25th Anniversary of Aerodynamics Labs, PINY, Farmingdale, NY, June 4-5, 1979.

16. Szema, K.Y. and Shankar, V., "Nonlinear Computation of Wing-Body-Vertical Tail-Wake Flows at Low Supersonic Speeds," AIAA Paper No. 84-0427.

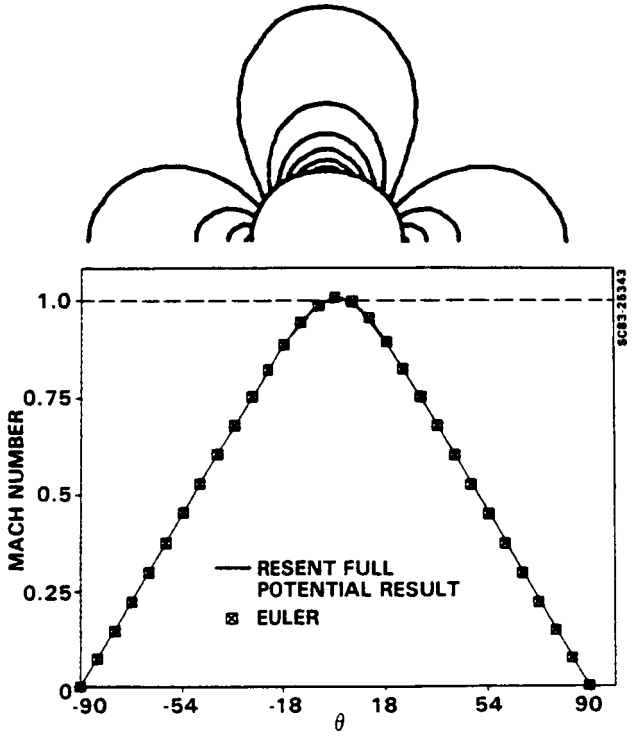

Fig. 2 Mach number distribution for cylinder flow at $M_\infty = 0.4$.

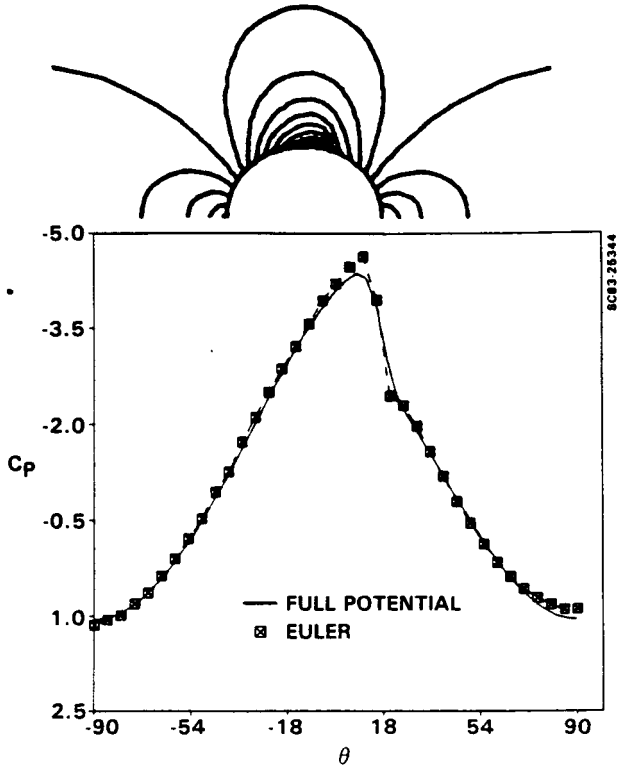

Fig. 3 Mach number distribution and contours for cylinder flow at $M_\infty = 0.45$.

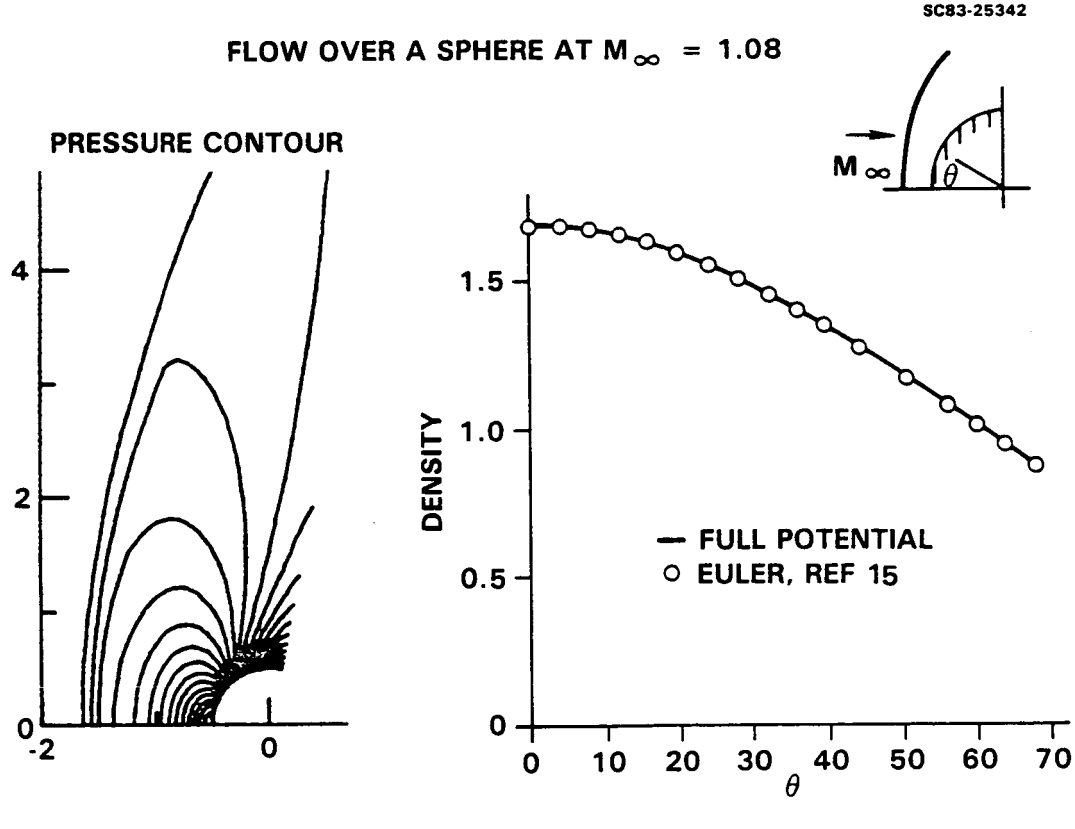

Fig. 4 Density distribution and Mach number contours for flow over a sphere at $M_\infty = 1.08$.

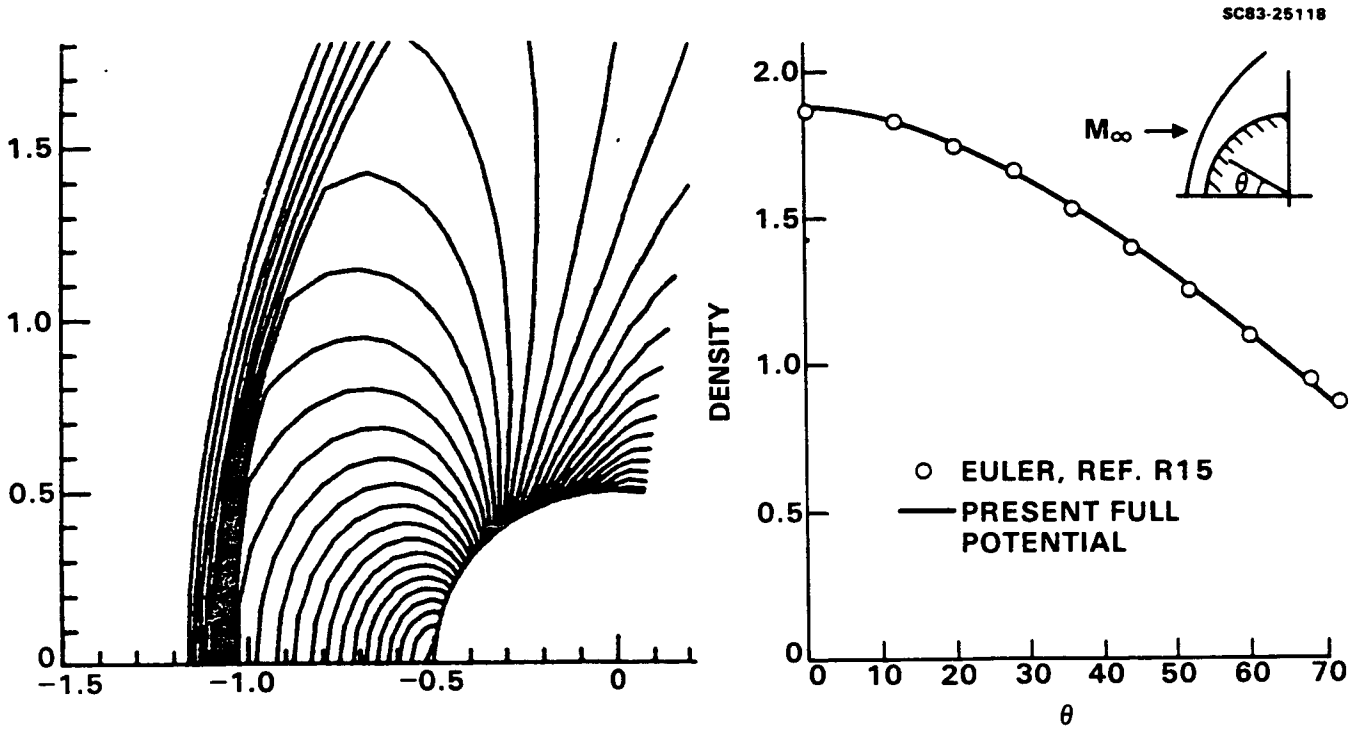

Fig. 5 Density distribution and Mach number contours for flow over a sphere at $M_\infty = 1.2$.

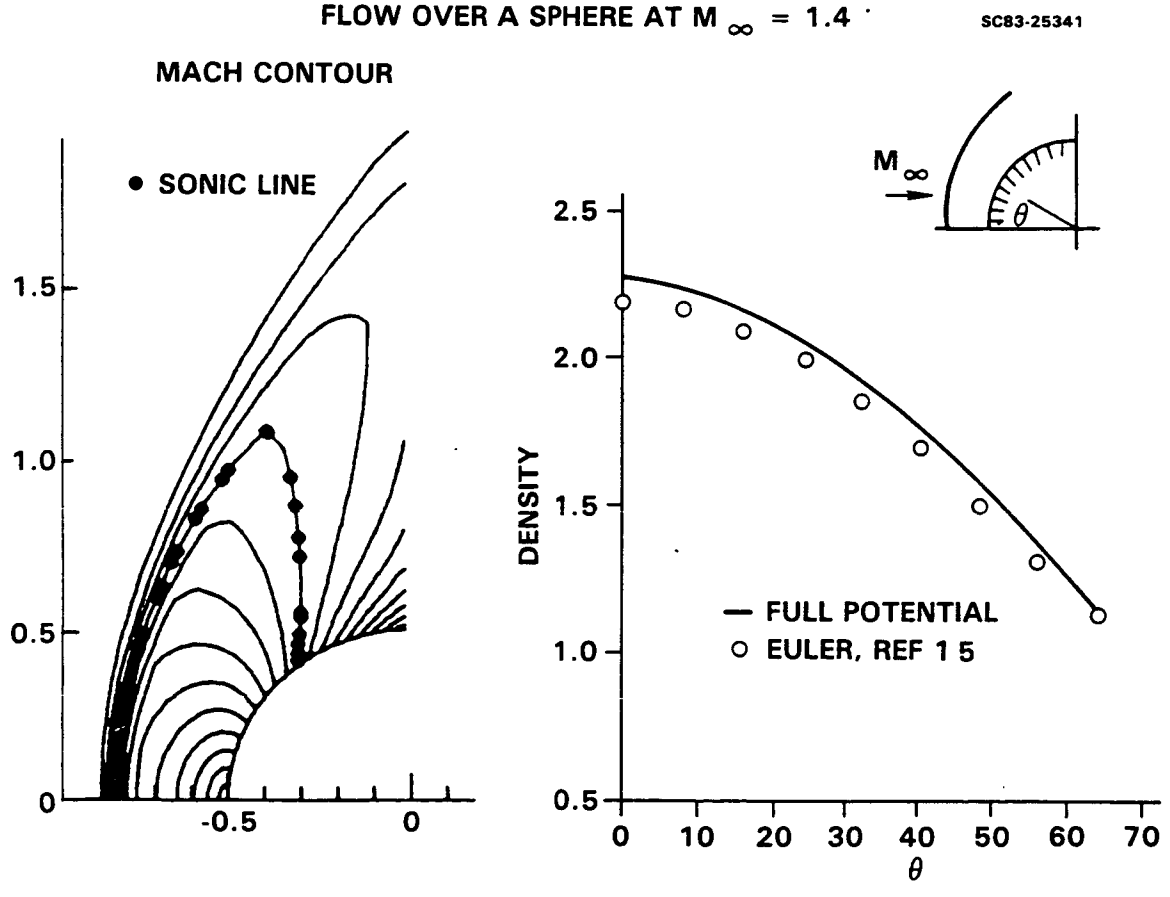

Fig. 6 Density distribution and Mach number contours for flow over a sphere at $M_\infty = 1.4$.

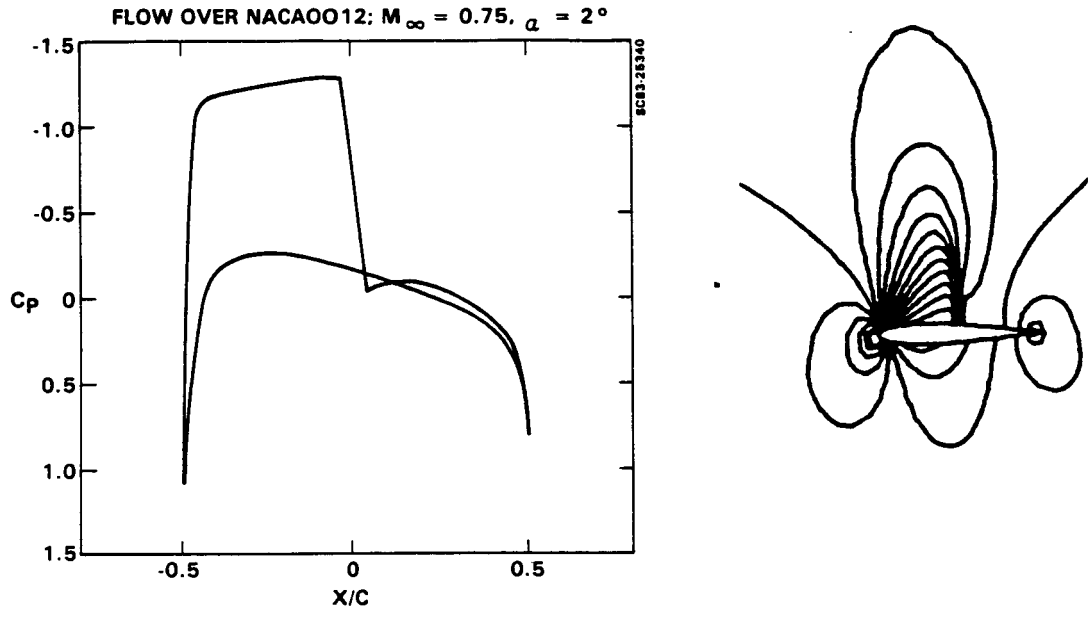

Fig. 7 Pressure distribution and Mach contours for flow over NACA 0012; M_∞ = 0.75, α = 2°.

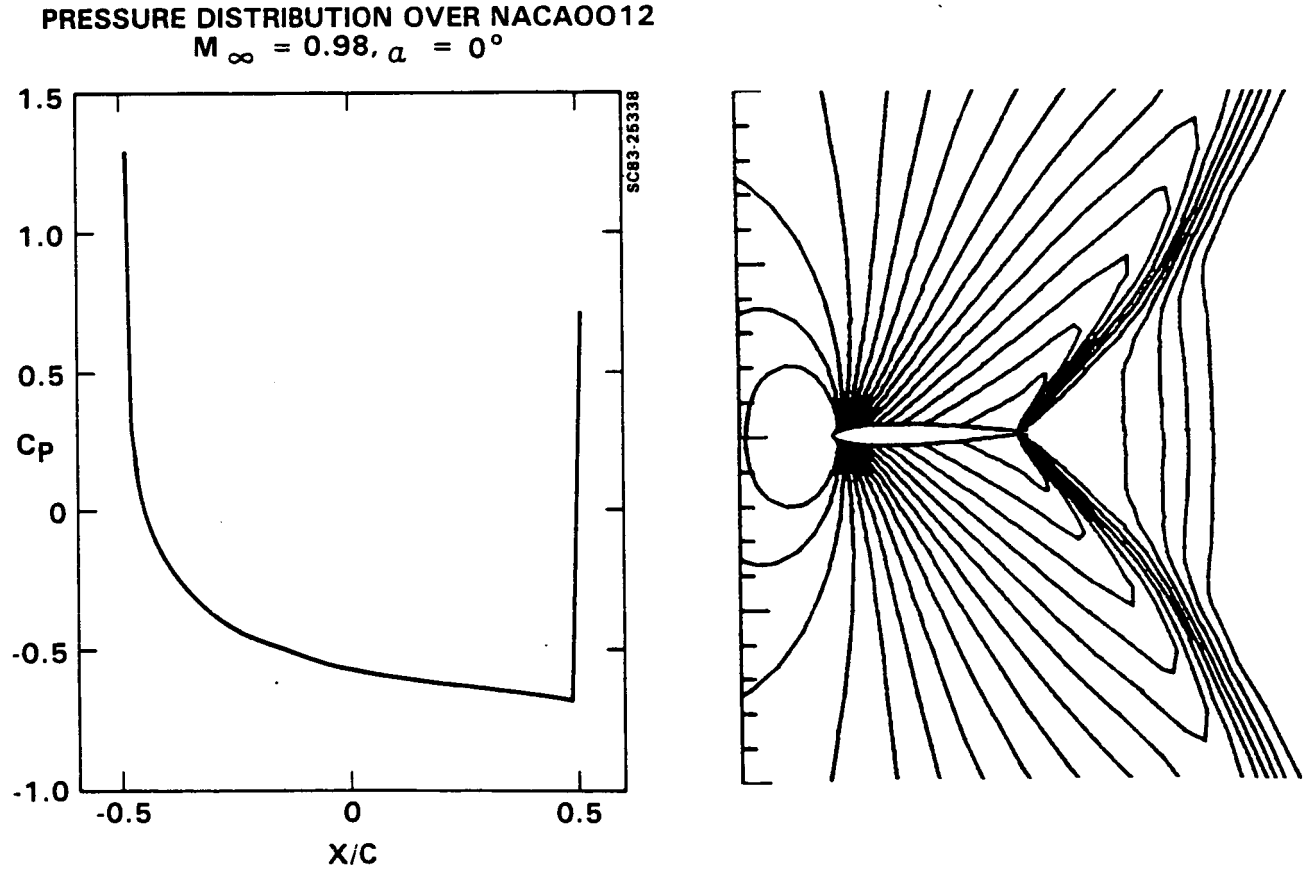

Fig. 8 Pressure distribution and Mach contours for flow over NACA 0012; M_∞ = 0.98, α = 0°.

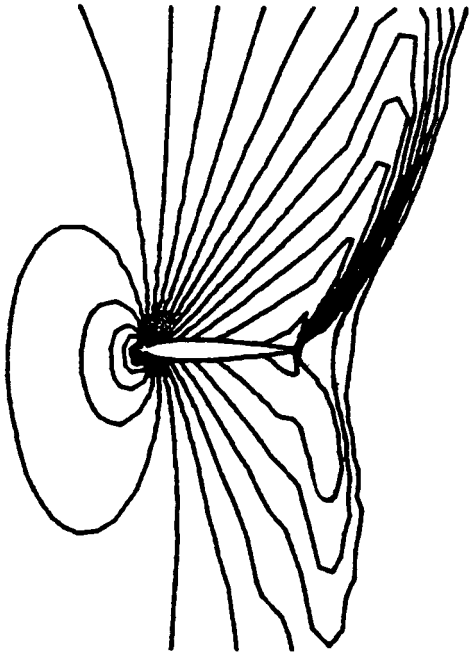

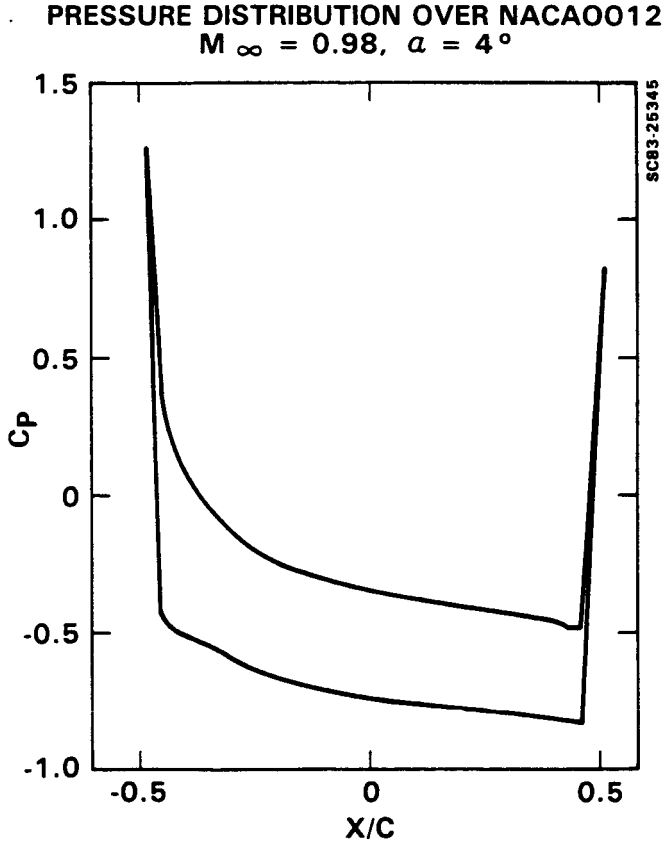

Fig. 9 Pressure distribution and Mach contours for flow over NACA 0012; $M_\infty = 0.98$, $\alpha = 4°$.

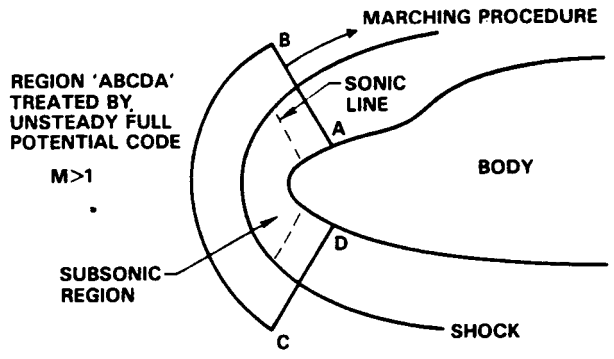

Fig. 10 Blunt body starting solution for a marching code.

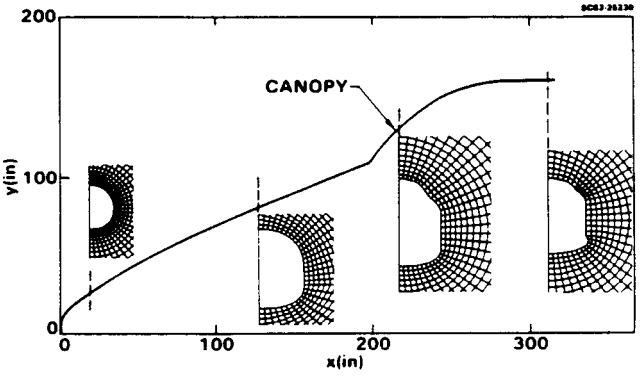

Fig. 11 Nose region geometry of Shuttle Orbiter.

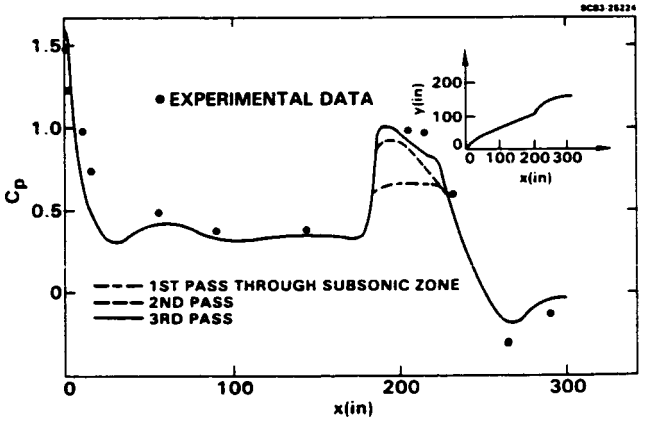

Fig. 12 Hybrid unsteady blunt body/supersonic marching calculation for the Orbiter at $M_\infty = 1.4$, $\alpha = 0°$.

ICAS

ICAS-84-1.6.2

Relaxation and Approximate Factorization Methods for the Unsteady Full Potential Equation

V. Shankar, H. Ide, and J. Gorski

14TH CONGRESS OF THE INTERNATIONAL COUNCIL OF THE AERONAUTICAL SCIENCES

September 9 – 14, 1984 Toulouse, France

RELAXATION AND APPROXIMATE FACTORIZATION METHODS FOR THE UNSTEADY FULL POTENTIAL EQUATION

Vijaya Shankar*, Hiroshi Ide**, and Joseph Gorski†
Rockwell International Science Center
Thousand Oaks, California 91360

Abstract

The unsteady form of the full potential equation is solved in conservation form using implicit methods based on approximate factorization and relaxation schemes. A local time linearization for density is introduced to enable solution to the equation in terms of ϕ, the velocity potential. A novel flux biasing technique is applied to generate proper forms of the artificial viscosity to treat hyperbolic regions with shocks and sonic lines present. The wake is properly modeled by accounting not only for jumps in ϕ, but also for jumps in higher derivatives of ϕ, obtained from requirements of density continuity. The far field is modeled using the Riemann invariants to simulate nonreflecting boundary conditions. Results are presented for flows over airfoils, cylinders, and spheres. Comparisons are made with available Euler and full potential results.

I. Introduction

Nonlinear aerodynamic prediction methods based on the steady form of the full potential equation are used regularly for treating transonic[1,2] and supersonic[3-6] flows over realistic wing–body configurations. Numerical algorithms to compute the unsteady form of the full potential equation are still in a developmental stage, and several researchers[7-11] have recently made significant progress in this area. There are several issues involved in the construction of a robust and efficient numerical algorithm for the unsteady full potential equation. They are: 1) proper treatment of boundary conditions in a nonorthogonal grid system, 2) correct formulation for the production of artificial viscosity to capture sharp shocks, 3) proper time linearization concepts, 4) unsteady wake treatment, and 5) nonreflecting outer boundary conditions.

The objective of the present paper is to present a numerical treatment of the unsteady full potential equation that properly takes into account the importance of the above listed items. The paper discusses a local time linearization procedure for treating the time derivative term, a flux biasing concept based on sonic conditions (instead of the usual density biasing procedures) for the treatment of spatial derivative terms, split boundary condition procedures consistent with approximate factorization schemes, unsteady wake models with proper jumps in ϕ and higher derivatives of ϕ taken into account from density relationships, and nonreflecting unsteady far field procedures based on Riemann invariants derived from the characteristic theory.

Use of unsteady methods has application not only to unsteady problems, but also to time asymptotic steady state solutions. If the unsteady method is constructed properly (robust and efficient), then it can even be made to generate steady state solutions faster than methods based on the steady form of the equation. Also, in the unsteady method, since the time direction is always present, the hyperbolicity of the unsteady full potential equation will allow one to obtain solutions to problems across the Mach number range (subsonic, transonic, and supersonic), whether steady or unsteady. The unsteady method of this paper, when combined with the steady marching method of Refs. 4–6, provides a complete treatment of the full potential equation.

Results are presented for flows over cylinders, spheres, and airfoils at various Mach numbers, and some comparisons are made with Euler solutions. Use of the split boundary condition technique, combined with the flux biasing concepts[12,13], has produced a very robust method which, even for a difficult case with a fishtail shock at the trailing edge of an airfoil, did not require any user-specified "constants", such as the ones discussed in Ref. 2.

The paper also presents the results from a "hybrid" calculation, wherein the spherical blunt body solution from the unsteady code has been effectively used to provide the initial data plane for a supersonic marching calculation performed over the Shuttle Orbiter geometry.

II. Formulation

The two–dimensional/axisymmetric unsteady full potential equation written in a body–fitted coordinate system represented by $\tau = t$, $\zeta = \zeta(x,y,t)$ and $\eta = \eta(x,y,t)$ takes the form

$$\left(\frac{\rho}{J}\right)_\tau + \left(\rho\frac{U}{J}\right)_\zeta + \left(\rho\frac{V}{J}\right)_\eta + S\rho\frac{v}{yJ} = 0 \qquad (1)$$

where

$S = 0$ for two dimensions, $= 1$ for axisymmetric

$$\rho = \text{density} = \left[1 - \tfrac{\gamma-1}{2}M_\infty^2\,(2\phi_\tau + \bar{U}\phi_\zeta + \bar{V}\phi_\eta - 1\right]^{1/(\gamma-1)}$$

$U = \zeta_t + a_{11}\phi_\zeta + a_{12}\phi_\eta$; $\bar{U} = U + \zeta_t$

$V = \eta_t + a_{12}\phi_\zeta + a_{22}\phi_\eta$; $\bar{V} = V + \eta_t$

$a_{11} = \zeta_x^2 + \zeta_y^2$; $a_{12} = \zeta_x\eta_x + \zeta_y\eta_y$

$a_{22} = \eta_x^2 + \eta_y^2$

J = Jacobian $= \zeta_x\eta_y - \zeta_y\eta_y$

The density ρ and the fluxes ρU and ρV are complicated nonlinear functions of ϕ, the velocity potential.

*Manager, Computational Fluid Dynamics Group

**Member Technical Staff, Aircraft Operations Div.

†Senior Technical Associate

Hence, to solve for ϕ from Eq. (1) will require a local linearization.

Let 'n' be the running index in the time direction, 'k' in the ς direction, and 'j' in the η direction leading out of the surface. The objective is to solve Eq. (1) for $\phi_{j,k}^{n+1}$ at the current time plane, knowing the information at n, $n-1$, $n-2$, $\cdots$ planes.

A. Treatment of $\frac{\partial}{\partial\tau}\left(\frac{\rho}{J}\right)$ in Eq. (1)

$$\frac{\partial}{\partial\tau}\left(\frac{\rho}{J}\right)^{n+1} =$$

$$\frac{(a_1-\theta b_1)\left\{\left(\frac{\rho}{J}\right)^{n+1}-\left(\frac{\rho}{J}\right)^{n}\right\}-\theta b_1\left\{\left(\frac{\rho}{J}\right)^{n}-\left(\frac{\rho}{J}\right)^{n-1}\right\}}{a_1\Delta\tau_1-\theta b_1\left(\Delta\tau_1+\Delta\tau_2\right)} \tag{2}$$

where

$a_1 = (\Delta\tau_1+\Delta\tau_2)^2$

$b_1 = \Delta\tau_1^2$

$\theta = 0$ for first order time accuracy

$\theta = 1$ for second order accuracy

$\Delta\tau_1 = \tau^{n+1}-\tau^n$

$\Delta\tau_2 = \tau^n-\tau^{n-1}$

In order to write Eq. 2 in terms of ϕ^{n+1}, a local time linearization procedure is introduced.

$$\rho^{n+1} \doteq \rho^n + \left(\frac{\partial\rho}{\partial\phi}\right)^n \Delta\phi + \cdots \tag{3}$$

where $\Delta\phi = \left(\phi^{n+1}-\phi^n\right)$. The term $\left(\frac{\partial\rho}{\partial\phi}\right)$ is a differential operator given by

$$\left(\frac{\partial\rho}{\partial\phi}\right)^n = -\frac{\rho^n}{a^2}\left(\frac{\partial}{\partial\tau}+U^n\frac{\partial}{\partial\varsigma}+V^n\frac{\partial}{\partial\eta}\right) \tag{4}$$

where 'a' is the local speed of sound.

Combining Eqs. (3) and (4), the nonlinear density function in terms of ϕ has been linearized, and the coefficients multiplying $\Delta\phi$ are evaluated at the known previous time level. To maintain conservation form, both ρ^{n+1} and ρ^n appearing in the first term of Eq. (2) are linearized according to Eq. (3).

B. Treatment of $\frac{\partial}{\partial\varsigma}\left(\rho\frac{U}{J}\right)$

$$\begin{aligned}\left(\rho\frac{U}{J}\right)_{\varsigma}^{n+1} &= \frac{\overleftarrow{\partial}}{\partial\varsigma}\left(\frac{\tilde{\rho}_{j,k+1/2}U_{j,k+1/2}^{n+1}}{J_{j,k+1/2}}\right)\\ &= \frac{\overleftarrow{\partial}}{\partial\varsigma}\left\{\frac{\tilde{\rho}}{J}\left(a_{11}\left\{\Delta\phi+\phi^n\right\}_{\varsigma}\right.\right.\\ &\quad\left.\left.+\,a_{12}\left\{\Delta\phi+\phi^n\right\}_{\eta}\right)\right\}_{j,k+1/2}\end{aligned} \tag{5}$$

where $\rho_{j,k+1/2}^{n+1}$ appearing in the spatial derivative term has been linearized to $\tilde{\rho}_{j,k+1/2}$. The symbol $\tilde{}$ appearing over ρ denotes that the density has been modified to produce the necessary artificial viscosity. The modified density is obtained from a flux biasing concept to be described later in this paper. For a genuine unsteady problem (where a time asymptotic steady state does not exist), initially, $\tilde{\rho}$ is set to $\tilde{\rho}^n$ and then subsequently iterated to convergence by setting $\tilde{\rho}$ to the pre-time plane. For problems where the steady state exists and is of interest (steady transonic flow over airfoils or blunt objects), $\tilde{\rho}$ is always set to $\tilde{\rho}^n$ and requires no internal iterations at the $n+1$ plane.

The only unknown in Eq. (5) is $\Delta\phi$.

C. Treatment of $\frac{\partial}{\partial\eta}\left(\rho\frac{V}{J}\right)$

$$\begin{aligned}\left(\rho\frac{V}{J}\right)_{\eta}^{n+1} &\doteq \frac{\overleftarrow{\partial}}{\partial\eta}\left(\tilde{\rho}\frac{V^{n+1}}{J^{n+1}}\right)_{j+1/2,k}\\ &= \frac{\overleftarrow{\partial}}{\partial\eta}\left\{\frac{\tilde{\rho}}{J^{n+1}}\left(a_{12}\left\{\Delta\phi+\phi^n\right\}_{\varsigma}\right.\right.\\ &\quad\left.\left.+\,a_{22}\left\{\Delta\phi+\phi^n\right\}_{\eta}\right)\right\}_{j+1/2,k}\end{aligned} \tag{6}$$

Similarly, $\tilde{\rho}_{j+1/2,k}$ is a modified density based on flux biasing.

D. Biasing Procedure

The spatial derivative terms given by Eqs. (5) and (6) are central differenced expressions about the node point (j,k) and are symmetric operators. For shocked flows and for treatment of hyperbolic regions, these operators are desymmetrized by introducing the biased value of density in the upwind direction. This will create the necessary artificial viscosity to form shocks and exclude the expansion shock. The biased value of density $\tilde{\rho}$ can be obtained in several ways. Some of them are presented here.

a) Density Biasing[2] (in the ς-direction)

$$\tilde{\rho}_{k+1/2} = \rho_{k+1/2} \mp \nu\Delta\varsigma\left(\frac{\overleftrightarrow{\partial\rho}}{\partial\varsigma}\right)_{k+1/2},$$

$$\nu = \max\left(0, 1-\frac{1}{M^2}\right)_{k+1/2} \tag{7}$$

where M is the local Mach number. For $U>0$, the $-$ sign and backward differencing ($\leftarrow$) is used in Eq. (7), while for $U<0$, the $+$ sign and ($\rightarrow$) operator is used.

b) Directional Flux Biasing

$$\tilde{\rho} = \frac{1}{q}\left\{\rho q \mp \Delta\varsigma\frac{\overleftrightarrow{\partial}}{\partial\varsigma}(\rho q)^{-}\right\} \tag{8}$$

c) Streamwise Flux Biasing

$$\tilde{\rho} = \frac{1}{q}\left\{\rho q \mp \Delta S \overleftrightarrows{\frac{\partial}{\partial S}}(\rho q)^{-}\right\} \tag{9}$$

where S is the local streamwise direction. Equation (9) can be rearranged as

$$\tilde{\rho} = \frac{1}{q}\left[\rho q \mp \left\{\frac{U}{Q}\Delta\zeta \overleftrightarrows{\frac{\partial}{\partial\zeta}} + \frac{V}{Q}\Delta\eta \overleftrightarrows{\frac{\partial}{\partial\eta}}\right\}(\rho q)^{-}\right] \tag{10}$$

where $Q = \sqrt{U^2 + V^2}$.

In Eqs. (8) and (10), the term $(\rho q)^{-}$ is defined to be

$$\begin{aligned}(\rho q)^{-} &= \rho q - \rho^* q^* \qquad \text{if } q > q^* \\ &= 0 \qquad\qquad\quad \text{if } q \le q^*\end{aligned} \tag{11}$$

The quantities $\rho^* q^*$, ρ^*, and q^* represent sonic values of the flux, density, and total velocity, respectively. These sonic conditions are given by (using the density and speed of sound relationships)

$$(q^*)^2 = \frac{1 + \frac{(\gamma-1)}{2}M_\infty^2\,(1 - 2\phi_\tau - \zeta_t\phi_\zeta - \eta_t\phi_\eta)}{\frac{\gamma+1}{2}M_\infty^2}$$

$$\rho^* = (q^* M_\infty)^{2/(\gamma-1)}. \tag{12}$$

Note that for steady flows, the sonic conditions ρ^* and q^* are only a function of the freestream Mach number, and for a given flow they are constants. For unsteady flows, ρ^* and q^* need to be computed everywhere due to the presence of ϕ_τ and other unsteady terms in Eq. (12).

The density biasing based on flux, Eq. (10), is more accurate than the one presented in Eq. (7), since it is based on sonic reference conditions. To illustrate the flux biasing procedure for various situations, Eq. (8) is considered.

1) Subsonic Flow ($q < q^*$ at $(j, k+1/2)$ and $(j, k-1/2)$) for $U > 0$, the modified density in Eq. (8) becomes

$$\begin{aligned}\tilde{\rho}_{j,k+1/2} &= \frac{1}{q_{j,k+1/2}}\left\{(\rho q)_{j,k+1/2}\right. \\ &\quad \left. - \left[(\rho q)^{-}_{j,k+1/2} - (\rho q)^{-}_{j,k-1/2}\right]\right\}\end{aligned} \tag{13}$$

$= \rho_{j,k+1/2}$ (since $(\rho q)^{-}$ at $(j, k+1/2)$ and $(j, k-1/2)$ is zero, according to Eq. (11).

2) Supersonic Flow ($q > q^*$ at $(j, k+1/2)$ and $(j, k-1/2)$) for $U > 0$,

$$\begin{aligned}\tilde{\rho}_{j,k+1/2} &= \frac{1}{q_{j,k+1/2}}\{(\rho q)_{j,k+1/2} \\ &\quad -[(\rho q - \rho^* q^*)_{j,k+1/2} - (\rho q - \rho^* q^*)_{j,k-1/2}]\} \\ &= \frac{(\rho q)_{j,k-1/2}}{q_{j,k+1/2}} + \frac{1}{q_{j,k+1/2}}[\{(\rho^* q^*)_{j,k+1/2} \\ &\quad -(\rho^* q^*)_{j,k-1/2}\}].\end{aligned} \tag{14}$$

For steady supersonic flows where $(\rho^* q^*)$ is a constant everywhere, Eq. (14) reduces to

$$\tilde{\rho}_{j,k+1/2} = \rho_{j,k-1/2}\left\{\frac{q_{j,k-1/2}}{q_{j,k+1/2}}\right\}. \tag{15}$$

3) Transition Through Sonic Line ($q > q^*$ at $k+1/2$ and $q < q^*$ at $k-1/2$. Refer to Fig. 1a.) For $U > 0$,

$$\begin{aligned}\tilde{\rho}_{j,k+1/2} &= \frac{1}{q_{j,k+1/2}}\{(\rho q)_{j,k+1/2} \\ &\quad -[(\rho q - \rho^* q^*)_{j,k+1/2} - \cancelto{0}{(\rho q)^{-}_{j,k-1/2}}]\} \\ &= \frac{\rho^* q^*}{q_{j,k+1/2}}.\end{aligned} \tag{16}$$

4) Transition Through Shock ($q > q^*$ at $k-1/2$ and $q < q^*$ at $k+1/2$. Refer to Fig. 1b.) For $U > 0$,

$$\begin{aligned}\tilde{\rho}_{j,k+1/2} &= \frac{1}{q_{j,k+1/2}}\{(\rho q)_{j,k+1/2} \\ &\quad -[\cancelto{0}{(\rho q)^{-}_{j,k+1/2}} - (\rho q - \rho^* q^*)_{j,k-1/2}]\} \\ &= \rho_{j,k+1/2} + \frac{1}{q_{j,k+1/2}}\{\rho q - \rho^* q^*\}_{j,k-1/2}\end{aligned} \tag{17}$$

For steady flows where $\rho^* q^*$ is a constant, it can be shown that at a pure supersonic point (case 2 above), the

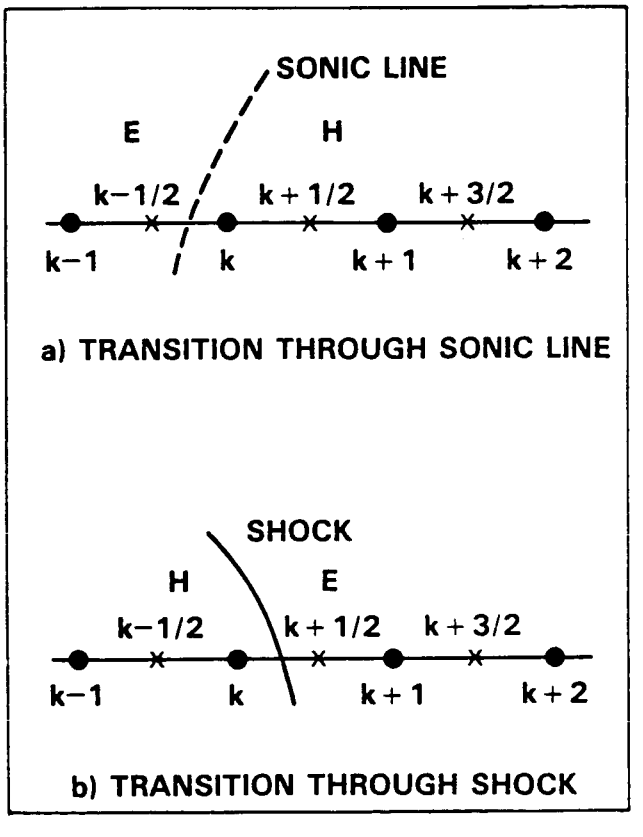

Fig. 1. Notation for flux biasing.

flux biasing procedure, Eq. (8), and the usual density biasing technique of Ref. 2, Eq. (7), are identical.

$$\frac{\partial \rho}{\partial q} = -\frac{\rho}{a^2} q \tag{18}$$

$$\frac{\partial \rho}{\partial \zeta} = \frac{\partial \rho}{\partial q}\frac{\partial q}{\partial \zeta} = -\frac{\rho}{a^2} q q_\zeta \tag{19}$$

$$\begin{aligned} \frac{\partial}{\partial \zeta}(\rho q)^- &= \frac{\partial}{\partial \zeta}(\rho q - \rho^* q^*) \\ &= \frac{\partial}{\partial \zeta}(\rho q) \text{ (for steady flows only)} \\ &= \rho_\zeta q + \rho q_\zeta \end{aligned} \tag{20}$$

Using Eq. (20)

$$\begin{aligned} \frac{\partial}{\partial \zeta}(\rho q)^- &= \rho_\zeta q \left\{1 - \frac{a^2}{q^2}\right\} \\ &= \rho_\zeta q \left\{1 - \frac{1}{M^2}\right\}. \end{aligned} \tag{21}$$

Using Eq. (21), thus, for a pure supersonic point, Eq. (8) becomes, for $U > 0$

$$\tilde{\rho}_{j,k+1/2} = \frac{1}{q_{j,k+1/2}} \left\{\rho q - \Delta\zeta \overleftarrow{\rho}_\zeta q \left(1 - \frac{1}{M^2}\right)\right\}_{j,k+1/2} \tag{22}$$

Using $\nu = \left(1 - \frac{1}{M^2}\right)$, Eq. (22) can be written as

$$\begin{aligned} \tilde{\rho}_{j,k+1/2} &= \rho_{j,k+1/2} - \nu(\rho_{j,k+1/2} - \rho_{j,k-1/2}) \\ &= (1-\nu)\rho_{j,k+1/2} + \nu\rho_{j,k-1/2}. \end{aligned} \tag{23}$$

Equation (23) is the usual density biasing technique of Holst[2]. However, while transitioning through a sonic line (case 3) or through a shock (case 4), the flux biasing procedure of Eq. (8) accurately monitors the sonic conditions ρ^* and q^*, as given by Eqs. (16) and (17).

The advantages of flux biasing over the density biasing[2] scheme are:

1. Does not require any user–specified constants (the parameter 'c' in Ref. 2) that depend on the severity of the flow.
2. Provides a monotone profile through the shock wave (for details, see Refs. 12 and 13).
3. Allows for larger Courant numbers to be taken during the calculation (by not producing undesired pressure overshoots at shocks, which could cause instability during transient calculations).
4. Provides a two point transition through a shock wave.

A detailed mathematical description of the flux biasing procedure can be found in the works of Osher[12] and Hafez[13].

E. Unsteady Wake Treatment

Figure 2 shows the schematic of a wake cut behind the trailing edge of an airfoil. This wake cut has to be properly modeled in the unsteady formulation. An expression for the jump in ϕ across the wake cut can be derived by requiring that the pressure be continuous across the cut. In the full potential framework, this results in the continuity of density. Equating the density $\rho_u = \rho_\ell$ at any point along the wake (refer to Fig. 2), one can write

$$2\Gamma_t + (U_u + U_\ell)(\phi_\zeta)_u - U_\ell \Gamma_\zeta = 0 \tag{24}$$

assuming $[V\phi_\eta] \cong 0$, where $[f]$ stands for the jump in the quantity given by $(f_u - f_\ell)$. Equation (24) is integrated from the trailing edge to the downstream boundary (along TE in Fig. 2) to obtain the Γ distribution along the wake cut. To maintain stability, the ζ derivatives in Eq. (24) are upwind differenced. For a steady flow, Eq. (24) will result in a constant value for Γ along the wake given by $\Gamma = \phi_T - \phi_{T'}$ in Fig. 2.

Beside the Γ evaluation, solution to the unsteady equation also requires information on (ϕ_η) at a wake point. Referring to Fig. 2 for notation, one can write the following using Taylor's series expansion.

$$\begin{aligned} \phi_2 &= \phi_3 - (\phi_\eta)_u + (\phi_{\eta\eta})_u/2 + \cdots \\ \phi_{\bar{2}} &= \phi_{\bar{3}} - (\phi_\eta)_\ell + (\phi_{\eta\eta})_\ell/2 + \cdots \end{aligned} \tag{25}$$

The subscripts 'u' and 'ℓ' stand for upper and lower, respectively.

For the chosen coordinate system, requiring that $(\phi_\eta)_u = -(\phi_\eta)_\ell$ and defining $\phi_2 - \phi_{\bar{2}} = \Gamma$, using Eqs. (25) one can write

$$(\phi_\eta)_u = \frac{\phi_{\bar{3}} - \{\phi_{\bar{3}} + \Gamma + [\phi_{\eta\eta}]/2\}}{2} \tag{26}$$

Equation (26) requires an estimate for the jump in $\phi_{\eta\eta}$ at the wake cut. This can be obtained by setting the jump in the equation to be zero at a wake point.

$$\left[\left(\frac{\rho}{J}\right)_\tau + \left(\rho\frac{U}{J}\right)_\zeta + \left(\rho\frac{V}{J}\right)_\eta\right] = 0. \tag{27}$$

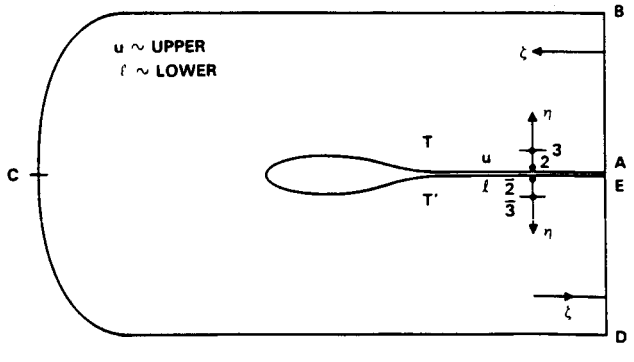

Fig. 2. Wake and outer boundary treatment.

Writing down Eq. (27) in terms of the transformation metrics and requiring that $\rho_u = \rho_\ell$, the following relationship is obtained.

$$[\phi_{\eta\eta}] = -\frac{(\rho a_{11}\Gamma_\varsigma)_\varsigma}{\rho a_{22}}. \tag{28}$$

For steady flows, the jump in $\phi_{\eta\eta}$ along the wake is zero because $\Gamma_\varsigma = 0$. For unsteady flows, to maintain accuracy, Eqs. (24)–(28) have to be employed.

F. Far Field Boundary Condition

Along the outer boundary ABCDE in Fig. 2, appropriate Riemann invariants are prescribed. The concept can be explained by considering the Cartesian form of the full potential equation cast in terms of the Riemann invariants.

$$\begin{aligned}
&\frac{\partial}{\partial t}\left(u + \frac{2}{\gamma-1}a\right) + (u+a)\frac{\partial}{\partial x}\left(u + \frac{2}{\gamma-1}a\right) = 0 \\
&\frac{\partial}{\partial t}\left(u - \frac{2}{\gamma-1}a\right) + (u-a)\frac{\partial}{\partial x}\left(u - \frac{2}{\gamma-1}a\right) = 0
\end{aligned} \tag{29}$$

Equation (29) implies that along the $(u+a)$ positive characteristics the quantity $\left(u + \frac{2}{\gamma-1}a\right)$ is invariant, and along the $(u-a)$ negative characteristics the quantity $\left(u - \frac{2}{\gamma-1}a\right)$ is invariant, known as the Riemann invariants. Usually, along the outer boundary, the Riemann invariant that corresponds to the positive characteristics with respect to the inward normal can be prescribed as a boundary condition.

For an arbitrary coordinate system (τ, ς, η), such as the one in Fig. 2, the following boundary conditions are appropriate.

$$\begin{aligned}
&\frac{U}{\sqrt{a_{11}}} + \frac{2}{\gamma-1}a = \text{constant along AB} \\
&-\frac{U}{\sqrt{a_{11}}} + \frac{2}{\gamma-1}a = \text{constant along ED} \\
&-\frac{V}{\sqrt{a_{22}}} + \frac{2}{\gamma-1}a = \text{constant along BCD}
\end{aligned} \tag{30}$$

Equation (30) is nonlinear in nature. Hence, to implement the Riemann invariant boundary condition, a linearization technique similar to Eq. (3) is employed. For example, equating the right hand side of Eq. (30) to the freestream value, along BCD one can write

$$\begin{aligned}
&-\frac{\left(a_{12}\frac{\partial}{\partial\varsigma} + a_{22}\frac{\partial}{\partial\eta}\right)^n \Delta\phi}{\sqrt{a_{22}}} \\
&-\frac{1}{a^n}\left(\frac{\partial}{\partial\tau} + U\frac{\partial}{\partial\varsigma} + V\frac{\partial}{\partial\eta}\right)^n \Delta\phi \\
&= \left(-\frac{V}{\sqrt{a_{22}}} + \frac{2}{\gamma-1}a\right)_{\text{freestream}} - \left(-\frac{V}{\sqrt{a_{22}}} + \frac{2}{\gamma-1}a\right)^n
\end{aligned} \tag{31}$$

The finite differenced form of Eq. (31) will provide an estimate for $(\Delta\phi)$ along the outer boundary. Use of the Riemann invariant boundary conditions is better than prescribing ϕ_∞ from the compressible vortex solution, and will serve as a nonreflecting boundary condition.

G. Relaxation and Approximate Factorization Schemes

When all the terms of Eq. (1) are put together, it will be in terms of the unknown $\Delta\phi$. It can be written as

$$F(\Delta\phi) + R(\phi^n, \phi^{n-1}, \cdots) = 0 \quad , \quad \Delta\phi = \phi^{n+1} - \phi^n. \tag{32}$$

The Newton iterative procedure for solving Eq. (32) becomes

$$\frac{\partial F}{\partial \Delta\phi}(\Delta\phi^{n+1} - \Delta\phi^i) = -R(\phi^n, \phi^{n-1}, \cdots) - F(\Delta\phi^i) \tag{33}$$

The off-diagonal elements of $\frac{\partial F}{\partial \Delta\phi}$, which cannot be accommodated within the tridiagonal setup of SLOR, can be set to zero. In Eq. (33), $\Delta\phi^i$ represents the intermediate iterative value of $\Delta\phi$. For steady state problems, $\Delta\phi^i$ can be set to $\Delta\phi^n$. If all the off-diagonal terms of $\frac{\partial F}{\partial \Delta\phi}$ are set to zero, then the relaxation process becomes the point Jacobi iteration. Results based on the relaxation procedure of Eq. (32) are presented in this paper.

Another procedure to solve Eq. (32) is the approximate factorization technique. This can be written as

$$L_\varsigma L_\eta \Delta\phi = R \tag{34}$$

where

$$L_\varsigma = \left[1 + \Delta\tau_1 U\frac{\partial}{\partial\varsigma} + \frac{\alpha}{\beta}\frac{\partial}{\partial\varsigma}\frac{\bar{\rho}^*}{J}a_{11}\frac{\partial}{\partial\varsigma}\right]$$

$$L_\eta = \left[1 + \Delta\tau_1 V\frac{\partial}{\partial\eta} + \frac{\alpha}{\beta}\frac{\partial}{\partial\eta}\frac{\bar{\rho}^*}{J}a_{22}\frac{\partial}{\partial\eta}\right]$$

$$\beta = -\left(\frac{\rho^n}{J^{n+1}(a^n\Delta\tau_1)^2}\right)_{j,k}$$

$$\alpha = (1-\theta) + \theta\left|\{a_1 - b_1(\Delta\tau_1 + \Delta\tau_2)/\Delta\tau_1\}/\{a_1 - b_1\}\right|$$

Equation (34) is solved at the $(n+1)$ plane in two steps.

$$L_\varsigma\overline{\Delta\phi} = R \quad , \quad \text{Step 1}$$

$$L_\eta\Delta\phi = \overline{\Delta\phi} \quad , \quad \text{Step 2}$$

$$\phi^{n+1}_{j,k} = \phi^n_{j,k} + \Delta\phi_{j,k}$$

Both L_ς and L_η result in tridiagonal matrices.

H. Body Boundary Condition

For inviscid flows, the surface flow tangency condition dictates that the contravariant velocity, V, be zero at the body. Implementation of the condition, $V = 0$, in the L_η operator is a crucial step in achieving a true implicit scheme. Usually, the boundary condition $V = 0$ is set only in the right hand side term R, and a careless or no boundary condition treatment is imposed in the left hand side L_η operator[2]. In the present method, the condition $V = 0$ is imposed on both sides of Eq. (34). Let $j = J$ denote the body point. Then,

$$V = (a_{12}\phi_\varsigma + a_{22}\phi_\eta)_{J,k} = 0 \tag{35}$$

or

$$(\phi_\eta)_{J,k} = -\left(\frac{a_{12}}{a_{22}}\phi_\zeta\right)_{J,k} . \tag{36}$$

Using Eqs. (35) and (36), and the relationship

$$\left(\rho\frac{V}{J}\right)_{J-1/2} = -\left(\rho\frac{V}{J}\right)_{J+1/2} , \tag{37}$$

the L_ζ and the L_η operators in Eq. (34) can be modified to the form, for a body point J,

$$\tilde{L}_\zeta \tilde{L}_\eta \Delta\phi = \tilde{R} \tag{38}$$

where

$$\tilde{L}_\zeta = \left[1 + \Delta\tau_1 U\frac{\partial}{\partial\zeta} + \frac{\alpha}{\beta}\frac{\partial}{\partial\zeta}\frac{\tilde{\rho}}{J}\left(a_{11} - \frac{a_{12}^2}{a_{22}}\right)\frac{\partial}{\partial\zeta}\right]$$

$$\tilde{L}_\eta = \left[1 + \frac{2}{\Delta\eta}\frac{\alpha}{\beta}\left(\frac{\tilde{\rho}}{J}a_{22}\frac{\partial}{\partial\zeta}\right)_{J+1/2}\right].$$

In Eq. (38), the boundary condition is split between the two operators, $\tilde{L}_\zeta$ and $\tilde{L}_\eta$. Even for nonorthogonal mesh at the body ($a_{12} \neq 0$), the boundary condition is set implicitly. This allows for large time steps, or Courant numbers, to be taken during the calculation.

III. Results

Computer codes based on both the relaxation method (Eq. (33)) and the approximate factorization method (Eq. (34)) have been constructed for two-dimensional and axisymmetric problems. The grid around the geometry can be either a C-type (Fig. 2) or an O-type. At present, the relaxation method is somewhat slower (at least 50%) in convergence than the approximate factorization code. However, the future implementation of multigrid techniques[17] and implicit relaxation concepts[14] to the present relaxation code can make it competitive to approximate factorization methods in three-dimensional applications, where the approximate factorization methods with triple factorization can be less flexible to handle complex geometries[14].

The unsteady code has been applied, at present, only to steady state problems. Calculations involving unsteady motions such as plunge, pitch, and oscillating flaps are currently in progress. For steady state problems, the time step $\Delta\tau_1$ appearing in Eq. (34) is computed from a prescribed Courant number, usually set much greater than one (~ 50).

Figure 3 shows the result for a flow over a cylinder at $M_\infty = 0.4$. The flow is barely critical, and a comparison with an efficient Euler code[14] is excellent. Figures 4 and 5 show results for supersonic flows over a sphere at low Mach numbers of 1.08 and 1.4. The density distribution for these cases are compared with benchmark Euler calculations[15]. The present full potential code required approximately 80 time steps to converge (residual $< 10^{-5}$). It is worth noting at this point that the Euler code of Ref. 15 requires in excess of 20,000 iterations to perform the low Mach number calculation of 1.08.

Figure 6 shows the pressure distribution obtained over the NACA 0012 airfoil at $M_\infty = 0.8$ and $\alpha = 0°$ with

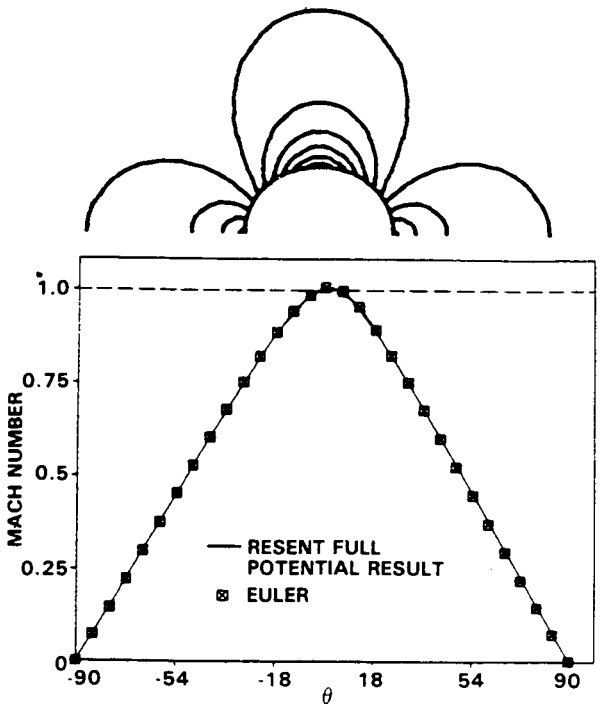

Fig. 3. Mach number distribution for cylinder flow at $M_\infty = 0.4$.

a grid of 84 points around the airfoil and 18 in the η-direction. The comparison with an Euler code[14] is good. Figure 7 shows the results for $M_\infty = 0.75$ and $\alpha = 2°$ over the same airfoil. Even with a crude grid, the formation of a strong shock without any overshoots is made possible by the use of flux biasing concepts. Calculations of this type require no user-specified "constants" to increase or decrease the amount of dissipation. Depending on the strength of the shock, the flux biasing automatically chooses the right amount of dissipation, since it is based on sonic reference conditions. The perfect matching of pressure contours across the wake cut (Fig. 7) illustrates the correctness of the unsteady wake model described in this paper. Figure 8 shows some difficult cases with fishtail shocks.

The unsteady code can also be effectively used to generate the blunt body solution, the outflow of which is to be prescribed as an initial data plane for a full potential supersonic marching code[6]. Figure 9 shows the schematic of such a hybrid calculation. The flow over the entire Shuttle Orbiter with a blunt nose has been simulated at $M_\infty = 1.4$ and $\alpha = 0°$. The results of Fig. 5 were used as a starting solution for the marching calculation[16]. The nose region geometry and the pressure distribution along the leeside symmetry of the Orbiter are shown in Figs. 10 and 11.

Simulation of unsteady phenomena, such as flutter and control surface oscillations will be presented in the future.

IV. Conclusions

A computational treatment for the unsteady full potential equation is presented. The method employs a local time linearization, flux biasing concepts for generation of

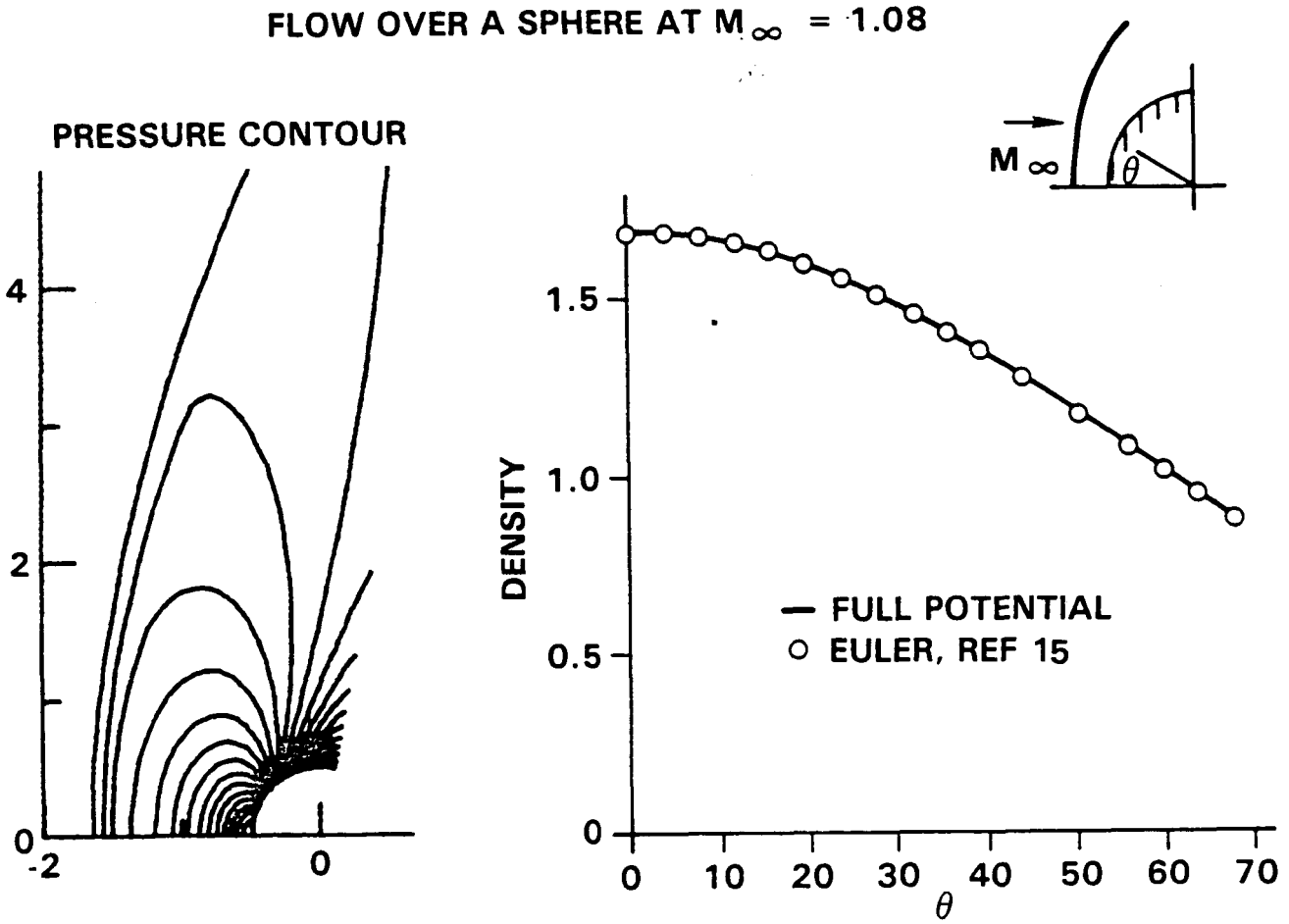

Fig. 4. Density distribution and Mach number contours for flow over a sphere at $M_\infty = 1.08$.

artificial viscosity, unsteady wake treatment, outer boundary conditions based on the Riemann invariants, and relaxation and approximate factorization algorithms. Use of the code for problems with steady state solution has been very effective and computationally fast. Extensions of this work to simulate unsteady phenomena such as flutter, and to three dimensions to treat wings, and wing-body combinations, are currently in progress.

V. Acknowledgement

The authors express their thanks to Prof. Osher of U.C.L.A., and Drs. Chakravarthy and Szema of Rockwell for many valuable discussions. This work was partially funded by NASA-Langley Research Center under Contract NAS1-15820.

VI. References

1. Jameson, A., "Transonic Potential Flow Calculations using Conservation Form," AIAA 2nd Computational Fluid Dynamic Conference Proceedings, 1975, pp. 148-155.
2. Holst, T.L., "Fast, Conservative Algorithm for Solving the Transonic Full Potential Equation," AIAA Journal, Vol. 18, No. 12, December 1980, pp 1431-1439.
3. Siclari, M.J., "Computation of Nonlinear Supersonic Potential Flow over Three-Dimensional Surfaces," AIAA Paper No. 82-0167, presented at the AIAA 20th Aerospace Sciences Meeting, Orlando, Florida, January 1982.
4. Shankar, V., "A Conservative Full Potential, Implicit, Marching Scheme for Supersonic Flows," AIAA Journal, Vol. 20, No. 11, November 1982, pp. 1508-1514.
5. Shankar, V. and Osher, S., "An Efficient Full Potential Implicit Method Based on Characteristics for Analysis of Supersonic Flows," AIAA Paper No. 82-0974, June 1982; AIAA Journal, Vol. 21, No. 9, p. 1262, September 1983.
6. Shankar, V., Szema, K.-Y., and Osher, S., "A Conservative Type-Dependent Full Potential Method for the Treatment of Supersonic Flows with Embedded Subsonic Regions," AIAA Paper No. 83-1887; to appear in the AIAA Journal, November 1984.
7. Chipman, R. and Jameson, A., "An Alternating Direction Implicit Algorithm for Unsteady Potential Flow," presented at the AIAA 19th Aerospace Sciences Meeting, January 1981.

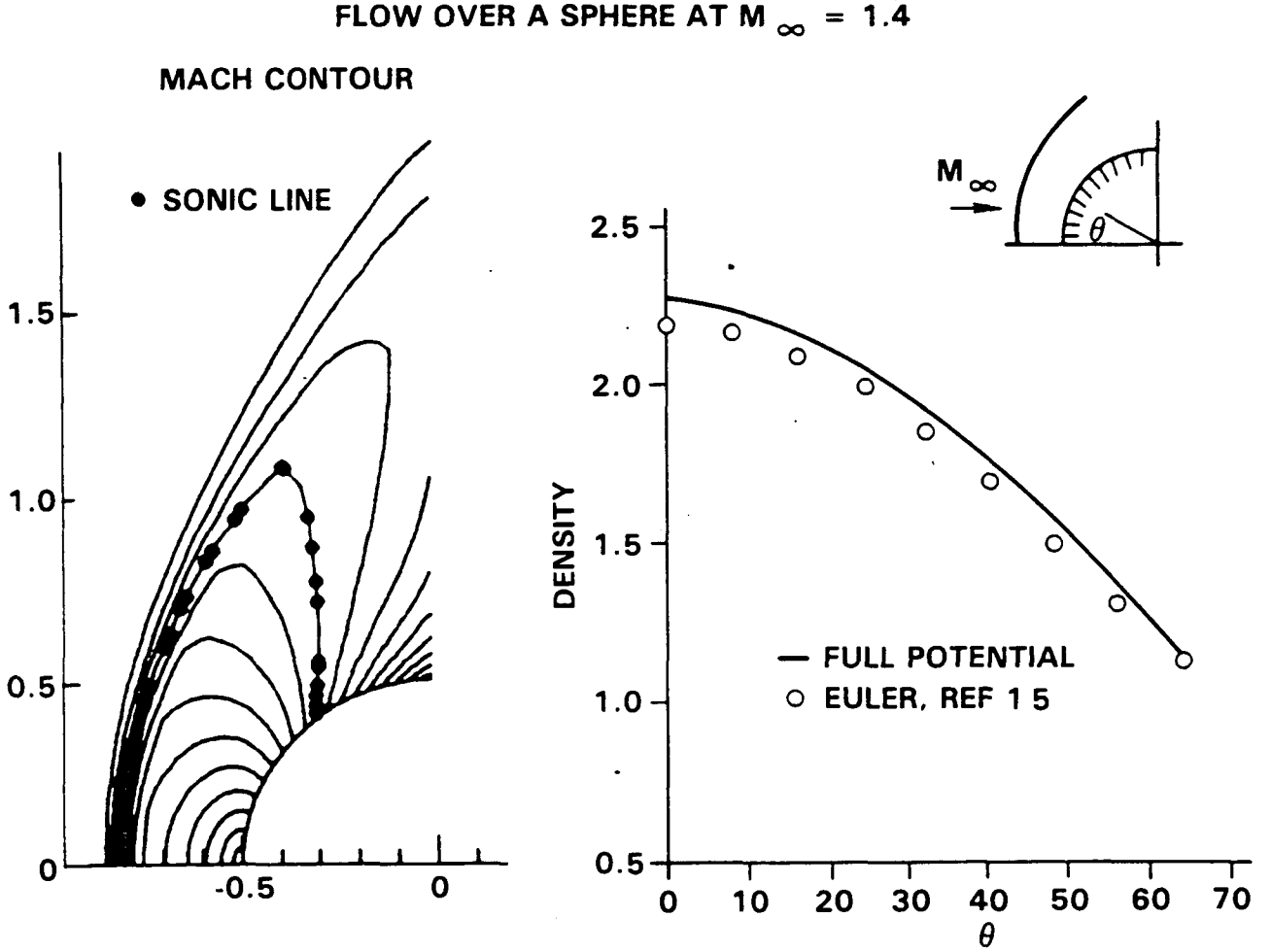

Fig. 5. Density distribution and Mach number contours for flow over a sphere at $M_\infty = 1.4$.

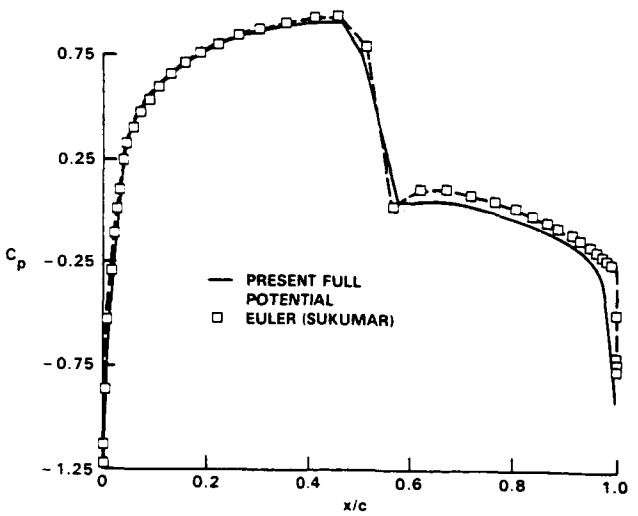

Fig. 6. Flow over NACA 0012, $M_\infty = 0.8$, $\alpha = 0°$.

8. Goorjian, P.M., "Computations of Unsteady Transonic Flow Governed by the Conservative Full Potential Equation using an Alternating Direction Implicit Algorithm," NASA CR-152274, June 1979.

9. Sankar, N.L. and Tassa, Y., "An Algorithm for Unsteady Transonic Potential Flow Past Airfoils," paper presented at the 7th International Conference on Numerical Methods in Fluid Dynamics, June 1980.

10. Steger, J. and Caradonna, F., "A Conservative Implicit Finite Difference Algorithm for the Unsteady Transonic Full Potential Equation," AIAA Paper No. 80–1368, presented at the 13th Fluid and Plasma Dynamics Conference, July 1980.

11. Malone, J.B. and Sankar, N.L., "Numerical Simulation of 2-D Unsteady Transonic Flows using the Full Potential Equation," AIAA Paper No. 83-0233.

12. Osher, S., "Scheme Design for Transonic Unsteady Aerodynamics Based on Riemann Solvers and the Entropy Condition," Transonic Unsteady Aerodynamics and Aeroelasticity Workshop, NASA-Langley Research Center, June 1983.

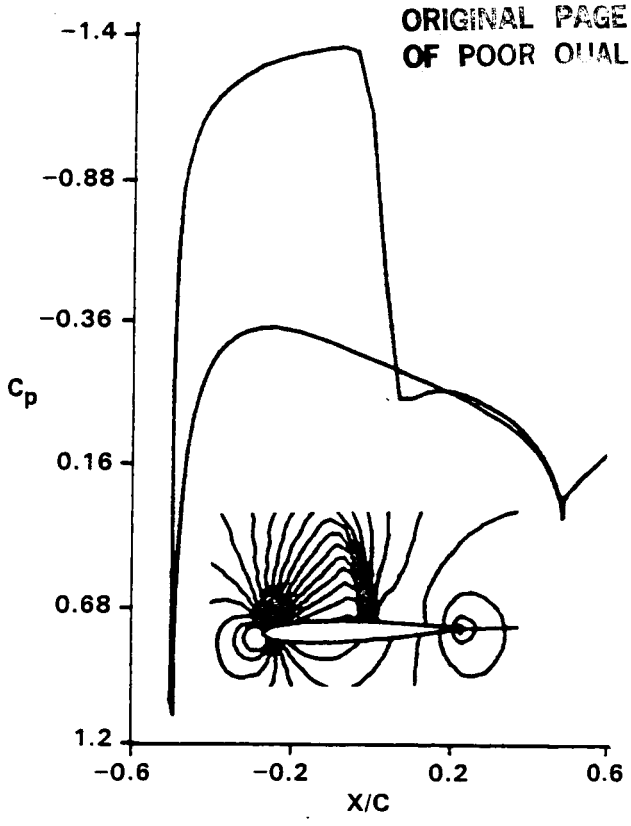

Fig. 7. Flow over NACA 0012, $M_\infty = 0.75$, $\alpha = 2°$.

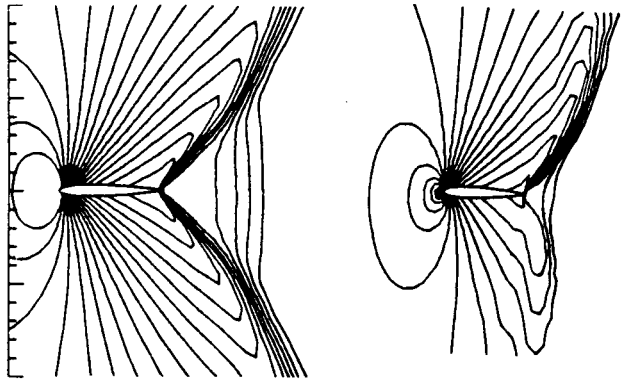

Fig. 8. Mach number contours for NACA 0012, M_∞ = 0.98.

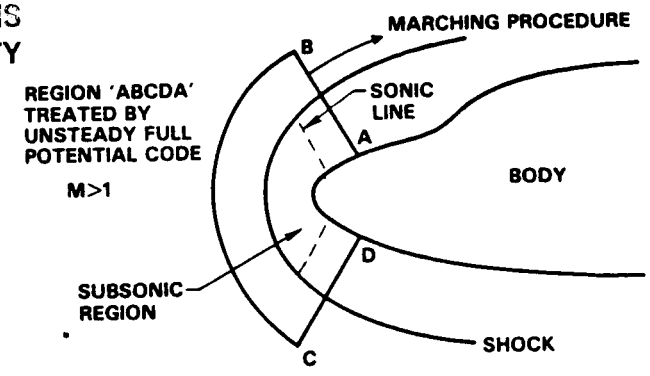

Fig.9. Blunt body starting solution for a marching code.

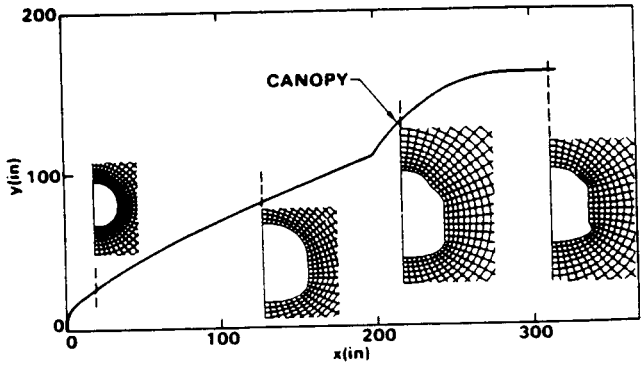

Fig. 10. Nose region geometry of Shuttle Orbiter.

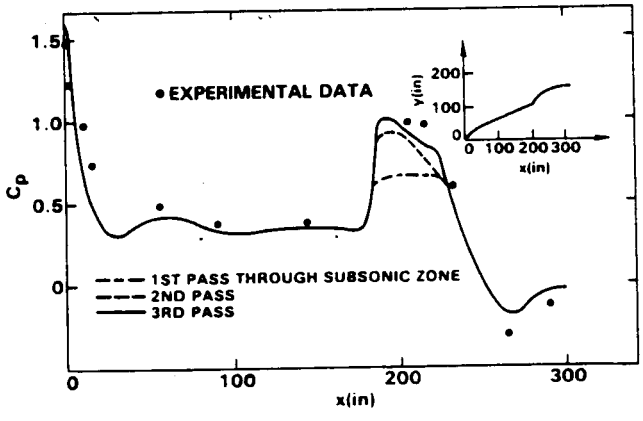

Fig. 11. Hybrid unsteady blunt body/supersonic marching calculation for the Orbiter at $M_\infty = 1.4$, $\alpha = 0°$.

13. Hafez, M., "Entropy Inequality for Transonic Flows," Transonic Unsteady Aerodynamics and Aeroelasticity Workshop, NASA-Langley Research Center, June 1983.

14. Chakravarthy, Sukumar, "Implicit Upwind Schemes without Approximate Factorization," AIAA Paper No. 84-0165.

15. Salas, M.D., "Flow Properties for a Spherical Body at Low Supersonic Speeds," Symposium on Computers in Aerodynamics, 25th Anniversary of Aerodynamics Labs, PINY, Farmingdale, NY, June 1979.

16. Szema, K.-Y. and Shankar, V., "Nonlinear Computation of Wing-Body-Vertical Tail-Wake Flows at Low Supersonic Speeds," AIAA Paper No. 84-0427.

17. South, Jr., J.C. and Brandt, A., "Application of a Multi-Level Grid Method to Transonic Flow Calculations," ICASE Report 76-8, NASA, 1976.

1. Report No.	2. Government Accession No.	3. Recipient's Catalog No.
NASA CR-172507		

4. Title and Subtitle	5. Report Date
NONLINEAR POTENTIAL ANALYSIS TECHNIQUES FOR SUPERSONIC AERODYNAMIC DESIGN	MARCH 1, 1985
	6. Performing Organization Code

7. Author(s)	8. Performing Organization Report No.
V. Shankar and K. Y. Szema	
	10. Work Unit No.

9. Performing Organization Name and Address	11. Contract or Grant No.
Rockwell International P. O. Box 92098 Los Angeles, California 90009	NAS1-15820
	13. Type of Report and Period Covered
12. Sponsoring Agency Name and Address	Contractor report
National Aeronautics and Space Administration Langley Research Center Hampton, Virginia 23665	14. Sponsoring Agency Code

15. Supplementary Notes

Technical monitors: Noel A. Talcott, Jr. and Kenneth M. Jones

16. Abstract

A numerical method based on the conservation form of the full potential equation has been applied to the problem of three-dimensional supersonic flows with embedded subsonic regions. The governing equation is cast in a nonorthogonal coordinate system, and the theory of characteristics is used to accurately monitor the type-dependent flow field. A conservative switching scheme is employed to transition from the supersonic marching procedure to a subsonic relaxation algorithm and vice versa. The newly developed computer program can handle arbitrary geometries with fuselage, canard, wing, flow through nacelle, vertical tail and wake components at combined angles of attack and sideslip. Results are obtained for a variety of configurations that include a Langley advanced fighter concept with fuselage centerline nacelle, Rockwell's Advanced Tactical Fighter (ATF) with wing mounted nacelles, and the Shuttle Orbiter configuration. Comparisons with available experiments were good.

17. Key Words (Suggested by Author(s))	18. Distribution Statement
Aerodynamic theory Potential analysis Supersonic/hypersonic	[redacted]

19. Security Classif. (of this report)	20. Security Classif. (of this page)	21. No. of Pages	22. Price
Unclassified	Unclassified	143	

Available: NASA's Industrial Applications Centers